Biogeomorphology shaping coastal and estuarine systems

the long-term development of landscapes

Biogeomorfologie van kust- en estuariene systemen

de langetermijnontwikkeling van landschappen

(met een samenvatting in het Nederlands)

P R O E F S C H R I F T

ter verkrijging van de graad van doctor aan de Universiteit Utrecht
op gezag van de rector magnificus, prof. dr. H.R.B.M. Kummeling,
ingevolge het besluit van het college voor promoties in het openbaar te verdedigen
vrijdag 8 december 2023 des middags te 2.15 uur

door

Márcio Boechat Albernaz
geboren op 27 juli 1986 te Guaratinguetá-SP, Brazilië

Promoters:
Prof. dr. Maarten. G. Kleinhans
Prof. dr. Gerben Ruessink

co-Promoters:
Dr. Ad van der Spek
Dr. Harm Jan Pierik

This work was financially supported by the European Research Council Consolidator grant to MGK (grant ERC-Consolidator 647570)

Biogeomorphology shaping coastal and estuarine systems

Promoters:
Prof. dr. Maarten G. Kleinhans
Prof. dr. Gerben Ruessink

Examination committee:
Prof. dr. Piet Hoekstra
Utrecht University, The Netherlands

Prof. dr. Vera van Lancker
University of Gent, Belgium

Prof. dr. Ian Townend
University of Southampton, UK

Prof. dr. Jakob Wallinga
Wageningen University, The Netherlands

Prof dr. Zheng Bing Wang
Delft University of Technology, The Netherlands

Dr. Meagan Wengrove
Oregon State University, USA

ISBN 978-90-6266-672-0

Published by Faculty of Geosciences, Universiteit Utrecht, The Netherlands, in:
Utrecht Studies in Earth Sciences (USES 299), ISSN 2211-4335

Typeset using XeLaTeX

Cover picture: Wadden Sea near Lauwersoog, NL. Source: author.
Cover design: Margot Stoete

Printed by Ipskamp Printing BV, Enschede, The Netherlands

Correspondence to: Márcio Boechat Albernaz, albernaz.oceano@gmail.com

Utrecht Studies in Earth Sciences 299

Biogeomorphology shaping coastal and estuarine systems

the long-term development of landscapes

Márcio Boechat Albernaz

Utrecht 2023

Faculty of Geosciences, Utrecht University

"I made a big decision a little while ago.
I don't remember what it was, which prob'ly goes to show
That many times a simple choice can prove to be essential
Even though it often might appear inconsequential.

I must have been distracted when I left my home because
Left or right I'm sure I went. (I wonder which it was!)
Anyway, I never veered: I walked in that direction
Utterly absorbed it seems, in quiet introspection.

For no reason I can think of, I've wandered far astray.
And that is how I got to where I find myself today."

Bill Watterson, Calvin and Hobbes

"Não quero regra nem nada
Tudo tá como o diabo gosta, tá
Já tenho este peso, que me fere as costas
E não vou, eu mesmo, atar minha mão
O que transforma o velho no novo
Bendito fruto do povo será
E a única forma que pode ser norma
É nenhuma regra ter
É nunca fazer nada que o mestre mandar
Sempre desobedecer
Nunca reverenciar"

Antônio Carlos Belchior, Como o diabo gosta

Contents

Summary

Coastal and estuarine environments are home to a wide variety of habitats and ecosystems. They provide ecosystem services such as nursery grounds and habitats for (non-)commercial fishes and other aquatic species, and offer natural protection to coastlines, shelter for harbors, tourism and leisure. Understanding the morphodynamics of coastal areas is vital as hundreds of millions of people live near the coast around the globe. Due to human pressure and climate change, many deltas and coastal areas are under threat. Therefore, the ability to understand and predict the long-term evolution (i.e. decades to millennium) of these systems is crucial for supporting policies and management towards more sustainable and safe usage of coastal environments.

Coastal, fluvial and estuarine landscapes develop through interaction of water, sediments and biota. These landscapes are an ever evolving product of hydrodynamic forces, such as river discharges, tides and waves, sediment transport and interactions with biota on the pre-existing morphology. As such, a landscape is a product of the initial conditions (e.g. the geological legacy), the boundary conditions (tides, waves, fluvial discharges, sediment supply and longer-term sea level fluctuations) and internal conditions (roughness, friction, inertia and turbulence steered by channels, shoals, bars, bedforms and vegetation) controlling the hydrodynamics and sediment transport which in turn modify the morphology and the abiotic conditions for biota. Biota affect the hydrodynamics in various ways and may also directly change morphology by organic material accretion. Thus the landscape is a result of dynamic biogemorphodynamic interactions between water, sediment, morphology and biota.

Two major but contrasting methodologies of studying long-term geomorphology and morphodynamics are: historical-paleogeographical reconstructions and morphodynamic modelling. Both methods have their own advantages and disadvantages in reconstructing past conditions, forecasting future conditions and understanding the morphodynamic drivers. Yet, scientific communities tend to concentrate on either method with limited interaction in spite of studying the same systems and processes. The reconstruction and hindcast of past conditions as well as the forecast of future scenarios are challenges for scientists. For example, paleogeographical reconstructions are commonly hampered by the ability to isolate variables and testing alternative hypotheses from often limited past data. On the other hand, morphodynamic models often need to be simplified in their initial and boundary conditions and in the acting mechanisms, in comparison to nature, due to a combination of limited available data (in terms of detailed model inputs), limited physical process formulations and limitations of computational power. That means, predicting the evolution of beaches, tidal basins and estuaries is challenging due to the limitations on our knowledge about the individual and combined effects of changing forces, such as sea level rise and sediment supply, within the morphodynamic feedback; as well as due to shortcomings in our knowledge of physics and the uncertainties of predicting future hydrodynamic conditions, sediment fluxes and composition and the biota composition for decades to centuries ahead. Consequently, there is

an urgent need to identify and address important knowledge gaps between paleogeographical reconstructions and morphodynamic models regarding the response of coastal-estuarine systems under varying sediment supply, fluvial discharges and increasing sea level, especially in combination with vegetation.

The objective of this thesis is to systematically determine the long-term and large-scale development of coasts, estuaries and tidal basins under combinations of tides, waves, river discharges, sea level rise, sediment supply and vegetation. Hypotheses posed by paleogeographical reconstructions were tested with numerical models.

The hypotheses tested in this thesis were largely derived from the data-rich geological record of the Netherlands. During the Holocene, the Dutch landscape evolved under a combination of sea level rise, marine and fluvial forces and sediment supply, and their interaction with vegetation and peat. By the mid-late Holocene, around 6000 cal BP, a large portion of the present Dutch territory was infilled by fluvial sediments from the Rhine-Meuse rivers and marine sediments from the North Sea. This infilling of the Dutch coastal plain occurred when the sea level rise decelerated around 6000 BP. During this infilling period, the rivers distributed freshwater and sediments along their path creating dynamic fluvial-estuarine landscapes with bifurcations, levees, floodplains and peat. Towards the coast, the rivers connected with the marine environment that also provided sediments and hydrodynamic forces through waves and tides which shaped the open coast, estuaries and tidal basins. Two environments within the Dutch coastal landscape were particularly relevant for this thesis. One is the Rhine-Meuse estuaries that fed the low-lying areas with fresh water and sediments, and where abundant peat formed and infilled the accommodation space. The other environment comprised the barrier islands along sections of Dutch coast that had little fluvial influence and limited effects of vegetation.

The hypotheses were tested in the Delft3D numerical model. Numerical models are based on detailed and complex physics to simulate hydrodynamics, sediment transport and morphology. They are commonly applied in engineering contexts of short-term scenarios (days to years) including simplifications of the natural system and parameterizations of physical and biological mechanisms. The consequence of being comprehensive is that such morphodynamic numerical models are often limited in application to short-term simulations. These limitations commonly hamper the ability to simulate long-term biogeomorphodynamics where small deviations in the short-term may lead to unrealistic long-term results. Some of these shortcomings were identified and further studied in this thesis in order to allow for the desired long-term simulations. Specifically, three key improvements were necessary for modelling the long-term biogeomorphodynamics: (1) vegetation development and effects were coupled to the Delft3D morphodynamic model; (2) the wave-driven sediment transport was improved by implementation and testing of an alternative for the classical near-bed wave orbital velocity parameterization by Isobe-Horikawa, that may overpredict onshore sediment transport due to excessive wave skewness; (3) the model tendency to promote excessive channel incision and morphological diffusion was studied and an improvement of the use of counteracting transverse bed slope parameterizations for sediment transport under currents and waves was developed.

The results after model improvements (2) and (3) showed that the long-term evolution of coastal-fluvial landscapes in numerical models are strongly controlled by the parameterization of the transverse bed slope sediment transport and the near-bed wave orbital velocities. Using an improved parameterization of transverse bed slope (TBS) sediment transport and parameterization for net sediment transport driven by near-bed wave orbital velocities improved long-term morphodynamic simulations in the sense that the simulated morphological development is now more realistic compared to nature. Without the improvements, unrealistically deep channels and fast coastal expansion are modelled. The TBS values applied in numerical models deviate from the empirical values derived from physical experiments. This discrepancy is likely due to the fact that the TBS needs to compensate for other model artifacts such as grid-size (dependency) and erosion-sedimentation processes. Thus, the choice of TBS varies with the sediment transport formulation, the grid size and the dominance of erosion or sedimentation. Furthermore, when coupling to wave-related sediment transport, the TBS also needs to be changed (mainly lowered) to account for the higher mobility condition induced by waves.

The parameterization of near-bed orbital velocity from Ruessink (RUE) showed better results in terms of onshore-directed but also alongshore sediment transport in open coasts when compared to the IH. The RUE parameterization takes into account both wave-induced velocity skewness and asymmetry, which when coupled to the skewness-based VR04 sediment transport predictor, resulted in more realistic coastal profiles compared to data from Katwijk (NL) and Duck (USA). Furthermore, when this parameterization was applied to the more complex case of a barrier island, the model showed dynamic ebb-tidal deltas that grew, migrated and even merged with the downdrift coast. These ebb-tidal delta dynamics and the overall inlet development were not possible with the previous (default) version of Delft3D.

Vegetation was implemented in the numerical models as eco-engineering plant species (i.e. functional types of vegetation with effects on the hydrodynamics). With the biogeomorphodynamic models, hypotheses derived from paleogeographical reconstructions were tested, such as that vegetation enhances sedimentation on levees and on the entire floodplain and saltmarsh. Scenarios of landscape evolution with various boundary conditions and sediment availability, with and without vegetation were explored in two contrasting idealized settings: a fluvial-tidal estuary, and a barrier coast (wave-tidal) system. The fluvial-tidal estuarine setup allowed levees to form and evolve under combinations of fluvial and tidal discharges, sediment supply and different eco-engineering species, namely reeds and trees. The wave-tidal setup of a comprehensive sand-mud barrier coast system tested combined effects of wave climate, tides, sea level rise and formation of marshes.

The tidal-fluvial basin model, inspired by paleoreconstructions of the Old Rhine, showed that vegetation played a major role in transforming the coastal landscape from subtidal to intertidal and supratidal. Over a hundred scenarios unravel the individual and combined effects of fluvial-tidal discharges, sediment supply and vegetation in building levees and crevasses that infilled the landscape. The dense reed vegetation in the floodbasin reduced the floodbasin sedimentation and the levee width but, more importantly, it inhibited the formation of crevasses that could have conveyed sediment to the floodbasins. Conversely, trees (sparse vegetation) enhanced the formation of crevasses. Furthermore, the set of mod-

els showed that vegetation alone was able to reduce the tidal effect in the floodbasin over time while enabling the seaward expansion of levees. The seaward levee expansion continued until the levees connected to the coastal barrier, which closed off the floodplains and thus transformed the tidal basin into an estuary. Essentially, this shows that the transition of the Old Rhine from a tidal basin to an estuary can have been entirely driven by the settling of reeds (followed by later peat formation) with all other boundary conditions (offshore tides and fluvial discharge) being equal.

The back-barrier basin model responded strongly to the presence of marsh vegetation in a similar way. The vegetation in the tidal basin changed the local configuration of channels and shoals. This triggered a cascade of effects beyond the vegetation patches: it changed the sediment import-export balance of the basin. The unvegetated basins, regardless the magnitude of the offshore supply of mud, imported sediments and kept up with sea level rise. On the other hand, the vegetated basins showed a net export of sediments after the marsh establishment. Without sea level rise, the basin reached a steady-state (equilibrium). However, with sea level rise the growth of accommodation space and tidal prism combined with the net sediment export trend led to basin drowning and extensive marsh mortality. This suggests that, in contrast with most literature, vegetation may not invariably contribute to the infilling that potentially counters sea level rise.

Samenvatting

Kustgebieden en getij-gedomineerde bekkens (wadden) en riviermondingen (estuaria) herbergen een grote verscheidenheid aan habitats en ecosystemen. Ze leveren ecosysteemdiensten zoals kraamkamers en habitats voor verschillende (niet-) commerciële vissoorten en andere aquatische organismen, bieden natuurlijke bescherming tegen overstroming en kustafslag en beschutting voor havens, toerisme en recreatie. Inzicht in de morfodynamiek van kustgebieden is van vitaal belang omdat wereldwijd honderden miljoenen mensen aan de kust wonen. Door toenemende intensiteit en ruimtebeslag van menselijke activiteiten en klimaatverandering wordt het functioneren van veel delta's en kustgebieden bedreigd. Daarom is het cruciaal om de ontwikkeling op lange termijn (d.w.z. decennia tot millennia) van deze systemen te begrijpen en te voorspellen, ten behoeve van een duurzaam beleid en beheer en veilig gebruik van kustgebieden.

Kust-, fluviatiele en estuariene landschappen ontwikkelen zich door de interactie van water, sedimenten en biota. Deze landschappen ontwikkelen zich doorlopend onder invloed van waterbeweging (rivierafvoer, getijden en golven), sedimenttransport en interacties met biota. Een landschap is daarbij een resultante van de initiële condities (bijv. de geologische ontwikkeling), de randvoorwaarden (getijden, golven, rivierafvoer, aanvoer van sediment en zeespiegelfluctuaties op de langere termijn) en interne omstandigheden (ruwheid, wrijving, traagheid en turbulentie beïnvloed door geulen, banken, platen, beddingvormen en vegetatie). Deze factoren bepalen de waterbeweging en het sedimenttransport, welke op hun beurt de morfologie en de abiotische omstandigheden voor biota weer veranderen. Biota beïnvloeden de hydrodynamica op verschillende manieren en kunnen ook direct de morfologie veranderen door accumulatie van organisch materiaal, bijvoorbeeld als veen. Het landschap is, kortom, het resultaat van biogeomorfodynamische interacties tussen water, sediment, morfologie en biota.

Twee belangrijke, essentieel verschillende maar complementaire methodologieën voor het bestuderen van geomorfologie en dynamiek op lange termijn zijn historische paleogeografische reconstructies en morfodynamische modellering. Beide methoden hebben hun voor- en nadelen bij het reconstrueren van omstandigheden in het verleden, het voorspellen van toekomstige omstandigheden en het begrijpen van de mechanismen en processen. Toch neigen wetenschappelijke disciplines zich te specialiseren in één van beide methoden, wat leidt tot beperkte uitwisseling met de andere, ondanks het feit dat ze dezelfde systemen en processen bestuderen. De reconstructie van vroegere omstandigheden en de voorspelling van toekomstige situaties zijn uitdagend. Zo leveren paleogeografische reconstructies de basis voor het opstellen van hypothesen over de sturing van de landschapsontwikkeling. Voor het toetsen van deze hypothesen en het vaststellen van de mogelijke sturende factoren, zijn modellen nodig. Anderzijds zijn morfodynamische modellen vereenvoudigd in hun begin- en randvoorwaarden en in de werkingsmechanismen in vergelijking met de natuur, mede door een combinatie van beperkte beschikbare gegevens (in termen van gedetailleerde modelinput), beperkte fysische procesformuleringen en beperkingen in rekenkracht. Dat betekent

dat het voorspellen van de langetermijnontwikkeling van stranden, getijdebekkens en estuaria een uitdaging is vanwege de beperkingen in onze kennis over de enkelvoudige en gecombineerde effecten van veranderende forceringen, zoals zeespiegelstijging en aanvoer van sediment, op het morfodynamisch systeem. Daarbij komen tekortkomingen in onze kennis van de relevante natuurkunde en de onzekerheden bij het voorspellen van hydrodynamische omstandigheden, sedimentfluxen en -samenstelling en de samenstelling van de biota voor de komende decennia tot eeuwen. Daarom is er dringend behoefte aan het identificeren en invullen van belangrijke leemtes in de kennis van de respons van kustsystemen op variërende sedimentaanvoer, fluviatiele afvoer en stijgende zeespiegel, vooral in combinatie met vegetatie, en dan in het bijzonder daar waar deze leemtes de potentieel krachtige combinatie van paleogeografische reconstructies en morfodynamische modellen hinderen.

Het doel van dit proefschrift is het systematisch bepalen van de langetermijn- en grootschalige ontwikkeling van kusten, estuaria en getijdengebieden onder verschillende combinaties van getijden, golven, rivierafvoeren, zeespiegelstijging, sedimentaanvoer en vegetatie. Hypotheses hieromtrent, gebaseerd op paleogeografische reconstructies, worden getest met numerieke modellen.

De hypotheses die in dit proefschrift worden getest, werden grotendeels afgeleid uit het rijke geologische archief van Nederland. Tijdens het Holoceen ontwikkelde het Nederlandse landschap zich onder invloed van een combinatie van zeespiegelstijging, mariene en fluviatiele krachten, sedimentaanvoer en hun interactie met vegetatie en veen. Tegen het midden van het Holoceen, rond 6000 jaar geleden , werd een groot deel van het huidige Nederlandse landschap opgevuld door sedimenten uit de Rijn en Maas en uit de Noordzee, en door veen. Deze opvulling van de Nederlandse kustvlakte vond plaats vanaf dat de zeespiegelstijging rond 6500 jaar terug afnam. Tijdens deze periode van netto sedimentatie voerden de rivieren zoet water en sediment aan, waardoor een dynamisch landschap ontstond waarin de rivier zich vertakte, riviertakken zich verlegden en veen werd gevormd, en waarin men dijken aanlegde waardoor uiterwaarden ontstonden. Richting de kust, waar de rivieren rechtstreeks in verbinding stonden met de zee, waren in toenemende mate golven en getijden van belang die sediment vanuit zee aanvoerden en de open kust, de estuaria en getijdenbekkens vormgaven. Twee milieus binnen het Nederlandse kustlandschap zijn bijzonder relevant voor dit proefschrift. De eerste is de Rijn-Maasmonding die de laaggelegen gebieden voedde met zoet water en sediment en waar overvloedig veen werd gevormd, waardoor de ruimte tussen waterbodem en gemiddeld wateroppervlak (accommodatieruimte) opvulde. Het andere milieu is het systeem van de barrière-eilanden en getijbekkens dat voorkwam langs de westelijke en noordelijke delen van de Nederlandse kust , waar de invloed van de rivieren en de effecten van vegetatie beperkt waren. De op de reconstructies gebaseerde hypothesen hadden met name betrekking op de sedimentbalans van de kustvlakte, de bronnen van sediment en de verspreiding ervan door rivieren, getij en golven en de invloed van vegetatie op sedimentatie en vorming van het land.

De hypothesen werden systematisch getest in een uitgebreide versie van het Delft3D numerieke model. Numerieke simulatiemodellen zijn gebaseerd op gedetailleerde en complexe natuurkunde om de interacties van waterbeweging, sedimenttransport en morfologie te simuleren. Ze worden vaak toegepast in kortetermijnscenario's (dagen tot jaren) voor ont-

werpen ten behoeve van scheepvaart en hoogwaterveiligheid. Het gevolg van deze veelomvattendheid en van vereenvoudigingen van het natuurlijke systeem en parametrisaties van fysische en biologische mechanismen is dat dergelijke morfodynamische numerieke modellen vaak beperkt zijn tot toepassing op kortetermijnsimulaties. Deze beperkingen belemmeren de vergelijking met reconstructies, omdat op zich kleine afwijkingen op die lange termijn kunnen uitgroeien tot onrealistische resultaten. De belangrijkste tekortkomingen werden geïdentificeerd en verder bestudeerd in dit proefschrift om de gewenste langetermijnsimulaties mogelijk te maken. Specifiek waren er drie belangrijke verbeteringen nodig voor het modelleren van de biogeomorfodynamiek op lange termijn: (1) vegetatieontwikkeling en -effecten ontbraken: deze werden gekoppeld aan het Delft3D morfodynamische model; (2) het golfgedreven kustwaartse zandtransport werd fors overschat door een klassieke parametrisatie voor vervormende golven die de kust naderen, waarvoor een betere parametrisatie werd geïmplementeerd en getest; (3) de neiging van het model tot overmatige insnijding van geulen werd bestudeerd en er werd een verbetering ontwikkeld voor de parameters die de insnijding tegenwerken onder stromingen en golven, namelijk voor sedimentbeweging op de hellingen naast de geulen.

De resultaten na modelverbeteringen (2) en (3) toonden aan dat de langetermijnontwikkeling van kust- en rivierlandschappen in numerieke modellen sterk wordt bepaald door de parametrisaties van het sedimenttransport op dwarshellingen van de geulbodem en de orbitaalsnelheden aan de bodem onder golven. Het gebruik van een verbeterde parametrisering van het sedimenttransport op de dwarshelling van de geulbodem (TBS) en een parametrisering voor het netto sedimenttransport, aangedreven door de orbitaalsnelheden aan de bodem onder golven, verbeterde de morfodynamische simulaties op lange termijn in die zin dat de gesimuleerde morfologische ontwikkeling nu realistischer is vergeleken met de natuur. Zonder deze verbeteringen worden onrealistisch diepe geulen en een te snelle kustuitbreiding gemodelleerd. De TBS-waarden die in numerieke modellen worden toegepast wijken af van de empirische waarden die uit fysische experimenten zijn afgeleid. Deze discrepantie is waarschijnlijk te wijten aan het feit dat de TBS moet compenseren voor modelartefacten zoals afhankelijkheid van de resolutie en of er netto erosie of sedimentatie plaatsvindt. De optimale keuze van de TBS-waarden hangt bovendien af van de formulering van het sedimenttransport. Daarnaast moet bij koppeling aan golfgerelateerd sedimenttransport de TBS worden verlaagd om rekening te houden met de hogere mobiliteitsvoorwaarde die door golven wordt veroorzaakt, wat ook het sedimenttransport op de hellingen versterkt.

De parametrisatie van Ruessink (RUE) van de waterbeweging door golven nabij de bodem liet in vergelijking met de klassieke parametrisatie betere resultaten zien bij kustdwars gericht én kustlangs sedimenttransport aan de kust. De RUE parametrisatie houdt rekening met zowel de scheefheid als de asymmetrie van de door golven veroorzaakte stroomsnelheden nabij de bodem, wat in combinatie met de op scheefheid gebaseerde gebruikte sedimenttransportformulering resulteerde in meer realistische kustprofielen, zoals bleek bij vergelijking met gegevens van de veel bestudeerde kusten van Katwijk (NL) en Duck (USA). Toen deze parametrisatie werd toegepast op de meer complexe situatie van een zeegat in een strandwal, of tussen twee waddeneilanden, toonde het model bovendien voor het eerst een dynamische ontwikkeling van ebdelta's, die groeiden, migreerden en zelfs samensmolten met de bene-

denstroomse kust, zoals dit ook in de natuur voorkomt. Het simuleren van de dynamiek van een ebdelta, en de morfodynamische ontwikkeling van een zeegat in het algemeen, waren met de eerdere (standaard) versie van Delft3D niet mogelijk.

Vegetatie werd in de numerieke modellen ingebouwd als eco-engineering plantensoorten, d.w.z. vegetatietypen waarvan de standplaats niet alleen afhangt van de omstandigheden, maar die ook effecten hebben op de hydrodynamica waardoor een extra terugkoppeling ontstaat in het model. Met de biogeomorfodynamische modellen werden hypotheses gebaseerd op paleogeografische reconstructies getest, bijvoorbeeld dat vegetatie de sedimentatie op oeverwallen en op de hele overstromingsvlakte en de schorren (of kwelders) versterkt. Scenario's van landschapsontwikkeling onder verschillende randvoorwaarden en beschikbaarheid van sediment, met en zonder vegetatie werden onderzocht in twee contrasterende geïdealiseerde omgevingen: een estuarium met rivierinvloed en een getijsysteem zonder rivier maar met grote invloed van golven. In het estuarium vormden zich sterk verschillende oeverwallen afhankelijk van de sterkte van getij- en rivierstroming, de sedimentaanvoer en de verschillende eco-engineering soorten, namelijk riet en bomen. De langetermijnontwikkeling van het golfgedomineerde systeem bleek niet alleen afhankelijk van het gecombineerde effect van golfklimaat, getij en zeespiegelstijging, maar bleek tevens erg gevoelig voor de vorming en het verdrinken van schorren (kwelders).

Het estuariummodel, geïnspireerd op reconstructies van de ontwikkeling van de monding van de Oude Rijn, toonde aan dat vegetatie een grotere rol dan verwacht speelde bij de transformatie van het kustlandschap van subgetijde naar intergetijde en supragetijde. Het doorrekenen van meer dan honderd scenario's ontrafelde de individuele en gecombineerde effecten van fluviatiele en getijdedebieten, sedimentaanvoer en vegetatie bij de vorming van oeverwallen en doorsnijdingen (crevasses) hiervan. Een dichte rietvegetatie op de overstromingsvlakte verminderde de sedimentatie daar fors en leidde tot veel smallere oeverwallen, maar, nog belangrijker, verhinderde de vorming van crevasses die sediment naar de overstromingsvlakten hadden kunnen voeren. Daarentegen bevorderden bomen met hun minder dichte begroeiing juist de vorming van crevasses. Bovenal toonde de reeks modelsimulaties aan dat vegetatie op zichzelf in staat was om het getijdeneffect in het overstromingsgebied in de loop van de tijd te verminderen, waarbij het de zeewaartse uitbreiding van oeverwallen bevorderde. De uitbreiding ging door totdat de oeverwallen verbonden raakten met de strandwal, waardoor de overstromingsvlakte werd afgesloten van de getij-invloed en zo het getijdenbekken in een estuarium veranderde. In wezen laat dit zien dat de overgang van de Oude Rijn van een getijdenbekken naar een estuarium volledig aangedreven zou kunnen zijn door de vestiging van riet (gevolgd door latere veenvorming), maar niet, zoals in veel literatuur wordt gesuggereerd, doordat de vegetatie de sedimentatie versterkte.

Het model voor het golfgedomineerde getijbekken (waddenbekken) reageerde op een vergelijkbare manier op de aanwezigheid van moerasvegetatie. Door de vestiging van vegetatie op de hogere delen veranderde de vorm van geulen en platen in het bekken. Dit veroorzaakte een zichzelf versterkend effect: de vegetatie hinderde de verspreiding van sediment en netto veranderde de import van sediment naar export. De niet-begroeide bekkens daarentegen bleven sediment importeren en hielden gelijke tred met de zeespiegelstijging, ook voor lage concentraties slib op zee. De begroeide bekkens exporteerden juist sediment na de vorming

van schorren. Zonder zeespiegelstijging bereikte het begroeide bekken wel een evenwicht, maar met zeespiegelstijging verdronk het bekken en stierven de schorren goeddeels af. Dit suggereert dat, in tegenstelling tot wat de meeste literatuur stelt, vegetatie niet altijd bijdraagt aan het bijhouden van de zeespiegelstijging met sedimentatie.

Chapter 1

Introduction

1.1 Problem definition

Coastal, fluvial and estuarine landscapes develop upon the interaction of water, sediments and biota. Such landscapes are an ever evolving product of hydrodynamic forces, such as river discharges, tides and waves, and sediment transport on the pre-existing morphology and their interaction with biota. This triad of hydrodynamics, sediment transport and morphology is the basis of the morphodynamic feedback loop (e.g. Wright and Thom, 1977) that drives the evolution of environments such as fluvial-tidal basins, estuaries, rivers, lakes, deltas and coastal plains. The landscape is a product of the initial conditions (e.g. the geological heritage), the boundary conditions (tides, waves, fluvial discharges, sediment supply and sea level fluctuations) and internal conditions (roughness, friction, inertia and turbulence steered by channels, shoals, bars, bedforms and vegetation) controlling the hydrodynamics and sediment transport, which in turn, modify the morphology (Boyd et al., 1992) and the abiotic conditions for biota. Biota affect the hydrodynamics in various ways and may also directly change morphology by organic material accretion. Therefore, the landscape is a result of dynamic biogemorphodynamic interactions between water, sediment, morphology and biota.

Coastal and estuarine environments are home to a wide variety of habitats and ecosystems. They provide ecosystem services such as nursery grounds and habitats for several (non-)commercial fishes and aquatic species, in addition of offering natural protection to coastlines and shelter for harbors, tourism and leisure. Understanding the morphodynamics of coastal areas is vital as hundreds of millions of people live near the coast, mostly in vulnerable areas, around the globe (Edmonds et al., 2020). Due to human pressure and climate change, many deltas and coastal areas are under threat (Syvitski et al., 2005; Nienhuis et al., 2020). Therefore, the ability to understand and predict the long-term evolution (i.e. decades to millennium) of these systems is crucial for supporting policies and management towards more sustainable and safe usage of coastal environments.

Two major but contrasting methodologies of studying long-term geomorphology and morphodynamics are: historical-paleogeographical data and the use of morphodynamic models. Both methods have their own advantages and disadvantages in reconstructing-forecasting past-future conditions and understanding the morphodynamic drivers. Yet, the scientific communities concentrating on either method have limited interaction in spite of studying the same systems and processes. The reconstruction and hindcast of past conditions as well as the forecast of future scenarios are a challenge for scientists. For example, paleogeographical reconstructions (and hindcast based on these) are commonly hampered by the ability to isolate variables and testing alternative hypotheses from often limited field data. An extra challenge is posed by the uneven representation in the stratigraphy of extreme events, peri-

ods of inactivity, erosional features and deposit hiatuses (Paola et al., 2018). On the other hand, morphodynamic models often need to be simplified in their initial and boundary conditions and in the acting mechanisms, in comparison to nature, due to a combination of limited available data (in terms of detailed model inputs), the lack of physical process formulations and limitations of computational power. The forecast is likewise challenging due to our limited capacity in predicting the future hydro-sediment-biota conditions especially in view of human interventions (e.g. river dams, dikes, dredging, breakwaters) and climate change (sea level change, droughts, biota distribution). The ability to assess the morphodynamic evolution of coastal environments through numerical simulations is especially troublesome on the large spatial (*O* 10-100's Km) and long-time scales (*O* decades to centuries) as small residual (net) effects in the short-term can lead to different large-scale effects due to the morphodynamic feedback (De Vriend, 1991a). That means, predicting the evolution of beaches, tidal basins and estuaries are challenging due to the limitations on our knowledge about the individual and combined effects of changing forces (e.g. sea level rise and sediment supply) within the morphodynamic feedback; as well as due to shortcomings in our knowledge of physics and the uncertainties of predicting future hydrodynamic conditions, sediment fluxes and composition and the biota composition for a decade-century ahead.

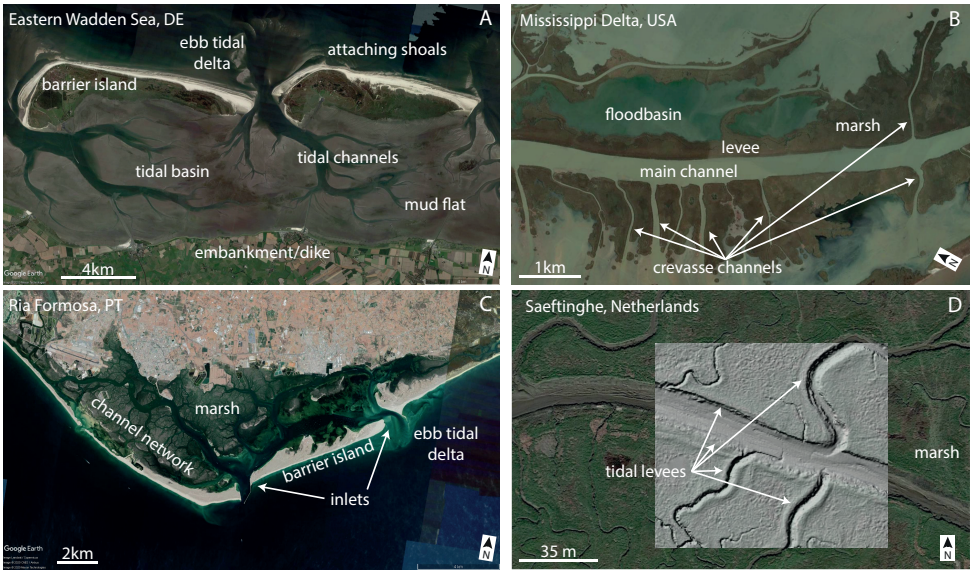

Figure 1.1: Natural systems around the World.

Landscapes, at least on Earth, are teeming with life but, while vegetation is abundant in fluvial, estuarine and coastal environments (e.g. Cazanacli and Smith, 1998; Corenblit et al., 2011; Pierik et al., 2017b; Temmerman et al., 2007, and Figure 1.1), the vegetation effects on hydrodynamics and morphology are understudied and often poorly represented in reconstructions and models despite their strong influence on morphodynamics (D'Alpaos et

al., 2007; Kirwan and Murray, 2007; Temmerman et al., 2007; Davies and Gibling, 2011; van Maanen et al., 2015; Kleinhans et al., 2018; Lokhorst et al., 2018; McMahon and Davies, 2018; Brückner et al., 2019). Vegetation is responsible for reducing flow velocity and therefore affects erosion and sedimentation (Leonard and Luther, 1995; Kirwan et al., 2016), which further changes the environmental conditions for the vegetation itself. This feedback between vegetation and morphology alters the environment in a process called eco-engineering (see Jones et al., 1994). The eco-engineering effects include, for example, increasing channel formation in salt marshes resulting in a richer drainage network (Temmerman et al., 2007; Schwarz et al., 2015). Vegetation effects also include controls beyond the local scale of vegetation patches through backwater effects (Oorschot et al., 2016; Kleinhans et al., 2018) and their ability to control crevasse formation and avulsions on fluvial-tidal systems (Mohrig et al., 2000; Nienhuis et al., 2018). As such, vegetation is not only affected by the physical processes but it also affects the physical processes at local and landscape scales. Although, the long-term and large-scale effects of these biogeomorphodynamic interactions are poorly understood and often neglected.

There is an urgent need to identify and address important knowledge gaps between paleogeographical reconstructions and morphodynamic models regarding the response of coastal systems under varying sediment supply, fluvial discharges and increasing sea level (Dunn et al., 2019; Eslami et al., 2019), especially in combination with vegetation. Commonly, long-term studies rely on paleogeographical reconstructions (e.g. Törnqvist et al., 2004; Stouthamer and Berendsen, 2007; Hein et al., 2016; Esposito et al., 2017; Pierik et al., 2017b; de Haas et al., 2018), physical experiments (e.g. Paola et al., 2001; Leuven et al., 2018a; Braat et al., 2019) and numerical models (Braat et al., 2017; Kleinhans et al., 2018; Lokhorst et al., 2018; Nienhuis et al., 2018; van Dijk et al., 2018) in isolation and without considering the effects of vegetation on the morphodynamics. But there is a clear need to integrate these knowledge fields towards better understanding the natural systems and improving our predictions. Specifically, reconstructions of vegetated coastal systems need to be enriched and compared with numerical models with and without vegetation effects in order to assess the long-term effects of vegetation. This, in turn, may aid improvements to paleogeographical reconstructions and their value for system understanding and forecasting.

Here I focus on bridging the knowledge gap between the paleogeographical reconstructions of coastal and estuarine systems, and the processes and mechanisms from biogeomorphodynamic models to improve our understanding of the long-term and large-scale development of these natural systems. By connecting these two fields of expertise, I can test hypotheses posed by paleogeographical reconstructions with numerical models. This combination allows the investigation of important physical processes and mechanism that shape the coastal-fluvial landscapes. This requires that testable hypotheses are inferred from the literature on paleoreconstructions, and that a numerical model system is developed to incorporate the necessary processes. **The objective of this thesis is therefore to determine the long-term and large-scale development of coasts, estuaries and tidal basins under combinations of tides, waves, river discharges, sea level rise, sediment supply and vegetation.** I will first review the key geological literature that inspired this thesis to derive hypotheses from the paleogeographical reconstructions. Then I will assess the present capabilities and

limitations of numerical models to identify the key areas for improvements and how to best test the paleographical hypotheses with schematized models. Finally, with the developed biogeomorphodynamic model I tested alternative conditions derived from the paleogeographical reconstructions to unravel the effects of individual and combined drivers in shaping the landscapes.

1.2 Inferred mechanisms from Holocene evolution of the Dutch landscape

The hypotheses tested in this thesis are largely derived from the data-rich geological record of the Netherlands. During the Holocene, the Dutch landscape evolved under a combination of sea level rise, marine and fluvial forces and sediment supply, and their interaction with vegetation and peat (see for reviews Beets and van der Spek, 2000; Vos, 2015; Pierik et al., 2017b; de Haas et al., 2018).

By the mid-late Holocene, around 6000 cal BP, a large portion of the modern Dutch territory was infilled by fluvial sediments from the Rhine-Meuse rivers and marine sediments from the North Sea (Figure 1.2 and Beets and van der Spek, 2000). This infilling of the Dutch coastal plain occurred when the sea level rise decelerated around 6000 BP. During this period the western backbarrier was filled with sediments and peat and the northern barrier developed towards the shape of the modern Wadden Sea. During this infilling process, tides, fluvial discharges and waves together with sediment supply and vegetation shaped and transformed the Dutch landscape. The rivers distributed freshwater and sediments along their path creating dynamic fluvial-estuarine landscapes with bifurcations, levees, floodplains and peat. Towards the coast, the rivers connected with the marine system which also provided sediments and hydrodynamic forces through waves and tides that shaped the open coast, estuaries and tidal basins.

Two environments within the Dutch coastal landscape are particularly relevant for this thesis. One is the Rhine-Meuse delta that fed the low-lying areas with fresh water and sediments, and where abundant peat formed and infilled the accommodation space (Figure 1.2). The other environment comprises the collection of two barrier island complex spread along sections of Dutch coast: one along the current Zeeland (southwest) and Holland Coast (western Barrier) and another one, the Wadden Sea, on the north. While both environments are situated in a developing delta and back-barrier system, the main differences are the fluvial influence, the exposure to waves and the effects of vegetation. Their contrasting pathways and the different degrees of infilling raise questions about the driving mechanisms in terms of boundary tidal-fluvial-sedimentary conditions and their biomorphodynamic interactions.

The large backbarrier system on the western (Holland) Dutch coast, near Leiden-Katwijk, was transformed into an estuary after an upstream river avulsion routed the main branch of the River Rhine to this area in the mid-Holocene (Figure 1.2 and de Haas et al., 2019). This branch, called the Old Rhine, infilled the landscape with levees, crevasses and floodbasin deposits together with reed and wood peat accumulation until its discharge was again rerouted after new consecutive avulsions upstream (Pierik et al., 2018; de Haas et al., 2019; Pierik et al.,

2023). While the Old Rhine was active in that area, the landscape completely transformed from a tidal backbarrier basin into a leveed estuary flanked by peatlands.

Conversely, the Wadden Sea in the north remains a barrier island. Apart from differences in wave climate, offshore slope and subsidence rates (Vos, 2015), two key differences may hypothetically explain the contrasting fates between the Dutch basins: first, the infilled Old Rhine system had a large fluvial connection after the avulsion of the Rhine river while only smaller rivers debouched in the Wadden Sea. Second, the western Dutch coast had more sediments available on the shallow North Sea in combination with a predominantly onshore (sand) sediment transport while the northern Coast (Wadden Sea) was poorer in sediment availability combined with a dominant alongshore sediment transport trend (van der Molen and de Swart, 2001). Moreover, throughout the last centuries, especially the western (Dutch) portion of the Wadden Sea was heavily transformed by human interventions such as the closures of the IJsselmeer and Lauwerszee (Wang et al., 2009; van der Spek, 2018; Wang et al., 2018; Elias et al., 2019), the landward construction of dikes and embankments that disconnected landward intertidal and vegetated areas and reduced tidal prism. Nowadays, the Wadden Sea is also affected by local (extra) subsidence due to the gas and salt extraction from the subsoil (Fokker et al., 2018; van der Spek, 2018). Despite the long-term changes in the boundary conditions and all these human-induced changes, the Wadden Sea is still an extensive barrier system that covers the northern Dutch coast and part of the German and Danish coast.

The Dutch coast provides much evidence and data through the paleogeographical Holocene reconstructions, but also raises questions about the biomorphodynamic processes that controlled the observed evolution. The following questions remain open about how the interactions between tides, rivers and waves together with sediment supply and vegetation can transform and shape large-scale landscapes. Here I enumerate the prominent questions derived from the Dutch paleogeographical literature:

- What are the possible mechanisms behind the closure of the Western Barrier Island system with the Old Rhine river-estuary? Did vegetation and levees-crevasses play a major role in infilling the accommodation when the Old Rhine connected to the basin? What were the system-scale effects of eco-engineering vegetation?
- How tidal basins without fluvial supply, such as the Wadden Sea, evolved under combinations of coastal sediment supply and vegetation under sea level rise? Could they develop a steady state equilibrium in terms of accommodation space?
- To what degree can vegetation help to infill coastal landscapes to keep pace with (future) sea level rise? What is the effect of limited sediment supply on vegetated tidal systems?

These questions cannot be answered by relying on paleogeographical reconstructions alone. Not only are the reconstructions subject to preservation issues, but also the principle of equifinality (i.e. multiple conditions that have the same result, see Bertalanffy, 1950; Thorn and Welford, 1994) creates an extra challenge to unravel the mechanics and conditions that created the observed landscape (Brierley et al., 1997; Burns et al., 2019). Even with the well-studied and data-rich Dutch coastal landscape, it is not possible to determine cause-effect relations or to test and isolate variables and mechanisms behind the evolution of the coastal

and estuarine system from the geological record. For that, we need analogue biogeomorphodynamic models that can reproduce key aspects and evolution phases of these natural systems. With such models, it is possible to isolate and understand the individual and combined effects of tides, waves, rivers, sediments and biota in shaping the landscape. This knowledge can then be used to further interpret palegeographical reconstructions and to better predict the future evolution of our coastal systems. This leads to the methodological challenge addressed next: the complexity of these landscapes requires complex numerical models that include all relevant processes and interactions.

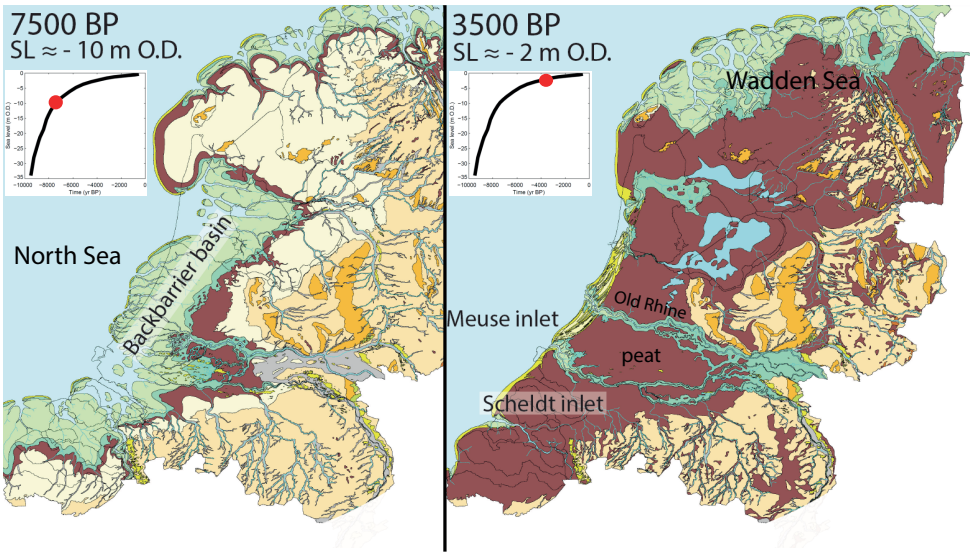

Figure 1.2: Geological reconstruction of the Netherlands for 7500 BP and 3500 BP after Vos (2015). The curves indicate the sea level height.

1.3 Issues of biomorphodynamic models applied to long-term development of large-scale coastal systems

The study of long-term morphodynamics started with equilibrium relationships. In simple words, morphodynamic equilibrium means that over a certain spatial-temporal scale the erosion and deposition are balanced, while on smaller scales fluctuations may occur (see discussion in Paola and Voller, 2005; Zhou et al., 2017). This equilibrium concept is the basis of several classical works and their later developments, such as the beach profile equilibrium of Bruun (1954) and Dean (1991) and its derivations, beach and dune erosion under storms (Vellinga, 1982), the equilibrium beach planform of Hsu and Evans (1989), González and Medina (2001), and Raabe et al. (2010), the relationship between inlet dimensions and tidal prism (Escoffier, 1940; O'Brien, 1967; Escoffier, 1977; Powell et al., 2006), the volume of ebb and flood deltas related to basin dimensions (Walton and Adams, 1976; Dronkers, 1998;

Powell et al., 2006) and fluvial channel and bar dimensions (Parker, 1978; Kleinhans and van den Berg, 2011). Some of these classic relations inspired the development of equilibrium-based models that function between the simple original relations and the more comprehensive process-based models that rely primarily on small-scale physical processes (De Vriend, 1991b), for example, González and Medina (2001), Raabe et al. (2010), den Heijer et al. (2012), and Townend et al. (2016). The equilibrium-based models consist of simple and robust tools that can effectively assess long-term development of relatively complex systems in response to a change in conditions that can hardly be achieved with physical experiments or process-based numerical models (De Vriend, 1991b). However, the equilibrium-based models are supported by semi-empirical relations with several (hidden) assumptions and limitations that often hamper their capability of predicting changes in conditions that violate their underlying assumptions. For example, the concept of equilibrium beach profile or planform of Vellinga (1982) and Hsu and Evans (1989) do not account for external (alongshore or cross-shore) supply of sediments, and therefore its validity is questioned when shoreface development is the result of external sources of sediments and gradients in littoral drift, as it is the case for the Dutch shoreface (Beets and van der Spek, 2000). Recently, a discussion was once again posed about the use of the Bruun (1962) rule for predicting the long-term beach evolution under sea level rise worldwide (Vousdoukas et al., 2020; Cooper et al., 2020) as its assumptions of beach slope and beach migration (transgression) were overlooked in several sites (Cooper et al., 2020) regardless of previous discussions about the validity of the Bruun's rule for sea level rise predictions (e.g. Cooper and Pilkey, 2004). These examples show the limited capability of the equilibrium-based relations, and the need for complex numerical models, in predicting changes in environmental conditions such as human interventions, climate change and the effects of sea level rise on complex coastal systems.

Morphodynamic numerical models are based on detailed and complex physics to simulate hydrodynamics, sediment transport and morphology. They are usually applied in engineering contexts of short-term scenarios (days to years). Also, some physical processes need to be simplified (parameterized) in order to accommodate our lack of knowledge (e.g. sediment transport, see Walstra et al., 2007a) and the extreme computational costs (e.g. resolving the wave phase, see Zijlema et al., 2011; Malej et al., 2015). The consequence is that comprehensive morphodynamic numerical models are limited to short-term simulations, while simplified models in physics or dimensions are more commonly applied in long-term morphodynamic studies (e.g. Murray and Paola, 2003; Kirwan and Murray, 2007; Guo et al., 2014; Townend et al., 2016; Leuven et al., 2019). Furthermore, comprehensive models require comprehensive information on settings, inputs and on the selection of relevant physical processes. Due to the complexity of these models, they often result in large cumbersome datasets that are difficult to interpret, not to mention the larger computational costs of calculations, storage and handling. Therefore, it is common practice to simplify the setup and boundary conditions especially when modelling long-term morphology. That means choosing for example only one (e.g. M2) tidal component, one wave condition and one sediment fraction per model scenario (e.g. van der Wegen and Roelvink, 2008; Nienhuis et al., 2016; Lenstra et al., 2019) due to difficulties in interpretation, calibration and the large computational costs involved when modelling waves and multiple sediment fractions altogether.

Furthermore, the presence and the effects of vegetation on the morphodynamics are rarely taken into account in process-based models. However, we know that in nature, coastal environments consist of a wide range of sediment fractions subjected to varying wave climate, and are often populated by vegetation species and biota. These limitations hamper the study of the complex environments of interest in this thesis, such as barrier coasts and coastal plains, where those elements act altogether in tight biogeomorphodynamic feedbacks.

Morphodynamic numerical models such as Delft3D, Mike21, Regional Ocean Modeling System (ROMS) and Telemac, need simplifications and parameterizations for sediment transport (Walstra et al., 2007a; Ganju et al., 2009; Davies and Robins, 2017; Olabarrieta et al., 2018). Shortcomings of these simplifications arise, for example, where the near-bed orbital velocities and bed slope effects are parameterized (Ruessink et al., 2012; Walstra et al., 2007a). That means, due to difficulties in computing flow and sediment transport associated with wave-current conditions near the shore, the cross-shore and alongshore processes and the resulting morphology cannot be both properly represented in one model configuration as discussed by Lenstra et al. (2019). A choice is needed to either match the cross-shore profile (with 1D or 2DV models) or the alongshore sediment transport by user-defined calibration (e.g. Grunnet et al., 2004; Ruessink et al., 2007; Briere et al., 2011; Walstra et al., 2012; Nienhuis et al., 2016; Luijendijk et al., 2017; Tonnon et al., 2018; Lenstra et al., 2019). Another shortcoming has been that long-term fluvial and estuarine morphology is commonly predicted with general bulk sediment transport formulations such as Engelund and Hansen (1967) and Meyer-Peter and Müller (1948) as they produce better channel patterns in fluvial-estuarine environments (e.g. Braat et al., 2017). However, there is a need for more comprehensive formulas such as van Rijn et al. (2004) to predict distinct sediment transport modes between wave and currents and bed load and suspended load. However, practical applications of van Rijn et al. (2004) often produce large channel incision (this thesis), extreme beach accretion or erosion (this thesis) and lack channel-bar pattern formation (see Figure 1.3 for examples of pilot models from the author). Nonetheless, the same van Rijn et al. (2004) predictor creates diffusive morphology when modelling with waves (Figure 1.3b). These shortcomings mean that we currently cannot perform reliable long-term simulations where waves and currents and the separation between bed load and suspended load are important.

Although numerical models will always have room for improving formulations and physical processes, here I identified three important limitations for modelling long-term biogeomorphodynamics of estuaries and tidal basins. First, very often, morphodynamic models lack the interplay of vegetation within the morphodynamic loop. Second, long-term morphodynamic models of fluvial-tidal dominated estuaries often predicted either extreme erosion (incision) or diffusive morphology (lack of bars and shoals). These problems of erosion-diffusion strongly depended on the applied sediment transport formulations but also on interactions between implemented processes, namely tides-fluvial discharge and waves. Third, coastal models enclosing long-term beach evolution struggle to match the observed beach profiles, and to form and keep nearshore sandy bars. The models often overpredict the onshore directed sediment transport which results in overestimating coastal progradation (i.e seaward migration or regression) and steep beach profiles. To overcome these issues, the

models need to be calibrated in sediment transport settings that affect other processes, such as the alongshore sediment transport.

Therefore, three key improvements were necessary for modelling the long-term biogeomorphodynamics in this thesis. (1) To model long-term biogeomorphodynamics, I incorporated vegetation effects in my models via either static vegetation (i.e. no vegetation dynamics such as settling and mortality) or the more comprehensive eco-engineering model of Brückner et al. (2019) coupled to Delft3D. Then, the two relevant limitations in modeling long-term coastal-estuarine sediment transport were addressed in this thesis: (2) I implemented and tested an alternative for the nearbed wave orbital velocity parameterization of Isobe and Horikawa (1982) that may overpredict onshore sediment transport due to wave skewness. (3) I studied the tendency of excessive channel incision and morphological diffusion induced by the transverse bed slope parameterizations for sediment transport under currents and waves by Ikeda (1984) and Koch and Flokstra (1981) (see Walstra et al. (2007a)). Figure 1.3 shows examples of how the combination of these issues leads to unrealistic model results.

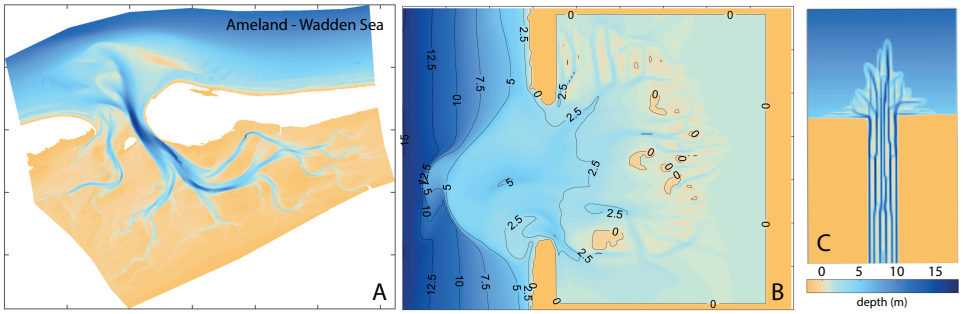

Figure 1.3: Examples of model issues due to limitations in implemented mechanisms. (a) Measured bathymetry at Ameland on the Dutch Wadden Sea for comparison. Data from Rijkswaterstaat. (b) Idealized tidal basin modeled in Delft3D with tides and waves. The model shows unrealistic morphological evolution due to excessive diffusion and lack of formation of channels and shoal. Source: own model presented during DSD2018. (c) Idealized tidal-fluvial model with VR93 (Delft3D default sediment transport formula) showing excessive incision of channels only one grid cell wide and without bends. Source: own unpublished model.

1.4 Development of hypotheses

The review presented above shows how both the data-driven (geological and historical data) and numerical modelling approaches leave open important questions and limitation in exploring long-term biomorphodynamics processes in building the coastal and estuarine landscapes. The paleogegraphical reconstructions rely on what is preserved, sampled and interpreted from the geological record and geomorphology to reconstruct past landscapes and to infer the causes, namely the initial and boundary conditions as well as the underlying mechanisms that created such environments (i.e. abduction, see Kleinhans et al., 2010a). Conversely, the numerical models rely on comprehensive physics to reproduce the mor-

phodynamics based on our knowledge and open up the possibility to isolate and combine several variables and possible boundary-internal conditions (i.e. deductive) that build and transform the landscape. However, models simplify and neglect several natural processes that may change the long-term development. In principle, the two approaches can be used as complementary as they follow opposed reasoning pathways to understand the same biogeomorphodynamic system (Figure 1.4). Therefore, in this thesis I want to bridge this gap between geology and process-based morphodynamics by exploring the complementary usage of comprehensive numerical models for long-term system development to test hypotheses supported by geological reconstructions, and to unravel important processes in estuaries and coastal systems and quantify their roles and interactions.

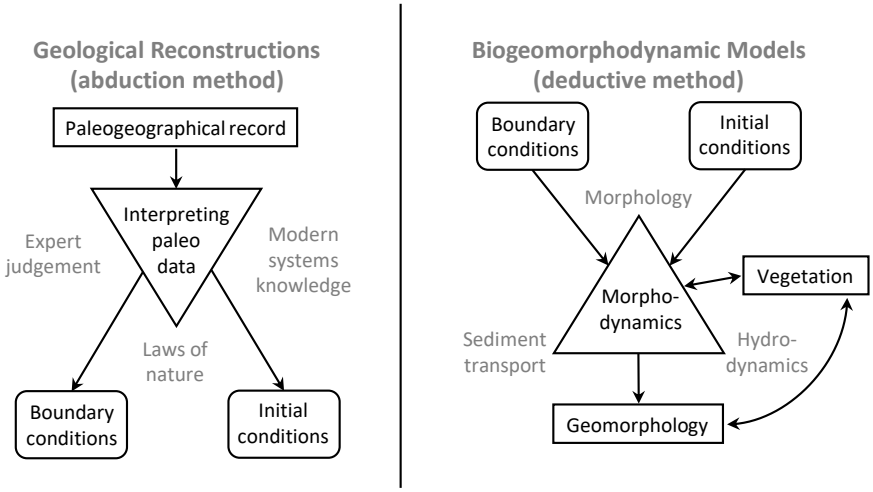

Figure 1.4: Concept graphic of the geological and numerical methods to study long-term biogeomorphodynamics. The shapes indicate the counterparts of aspects of geology and numerical models. Rounded polygons: external driving forces, antecedent geology or landscape and forcing of a selected system. Triangles: the core of the method including geological investigation, analyses and interpretation, which are analogue to the set of equations, parameterization and relations included in morphodynamic models. Rectangles: the subsurface or landscape that is present in nature and is produced as output of numerical models. For geologists the paleogeographical record and geomorphology is the data to be interpreted, while for modelers the geomorphology is the end-product. Vegetation: the biotic addition to the classic (bio)morphodynamic system.

The approach to address the objective of this thesis is to perform numerical modelling studies to explore the long-term effects (i.e. decades to centuries) of boundary and internal conditions on building coastal-estuarine-fluvial landscapes. Inspired by the data-rich geological reconstructions of the Netherlands and contrasting systems worldwide, I isolated and combined the effects of fluvial-tidal-wave hydrodynamics, sand-mud sediment supply and vegetation on the morphodynamic numerical model of Delft3D to study the physical processes and mechanics that shape coasts, tidal basins, estuaries and levees. For the interpretations, the idealized model scenarios are linked to the paleogeographical reconstructions of specific coastal landscapes.

Based on the above, I formulate the following hypotheses that are tested in this thesis:

1. *In numerical models, entire fluvial-tidal systems are strongly affected by the choices of transverse bed slope (TBS) parameterization combined with the sediment transport formulation. The choice of TBS parameterization and sediment transport formulation need to compensate for other models weaknesses, such as, the imbalance between bed load and suspended load and grid-dependent diffusion;*
2. *The overall nearshore sediment balance and morphological evolution of coasts and tidal basins in morphodynamic models, and the possibility of large-scale, long-term dynamic equilibrium, depend on the wave-related sediment transport associated to the parameterization of the near-bed orbital velocities induced by wave skewness and asymmetry in shallow nearshore waters;*
3. *The development of levees, floodplain and the crevasses in between is controlled by the fluvial and tidal conditions, the sediment supply and the interplay with vegetation. Water discharge and sediment supply, in particular of grain sizes between channel sand and floodplain mud, favor larger levees and the formation of crevasses while floodbasin vegetation reduces the exchange of flow and sediment away from the main channel and therefore affect the levee dimensions and the formation of crevasses;*
4. *The infilling of accommodation space in fluvial-tidal basins depends not only on the offshore tidal-sediment boundary conditions but also on the internal development of the fluvial-tidal morphology and its interaction with vegetation. The interdependence and connectivity of the barrier coast elements, namely, open coast, inlet, ebb-tidal delta, tidal basin, channels-shoals and vegetation will together determine the evolution of the barrier coast as a whole;.*
5. *Vegetation acts as a direct and indirect mechanism to fill accommodation space. The vegetation itself occupies space and reduces hydrodynamics via added friction, and in the long-term can form peat-lands (direct effect) while vegetation also increases sediment trapping due to its effects on reducing shear stress that favors sediment deposition (indirect effect). Therefore vegetation can help to infill the accommodation space and keep up with sea level rise even when the sediment availability is low, if the rise in sea level is not leading to vegetation drowning and collapse.*

1.5 Outline of chapters

To test the hypotheses, I developed a range of morphodynamic models covering large-scale systems over centuries. These models included the necessary and novel improvements regarding the parameterization of slope effects and wave orbital velocities on the sediment transport.

I started with changes in the sediment transport mechanisms and improving the model skills and performance in order to overcome the aforementioned limitations of modeling large environments through decades to centuries when including waves, tides, rivers, multiple sediment fractions and vegetation. Chapter 2 addresses hypothesis 1 concerning the transverse bed slope sediment transport parameterizations (Ikeda, 1984; Koch and Flokstra, 1981), in combination with two broadly applied sediment transport formulations, namely

Engelund and Hansen (1967) (total transport formulation designed for current-only) and the more comprehensive TRANSPOR2004 wave-current formulation (van Rijn et al., 2004) based on van Rijn (2007a) and van Rijn (2007b) and van Rijn et al. (2007). This choice is made to allow sediment transport calculation for a range of grain size fractions from mud to sand as well as current- and wave-related transport that is not straightforwardly possible with alternative transport formulations. As the focus of this thesis is also on modelling coastal environments that are subject to wave action, Chapter 4 addresses the improvements on the wave-related sediment transport (hypothesis 2), also in combination with van Rijn et al. (2004). Here I introduced and tested a recently derived parameterization of wave shape and near-bed orbital velocities in the coastal zone (Ruessink et al., 2012) into the Delft3D source code. The model performance was compared together with the old default parameterization of Isobe and Horikawa (1982) against field measured data in the Netherlands and in the USA.

With the improved modelling tools, I investigated the effects of fluvial-tidal discharges, sediment supply and reed-tree vegetation on building levees and crevasses (hypothesis 3-5; Chapter 3) that are important controls on water and sediment fluxes between the main channel and floodbasins. These models target coastal-estuarine systems with a river connecting to a basin, which is relevant to the Old Rhine system in the Netherlands. Here levees and crevasses developed freely in a large-scale model allowing the study of key controls on levee dimensions and the formation and persistence of crevasses, with and without vegetation in the floodbasin. By means of a comprehensive set of models (i.e. 60 scenarios of 100 years morphology each) I was able to unravel the mechanisms controlling the growth of levees and crevasses in fluvial but also tidal influenced environments with different vegetation typologies. This was the first study that built levees and crevasses in a long-term morphodynamic model and tested comprehensively combinations of boundary conditions, including tides, and vegetation altogether. The levee setup and scenarios were largely inspired by the Saskatchewan and Columbia Rivers in Canada (Cazanacli and Smith, 1998; Adams et al., 2004; Smith and Pérez-Arlucea, 2008), and the ancient Old Rhine estuary in the Netherlands (de Haas et al., 2019). The model results were also compared to levees in several other systems worldwide.

With another set of models I studied how a barrier coast and associated backbarrier basin evolve under sea level rise in combination with waves, offshore sediment supply and vegetation (hypotheses 4–5; Chapter 5). The applied increasing sea level rate has been observed in the late Holocene, and will be important to better manage our coastal landscapes in view of future sea level rise. Here I modeled a barrier island over a century with comprehensive wave climate, sediment composition and dynamic (marsh) vegetation to assess how the backbarrier basin evolves under sea level rise with varying mud supply and the effects of vegetation along this process. This was the first set of models enclosing an entire barrier coast with this level of complexity and time-spatial scales, allowing proper establishment of the connections between the open coast, ebb-tidal delta, inlet and the tidal basin including the eco-engineering effects of vegetation in the tidal basin.

In Chapter 6 I discuss the combined outcomes of this thesis and present ideas for future developments and the conclusions from this thesis.

Chapter 2

All models are wrong, but some are useful: critical dependence of morphodynamic models on empirical downslope sediment transport

The morphological development of fluvial and tidal systems is forecast more and more frequently by models in scientific and engineering studies for decision making regarding climate change mitigation, flood control, navigation and engineering works. However, many existing morphodynamic models predict unrealistically high channel incision, which is often dampened by increased gravity-driven sediment transport on side-slopes by up to two orders of magnitude too high. Here we show that such arbitrary calibrations dramatically bias sediment dynamics, channel patterns, and rate of morphological change. For five different models bracketing a range of scales and environments, we found that it is impossible to calibrate a model on both sediment transport magnitude and morphology. Consequently, present calibration practice may cause an order magnitude error in either morphology or morphological change. We show how model design can be optimized for different applications. We discuss the major implications for model interpretation and a critical knowledge gap.

Published as: Baar, A. W., Boechat Albernaz, M., van Dijk, W.M., Kleinhans, M.G. (2019), Critical dependence of morphodynamic models of fluvial and tidal systems on empirical downslope sediment transport, *Nature Communications* 10 (1), 1-12 DOI: 10.1038/s41467-019-12753-x.

Contributions

This article was the result of a fruitful collaboration between the first and second authors during their (Anne Baar and Marcio Boechat Albernaz) PhD with Maarten Kleinhans (PI of the NWO-Vici and ERC projects). The two lead authors contributed with equal importance. Anne Baar had the knowledge and experience with Transverse Bed Slope (TBS) from physical experiments and analytical models while Marcio Boechat Albernaz built and tested several models and parameterizations of TBS in the Delft3D model focusing on long-term morphodynamics. This close collaboration culminated with this Nature Communication article which was a key component for the long-term morphodynamic modeling developed in this PhD thesis.

2.1 Introduction

River valleys, coastal plains and deltas are changeable landscapes with a large part of the human population that will be at risk from climate change effects and sea level rise. Adaptation requires a system approach (Brown et al., 2014; Best, 2019) with combinations of hard engineering measures and sediment attrition (Smajgl et al., 2015). Reliable forecasting of effects of combined measures requires morphodynamic models for rivers, estuaries, deltas and coasts. Morphodynamic models are therefore widely used tools to study and forecast the development of these landscapes. However, in practice, all large-scale models depend on model choices and need some form of calibration to converge to a stable morphology, for example by the choice in roughness predictor (Kleinhans et al., 2008; Schuurman et al., 2018), adding coarser grain sizes in the channels (Dastgheib and Roelvink, 2010) or include a non-erodible layer that limits channel depth (Nnafie et al., 2018), and increasing the transverse bed slope parameter which determines the amount of sediment transported on channel side-slopes. The latter has proven to be most effective, since the bed slope parameter linearly increases downslope sediment transport and thereby directly affects channel depth and bar dimensions, and therefore has the largest effect on large-scale morphology (van der Wegen and Roelvink, 2012; Schuurman et al., 2013).

The problem is that morphodynamic models show severe and unrealistic channel incision and require artificially and seemingly arbitrarily transverse bed slope parameters up to a 100 times higher (van der Wegen and Roelvink, 2012; Schuurman et al., 2013; Braat et al., 2017) than physically correct (Ikeda and Nishimura, 1986; Sekine and Parker, 1992; Baar et al., 2018b) to counteract this incision and obtain realistic bar and channel patterns. A recent comprehensive set of experiments showed that a physically realistic value for the slope parameter is in the order of 1 and a realistic calibration range is within a factor of two(Baar et al., 2018b). This calibration range is therefore much smaller than needed in recent model studies. The need to apply unrealistically intense bed slope effects implies a flaw in the balance between the non-linearity of sediment transport that carves out channels, and downslope sediment transport that counteracts this incision. Increasing the magnitude of downslope sediment transport by more than an order of magnitude raises doubts about the physical validity and predictive power of these models. It begs the question whether these models converge to a balance between erosion and deposition for the right reasons, whether sediment transport magnitudes can be correct at the same time, and what aspects of the forecasts on timescales of a century are most unreliable.

The severe channel incision is best known for sensitive codes such as Delft3D (van der Wegen and Roelvink, 2012; Schuurman et al., 2013), but is also an issue in studies with other morphodynamic models. Studies with for example the Regional Ocean Modeling System (ROMS) or Telemac report the need of a bed slope diffusion term (Olabarrieta et al., 2018) or a coarsening of the bed (Ganju et al., 2009; Davies and Robins, 2017) to prevent unrealistic bed erosion and sharp morphodynamic features. An inventory in typical geomorphology journals showed that only 13 (19%) out of 68 model studies discussed the need to increase the slope effect due to the imbalance between severe incision and downslope sediment transport,

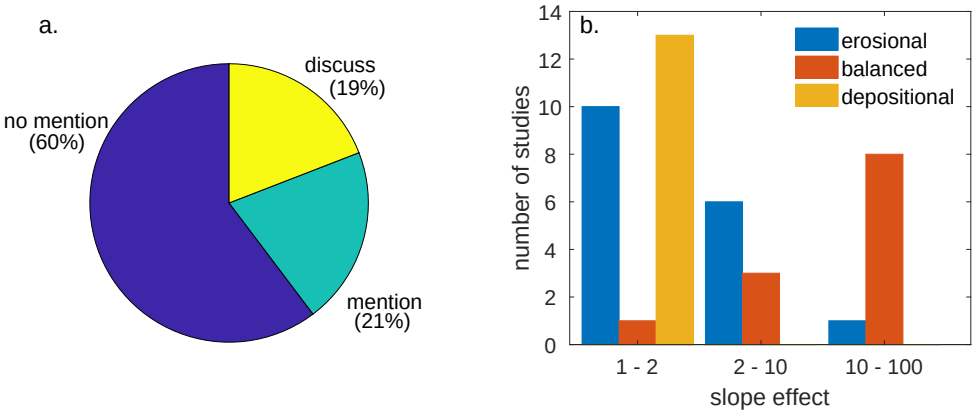

Figure 2.1: Literature inventory of slope effects in morphodynamic models (a) Model studies that mentioned, discussed or overlooked the severe channel incision and the artificial increase in slope effect that was necessary to counteract this (see Baar et al. (2019) for inventory). (b) Studies that mention the magnitude of the slope effect subdivided by modeled environment and the applied slope effect value (1=default).

and 14 (21%) studies only mentioned the magnitude of the slope parameter in their model (Figure 2.1)(see Supplementary Information in Baar et al. (2019) for the complete inventory).

The literature inventory suggests that sensitivity to incision depends on the environmental settings (Figure 2.1b). Here, environment means initial and boundary conditions, which determine sediment characteristics, flow conditions, channel pattern and bar regime. Models of environments with a large-scale balance between erosion and deposition, such as estuaries and rivers, particularly have the tendency to overpredict channel depth and number of channels and required very high slope effects up to a factor of 100 (Van der Wegen and Jaffe, 2014; Schuurman et al., 2018). In contrast, models of systems with dominant erosion such as a tidal channel network, usually had slope factors lower than 10 (Marciano et al., 2005; Dissanayake et al., 2009; Zhou et al., 2014), and depositional systems such as river deltas all used the default value (Edmonds and Slingerland, 2007; Leonardi et al., 2013; Caldwell and Edmonds, 2014). However, increasing the slope effect to obtain realistic channel depth and bar dimensions results in an unrealistically large downslope sediment flux, which determines the rate of bank erosion, channel formation and migration. On the other hand, default transverse slope parameters in both erosional and depositional models commonly show unrealistically deep channels and sharp angular bends (Edmonds and Slingerland, 2010; Kleinhans et al., 2010b; Caldwell and Edmonds, 2014; Van der Vegt et al., 2016). While these angular bends have been attributed to grid resolution, we here show that the underlying cause is in the sediment transport.

The use of different sediment transport predictors, which relate the sediment transport rate to flow velocity, and parameterizations for the deflection of sediment transport on transverse slopes reflect the present uncertainty about the nonlinearity of sediment transport and the negative feedbacks on run-away deepening. The frequently-used sediment transport pre-

dictor of Engelund-Hansen (EH) that relates sediment transport rate to flow velocity to the power of 5, has a higher sediment transport rate than the predictor of Van Rijn (VR), which relates sediment transport rate to flow velocity to the power of 3 for high mobility and much higher powers for lower mobility. Many other relations for bed load transport have qualitatively similar behavior. The predictor of Van Rijn furthermore makes a distinction between sediment transported over the bed and in suspension, and assumes the bed slope effect only acts on the bedload part. As a result, the predictor of Engelund-Hansen will deflect more sediment downslope than the predictor of Van Rijn and similar relations at the same flow velocity. The two most commonly used slope parameterizations, by Ikeda (Ikeda, 1984)(IK) and by Koch and Flokstra (Koch and Flokstra, 1981)(KF), calculate the downslope sediment transport vector differently (Figure 2.2). For KF the streamwise transport vector is rotated as a function of the transverse bed surface gradient, while for IK the normal transverse transport vector is enhanced before combination with the streamwise transport vector. As a result, the method of IK not only changes the direction, but also increases the flux of sediment transport. How this affects morphology and the rate of change thereof remains unquantified. Most other bed slope parameterizations have similar behavior to one of the aforementioned (Baar et al., 2018b).

Here we conduct five sets of numerical morphodynamic simulations for different scales and environments, i.e. erosional, depositional or balanced, to quantify the effects of increased downslope sediment transport on morphology (Fig 2.3). The flow velocities in all models are such that suspended sediment transport of sand plays a significant role, but we do not consider suspension of cohesive sediments. The objective is firstly to identify possible causes of the imbalance between incision and transverse sediment transport on the channel scale for typical combinations of sediment transport and slope parameterizations. Secondly, we quantify the effects of local sediment transport vectors on large-scale morphology of rivers, estuaries and deltas. Finally, we will discuss sensitivity to environment and the large range in slope effect that is applied between different model studies, and consequently give recommendations for an appropriate design of models depending on research objectives of future studies given the present limitations and uncertainties.

2.2 Results

2.2.1 Effects of slope parameterization on general morphology

All five models (Figure 2.3) generally showed deep incision and steep morphology with physically correct slope effects, leading to deep and narrow channels, a higher number of channels and shorter bars than typically observed in nature. Increasing the bed slope effect resulted in wider and shallower channels, longer bars, a smaller braiding index, and fewer bifurcations and a greater similarity to natural systems, although a very high slope effect caused overly subdued relief in models with the EH sediment transport predictor (Appendix A-Figure A.6 and A.8). However, different combinations of sediment transport predictor and slope parametrization lead to starkly contrasting morphologies. To quantify the difference in effect of both slope parameterizations on sediment transport processes and morphology, the parameter that determines the magnitude of the transverse slope effect was systemati-

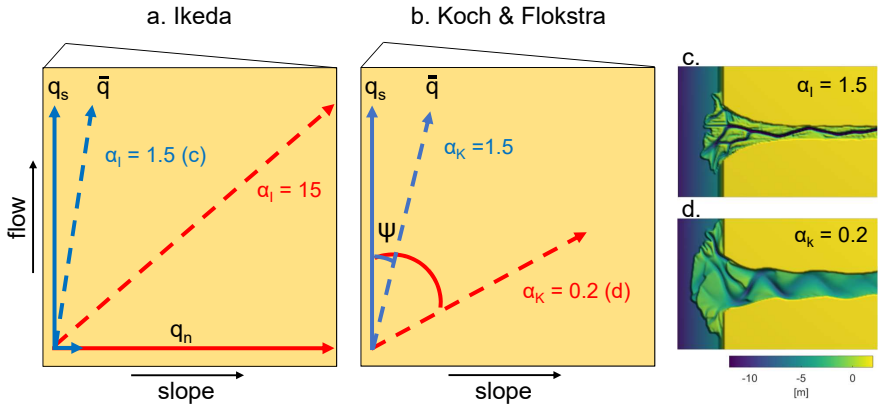

Figure 2.2: Schematic drawing of the two main slope parameterizations The parameterizations for sediment deflection by Ikeda (Ikeda, 1984) (α_I) and Koch and Flokstra (Koch and Flokstra, 1981) (α_K) drawn on a transverse bed slope. Both methods are drawn on a top view of a bed sloping towards the right. Blue solid arrows show sediment transport in streamwise direction (q_s) and transverse direction (q_n, only for Ikeda), and dashed blue arrows show the resulting transport vectors (q) with default values for the slope effect. Red arrows represent transport vectors when the slope effect is increased to typical values used in current model studies. (a) The method of Ikeda increases the transverse sediment vector as a function of slope and α_I, and thereby increases the resulting sediment transport vector. (b) The method of Koch and Flokstra rotates the streamwise transport vector over an angle (ψ) as a function of slope and α_k. α_k is roughly the inverse of α_I. See Appendix A Note 1 for detailed calculation method and how to translate α_k into α_I. c+d) examples of a modelled river delta for default (α_I = 1.5) and high (α_k = 0.2) slope effect (see Appendix A Figure A6 for more examples).

cally increased. Henceforth, the term slope effect refers to the magnitude of this parameter, which is the α_I in the method of Ikeda and the α_K in the method of Koch and Flokstra (Appendix A Note 1). Note that the parameter α_K is roughly the inverse of α_I. To be able to compare the differences between both options, the values for these parameters were not simply proportionately varied, but determined by requiring equal sediment transport in the transverse direction as explained in Appendix A Note 1 (Figure 2.1). The Appendix A shows all model DEM and cumulative bed slope distributions; here we use the braided river model as an example.

Models with the KF parameterization, which merely rotates the transport vector, had steeper slopes and deeper channels than models with the IK parameterization, which calculates an additional transverse vector and therefore increases sediment transport (Figure A.8).

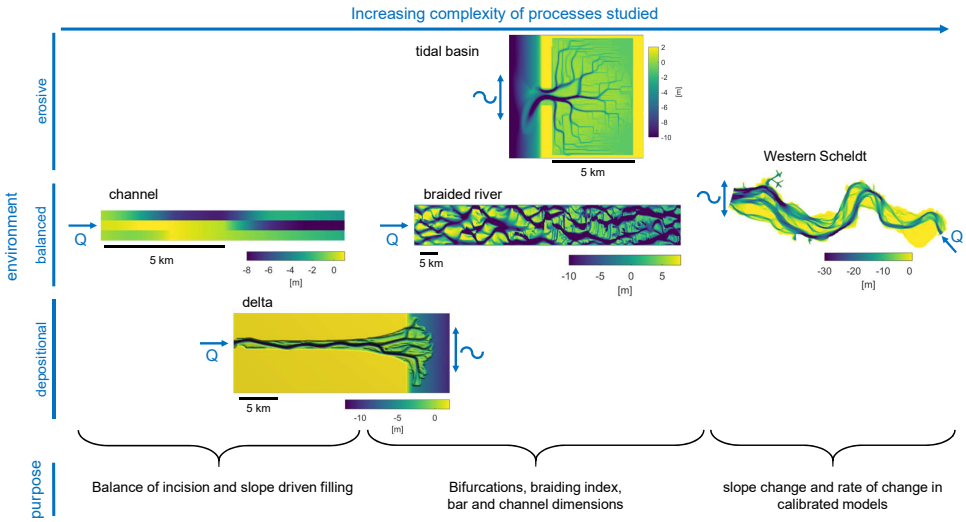

Figure 2.3: Overview of model environments and objectives in this study The narrow channel model and the river in the delta model are used to study local sediment transport processes. The delta model, the braided river model, and the tidal basin model quantify the effects of different slope parameterizations and magnitudes in combination with different sediment transport predictors on bifurcation dynamics, braiding index and channel dimensions. The calibrated Western Scheldt estuary model shows differences in dynamics between models with different slope parameterizations and magnitudes relevant for fairway dredging depth and intensity.

Increasing the slope effect with the IK parameterization in models with the EH sediment transport predictor resulted in significantly lower bed slopes, while this decrease in bed slopes was significantly less than when increasing slope effect with the KF parametrization. Models with the VR sediment transport predictor had much steeper slopes and deeper channels than with EH and showed unrealistically long thin bars with the default value (Figure A.8). The most worrying conclusion is that the braided river model with the EH transport predictor and an α_K of 0.7 (slope effect = 7) has similar morphology as with an α_I of 1 (slope effect = 1) (Figure A.8), but has seven times larger transverse sediment fluxes on the same slope, since the slope effect is seven times larger, which also means a large change in direction of sediment transport. The consequence is that the time scale of morphological adaptation differs considerably, which possibly has major implications for model studies that are used for management strategies. When using another sediment transport predictor this difference is even larger, since a hundred time larger slope effect is needed in the model with the VR transport predictor to get similar bed slopes as in the model with the EH transport predictor

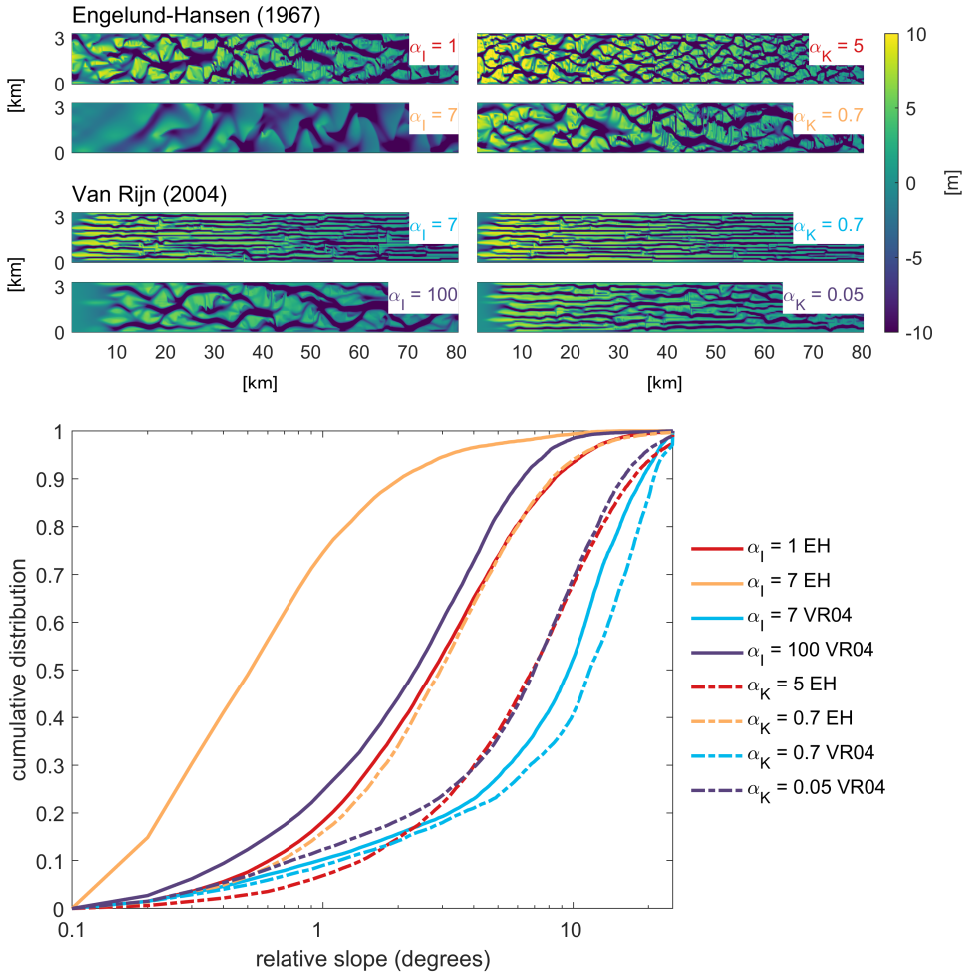

Figure 2.4: Influence of slope effect and transport predictor on morphology Morphology of 8 braided river model runs for different combinations of slope effect and sediment transport predictors. Models on the horizontal axis have equal slope effect. The α_I is the input parameter of the method of Ikeda (Ikeda, 1984), while the α_K is the input parameter of the method of Koch and Flokstra (Koch and Flokstra, 1981), both with defaults of order 1. The graph shows the cumulative distribution of the slopes of all gridcells in the same models at the same timestep. Solid lines are results with IK and dashed lines are results with KF. Colors indicate equal transverse sediment transport magnitudes and the same sediment transport predictor.

(Figure A.8). In the wide braided river model it was not possible to get a realistic morphology in combination with the KF slope parameterization.

2.2.2 Imbalance between incision and transverse sediment transport

The unrealistic channel erosion in numerical models suggest an imbalance between channel incision and transverse sediment transport. Therefore, the overdeepening of channels can be the result of either of these two processes. To understand this imbalance it is necessary to compare the different sediment transport predictors to the theoretical equilibrium between incision and downslope sediment transport at the channel scale. In nature, the width-to-depth ratio determines whether minor perturbations on a flat bed decay or grow into channels and bars, with the braiding index depending on the width-to-depth ratio (Struiksma et al., 1985). Growing perturbations mean channel erosion. This is caused by the nonlinear dependence of the sediment transport rate on flow shear stress at the bed, so that deeper channels that attract more flow have disproportionally more sediment transport capacity that is not balanced by the upstream supply of sediment. This positive feedback is strongest near the critical flow velocity for sediment motion, where the non-linearity of sediment transport is largest and therefore tends to deepen channels, albeit at a low rate. The most important negative feedback on channel formation is sediment transport deflection on the side slopes towards the center of the channel under the influence of gravity (van Bendegom, 1947; Sekine and Parker, 1992; Talmon et al., 1995), which is thus a crucial feedback in forming equilibrium channels. Wider and shallower channels tend to incise more, so that larger bed slope effects are needed to prevent deepening of channels, and this equilibrium determines the development of bars and sets the braiding index (Struiksma et al., 1985; Crosato and Mosselman, 2009). The transition between decay and growth of a perturbation is therefore a function between width-to-depth ratio and the transverse sediment flux and can be analytically described.

To determine the tendency to incise independently of numerics, we use an analytical model of a river channel cross-section, which is described in Appendix A Note 2. This analytical model calculates the theoretical equilibrium width-to-depth ratio of the channel. Channels with lower ratios should theoretically show decaying perturbations, while models with higher ratios should have growing perturbations. The equilibrium width-to-depth ratio depends on the nonlinearity of the sediment transport predictor and the magnitude of the slope effect, since incision is more dampened when more sediment is transported towards the channel center. For the sediment transport predictor of Van Rijn, we only take the bed load part into account in the analytical model, since in Delft3D slope effects only act on the bed load. This analytical model is compared to a very simple numerical model scenario of three grid cells wide. This prevents formation of complex patterns so that channel and bar formation are fundamentally the result of the balance of two processes: channel erosion and gravity-driven sediment motion towards the channel center. Channel width was varied between 21 and 210 m.

With the default value for the slope effect ($\alpha_I = 1.5$), the VR models corresponded reasonably well with the analytical model, since the transition from a dampened system towards a channel where the perturbation grows is around the theoretical equilibrium line (Figure 2.5).

However, the numerical models with increased slope effect significantly deviated from the analytical model. These models required a disproportionately larger slope effect to dampen the initial perturbation (more than 30 times higher than the default factor as opposed to 4 times the default in the analytical model). On the other hand, the initial perturbation in models with the EH predictor immediately decayed (Figure 2.5) until the channel has a width-to-depth ratio around 36, which is more than 15 times higher than the theoretical model. These results demonstrate a stronger tendency to incise in the numerical model with VR than expected from theory, and a weaker tendency to incise in numerical models with EH.

However, all large scale morphodynamic models show unrealistic channel incision independently of sediment transport predictor and need increased slope effects to balance this (van der Wegen and Roelvink, 2012)(Figures A.8 and A.6), which suggest that the imbalance at the channel scale does not only depend on the sediment transport predictor and the resulting amount of transverse sediment transport, but also on the rate of incision. To study if the overdeepening of channels is a numerical issue, grid size is systematically varied for the tidal basin model and braided river model. Results show that equilibrium channel depth increases with decreasing grid size in models with a low transverse slope effect (Figure 2.5). With increasing slope effect, grid size-dependent incision decreases and with a sufficiently large slope effect there is no trend with grid size. However, the transition between grid size-dependent incision and no grid size dependency differs for each sediment transport predictor and slope parametrization. The braided river model with the EH transport predictor shows this transition around a slope effect of $\alpha_I = 3$ (Figure 2.5a), while the tidal basin model with VR needs a slope effect of α_I=100 (Figure 2.5b). Furthermore, models with the KF slope parametrization again show a larger incision than models with the IK parametrization and the same slope effect. In the braided river models, also the horizontal eddy diffusivity was changed from 10 to 1, and this resulted in slightly different distributions of channel depth, but did not have the same amount of influence as increasing grid size or changing slope effect (Figure 2.5a).

2.2.3 Effect of grid size-dependent incision on channel dynamics

Large-scale morphology critically depends on the balance between incision and downslope sediment transport at the channel scale, which is illustrated in Figure A.6. The delta model (Figure 2.3) initially exists of only a straight channel, before it starts transporting sediment and depositing it in the sea basin. However, over time, the river in the models with the VR transport predictor stays within that initial channel without moving sideways, and only at a high slope parameter it starts to erode the initial banks. In contrast, models with the EH transport predictor are immediately much more dynamic. This illustrates the effect of the difference in slope effect needed to balance incision at the channel scale between both transport predictors. On the other hand, the delta is a depositional environment and depends on sedimentation instead of the non-linear incision, and therefore initially does not have to erode banks. As a result, depositional models with the EH transport predictor show a subdued morphology due to the large sediment transport rates, which is enhanced with increasing slope effects. However, the channels on the delta show similar dynamic behavior as in the

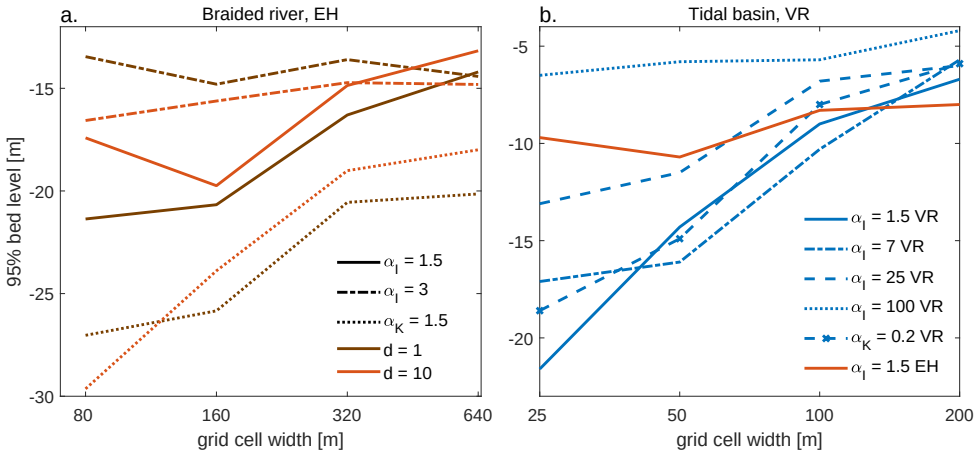

Figure 2.5: Grid size-dependent incision Tendency to incise quantified as 95% depth against size of the grid cells for different magnitudes of slope effect, of (a) the braided river model in combination with the sediment transport predictor of Engelund-Hansen and a horizontal eddy diffusivity d of 1 or 10, and (b) the tidal basin model.

river part of the model, since they incised in the deposited material. Once channels start to form in the models with the VR transport predictor, their location seems to be fixed due to the transverse sediment transport rate that is too low, while channels on the delta in models with the EH transport predictor show lateral movement and regular avulsions. Channels in the erosive tidal basin model showed the same behavior: once a channel was formed in models with the VR sediment transport predictor it was fixed to that location, while channels in models with EH were still able to migrate (Figure 2.9). This difference in channel dynamics shows that the model has to overcome extreme incision at the channel scale by increasing slope effects to model a dynamic system. Only when grid size-dependent incision is balanced by downslope sediment transport, the channel can migrate sideways.

2.2.4 Slope effect dependent bar and channel properties

The environment that is modelled, i.e. depositional, erosive or balanced, controls the growth or decay of perturbations at the channel scale, and therefore influences how likely models are to incise and how sensitive they are to changes in bed slope effect. We now quantify effects on bars and the degree of braiding, which are critical elements of fluvio-deltaic patterns. Here, the delta in the delta model is a perfect depositional environment. The braided river model represents a Brahmaputra-sized braided sand-bed river with a 3.2 km wide and 80 km long braidplain where erosion and deposition are on average in balance, and is exactly the same as the model of Schuurman and others (Schuurman et al., 2013). The tidal basin model consists of a channel network that is incised by the tidal motion, and therefore this model represents an erosional environment (Figure 2.3).

Downslope sediment transport counteracts incision but also balances effects of helical flows in curved channel sections. In nature, secondary currents alter the direction of the bed

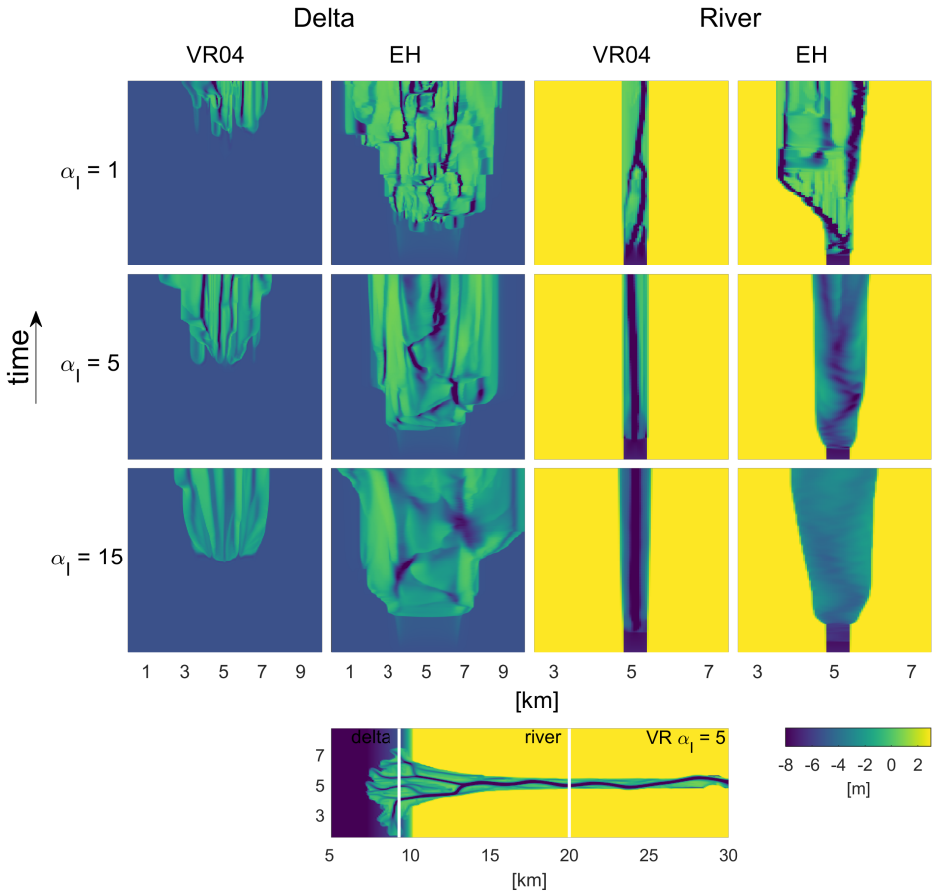

Figure 2.6: Effect of grid size-dependent incision on channel dynamics Development of the bathymetry of a cross-section at the river and at the delta over time in the delta model, for different combinations of sediment transport predictor and magnitude of the slope parameter with the method of Ikedalkeda, 1984.

shear stress towards the inner bend, which leads to a balance between the upslope directed drag force by the secondary flow and the downslope sediment transport under influence of gravity (Engelund, 1974; Struiksma et al., 1985). By balancing secondary flows, downslope sediment transport controls the adaptation of the bar morphology to spatial gradients in flow conditions and along meanders (Struiksma et al., 1985; Crosato and Mosselman, 2009; Kleinhans and van den Berg, 2011). Therefore, by both counteracting incision and balancing secondary flow, the magnitude of downslope sediment transport determines the developed active channel width, orientation of channels, and the length and migration rates of fluvial and tidal bars (Seminara and Turbino, 2001; Dissanayake et al., 2009; Schuurman et al., 2013; Van Dijk et al., 2014), and controls the division of bedload over bifurcates (Kleinhans and van den Berg, 2011). On the larger scale, the amount of downslope sediment transport therefore has a major influence on channel and bar patterns, by determining braiding index (Parker, 1979; Struiksma et al., 1985; Crosato and Mosselman, 2009) and the stability of river bifurcations and related tendency of channels on fans and deltas to avulse (Bolla Pittaluga et al., 2003; Kleinhans et al., 2008; Sloff and Mosselman, 2012; Bolla Pittaluga et al., 2015).

Braided river models with the KF slope parameterization had a larger braiding index and shorter bars than the models with the IK slope parameterization with the lowest slope effect, and the braiding index decreased with increasing the slope effect for both sediment transport predictors (Figure 2.7b). Models with the EH sediment transport predictor showed braiding indices that were lower than predicted with the braiding index predictor of Crosato and Mosselman (Crosato and Mosselman, 2009), especially at a lower slope effect. However, models with the KF slope parameterization had braiding indices that were only slightly lower with a higher slope effect than the braiding index predictor, and generally showed the same trend in decreasing braiding index with increasing slope effect. Models with the VR sediment transport predictor theoretically should have lower braiding indices due to the lower non-linearity of sediment transport, but in these models many deep and narrow channels developed separated by long bars (Fig A.8). Only with downslope sediment transport that was almost a hundred times larger than with the default value, realistically shaped bar patterns developed, but the braiding index was still too high.

In general, bar length in the braided river model increased with increasing slope effect in models with the EH sediment transport predictor, but for the models with the IK slope parameterization bar length showed a local decrease with an intermediate slope effect (Figure 2.7d). For strong slope effects, a subdued morphology is visible with short and wide bars. Bar length also decreased slightly in the model with the KF slope method and with the largest amount of downslope sediment transport. Predicted bar length by Struiksma et al. (1985) is in the same range as the models, but show a much more stable bar length with an increase in slope effect. As a result, bars in the braided river model are theoretically longer when the slope effect is weak, and shorter when the slope effect is strong. Models with the VR predictor showed a decreasing bar length with increasing slope effect, since here cross bar channels started to dissect the unnaturally long bars separating the deep channels, or started to show realistically shaped bar patterns in the case of the model with the IK slope parameterization. The bar length predictor predicts increasing bar lengths with increasing slope effect, which is therefore not comparable with bar lengths in the braided river models with the VR predictor.

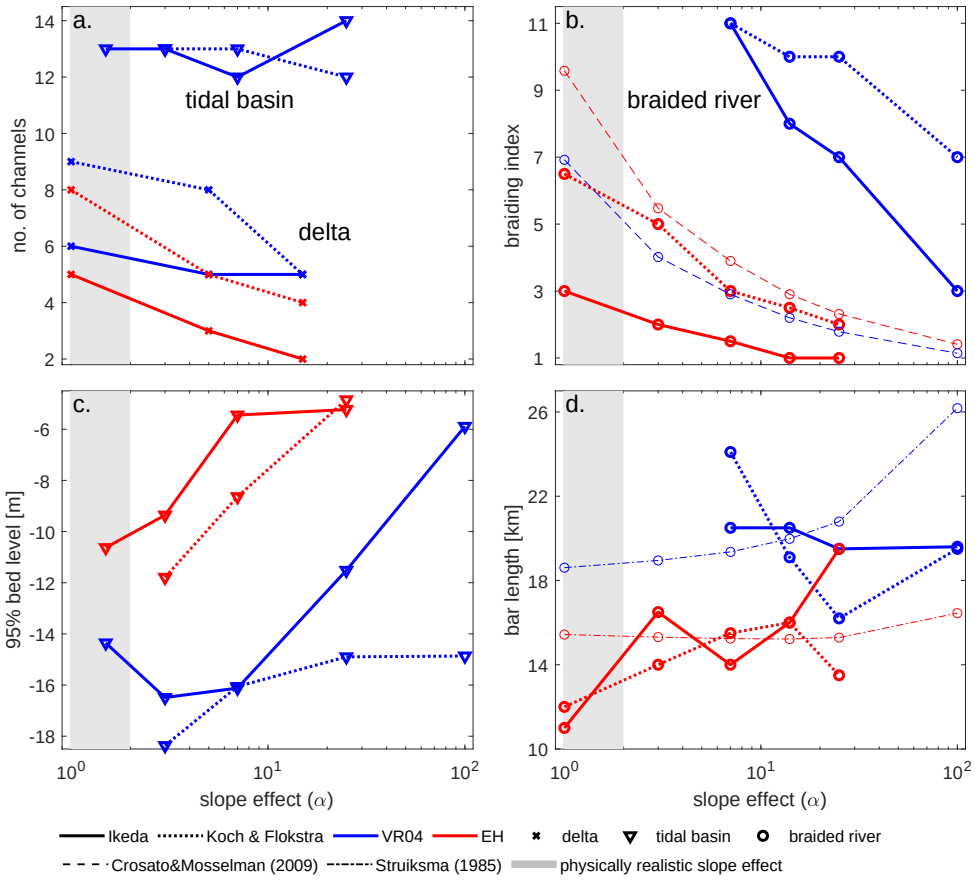

Figure 2.7: Relation between slope effect and morphodynamic element dimensions a) Number of channels at the delta front in the delta models, and the number of channels in the tidal basin models, against increasing slope effect. b) Braiding index with increasing slope effect in the braided river model, with the semi-analytical predictor for braiding index from Crosato and Mosselman (2009) in corresponding colors for comparison. c) The 95% depth of all tidal channels in the tidal basin models against slope effect. d) Mean bar length in the braiding river model when increasing the slope effect, including the predictor of Struiksma et al. (1985) for wave lengths of bars. Braiding index and bar length are computed according to the methods described in Schuurman et al. (2013). The method of determining the number of channels in the tidal basin models is explained in the methods section. Slope effect is given as the α_I for IK and transformed for KF.

The number of avulsions in the delta models is larger for runs with the KF bed slope predictor compared to runs with the IK parameterization, even though sediment transport rates were equal for models with an equal downslope sediment transport. Models with VR had a larger number of avulsions compared to models with the EH predictor with equal slope effect (Figure 2.7a). In contrast, the tidal basin model shows that the number of channels is not significantly affected by increasing downslope sediment transport in an erosive environment (Figure 2.7a). Furthermore, the amount of incised channels was also similar between models with different slope parameterizations. The magnitude of the bed slope effect did have an influence on channel dimensions, since in general channels became shallower with increasing downslope sediment transport (Figure 2.7c).

2.3 Discussion

The extreme incision common in morphodynamic models is the result of an imbalance at the channel scale between the non-linearity of sediment transport that carves out channels and transverse sediment transport that counteracts incision. The cause of this imbalance is twofold. Firstly, the amount of channel incision is highly dependent on grid size, suggesting strong numerical effects. When a channel incises, the channel will attract more flow and will experience a positive feedback. The flow seems to prefer flowing through as few grid cells as possible, and when grid cell width is smaller this means that there is more discharge flowing through a smaller area, which therefore results in more incision. The discharge flowing through a much smaller area than a natural channel width results in an unrealistically deep channel at equilibrium. Lateral channel migration requires erosion and movement of all sediment in the high banks, so that deep channels are effectively unable to migrate sideways. The transition from grid size-dependent incision to a more dynamic system is determined by the transverse sediment transport rate and can therefore be reached by increasing the transverse slope parameter (Figure 5). Some studies suggest the severe incision is caused by the use of uniform sediment instead of a sediment mixture, which would lead to coarser sediment to be deposited in the deeper parts and therefore a reduce in flow velocities (van Maren, 2007; Dastgheib and Roelvink, 2010). However, for realistic grain size mixtures active sediment sorting will not lead to different transverse slopes (Baar et al., 2019). Our results show that the extreme gridsize-dependent incision with uniform sediment is not natural, and therefore, adding coarser sediment fractions to the model does not solve the problem of severe incision, but can mask it by resulting in a non-erodible bed layer that prevents erosion.

Secondly, the magnitude of slope parameter that is needed to overcome grid size-dependent incision is determined by the bed load transport rate that is initially available for deflection downslope. This transport rate is calculated by the sediment transport predictor, which determines both the sediment transport rate and the ratio of bed load versus suspended load. Simple transport predictors such as EH overdampen perturbations due to the high total sediment transport rate and because slope effects act on all sediment transport. On the other hand, VR initially predicts the correct balance between incision and downslope transport in accordance with the analytical model (Appendix A Figure A5). However, once incision commences, it needs much higher slope effects to counteract incision than in theory. This can

be explained by the distinction of suspended and bedload transport, since VR and similar suspended load predictors assume that bed slope effects only act on bedload. Additional bed slope effects on suspended sediment and the influence of the vertical distribution in the water column are not accounted for (Talmon et al., 1995; Schuttelaars and De Swart, 1999; Walstra et al., 2007b). Consequently, the tendency to incise depends on grain size and sediment mobility, since this determines the amount of sediment that is transported in suspension (Dastgheib and Roelvink, 2010; Nicholas, 2013; Schuurman et al., 2013). More suspension means that there is less bedload available for deflection downslope and therefore leads to a higher slope parameter to counteract incision. However, there are some model studies with only suspended sediment or very high suspended sediment concentrations that do get realistic channel morphology. This can be explained by large numerical diffusion (Dam et al., 2016), dampening of the turbulence near the bed due to large suspended sediment concentrations (van Maren, 2007), or by modelling a small and constrained domain with well-defined boundary conditions (Lanzoni and D'Alpaos, 2015; Xu et al., 2019). Therefore, it is advised to further study the role of slope effects on, and diffusion of, suspended sediment transport by modelling and experiments.

To model a dynamic system, the model has to overcome extreme incision at the channel scale by increasing the transverse bed slope effect. The magnitude of the transverse slope parameter that is needed depends on if a model needs to be laterally dynamic or not, and thus if it has to overcome the grid size-dependent incision. Therefore, the difference in slope factor that is used in dynamic, erosional or depositional systems in previous model studies (Figure 2.1) is also explained by the research objective, next to flow conditions and the choice in sediment transport predictor. Environments with a large-scale balance between erosion and deposition, such as estuaries and rivers, particularly have the tendency to overpredict channel depth and braiding index and require very high slope effects to overcome the severe incision and show realistic morphology. The initial response determines whether a system tends to incise or goes towards an equilibrium channel with a constant width to depth ratio by eroding the banks. Once a channel incises, it attracts more flow and will deepen further through the aforementioned positive feedback, and therefore especially models with weak slope effects had a more extreme deviation in channel depth, braiding index and bar length compared to theory (Figure 2.7). In case of erosional models, in some studies bank erosion was calibrated and therefore slope effects were increased, which will set channel dimensions but not necessarily the number of channels (Figure 2.7). However, the majority of the models presumably only focused on the network characteristics and therefore saw no need to increase slope effect. As a result, many studies show unnaturally sharp angular bends in plan view. These angular bends that are observed in many models especially with the transport predictor of Van Rijn are also explained by grid size-dependent incision and the resulting lack of channel migration. The channels follow the grid configuration which is rectangular in this study, and therefore it is expected that models with an irregular shaped grid will show other bend shapes, but this does not mean that the problem of grid size-dependent incision and lack of channel migration is solved in this case. In contrast, depositional models like the delta model will show more natural looking bars with default slope parameters Appendix A Figure A6), since deposition does not depend on the non-linearity of sediment transport that

carves out channels. In this case, increasing the slope effect would quickly lead to a diffuse morphology. However, channels that form on the deposits will incise during the model run and often show the same rectangular bends as in the erosional models, as observed in previous model studies (Edmonds and Slingerland, 2010; Caldwell and Edmonds, 2014; Van der Vegt et al., 2016).

The slope parametrization determines local direction of sediment transport and thereby the magnitude of downslope sediment transport. The IK slope parameterization increases the total sediment transport by calculating an additional transverse transport vector, while the KF slope parameterization only causes a larger rotation of the transport vector. This difference between slope parameterizations in direction and magnitude of the transport vector significantly influences the development of morphology across scales (Figure A.8, 2.7). The larger magnitude of the total transport vector in models with the IK slope parameterization results in wider and shallower channels. The larger rotation of the transport vector in models with the KF slope parameterization results in a different distribution of sediment over bifurcates and a shorter adaptation length to changes in flow conditions, influencing bifurcation dynamics and bar dimensions. Since both slope parameterizations distribute sediment differently, this also modifies channel curvature and therefore the orientation of channels at bends and bifurcations. This orientation affects locations of bank erosion, migration rate, and chute cutoff processes (Van Dijk et al., 2014). On the larger scale, this alters the timescale of morphological adaptation and the frequency of avulsion (Kleinhans and van den Berg, 2011), and therefore has a large influence on the development of channel patterns.

The local balance between channel incision and downslope sediment transport has a large effect on sediment transport rates, bar and channel dynamics, and consequently large-scale morphology. Therefore, modeled morphology heavily depends on the combination of sediment transport predictor and slope parametrization. Pending further investigations into sediment transport parameterizations and numerical effects, the choice of sediment transport predictor and slope parametrization in future studies should depend on the environment that is modeled and the research objective, instead of arbitrary choices. Our recommendations based on the results of this study are summarized in figure 2.8, and are not a solution, but a way to limit unintended artifacts until the real problems are solved. These recommendations qualitatively hold for any sediment transport predictor that either is a bedload or total load predictor like Engelund-Hansen, or makes a distinction between bedload and suspended load like Van Rijn. Quantitatively, however, the predicted sediment transport rate and dimensions of morphodynamic features will depend on the non-linearity of the transport predictor and other predictor-specific parameters. Increasing the transverse bed slope effect leads to physically unrealistic sediment transport vectors (Baar et al., 2018b), but to more realistic bed slopes, channel depths, channel dynamics and bar patterns (Figure 2.7). Practically, this means that it is impossible to have both realistic sediment transport vectors and morphology in the same model study, and the choice of sediment transport predictor and slope parametrization depends on whether the objective is related to sediment transport processes or to channel and bar patterns (Figure 2.8).

The predictor of Engelund-Hansen will lead to more realistically shaped bars and channel networks in systems were lateral dynamics are essential, since it needs much lower slope

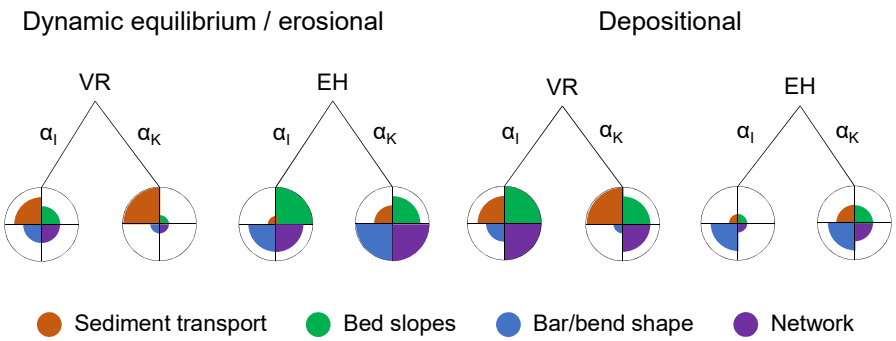

Figure 2.8: Model design recommendations Relative performance for each combination of transport predictor and slope method in models of either erosive or balanced environments where bank erosion is necessary, or depositional environments. Relative performance is divided in four categories, such that the choice of predictors can be made depending on the research objective. Network characteristics include braiding index and number of channels in e.g. a tidal basin or a delta.

effects to counteract the severe incision than Van Rijn. However, sediment transport rates are too high which overdampens perturbations. Therefore, if the objective is to have realistic sediment transport vectors and morphological adaptation, the predictor of Van Rijn works better. Furthermore, since this predictor makes a distinction between bed load and suspended load, it is the only option in models were suspended sediment is essential, for example in models of tidal environments with waves, varying flow directions, or cohesive sediments. In depositional environments where lateral dynamics are initially less important, the use of the predictor of Engelund-Hansen is difficult due to the diffusive nature of this predictor. This predictor should only be used if the channels that eventually form have to be dynamic. The choice of slope parametrization depends on the sediment transport predictor. In models with Engelund-Hansen, the best option is generally the KF parameterization, since this resulted in the most realistically shaped bars and braiding index (Struiksma et al., 1985; Crosato and Mosselman, 2009) (Figure 2.7). The IK slope parameterization will lead to even more subdued morphology (Figure A.8, Appendix A Figure A6), since the increase in total sediment transport with increasing slope parameter will further overdampen perturbations. In models with Van Rijn on the other hand, it is advisable to use the IK slope parameteri-

zation, since this is often the only way to counteract the higher incision rate. However, it should be noted that any model with slope parameters higher than $\alpha_I = 5$ in case of the IK slope parameterization or lower than $\alpha_K = 0.5$ for the KF slope parameterization for certain do not produce realistic sediment transport rates and direction, according to the range in experimental results.

In case models are designed to represent existing morphology for e.g. decision making or case studies, the effect of slope parametrization might seem less obvious due to often smaller or constrained model domains and shorter run time. Furthermore, the model runs start closer to the desired equilibrium with the existing flow conditions than when starting from incipient formation of channels as in the models discussed so far. However, starting with close-to-equilibrium morphology does not affect the final morphology and the model will incise when this is not balanced by an increased slope effect. This means that morphological models cannot produce more than one equilibrium morphology based on the initial conditions. This is illustrated by the Western Scheldt model, which started with measured bathymetry (Appendix A Note 3). After ten years, default values of the slope effect lead to slopes that are too steep even though the model started form the measured morphology and calibrated hydrodynamics (Appendix A Figure A8). When the model is run for longer, the slopes start to steepen further and experience the positive feedback that leads to unrealistic incision. On the other hand, with a sufficiently high slope effect and starting with a plane bed or a measured bathymetry, the same reasonable morphologies were obtained after centuries by van der Wegen and Roelvink (2012). Furthermore, local direction and magnitude of total sediment transport in calibrated models still critically depend on the choice of sediment transport predictor in combination with the slope parameterization. When the model is calibrated on bed slopes or the shape of morphological features, different slope parametrizations will lead to a different magnitude and direction of the transport vector on the same slope (Appendix A Figure A11), and therefore leads to different local channel dynamics, such as bank erosion rates and location of erosion and deposition. For calibrated models, it means that when a model is calibrated on morphology but used to make an estimate of time scales of erosion or sediment migration, these estimates will depend on the choice of slope parametrization. This is for example the case in models of existing estuaries that are used for dredging and dumping strategies, like the model of the Western Scheldt in Appendix A Note 3. When the objective is to determine time scales of erosion or sediment migration, it is better to calibrate the model on for example migration rates of channels instead of bed levels. On the other hand, when models are calibrated to sediment transport time scales, morphology and bed slopes will differ between different methods. These are for example models that focus on the migration rate of dumped sediment, the sediment distribution at bifurcations, or the rate of bank erosion. Therefore, when models are calibrated by increasing downslope sediment transport, either sediment transport magnitude or bed slopes match to measured data, while both is not possible.

Finally, idealized model scenarios are frequently used to study fundamental morphological behaviours under controlled conditions in wide-ranging environments (Dissanayake et al., 2009; Schuurman et al., 2013; Caldwell and Edmonds, 2014; Van der Vegt et al., 2016; Kleinhans et al., 2018), but the above demonstrates that conclusions from model-only studies are

Table 2.1: Overview of the default physical and numerical parameters of interest for all five Delft3D models used in this study.

model	channel	braided river	river delta	tidal basin	Western Scheldt estuary
environment	balanced	balanced	depositional	erosive	balanced
boundaries	river	river	river,tides	tides	river,tides
grain size [mm]	0.5	0.2	0.25	0.125	0.2
roughness coefficient	C=40	k_s=0.15	C=50	C=50	n=0.022-0.028
time step [min]	0.1	0.1	0.5	0.5	0.25
morphodynamic run time [yr]	0.33	2	1000	200	10
MorFac	1	25	200	200	20
gridsize LxW [m]	7x7 to 66.67x66.67	200x80	100x50	50x50	250x120 120x50
horizontal eddy diffusivity [m^2s^{-1}]	10	10	10	10	10

sensitive to a priori model choices. This shows a need for the use of converging evidence from complementary physical experiments and field data analyses.

2.4 Methods

The morphodynamic modelling package DELFT3D FLOW2D3D version 6.02.13.7658 was used in all models in this study. For all models, the depth-averaged version with parameterization of secondary flow was used. The sediment mobility in all models is such that suspended sediment transport of sand is important, but cohesive sediments are not considered, since this requires many more processes such as flocculation, hindered settling in near-bed fluff layers, cohesion and salinity effects. Here, we describe the set-up of each model in detail. In Table 2.1 the physical and numerical parameters of interest are summarized for all five models.

2.4.1 Channel model

We set up a simple river channel in Delft3D for comparison to the analytical model to study the tendency to incise due to imbalance between incision and downslope sediment transport (Appendix A Note 2). This river channel has 3 grid cells across the channel, and two additional outer cells with a bed level that is 7 meters higher than the inner three cells to avoid boundary effects. This means that these outer two cells are above the water level and do not interact with the channel. As a result, the active channel has the same cross-section as the analytical model (Appendix A Note 2). The discharge is equally partitioned over the three grid cells as three upstream boundary conditions.

The default model run has a channel with a length of 10 km, a slope of 0.5 m/km, a Chezy coefficient of 40 $\sqrt{m}/s$, a ratio between discharge Q and channel width W of Q/W=12.5 m^2/s, and a grain size of 0.5 mm, which is all equal to the default analytical model. As a result, the average water depth is 5.8 m. The IK method is used for slope effect, with an α_I of 1.5. To be able to compare the model behavior to the analytical model results, we varied the channel width between 21 and 210 m, the bed level difference of the middle grid cell and the surrounding cells between 0.01 and 3 m, and the α_I between 1.5 and 50. Furthermore, we either used the VR sediment transport predictor, which relates the transport rate to the flow

velocity to the power of 3 (k=3) at higher mobility, or the EH predictor, where the transport rate is related to the flow velocity to the power of 5 (k=5). To test if the model results depend on the varied parameters or on the implementation of the specific transport predictor, we run the same models with the general transport predictor (Appendix A Note 1) in combination with both the IK and KF slope parameterization, with and without the critical shear stress, and varied the non-linearity between 3 and 10 (Appendix A Note 2). The models were run for two months, after which either the perturbation caused larger bed level differences and 1 grid cell wide bars to form, or the perturbation decayed and the three grid cells showed the same bed level.

2.4.2 River delta model

The river delta model was inspired by the Old Rhine river mouth at Leiden, The Netherlands, from the mid-late Holocene and is similar to that of Geleynse et al. (2011). It consists of a 20 km long river that flows into the coastal domain delimited as a 10 km by 10 km sloping bed, where the sediment is deposited and a delta is formed. The river can freely migrate and forms its own topographic forcing by incising and forming meander bends. Initially, the river is a 7 m deep channel with a width of 0.5 km for the first 15 km from the upstream boundary, after which it exponentially expands over the last 5 km towards a width of 3 km at the river mouth. The sea has a depth around 4 meters at the river mouth, increasing towards the end of the model domain. The upstream boundary consists of a constant discharge of 1750 m^3/s and at the downstream water level boundary a M2 tide is prescribed with an amplitude of 0.7 m. The model is run for 5 years at the hydrological time scale with a morphological scale factor of 200, resulting in a morphological run time of 1000 years.

2.4.3 Tidal basin model

The tidal basin model consists of a coastal domain of 7 by 3 km and a tidal basin of 7 by 5 km, connected by a 1 km wide inlet. The water depth at the basin is initially 1 m, and the coastal domain slopes up to 15 meters depth. A 0.75 m amplitude M2 tide is prescribed at the north and south coastal boundary with a phase difference in order to create an alongshore tidal current. The initially flat tidal basin, evolves with incisions due to the tidal induced currents, promoting a rich channel network. The model is run for 12 months at the hydrological time scale with a morphological scale factor of 200, resulting in a morphological run time of 200 years. Figure 2.9 shows two bathymetries of model runs with the default slope parameter in the IK method ((α_I = 1.5), and with an α_I of 25. A characteristic number of channels is determined at a fixed distance from the inlet of 2.5 km.

2.4.4 Braided river

The braided river model was inspired by the Brahmaputra river and is the same model that is used and described in detail in the study of Schuurman and othersSchuurman et al., 2013. The model consists of a 3.2 km wide and 80 km long braidplain, with a slope of 0.093 mm/m. The total discharge was 40000 m^3/s, partitioned over 20 cells at the upstream boundary, with an initial water depth of 5 m. The initial bed and the discharge were slightly perturbated to stimulate bar development. The bed level of the upstream grid cells differed by 1 cm, and

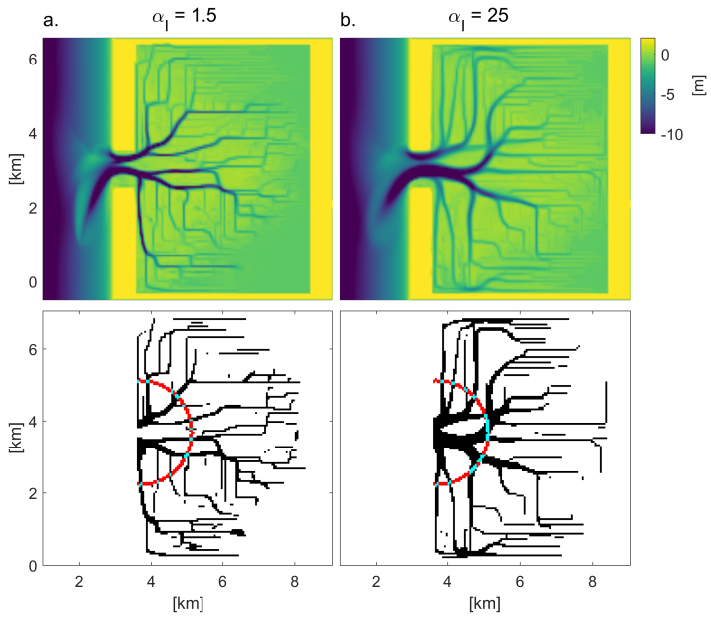

Figure 2.9: Bathymetries of the tidal inlet model Bathymetries are shown for models with the IK parameterization in combination with an α_I of (a) 1.5 (default) and (b) 25, and their corresponding binary image, where channels are black and the surrounding area is white.

the partitioning of the discharge between the upstream grid cells varied sinusoidally through time over the cross-section, with an amplitude of 200 m^3/s and a period of 2.28 days. In this study, the model was run for 2 years at the morphodynamic time scale.

2.4.5 Western Scheldt estuary

The Western Scheldt estuary model is based on the NeVla-Delft3D schematization of the Scheldt estuary, which includes the upstream Flemish branches of the estuary, the Western Scheldt and part of the North Sea. The NeVla-Delft3D model is a schematization from the fluid-flow behavior of the Simona simulation used by Rijkswaterstaat (the Netherlands) combined with the Delft3D component for sediment transport and morphodynamics. The NeVla model is a state-of-the-art numerical model that has been optimized for hydrodynamicsMaximova et al., 2009c; Vroom et al., 2015 and morphologyGrasmeijer et al., 2013; Schrijvershof and Vroom, 2016 and is applied by the Dutch and Belgian government.

Here, we used a nested model of the NeVla-Delft3D schematization focusing on the Western Scheldt partly for reducing the computational time, which is also used by van Dijk et al. (2018). The model boundaries include the Western Scheldt from the mouth at Vlissingen to the Belgian border, in which the seaward boundary includes a water level fluctuation due to tides and the landward boundary a current. For simplification the boundaries consist of a repeating spring-neap tidal cycles. Sediment fraction was uniform with a median grain-size of 200 μm. The roughness field in the model is defined in Manning n and is variable

over the model domain, which was 0.022 $s \cdot m^{-1/3}$ for the eastern part, and 0.027 $s \cdot m^{-1/3}$ for the western part (Maximova et al., 2009c; Maximova et al., 2009a; Maximova et al., 2009b; Vroom et al., 2015; van Dijk et al., 2018). The bed consisted of erodible and non-erodible layers (Gruijters et al., 2004; Dam and Bliek, 2013), and therefore sediment thickness varies within the Western Scheldt model, which reduces the morphological changes but not the transverse bed slopes. To reduce computational time the wind direction and magnitude as well as salinity were excluded because of they have no effect on the transverse bed slope. We applied a morphological factor of 20, to reduce computational time and evaluated the model runs after 10 years of morphological changes.

We assessed the effect of sediment transport predictor, slope parametrization and its calibration parameter α_I or α_K on the sediment transport and morphodynamics within the Western Scheldt model. The results are presented in the Appendix A.

Acknowledgements

This research was supported by the Dutch Technology Foundation (TTW) of the Netherlands Organization for Scientific Research (NWO) (Vici grant 016.140.316/13710 to MGK) and by the European Research Council (ERC) (Consolidator project 647570 to MGK). We acknowledge Kees Sloff, Wim Uijttewaal, Erik Mosselman, Mick van der Wegen, Zheng Bing Wang, Bas van Maren and Willem Ottevanger for valuable discussions.

Chapter 3

Natural levee evolution in vegetated fluvial-tidal environments

Natural levees are common features in river, delta and tidal landscapes. They are elevated near-channel morphological features that determine the connection between channel and floodbasin, and consequently affect long-term evolution up to delta-scales. Despite their relevance in shaping fluvial-tidal systems, research on levees is sparse and often limited to fluvial or non-tidal case studies. There is also a general lack of understanding of the role of vegetation in shaping these geomorphic units, and how levee morphology and dimensions vary in the transition from fluvial to coastal environments, where tides are increasingly important. Our goal is to unravel the effects of fluvial-tidal boundary conditions, sediment supply and vegetation on levee characteristics and floodbasin evolution. These conditions were systematically explored by 60 large-scale idealized morphodynamic simulations in Delft3D which self-developed levees over the course of one century. We compared our results to a global levee dataset compilation of natural levee dimensions. We found that levee height is determined by the maximum water level, provided sufficient levee building sediments are available. Discharge fluctuations increased levee width and triggered more levee breaches, i.e. crevasses, that effectively filled the fluvio-tidal floodbasin. The presence of wood-type (sparse) vegetation further increased the number of crevasses in comparison with the non-vegetated scenarios. Conversely, reed-type (dense) vegetation strongly dampened tidal amplitude and reduced the accommodation space and sedimentation further into the floodbasin, resulting in narrower levees, no crevasses and limited floodbasin accretion. However, dense vegetation reduced tidal forces which allowed levee growth further downstream. Ultimately, the levees merged with the coastal barrier, eliminating the floodbasin tides entirely. Our results elucidate the mechanisms by which levee and crevasse formation, and vegetation may fill fluvio-tidal wetlands and affect estuary evolution. This brings new insights for geological reconstructions as well as for the future management of deltas and estuaries under sea-level rise.

Published as: Boechat Albernaz, M., Roelofs, L., Pierik, H.J., Kleinhans, M.G. (2020), Natural levee evolution in vegetated fluvial-tidal environments, *Earth Surface Processes and Landforms*, 45(15), DOI: 10.1002/ESP.5003.

3.1 Introduction

Natural levees, hereafter called levees, are along-channel elevated areas (Fig. 3.1) that slope towards the adjacent floodbasin (Brierley et al., 1997). Levees are found in both fluvial and tidal environments, commonly associated with vegetation, and are formed by differential sedimentation between the active channel and floodbasin (Cazanacli and Smith, 1998). Levees control the distribution of water, nutrients and sediment onto the alluvial valley and delta (e.g. Hiatt and Passalacqua, 2015). Over the course of their lifetime, levees can experience several breaches, called crevasses. Crevasses tend to be temporary features as they silt up, unless the breach turns into a major avulsion or bifurcation (Slingerland and Smith, 1998; Törnqvist and Bridge, 2002; Kleinhans et al., 2013; Nienhuis et al., 2018). The formation of crevasses leads to effective distribution of water and sediment further into the floodbasin even after the levee has built up to flood levels. Understanding how levee and crevasse morphodynamics affect the geomorphic evolution of fluvial-tidal landscapes is vital for long-term management of deltas and estuaries in view of sea level rise and human interventions, and elucidating previous and future sediment budgets.

The definition of a levee, although straightforward, is difficult to be systematically applied between geomorphologists and geologists (Brierley et al., 1997). In general, levees are along-channel elevated areas which comprise intermediate sized sediments (e.g. very fine sand and silt) and are located between coarse active channel sediments and the fine floodbasin fill (Cazanacli and Smith, 1998; Makaske et al., 2002; Adams et al., 2004; Smith and Pérez-Arlucea, 2004; Filgueira--Rivera et al., 2007; Smith and Pérez-Arlucea, 2008; Burns et al., 2019). Geomorphologists tend to define a critical slope for levee definition (Cazanacli and Smith, 1998), whist for geologists overbank lithology is a more commonly followed criterion. This is because in ancient geological strata differential compaction subsequent to deposition may result in deviations from the original levee slope (Stouthamer, 2001; Burns et al., 2019; Pierik et al., 2017b). However, both definitions have practical limitations to clearly identify the transition between levee and floodbasin from field records, especially for quantitative assessments.

Levee research has so far largely focused on case studies of fluvial environments through geological and morphological field data (e.g. Umitsu, 1985; Cazanacli and Smith, 1998; Makaske et al., 2002; Adams et al., 2004; Smith and Pérez-Arlucea, 2004; Filgueira--Rivera et al., 2007; Smith and Pérez-Arlucea, 2008; Johnston et al., 2019), modelling studies of only hydrodynamics in jet and mouth bar configurations (Mariotti et al., 2013; Canestrelli et al., 2014), or small scale (experimental) morphology (e.g. Rowland et al., 2010). These previous works either cannot isolate the effects of individual variables from the field, or in the case of modelling, do not account for the complexity of morphodynamic feedbacks in the scale of a fluvial-tidal system. The field studies demonstrate a variety of possible levee shapes, slopes and total volumes, (Cazanacli and Smith, 1998; Adams et al., 2004; Gibling, 2006; Pierik et al., 2017b) even across short distances along an individual channel. What causes this variability is presently uncertain due to scarce available data and difficulties in isolating the effects of internal and boundary conditions from field observations, especially the presence and effects of vegetation. While vegetation is abundant in fluvial and estuarine environments (e.g. Cazana-

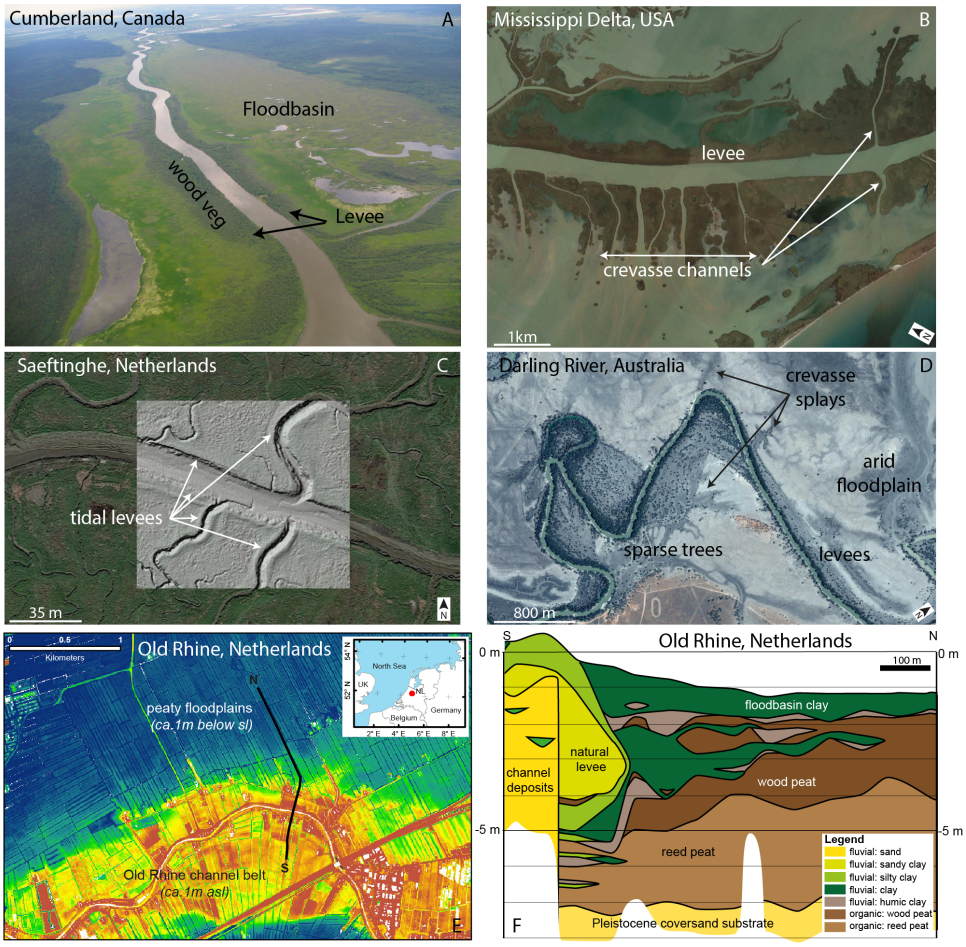

Figure 3.1: Overview of levees. (a) Levee complex at Cumberland, Canada - aerial photos by MGK. (b) Levees and crevasses at the lower Mississippi Delta, USA - from Google Earth imagery. (c) Tidal levees at Saeftinghe marsh, the Netherlands - color image from Google Earth and hillshade from AHN *www.ahn.nl*. (d) Levees and crevasses splays of Darling River on the arid environment of Australia - from Google Earth imagery. (f) Elevation map of the Old Rhine, NL from AHN *www.ahn.nl*. (g) Geological cross-section of the Old Rhine after Stouthamer (2001).

cli and Smith, 1998; Corenblit et al., 2011; Pierik et al., 2017b; Temmerman et al., 2007, and Figure 3.1), vegetation effects on hydrodynamics and morphology are often disregarded and understudied despite their strong influence on morphodynamics (D'Alpaos et al., 2007; Kirwan and Murray, 2007; Temmerman et al., 2007; Davies and Gibling, 2011; van Maanen et al., 2015; Kleinhans et al., 2018; Lokhorst et al., 2018; McMahon and Davies, 2018; Brückner et al., 2019). This paper aims to illustrate the growth processes, limiting factors and morphodynamic feedback of levee formation in fluvial-tidal environments, including the presence and effects of vegetation.

Levee incipience and growth occurs when water levels exceed channel heights and induce overbank discharge. This overflow is controlled by river discharge, sometimes in combination with tides. Coarser sediments are deposited in proximity to active channels with finer materials grading into more distal reaches of the floodbasin (Cazanacli and Smith, 1998; Adams et al., 2004). In the incipient growth stage, levees tend to be narrow and steep (Filgueira--Rivera et al., 2007). The progressive growth in height diminishes the transport of coarser material over channel banks. In this later stage, levees tend to widen with finer material (silt and clay) towards the floodbasin, which reduces the overall levee slope (Filgueira--Rivera et al., 2007) and generally creates a fining upward sequence (Törnqvist and Bridge, 2002; Pierik et al., 2017b; Burns et al., 2019).

Our lack of understanding of the importance of boundary conditions in levee formation means, for example, that we do not know whether fluvial-tidal levees develop relatively larger (or faster) than fluvial levees. We also do not know how levees and vegetation influence the fluxes of water and sediment distribution between channel and floodbasin, which determines long-term delta development.

We hypothesize that the interplay between fluvial and tidal boundary conditions, sediment supply and vegetation are key in determining the end-member morphology of levees-crevasses and floodbasins. We aim to understand levee-crevasse formation and floodbasin evolution, including the so far understudied effects of tides and floodbasin vegetation, in addition to variations in fluvial discharge and sediment supply.

We performed long-term (*i.e.* 100 years) idealized numerical simulations of an entire coastal-fluvial system using a morphodynamic model (Delft3D). In total, 60 scenarios were simulated under varying fluvial discharge, tidal amplitude, sediment concentration and under the effects of two vegetation types: reeds (dense) and trees (sparse). The model encompasses six sediment fractions grading from coarse sand to clay, and provides detailed stratigraphy and sediment sorting. With this approach we aim to self-develop levees, covering key end-member environments from nature. Our results are then compared to a large database of measured natural levees (compilation available in the supplementary material). Our model setup and scenarios were largely inspired by the Saskatchewan and Columbia Rivers in Canada (Cazanacli and Smith, 1998; Adams et al., 2004; Smith and Pérez-Arlucea, 2008), and the ancient Old Rhine estuary in the Netherlands (de Haas et al., 2019). The channels and boundary conditions in the Canadian rivers have been studied extensively, and one important finding was that the supply of silt from the formerly glaciated hinterlands facilitated the rapid formation of high levees (Cazanacli and Smith, 1998; Perez-Arlucea and Smith, 1999; Makaske et al., 2002; Adams et al., 2004; Filgueira--Rivera et al., 2007; Smith and Pérez-Arlucea, 2008). The Old Rhine is a data-rich fluvial-tidal system which contains levees and crevasses that evolved throughout the Holocene from a tidal basin into a river estuary. This evolution was partially steered by upstream avulsions that rerouted the full Rhine river discharge into this branch between 6000 and 3000 years BP. After that, upstream avulsions progressively diverted discharge away from the Old Rhine, and wave-induced sediment transport closed off the mouth (Berendsen and Stouthamer, 2000; Stouthamer, 2005; Cohen et al., 2012; Pierik et al., 2018; de Haas et al., 2019).

3.2 Methods

The morphodynamic simulations were performed in Delft3D FLOW2D3D version 6.02.13.7658 from tag 7545 (Deltares, 2020). Delft3D is an extensively applied morphodynamic model of finite differences solving the momentum and continuity equations for unsteady shallow-water flow in depth-averaged mode through the Navier-Stokes equation with hydrostatic pressure approximation (Deltares, 2017). The model computes accurate hydrodynamics and morphology, see Lesser et al. (2004), in addition to including the effects of vegetation on the hydrodynamics.

Below we detail the relevant model settings, including the initial and boundary conditions, and the basic data analysis.

3.2.1 Model settings

The model domain consist of a 20 by 10km idealized estuarine environment (Fig. 3.2) that provides enough time-space for the levee-crevasse development and the evolution of fluvial-tidal landscape. The estuary comprises a 12.5 by 10km flood-tidal basin enclosed by barriers, representing barrier islands, connected to a coastal zone of 7.5 by 10km on the seaside, while being fed by a river discharge on the landward upstream side of the basin.

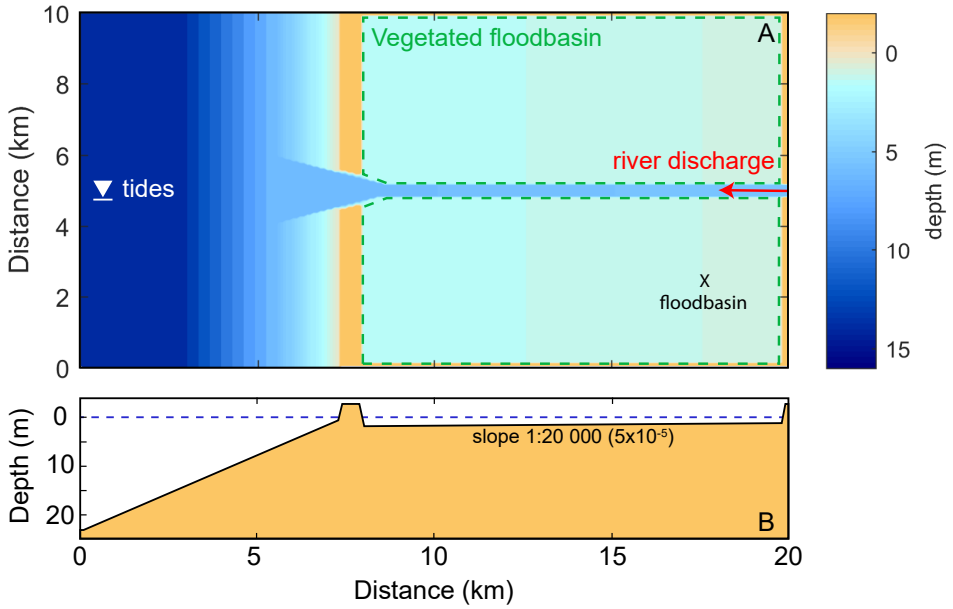

Figure 3.2: Delft3D model layout comprising initial bathymetry and boundaries. (a) plan view of model domain with boundary locations and the position of the floodbasin measurements denoted by the 'x' mark; (b) cross-section view along the domain.

The numerical simulations are depth-averaged models (2DH) with 100m resolution in the flow direction (along the river) and 50m across. The domain contains a null gradient

Neumann condition at the cross-shore sea boundary, water level on the seaward side and river discharge on the upstream basin limit. An initial channel was carved across the basin connecting the upstream river to the inlet, ending with a divergent shape at the coast. The width and depth dimensions of the initial river channel were determined based on geometric relation ($Q = whu\ [m^3/s]$ where Q is the river discharge; w the channel width; h the channel depth and u flow velocity) aiming for an initial flow velocity of 0.5 m/s and constant width-depth ratio of approximately 45. For example, a scenario with 700 m^3/s discharge consists of a channel with 250 m wide and 5.5 m depth dimensions. The basin slopes with $5x10^{-5}$ (*i.e.* 1:20,000), corresponding to approximately 0.6 m height difference between the inlet and river mouth. Six sediment fractions were deployed for simulating complex sediment sorting and allowing levee evolution out of a subset of these fractions for a wide range of flow conditions. The initial substrate contains four sand sizes ranging from coarse (300 μm) to very fine sand (75 μm). The two finest fractions, namely silt and clay material were supplied by a given concentration during the simulation via the upstream river boundary, while the other sand-sizes are supplied by an equilibrium concentration boundary condition.

The model scenarios were systematically varied with different combinations of (1) time-constant fluvial discharge magnitudes, (2) tidal amplitude, (3) fine sediment supply, (4) the time-variable fluvial discharge, (5) sediment starvation of very fine sand and silt, (6) and the presence of two types of vegetation (Table 3.1). The time-constant fluvial discharge magnitude varies among different runs between 400 m^3/s and 1500 m^3/s. The tidal amplitude of the M2 tidal component ranges between 0.5 and 1.25 m in steps of 0.25 m. Additionally, the M4 component was coupled with 10% of the M2 amplitude and 75 degrees phase lag, resembling the West (Holland) coast of the Netherlands on the North Sea. The fine sediment supply was delivered from the fluvial upstream boundary varying between 0 g/m^3 and 20 g/m^3 of equal amounts of clay and silt, resulting in a total mud concentration up to 40 g/m^3. We also performed simulations without very fine sand and silt to assess if these were limiting factors for levee development in a sediment-starved system. The influence of discharge variability was included with a yearly based peak discharge of different magnitudes. For comparison, the yearly integrated discharge was kept constant, at 700 m^3/s, for all variable discharge scenarios.

Finally, vegetation was included in the floodbasin (see Fig. 3.2) as dense and sparse type of plants. The vegetation typologies resemble the parameters (Table 3.2) of reeds (dense) and trees (sparse), based on van Oorschot et al. (2017). The vegetation was simulated with the Baptist et al. (2007) formula which affects the morphodynamics in two ways: first, it computes a new bed roughness (C) accounting for the vegetation ensemble in each grid cell, as follows:

$$C = \overbrace{\underbrace{C_b}_{\text{emerged}} + \frac{\sqrt{g}}{\kappa}\ \ln\left(\frac{h}{h_v}\right)\sqrt{1 + \frac{C_D\, n\, h_v\, C_b^2}{2g}}}^{\text{submerged}} \tag{3.1}$$

where: C = Chézy value added with vegetation $[m^{0.5}/s]$; C_b = base Chézy value $[m^{0.5}/s]$; C_D = drag coefficient induced by vegetation [-]; n = vegetation density $[1/m]$; h_v = vegetation height $[m]$; h = water depth $[m]$; g = gravity acceleration $[m/s^2]$; κ = von Kármán constant [-];
second, it introduces a drag force into the hydrodynamics as $\frac{\lambda}{2}u^2$, coupled into the momentum equation:

$$\lambda = \overbrace{\underbrace{C_D\, n}_{\text{emerged}}\ \frac{h_v\, C_b^2}{h\, C^2}}^{\text{submerged}} \tag{3.2}$$

where, λ = flow resistance due to vegetation $[1/m]$; u = flow velocity $[m/s]$. Therefore, the vegetation also affects the flow, via an additional drag force term λ, instead of solely increasing the bottom roughness which would lead to overprediction of sediment transport rates due to the increase of the bed shear stress. More details regarding the implementation of vegetation can be found in Baptist et al. (2007) and Deltares (2017).

In order to have a frame of comparison between the models, we elected the typical scenario (model 40) as our reference model run, with 700 m^3/s fluvial discharge, 0.75 m tides and 20 g/m^3 of mud (clay & silt).

Table 3.1: Overview of model scenarios and boundary conditions simulated in Delft3D. In total 60 scenarios combined: (1) Discharge magnitude, (2) tidal amplitude, (3) total concentration of fines, (4) discharge variability, (5) absence of very fine sand and silt, (6) and the inclusion of two types of vegetation. The reference scenario (model 40) is highlighted in **bold**.

Model Scenarios	**Unit**	**Absent**	**Low**	**Medium**	**High**	**Very high**
1. Discharge magnitude	m^3/s	-	400	**700**	1000	1500
2. Tidal amplitude (M2)	m	0	0.25-0.5	**0.75**	1.0	1.25
3. Mud Concentration	g/m^3	0	10	**20**	30	40
	Peak Q m^3/s	**Low Q** m^3/s	**Mean Q** m^3/s			
4. Discharge variability	1000	692	700			
	1250	685	700			
	1500	678	700			
5. Sediment-starved	no silt, no very fine sand					
6. Vegetation	Dense (reeds)			Sparse (trees)		

We selected the sediment transport predictor TRANSPOR2004 (van Rijn et al., 2004; van Rijn, 2007a; van Rijn, 2007b) because it is well-calibrated on a wide range of environments, including tidal-fluvial conditions. It conceptually separates bed and suspended load and allows calculations with multiple sediment size fractions. In Delft3D the mud fractions are treated as cohesive sediments and the deposition and erosional fluxes are computed according to Partheniades-Krone formulation (Partheniades, 1965) based on user-defined critical shear stresses. The erosion shear stress was set to 0.5 N/m^2 and the sedimentation threshold

Table 3.2: Vegetation parameters used as model inputs to simulate dense and sparse vegetation. *n* is vegetation density, h_v is vegetation height, C_b = Chézy value with considering vegetation, C_D = drag coefficient and *Area* is the coverage percentage.

	n	h_v	C_b	C_D	**Area**
units	$1/m$	m	$m^{0.5}/s$	-	%
sparse	0.05	3	45	1.2	0.5
dense	3	3	45	1.0	0.3

to 1000 N/m^2 (the high value means that it always allow for sedimentation), both default values. The transverse bed slope sediment transport was parameterized with Koch and Flokstra (1981) to have less morphological diffusion than Ikeda (1982), after Baar et al. (2019), wherein the sediment transport vector is rotated downslope as a function of transverse slope divided by $\alpha * \theta^{\beta}$, where θ is the sediment mobility, and here $\alpha = 0.2$ and $\beta = 0.5$.

The stratigraphic bed module from Van Kessel et al. (2012) was used to allow different sediment mixtures and the effect of differential bed composition on sediment transport rates for each sediment fraction. The module tracks and saves the bed composition with a user-defined vertical resolution, here 10cm, and the sediment transport is computed for the active top-layer on the basis of the top sediment mixture. With this approach, we were able to represent the sediment dynamics of different sub-environments, for example channel, floodplain and levees, similar to van der Vegt et al. (2016).

A constant morphological acceleration factor (morfac) of 200 was used to speed up the simulations and 100 morphological years were performed in total. Preliminary runs (not shown) demonstrated the limited effects of the acceleration factor on the final morphology, in agreement with Ranasinghe et al. (2011), whilst the high computational cost of multiple size fractions and one century development required a high morfac. The variable discharge scenarios included a time-varying morfac to incorporate the higher discharges by means of lower acceleration factors, here 20, during peak discharges.

Comprehensive model settings are specified in the supplementary material.

3.2.2 Data analysis

We quantified levee dimensions based on their morphology, similar to e.g. Cazanacli and Smith (1998), Adams et al. (2004), and Filgueira--Rivera et al. (2007). Levee height and width were extracted from the most upstream 5km of the floodbasin portion in order to avoid the disturbance by the main tidal channel network. The representative levee profile is the average elevation on the longitudinal direction along this section. Levee height was computed as the largest prominence in the cross-section, while the width corresponds to the lateral extent of half a levee height (Figure 3.3). The final value for height and width is the average between both sides of the floodbasin. The channel depth and width correspond to the bankfull channel depth (i.e. from the bottom of the channel up to the levee height) and bankfull channel width (i.e. distance between the two levee crests), respectively.

Crevasse channels were counted along the central channel whenever the breach reached more than 0.5 m depth in the main levee. For counting the number of crevasses, we consid-

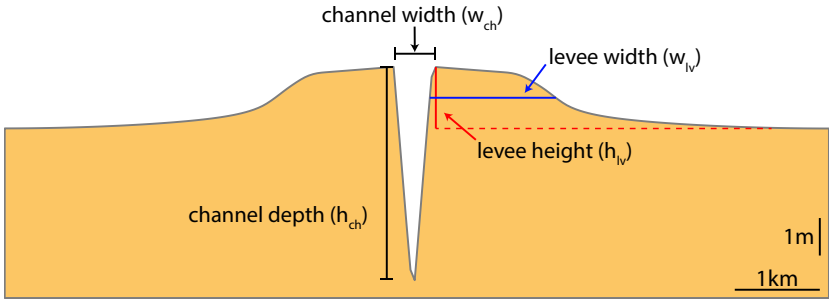

Figure 3.3: Discrimination of main levee and channel dimensions applied during analysis. This representative cross-section corresponds to the final levee of model 38. Levee height and width are quantified as the average between both sides of the levee.

ered the entire reach between the barrier and the upstream river, instead of restricting to the 5 km upstream reach, up to the point where the main levee could be identified.

3.3 Results

3.3.1 Levee development under fluvial-tidal conditions

Levee development predominantly starts with vertical growth towards the maximum water level, followed by the lateral expansion into the floodbasin (Fig. 3.4). The dimensions are larger near the upstream boundary, which is the main source of sediments, and decrease in size and volume towards the downstream portion of the domain. Levees are mainly formed by silt and very fine sand (VFS) along the main channel. The coarser sand fractions are dominant within the active main channel, while clay generally settles further into the floodbasin. The deposits near the channel are relatively coarser, fining upwards and laterally.

Distinct geomorphological patterns formed among the scenarios of time-constant fluvial discharge (model 38), time-varying fluvial discharge (model 93), and combined fluvial-tidal discharge (model 40). In the absence of discharge fluctuations, levees are smooth and continuous (Fig. 3.4,a) with a clearer transition from levee to floodbasin deposits (i.e. distal clays in Figure 3.4,d). In contrast, water level fluctuations, especially those induced by tides, trigger more crevasses (Fig. 3.4,b,c) and enhance sediment mixture between the levee and floodbasin deposits (Fig. 3.4,e,f), making the units and transitions among levee, floodbasin and tidal channels nearly indistinguishable in the lithological record.

As levee morphology and floodbasin evolution is considerably different after varying the fluvial-tidal boundary conditions (Fig. 3.4), we simulated a wide range of scenarios (Fig. 3.5) varying the relative force between fluvial and tidal discharges (Table 3.1). Both the channel and its associated levees became wider when subjected to increased mean fluvial discharge. No crevasses were formed under the constant discharge scenarios (Fig. 3.5,a-c). Conversely, fluvial-tidal conditions show abundant crevasse systems, together with tidal channels in the downstream portion of the basin closer to the inlet, and along the side flanks towards the upstream basin (Fig. 3.5,d-i). When both fluvial and tidal discharge are increased, the basin

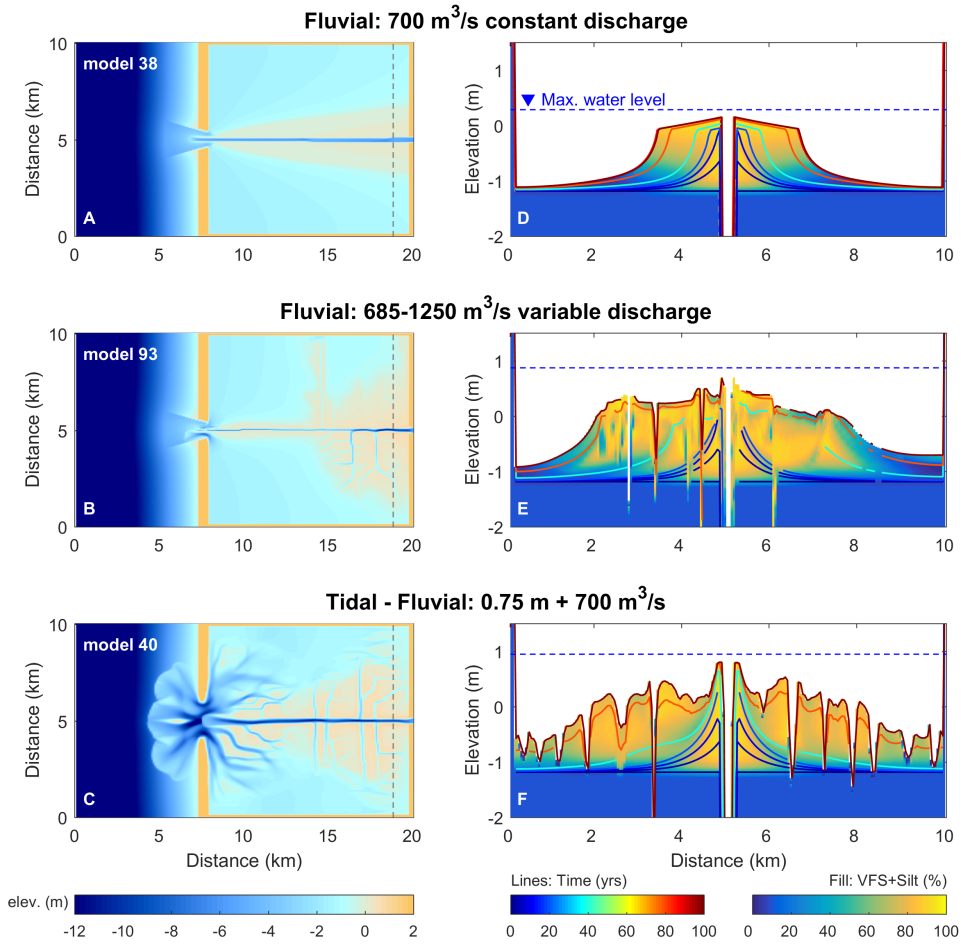

Figure 3.4: Levees after 100 years under a range of fluvial-tidal boundary conditions. Left panels (a-c) show the final plain-view morphology. Right panels (d-f) show the cross-section, illustrated in the correspondent map on the left, with combined percentages of very fine sand (VFS) and silt in the colored fill scale and the bed level evolution shown in colored lines.

fills with more sediment and develops larger and more complex crevasses and more extensive tidal channel network (see Fig. 3.5,g). The tidal channels tend to follow E-W direction along the basin, while crevasses are oriented N-S across the basin. The relative importance of fluvial versus tidal discharge leads to either more tidal or fluvial dominated morphology, which compete for space within the basin. Apart from the spatial dominance between tides and river, the general development of levees, channels and crevasses is rather similar across all scenarios (Fig. 3.5,d-g). In contrast, the models with time-constant fluvial discharge developed no crevasses, but instead developed continuous and unincised levees (Fig. 3.5,a-c). We

can therefore conclude that discharge fluctuations create an increasingly diverse morphology and deposits with larger crevasses and more complex channel networks.

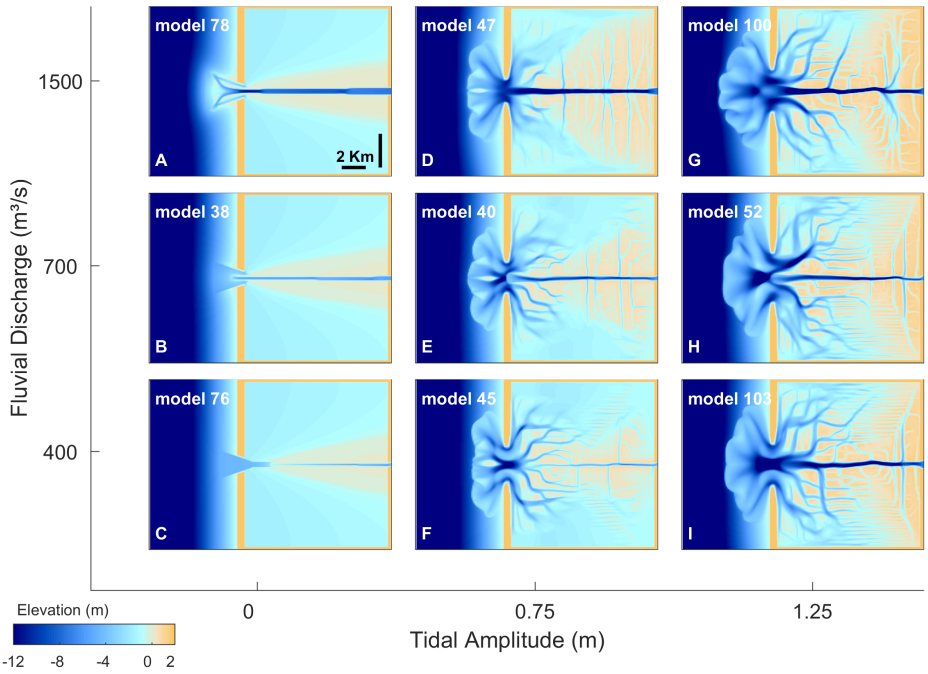

Figure 3.5: Morphological evolution after 100 years for combinations of fluvial discharge and tidal amplitude.

3.3.2 Effects of vegetation and sediment starvation

We introduced variations to the previous models regarding levee building sediment supply and inclusion of vegetation on the floodbasin. Starting from the reference fluvial-tidal model (model 40, Fig. 3.6,a) we included sparse (model 64, Fig. 3.6,c) and dense (model 63, Fig. 3.6,b) vegetation in the floodbasin, in addition to removing very fine sand and silt from the system (model 62, Fig. 3.6,d).

The sediment-starved scenario shows that without intermediate sediment sizes there is no levee formation and the near-channel deposits do not grow in height towards the maximum water level, as they do in other scenarios. Without levees, clay gradually fills the floodbasin in a homogeneous gently sloping deposit initiating from the main channel (Fig. 3.6,e).

The effect of vegetation is also pronounced on the levee and floodbasin development. The dense vegetation (reeds) creates narrower and steeper levees compared to other scenarios (Fig. 3.6,e). The main effects of dense plants are: (1) reducing the propagation of tidal flow into the basin and the resulting tidal prism (Fig. 3.7,d,e), (2) inhibiting both crevasse formation (Fig. 3.7,g) and lateral levee growth, and (3) leaving the basin sediment-starved (Fig. 3.7,h) as fluvial sediments are mainly exported to the ebb delta rather than stored in the basin.

In the dense vegetation scenario, the narrow levee progressed from the upstream river as far as the coastal barrier, connecting the main channel to the open coast after approximately 75 years (Fig. 3.6,b). This merging of levees and the coastal barrier ultimately inhibits the tidal propagation and isolates the floodbasin from fluvial-tidal dynamics, and thus it resembles a fluvial dominant system despite the presence of offshore tides. With the levees fully connected to the coastal barrier, the floodbasin turned into a near-stagnant water reservoir with higher mean water level in comparison to the main channel (Fig. 3.7,d) and currents are almost entirely absent inside the basin. This water level gradient together with the reduced sediment dynamics inhibited the formation of crevasses and the basin infilling. Sparse (trees) vegetation (1) reduces the tidal propagation into the basin to a lesser extent, (2) facilitates more crevasses along the levee, (3) inhibits the formation of tidal channels, although tides still penetrate the floodbasin generating water level fluctuations and currents (Figs. 3.6,c and 3.7).

In short, our scenarios demonstrate that no levee forms without the presence of specific sediment fractions, despite suitable boundary conditions and accommodation space. Vegetation creates higher but narrower levees. The models with sparse or no vegetation (reference scenario) induced more crevasses and trapped more sediment into the basin compared to the dense and sediment starved cases. The dense vegetation scenario was the only case where the sediment volume exported to the ebb delta topped the volume trapped inside the floodbasin (Fig 3.7,h).

Another remarkable effect of vegetation is the reduction of tidal prism and accommodation space. We compute accommodation space as the total water volume within the floodbasin, and tidal prism as the water discharge through the inlet during one tidal cycle. For the same fluvial-tidal boundary conditions, we observe a reduction of the initial tidal prism and accommodation space with the inclusion of vegetation on the floodbasin (Fig. 3.7e,f). Through time, both accommodation space and tidal prism decrease as the basin progressively fills with sediment (Fig. 3.7h). Hence, we expect different equilibrium states between the basin (hydro)dynamics and the import and export of sediment, for each scenario, after the initial morphological development. To test this hypothesis, we computed the basin dynamics, defined as the tidal prism divided by the accommodation space, as a proxy of how large and dynamic the basin is. Larger basin dynamics values indicate higher flushing per basin volume, while lower dynamics indicate a more stagnant condition. We plotted basin dynamics against the infilling percentage (defined as the sediment volume gain divided by the initial accommodation space) (Fig. 3.8). The sediment-starved and reference scenario, without vegetation, are the most dynamic cases with similar values. The starved scenario is slightly more dynamic than the reference case and does not show a decrease through time. Despite their similarity, those two cases have distinct infilling rates, as expected by the difference in sediment input. In contrast to the non-vegetated scenarios, the sparse vegetated model shows less dynamics with the same infilling percentage with respect to the reference case. Their behavior also display a similar evolution with increasing basin dynamics at the beginning, before decreasing as the model runs. Conversely, the dense vegetation shows a constantly decreasing dynamic from initiation. After approximately 75 years, and after the levee connected with the barrier, the system finds a new equilibrium accompanied with lower

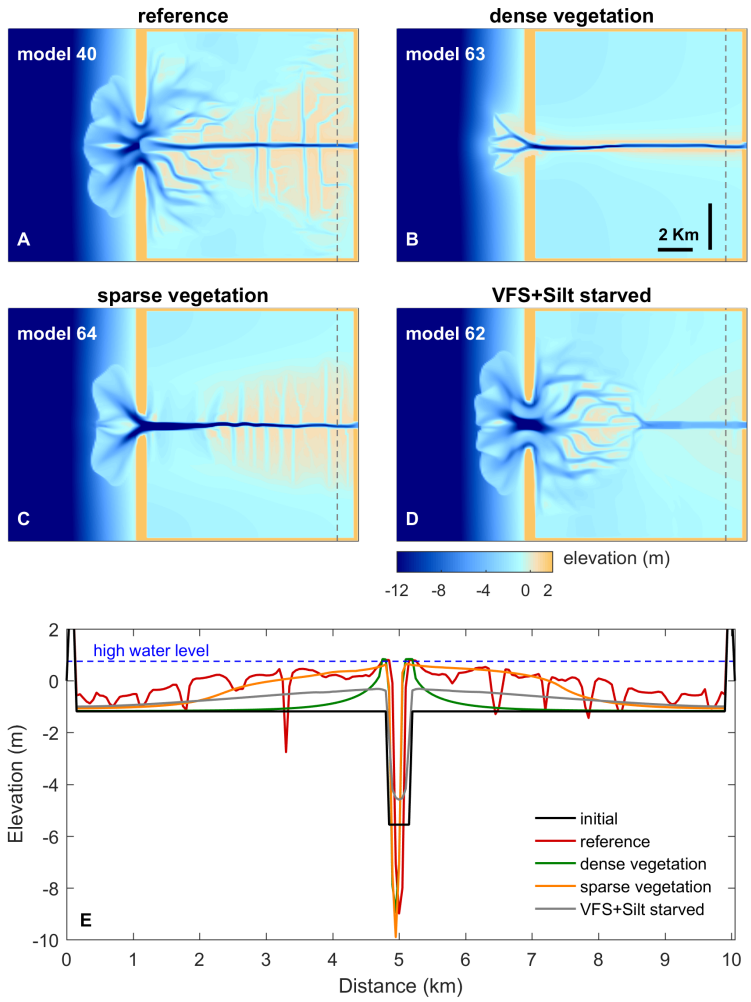

Figure 3.6: Effects of sediment starvation and vegetation on levee and floodbasin evolution. (a-d) Plan view of described models. (e) Cross-section of each model along the gray line in the top models.

infilling rate as sediments are predominantly carried out to the ebb delta at this later stage (Fig. 3.7h). We conclude that vegetation reduces the tidal propagation and thus the basin dynamics, with dense vegetation having the strongest effect, ultimately inhibiting all tidal penetration inside the basin.

3.3.3 Levee dimensions and evolution

We retrieved levee height and width from all 60 model scenarios (see Tables 3.1) according to Figure 3.3. In addition, we normalized the final levee height and width after 100 years (Fig. 3.9). Levee height was normalized by dividing the levee elevation by the maximum

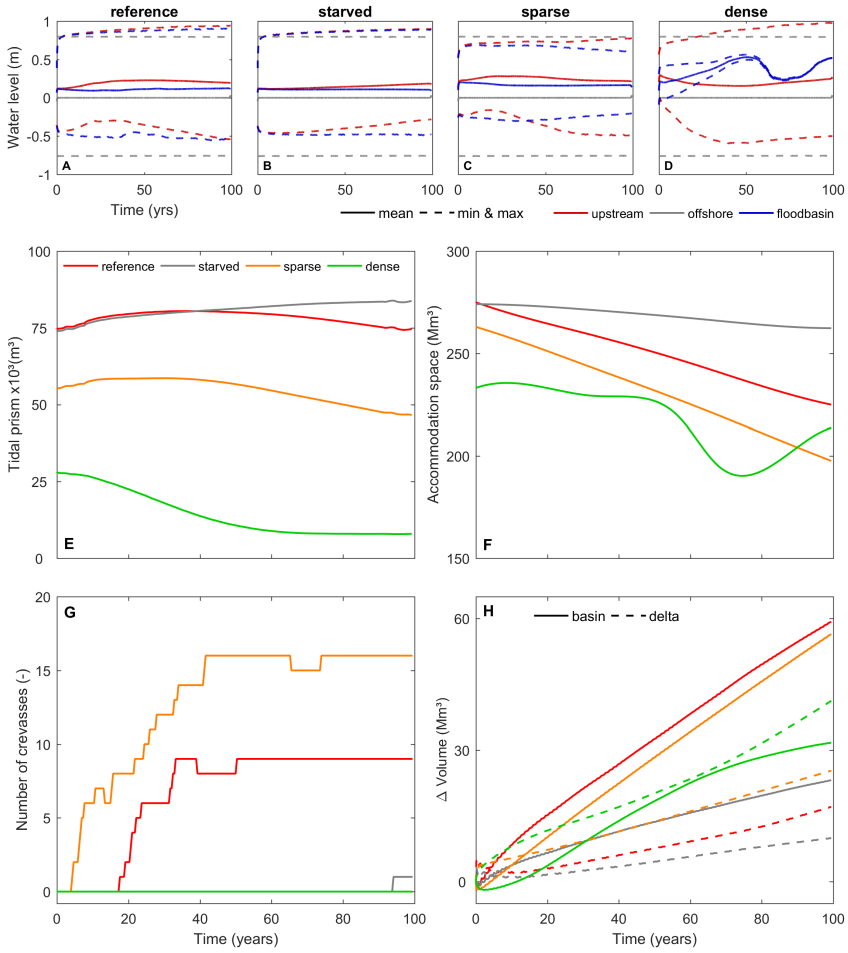

Figure 3.7: (a-d) Comparison of water levels in the upstream fluvial river, floodbasin and the offshore tidal range. Models shown are the same as in Figure 3.6. The position of the floodbasin measurement location is shown in Fig. 3.2. (e) Computed tidal prism and (f) accommodation space through time. (g) Number of crevasses along both sides of the main levee. (h) The sediment volume gain in the floodbasin and in the ebb delta.

water level, and levee width was divided by the floodbasin width. This normalization indicates how much the levee grew towards its maximum possible dimensions (i.e. maximum water level and floodbasin width). As levees grow towards the maximum water level, tides and floods are strong controls on levee height, and sediment concentration to a lesser extent (Fig. 3.9a-d). After the initial predominantly heightening phase, levees start to widen. Levee width shows a more constant growth through time, strongly related to fluvial discharge and sediment concentration. In general, no levees are formed in absence of very fine sand and silt (Fig. 3.6d,e). In this case, mud spreads all over the floodbasin, without a distinct near-channel elevated ridge but instead a low, gently sloping very wide deposit that does not follow

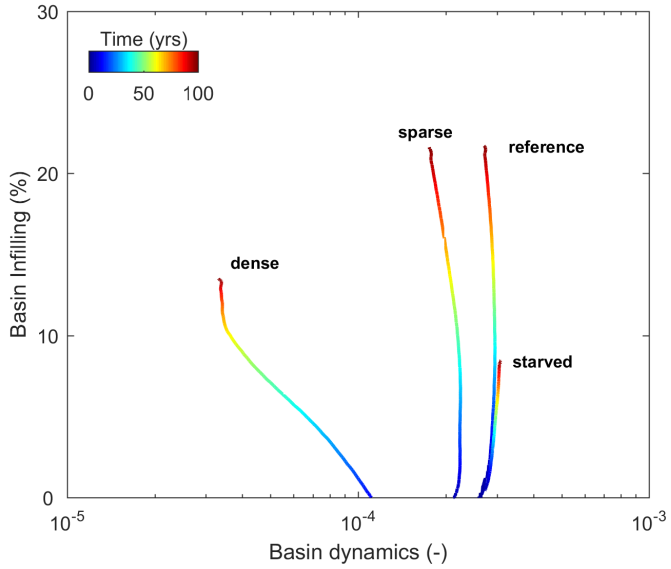

Figure 3.8: Basin dynamics versus basin infilling over time. Here the basin dynamics is defined as the tidal prism divided by the accommodation space, and basin infilling is the delta volume of deposited sediment divided by the initial accommodation space. Models shown are the same as in Figure 6.

the maximum water levels. Hence, it is arguable that this deposit should not be classified as a levee. Despite this, we quantified the dimensions to compare it with all other scenarios.

The inclusion of vegetation creates higher but narrower levees, especially for the dense vegetated floodbasin. The sparse vegetation scenarios generate levees dimensions that fall between the dense and reference scenarios. Increasing the fluvial discharge, especially in combination with tides, causes levees to grow higher, (Fig. 3.9a,e,i,m) whilst levee width has its maximum in mid-tidal ranges as larger tides create more tidal channels in the basin that flank the levees (Fig. 3.9b,f,j,n). Sediment supply only impacts levee height when there are very low concentrations, namely no mud (0 g/m^3). However, levee width shows a strong relation with increasing mud concentration. Finally, we observe that fluvial discharge variations affect both height and width. Floods promote similar morphological effects to tides. Although, tides are more efficient in widening and heightening levees as the water level fluctuates once or twice a day while floods occur in a yearly time-scale.

3.3.4 Comparison with natural levees

Following the self-development of levees from our numerical models, we compared our model results with measured data from several sites (Cazanacli and Smith, 1998; Latrubesse and Franzinelli, 2002; Makaske et al., 2002; Adams et al., 2004; Filgueira--Rivera et al., 2007; Makaske et al., 2007; Funabiki et al., 2012; Klasz et al., 2014; Kiss et al., 2018) and extracted relations between the relevant channel and levee dimensions. Beyond a simple comparison for model validation, we intend to highlight and explore the main similarities and discrep-

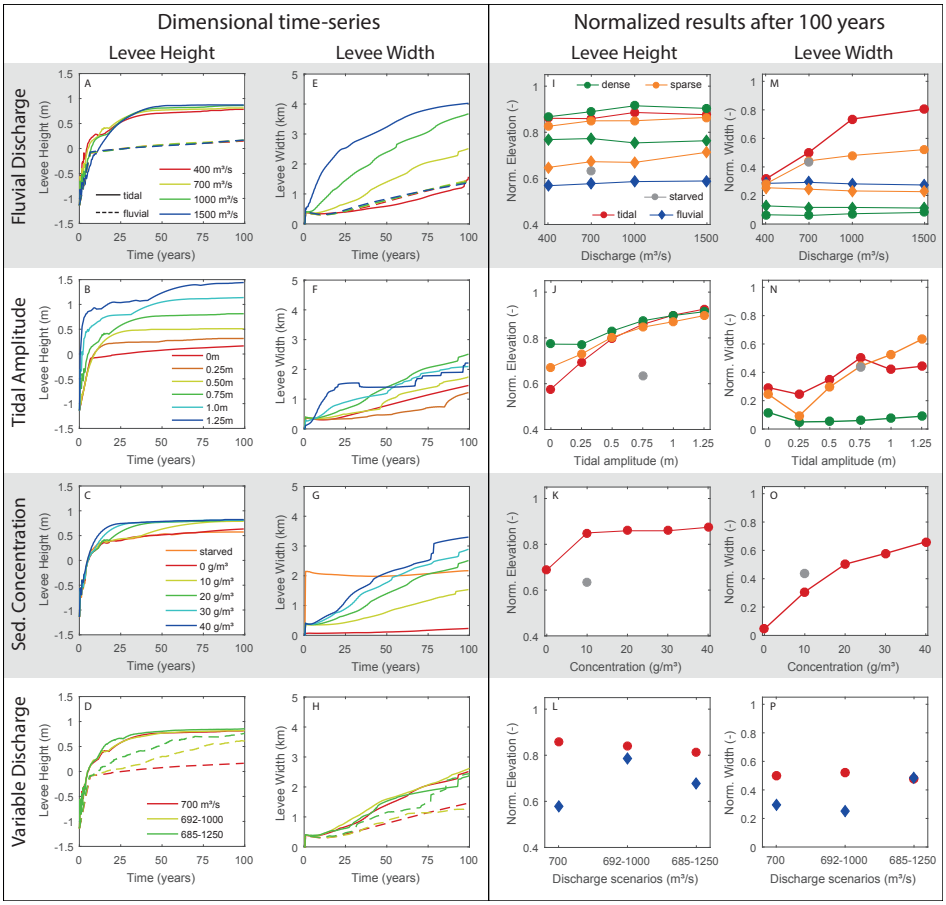

Figure 3.9: Dimensional time-series of levee height and width (left two columns) and normalized results after 100 years (right two columns) for all 60 runs. Levee height was normalized by the maximum recorded water level and levee width was normalized by floodbasin width. The first row (a,e,i,m) shows variations in fluvial discharge with 0.75 m tides (solid lines;circles) and without tides (dashed lines;lozenge). The second row (b,f,j,n) shows varying tidal amplitude combined with 700 m^3/s fluvial discharge. The third row (c,g,k,o) shows varying mud concentration, combined silt and clay, for 0.75 m tides and 700 m^3/s fluvial discharge. The fourth row (d,h,l,p) shows variable discharge cases with 0.75 m tides (solid lines;circles) and without tides (dashed lines;lozenge). On the normalized cases (right side) vegetation is depicted in orange (sparse) and green (dense) while the starved cases, without VFS and silt, is shown in gray.

ancies between the model results and the measurements. Both measured and model data are available in the supplementary material.

Modelled levee height (h_{lv}) collapsed within the measured dataset range (Fig. 3.10). Modelled levee width (w_{lv}) from the dense-vegetated scenarios also compared well with the measured levee dimension, while the sparse and non-vegetated modelled scenarios overestimated levee width by approximately one order of magnitude. This mismatch in width between our models and the measured levees demonstrates the importance of vegetation in

shaping morphology, and we address this topic more extensively in the discussion. Most natural vegetated levees have aspect ratios, calculated as width relative to height, between 10 to 100 times. The largest rivers, e.g. Amazon, Yellow River and Mekong, as well as our non-vegetated cases can reach aspect ratios of up to 1000. Levee height varies from a few centimeters up to 3 m, again with the exception of the large rivers which reach up to tens of meters. Levees in our models varied between 0.4 and 2.1 m in height and 160 to 4025 m wide. We also see a similar trend when normalizing the levee dimensions by the channel dimensions. Most natural and model data have levee heights that correspond to ca. 20% of their channel depths. Levee width usually has the same order of magnitude of channel width, especially with dense vegetation. For the scenarios without vegetation and the fluvial-tidal scenarios, we observe much wider levees, of around 4 times their channel widths.

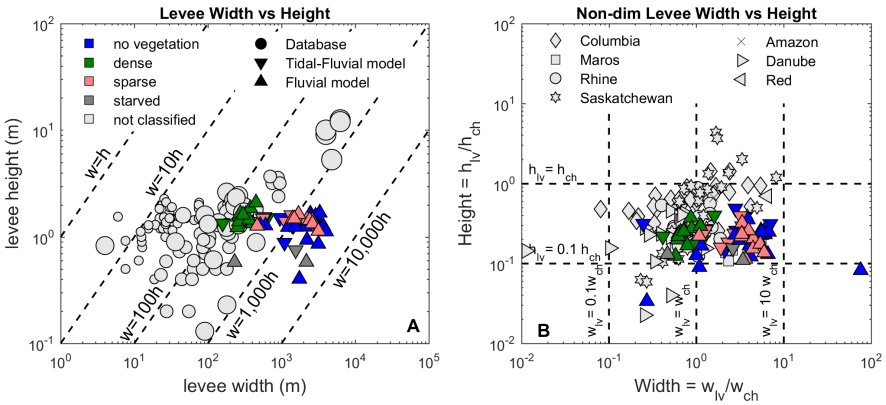

Figure 3.10: Comparison of levee height and width between model and dataset. The model scenarios are subdivided in tidal-fluvial (downward triangle) and fluvial (upward triangle) and color coded by the scenario. The database is displayed in gray, i.e. not classified. (a) The dimensional levee height versus width where the sized symbols for the database (circle) represents mean fluvial discharge values. (b) The non-dimensional height is the levee height divided by the bankfull channel depth and width is the levee width divided by the bankfull channel width.

The non-dimensional levee data from the Columbia and Saskatchewan rivers show relatively high levees and shallow channels compared to our compilation of field and model dataset. These observations agree with the fact that these rivers are rich in silt, anastomosing and multi-thread in pattern (Makaske et al., 2002), unlike the modelled scenarios and the other rivers from our database. The anastomosing character implies complex division of water and sediment discharges through the branches, which is relevant because individual channels tend to fill over time following inactivation (Kleinhans et al., 2012). Hence, levee dimensions from the anastomosing Canadian rivers show larger scatter in respect of channel dimensions, while the Rhine, Maros, Amazon and Danube rivers data agrees relatively well with our model results.

In summary, the best agreement between the measured data and model results comes from the model scenarios including vegetation. The non-vegetated scenarios result in wider levees that are rarely observed in nature nowadays. Those dimensions are comparable to the largest

rivers in the world, however this apparent similarity derives from a much higher water and sediment discharge and not the lack of vegetation.

3.4 Discussion

We self-developed levees and crevasses in a morphodynamic model under comprehensive fluvial-tidal boundary conditions, including the effects of vegetation and broad sediment composition and sorting. With our novel set of scenarios, we unraveled the most important conditions that control levee height and width and the formation of crevasses, and showed how vegetation alters levees, basin dynamics and consequently the overall landscape evolution. Now, we discuss the main findings about levee evolution and dimensions, and the implications for geological reconstructions and future delta management.

3.4.1 Levee development and dimensions

The models show that incipient levee formation occurs when intermediate grain sizes, i.e. silt and fine sands are transported over the channel where bed shear stress diminishes towards the calm floodbasin (Fig. 3.12a), which proves the hypothesized mechanism in Cazanacli and Smith (1998), Adams et al. (2004), Filgueira--Rivera et al. (2007), and Smith and Pérez-Arlucea (2008).

We found that levee formation occurs in two phases: an initial and faster heightening phase when levees grow towards the asymptote of water depth and a slower and more constant widening phase filling the floodbasin. Initially, coarser sediment fractions (e.g. silty sand) are deposited near the channel, contributing to the heightening phase, (i.e. resembling the initial rapid vertical levee growth) (see Fig. 3.4). During the widening phase finer material (e.g. silt) is deposited progressing into clay towards the distal floodbasin. In the absence of these key sediment fractions there is no levee formation and the floodbasin remains relatively flat and filled with clay (Fig. 3.6). In this case, there is not enough sediment transport from the main channel towards the basin to build levees, even with suitable local bed shear stresses (Fig. 3.12e). From our scenarios we conclude that the necessary conditions to create levees are (1) fluvial-tidal (overbank) discharge with high water (flood) levels that provide sufficient accommodation space for levee growth and (2) abundant supply of intermediate grain size fractions.

Levee height depends primarily on the maximum water level induced by tides and floods, given enough sediment availability, while levee width mainly responds to sediment supply (Fig. 3.9). Storms et al. (2005), Smith and Pérez-Arlucea (2008), and Esposito et al. (2017) show the importance of river floods in building levees, similarly to our simulations with variable fluvial discharge. In addition, our results demonstrate that vegetation further controls levee dimensions and overall morphology, including the formation and persistence of crevasses (Fig. 3.11). Vegetated levees are higher and narrower than their analogue non-vegetated scenario (Figs. 3.6, 3.9) as the vegetation reduces sediment mobility and transport (Fig. 3.12b,c), increasing sediment retention (Fagherazzi et al., 2012). To summarize, levee dimensions derive from the 3-way interaction between hydrodynamics, vegetation effects,

and sediment supply. By changing one of the aforementioned elements the resulting levee will be different in its dimensions and composition, or even nonexistent.

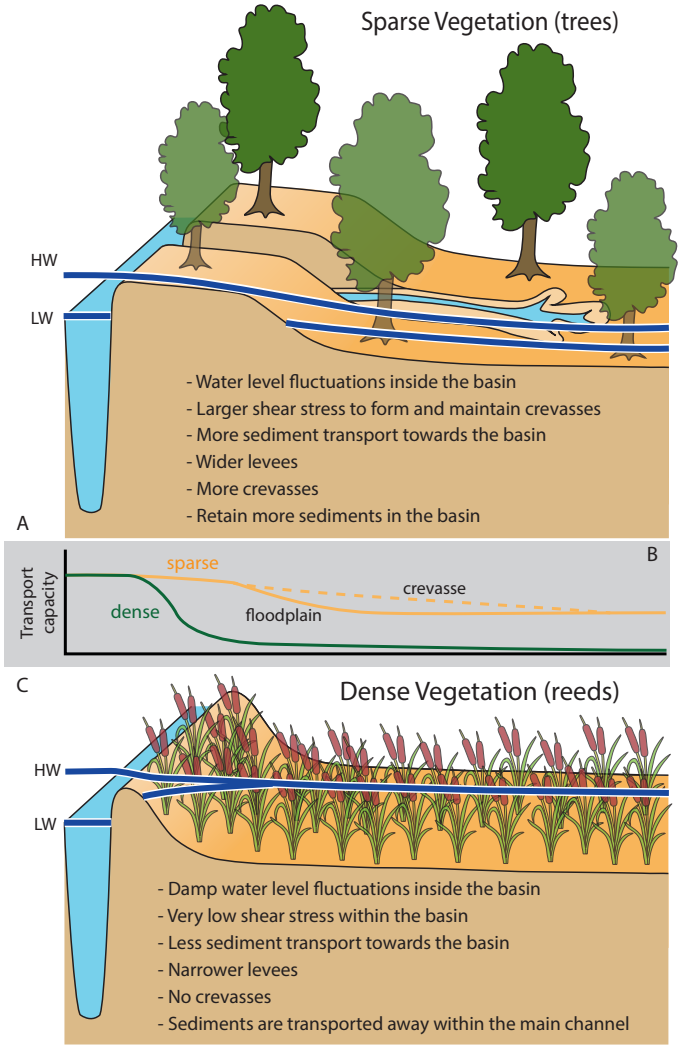

Figure 3.11: Sketch of levee and floodbasin evolution under fluvial-tidal boundary conditions with different vegetation typologies: (a) sparse (trees) vegetation and (c) dense (reeds) vegetation. (b) Sketch of sediment transport magnitude across the levee and floodbasin. Vertical dimensions are exaggerated for better visual representation. The minimum and maximum water levels drawn here were largely based on findings from Fig. 3.7c,d

.

These results partly explain the empirical findings of Cazanacli and Smith (1998) and Adams et al. (2004), who found strongly varying levee dimensions, without a clear relation between levee dimensions, channel size (or discharge) and sediment composition. We

demonstrate that, in addition to these boundary conditions considered by the authors, changes in the hydrodynamics (discharge and water level), vegetation pattern, and sediment supply strongly affect the end-morphology of levees and crevasses. These extra variables, hardly isolated in field studies but systematically explored in our models, may explain some of the scatter found by previous authors. The scatter in levee dimensions holds specifically for the silty-rich anastomosing rivers, such as the Columbia and Saskatchewan (Makaske et al., 2002), where bifurcations and the division of water and sediment discharge are irregular between the multi-thread channels (Kleinhans et al., 2012), leading to stronger variations in levee morphology.

Water level fluctuations driven by river discharge variations and tides further induce the formation of crevasses. Crevasse channels form through breaches in the levee and may establish a stable crevasse splay system. Crevasse channels diverge and focus the flow away from the main channel, and induce higher bed shear stress and sediment transport through the narrow gaps (Fig. 3.12a). After the incipient stage, the bed shear stress keeps the crevasse opened, whilst delivering sediments further into the floodbasin (Fig. 3.12b,d). As such, crevasses play a complex role: they deliver sediment to the distal parts of the levees and the basin, but also reduce unchannelized flow over the levees. The relation between crevasse formation and vegetation is unravelled below and in Figures 3.11 and 3.12.

Vegetation also plays an important role for the formation and persistence of crevasses and crevasse splays (Fig. 3.6). We see that the presence of dense vegetation inhibits tidal propagation and the formation of crevasses, while sparse vegetation triggers more crevasses compared to the reference non-vegetated case (Figs. 3.6, 3.7). Both types of vegetation induce larger water level gradients between the channel and floodbasin, however, the dense scenario induced higher water levels in the basin and therefore reduced the bed shear stress and sediment transport capacity from the channel into the floodbasin (Figs. 3.11 and 3.12c). This combination largely inhibited the formation of crevasses, which was also observed by Nienhuis et al. (2018) who modelled single crevasses, and by Mohrig et al. (2000) from the rock record. Now we were able to demonstrate the physical mechanism responsible for both the absence, and the inception and maintenance of crevasses. In contrast to dense vegetation, the sparse vegetation created higher water levels in the channel with respect to the basin, maintaining sufficient water flow, shear stress and sediment transport (Fig. 3.12d). This resulted in more crevasses along the levees in comparison with the same scenario without vegetation and dense vegetation. These results are confirmed along the Old Rhine system when reed peat was present in the landscape (Fig. 3.1f, Stouthamer, 2001; van Dinter, 2013; de Haas et al., 2019). As in our modelled scenarios, crevasses along the Old Rhine only appeared when wood peat (sparse vegetation) became dominant over denser reed vegetation (Pierik et al., *in prep.*). Because of these different tidal basin infilling modes, we conclude that vegetation not only affects levee and crevasses morphology, but also the infilling of an entire estuary. In contrast, dense plants on the floodbasin reduce the overall tidal prism, basin dynamics, flow velocity, bed shear stress and sediment transport which inhibits the formation and evolution of crevasses (Figs. 3.7, 3.11, 3.12b-e and Nienhuis et al., 2018).

Although we include only two end-members of vegetation (i.e. dense and sparse) fully covering the floodbasin, this approach clearly shows the isolated effect of these major veg-

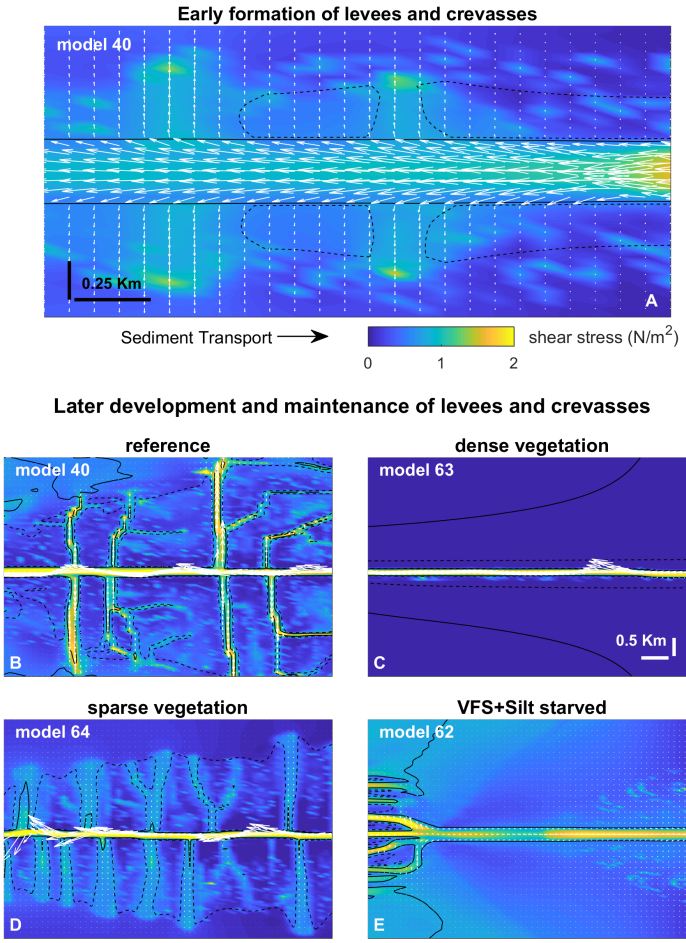

Figure 3.12: Mechanism of levee and crevasse formation and maintenance. Model scenarios are the same from Fig. 3.6. The plots consist of the maximum bed shear stress over a full tidal cycle (color maps), and tidally integrated (i.e. net) sediment transport (arrows). The channel-directed (U-component) sediment transport was reduced to 25% while the basin-directed (V-component) was increased by 50% for visualization purposes. The solid black line depicts the depth contour of the main channel and larger breaches, while the dashed lines represent the levees and the smaller breaches. (a) Early levee development from the reference scenario and the simultaneous formation of crevasses. Note the higher bed shear stress focused between the levee sections (dashed lines), and the sediment transport being diverted from the main channel. (b-e) later stage of levee and crevasse maintenance. These maps are based on the bed evolution stage shown in Fig. 3.6a-d.

etation typologies found in nature (see Figure 3.1 and Cazanacli and Smith, 1998; Adams et al., 2004; van Dinter, 2013). In reality, vegetation assemblages are patchier and more dynamic, with competition and succession between species (Silvestri et al., 2005). Therefore, we expect that dense vegetation creates higher and narrower levees, which could in turn trigger more crevasses due to the weaker geotechnical nature of such narrow and high levees (analogue to the superelevation in Mohrig et al., 2000). In this scenario, a temporary or local

disturbance of vegetation, e.g. studied in Kirwan et al. (2008), has high potential to start a successful crevasse. However, a densely vegetated floodbasin reduces the likelihood of such crevasses being successful as the breach tends to be quickly filled due to the limited water and sediment discharge through the crevasse towards the dense vegetated floodbasin (Fig. 3.12b), also demonstrated in Nienhuis et al. (2018). In fact, both scenarios and hypotheses are valid depending on the dynamics of vegetation, e.g. perennial versus ephemeral, spatial distribution, and the timing of events. For the latter, a reset of vegetation after winter, floods or drought, plays a different role compared to an upstream avulsion into a well established pre-vegetated (or peated) land, i.e. reoccupation of paleochannels (see Stouthamer, 2005). This dynamic behavior of vegetation and biota, including settling, growth, organic accumulation, and mortality is beyond the present scope but should be considered in future projects insofar it affects the location, distribution and density of vegetation (Kirwan et al., 2008; Marani et al., 2013; van Maanen et al., 2015; D'Alpaos and Marani, 2016; van Oorschot et al., 2017; Kleinhans et al., 2018; Lokhorst et al., 2018; Brückner et al., 2019) and the formation of peat.

Therefore, congruent to observations from Tal and Paola (2007), Davies and Gibling (2011), and McMahon and Davies (2018), the character of the vegetation and other biota controls the large scale landscape, for example, between braiding and meandering rivers end-members. Here we show that vegetation affects levee dimensions, especially width, and the overall levee evolution including the formation of crevasses. The best agreements between measured levees and our models are found when vegetation is included in the modelled scenarios (see Fig. 3.10). The non-vegetated scenarios create rather wide levees of similar dimensions to rivers much larger than our modelled discharge and sediment load.

3.4.2 Implications for interpreting geological records

Levees are acknowledged to have low preservation potential in the geological record (Brierley et al., 1997). Moreover, levees, crevasses (splay), overbank and floodbasin deposits have similar lithological signatures, which are difficult to identify in geological records (Brierley et al., 1997; Burns et al., 2017; Burns et al., 2019). This holds for more distal levees, where levee signature can be mixed with floodbasin, and also for levees that are disturbed by crevasses and other (tidal) channels (see Fig. 3.4 and Burns et al., 2019). Overbank deposits may extend beyond the scale of outcrops, which makes it challenging to recognize them in the field. Furthermore, similar lithological signatures identified in the field may have formed under different combinations of fluvial-tidal boundary conditions, i.e. the concept of equifinality (Figs. 3.4, 3.5). Hence, due to this challenge with interpretation, levees might be under-reported in the geological rock records. Once identified, difficulties remain in genetic interpretation, i.e. to explain the variations in sedimentology and stratigraphy either by changing boundary conditions (allogenic) or by internal variation (autogenic) (e.g. Stouthamer and Berendsen, 2007; Shiers et al., 2014; Shen et al., 2015; Hein et al., 2016; Ishii et al., 2016). This means that recognizing levees in geological records and inferring past boundary conditions from them is not straightforward. Therefore, the discussion of their presence, forming conditions and influence on morphology is essential to aid reconstructions.

The large-scale effects of vegetation on fluvial-tidal levee formation identified in this paper are relevant, if not essential, to the reconstruction and interpretation of ancient fluvial-tidal systems. Vegetation dampens the tides and hence controls the tidal influence on the deposits (Figs. 3.6, 3.7). Therefore, variations in overbank deposits, observed in the geological record, may reflect local vegetation variations instead of changes in boundary conditions offshore or from upstream rivers (Esposito et al., 2017; Burns et al., 2017). The same is valid for sequences of peat and inter-fingering crevasse and levee deposits, which might well be self-organizing features rather than forced by different boundary conditions (in line with e.g. Shen et al., 2015). Here we show that dense pioneer-riparian species affect the geomorphology and morphodynamics in several ways. Firstly, dense vegetation inhibits levee widening and crevasse formation. Secondly, it can dampen offshore tides to such an extent that the floodbasin resembles a fluvial-dominated system (Fig. 3.6b). These findings are summarized and illustrated in Figure 3.11. This second effect has long-term consequences for a succession from a tidal environment to a fresh water wetland or peat under constant boundary conditions.

We see these contrasting model scenarios (Fig. 3.6) mirrored in the fate of Holocene Dutch estuaries, some of which filled up and some of which remained open (Vos, 2015; de Haas et al., 2018). The key contrasting conditions between tidal inlets on the western coast of the Netherlands, including the Old Rhine, and the Wadden Sea are (1) the history of marine-fluvial sediment supply, (2) the abundance of vegetation and peat, (3) tidal basin shape and orientation affecting local generated wind-waves (Beets and van der Spek, 2000; Vos, 2015). The factor which causes the difference in morphology is that the Rhine-Meuse rivers supplied water and sediment discharge to the Old Rhine and Meuse estuary from the landward side (Vos, 2015; de Haas et al., 2018; de Haas et al., 2019). The freshwater supply was conducive to peat formation. The model results corroborate the theory that sediment supply and vegetation or peat growth are the main causes of infilling in basins and estuaries (Kirwan and Murray, 2007; Esposito et al., 2017; de Haas et al., 2018; Donatelli et al., 2019). On the other hand, the Wadden Sea system had no large sediment input, so the lack of both sediment and vegetation allowed tides and local wind waves to keep it open for longer time periods, similar to e.g. Marani et al. (2007), Mariotti and Fagherazzi (2010), Marani et al. (2011), Mariotti and Canestrelli (2017a), Nardin et al. (2018), Deng et al. (2018), and Donatelli et al. (2019).

In summary, the fate of estuaries can be explained by the two-way interaction of sedimentation facilitating vegetation to settle in shallower grounds and vegetation retaining more sediments. The shallow vegetated areas combined with sediment delivery reduce the hydrodynamics, including the tidal prism and the dissipation of local generated waves. This infilling feedback loop progressively reduces the basin dynamics allowing more deposition (Fig. 3.8).

3.4.3 Considerations for future delta and estuary management

Understanding the complex interplay between fluvial-tidal boundary conditions, sediment delivery and the presence of vegetation enlightens the future management of low lying areas. For example, the maintenance of water and sediment discharge is essential for infilling the accommodation space created by future expected accelerated sea level rise (e.g. D'Alpaos

et al., 2007; Kirwan and Murray, 2007). We show that vegetation may be beneficial in retaining sediments (Kirwan et al., 2008; Fagherazzi et al., 2012; Belliard et al., 2016; D'Alpaos and Marani, 2016; Esposito et al., 2017), creating levees and crevasses that acts as sediment conveyors (Figs. 3.6, 3.11, 3.12 and Nienhuis et al., 2018), while reducing the tidal prism and facilitating more quiet conditions, required for sediment deposition (Fig. 3.7 and Braat et al., 2019; Brückner et al., 2020). Even when sediment supply is too low to fill basins entirely, sedimentation corridors (e.g. crevasses) along channels may be an attractive way to distribute sediments that contribute to land rise. When building artificial levees that are never or rarely flooded, most sediments are carried downstream via main channel, and do not contribute to land level rise on the low-lying floodplains that used to benefit from it before the dikes and flood control measures were implemented. Our scenario with dense vegetation shows that the basin remains rather starved, but we expect that organic growth, not incorporated in our model, can still contribute to rise the bed level locally (Mariotti and Canestrelli, 2017a).

Although this seems straightforward, we demonstrate that a sediment starved system can enter an enlarging (erosional) positive feedback in the presence of tides, where the tidal prism grows in respect of the accommodation space (Fig. 3.8). Similar evolution has been observed by Marani et al. (2007) for the Venice Lagoon along the 20th century and by Eslami et al. (2019) on the Mekong Delta. This is an undesirable end situation for low-lying deltas and estuaries, because it will lead to land drowning. Therefore, human interventions such as the construction of artificial levees, river damming, sand mining and water intake, are severe threats to the future sediment budget of deltas and estuaries and land rise to counteract sea level rise (Eslami et al., 2019; Dunn et al., 2019). The combination of reducing the water discharge and floods, shortage of sediment supply and the sediment trapping in upstream dams are dooming several deltas (Syvitski et al., 2005; Nienhuis et al., 2020) and lowlands to be lost in the near future unless intensive (and expensive) engineering measurements are deployed (e.g. Louisiana and Authority, 2012).

Observations of the Holocene systems (Blum et al., 2003; Törnqvist et al., 2004; Vos, 2015) and more recent deltas (Nienhuis et al., 2020) have shown that a sediment surplus, inorganic and organic, combined with vegetation can overcome relative sea level rise and erosion from tides and waves. Complementary to the aforementioned studies, our modelling elucidates the mechanisms by which sediment supply, and vegetated levees-crevasses efficiently distribute and retain sediments to promote land level rise. Thus, by allowing levee and crevasse splay growth at strategic spots, high ridges can form in the landscape that protect drowning floodplains from storms (Temmerman et al., 2013; Giosan et al., 2014) and future sea level rise. Instead of providing a holistic solution to land loss, our results and model developments can help to guide the management of overbank discharges (floods), and sediment supply in combination of vegetation to restore the natural evolution of tidal basins and estuaries while adding value for flood safety.

3.5 Conclusion

The morphodynamic models presented here shows, in isolation and combination, the main effects of fluvial-tidal boundary conditions, sediment supply and the presence of vegetation in creating levees, crevasses and the overall estuary geomorphic evolution.

Levees grow in height and width when provided with key sediment size fractions, namely, fine sands and silt, (overbank) fluvial-tidal discharges and sufficient accommodation space. We found that maximum levee height is limited by water level fluctuations induced by tides and floods, while sediment supply and fluvial discharge control their lateral expansion. In general, the combined effect of river and tides creates higher and wider levees as well as trigger more crevasses when compared to fluvial conditions alone. We furthermore show that intermediate grain sizes, e.g. silt and very fine sand, are a prerequisite for levee formation. Otherwise mud fractions spread over the floodbasin without a clear morphological separation from the main channel.

Our model scenarios demonstrate the mechanisms by which vegetation controls the dimensions and the evolution of levees-crevasses and hence entire estuary morphodynamics. In general, vegetation creates higher but narrower levees when compared to the analogue non-vegetated scenario. Depending on the type of vegetation, the effect of plants on the morphodynamics is to inhibit crevasses (dense vegetation) or to trigger more crevasses (sparse vegetation). In addition, vegetation reduces the tidal prism and accommodation space within the basin, ultimately shifting the tidally dominated system towards a fluvially dominant state. Here we showed that even with offshore tidal conditions, the levee ended up fully connected to the barrier island, unlike the other tidal scenarios. This levee connection isolated the floodbasin from the main tidal-fluvial dynamics, which mimics what happened with the Old Rhine in The Netherlands during the Holocene. More importantly, this transition from tidal to fluvial dominated environment was induced solely by the presence of vegetation, allowing levee expansion further downstream, and not by a change in boundary conditions such as tidal or fluvial discharge. This example shows the importance of considering the effects of biota in geological reconstructions as well as its importance for forecasting future scenarios.

These findings have implications for future delta and estuary management. The human-induced long-term reduction of fluvial water and sediment discharge, for example through dams and sand mining, are leading to the loss of important coastal environments. Here we show that the natural discharge of water in combination with abundant sediment supply and vegetation is effective in developing levees and crevasses that distribute and retain more sediment into the floodbasin. This process represents a natural mechanism to keep up with relative sea level rise while preventing the loss of important ecosystems.

Acknowledgements

Supported by ERC Consolidator agreement 647570 to MGK. The computer resources were further supported by NWO-SurfSARA project 17635, and Utrecht University Geoscience Eejit cluster. The authors acknowledge the assistance from Edwin Sutanudjaja (UU), Lukas van de Wiel (UU) and Maxime Moge (SurfSARA) to compile and run Delft3D in the HPC Linux clusters. We appreciated the advices of Muriel Brückner on the implementation of vegetation, and the comments from William McMahon, Jana Cox and Jaap Nienhuis on the final draft. Levee dimensions used in this article are available as sup-

plementary material (see ESPL article). Delft3D steering settings from our reference scenario (model 40) are available as supplementary material. Complete data sets and model inputs/results used and/or analyzed during the current study are available from the corresponding author on reasonable request. Delft3D source code is freely distributed and available at the Deltares (SVN) repository:

https://svn.oss.deltares.nl/repos/delft3d/tags/delft3d4/7545.

Chapter 4

Effects of Wave Orbital Velocity Parameterization on Nearshore Sediment Transport and Decadal Morphodynamics

Nearshore morphological modelling is challenging due to complex feedback between hydrodynamics, sediment transport and morphology bridging scales from seconds to years. Such modelling is, however, needed to assess long-term effects of changing climate on coastal environments, for example. Due to computational efficiency, the sediment transport driven by currents and waves often requires a parameterization of wave orbital velocities. A frequently used parameterization of skewness-only was found to overfeed the coast unrealistically on timescales of years-decades. To improve this, we implemented a recently-developed parameterization accounting for skewness and asymmetry in a morphodynamic model (Delft3D). The objective is to compare the effects of parameterizations on long-term coastal morphodynamics. We performed simulations with default and calibrated sediment transport settings, for idealized coastlines, and compare the results with measured data from analogue natural systems. The skewness-asymmetry parameterization was found to predict overall stable coastlines within the measured envelope with wave-related calibration factors within a factor of 2. In contrast, the original parameterization required stronger calibration, which further affected the alongshore transport rates, and yet predicted erosion in deeper areas and unrealistic accretion near the shoreline. The skewness-asymmetry parameterization opens up the possibility of more realistic long-term morphological modelling of complex coastal systems.

Published as: Boechat Albernaz, M., Ruessink, R.B., Jagers, H. R. A., Kleinhans, M.G. (2019), Effects of Wave Orbital Velocity Parameterization on Nearshore Sediment Transport and Decadal Morphodynamics, *Journal of Marine Science and Engineering*, 7(6), 188, DOI: 10.3390/JMSE7060188.

4.1 Introduction

As deep-water linear waves approach shallow coastal zones they begin to interact with the bottom and change their shape and orbital motion towards the shoreline. Along the propagation path, non-linearities arise with the waves first becoming skewed with a shorter, higher crest and longer shallower trough, and, in the shallow surf zone, gradually changing into asymmetric waves with a saw-tooth shape, pitched forward with a steep front and gentle rear (Elgar and Guza, 1986). This process modifies the near-bed orbital velocities, which impacts the sediment transport and long-term, large-scale morphological evolution, here defined as years to decades covering kilometers. The wave shape transformation can be fully computed by means of phase-resolving models (Zijlema et al., 2011; Malej et al., 2015); however, this requires large computational efforts, restricting simulations to hydrodynamics-only scenarios of small temporal-spatial scales (*O* hours-meters). Therefore, for reasons of computational efficiency, the wave shape transformation and orbital velocities are often parameterized in phase-averaged morphodynamic models. Nonetheless, the parameterization effects starting from the hydrodynamics of orbital motion up to long-term morphological evolution remain highly uncertain. Small deviations in orbital velocities between parameterizations combined with non-linear response of sediment transport makes morphological predictions rather uncertain and ultimately inaccurate over such long time-scales. Yet this is a societal relevant scale for coastal protection by sediment management in view of climate change and sea level rise (van der Spek and Beets, 1992; van Rijn, 1995; Beets and van der Spek, 2000).

Various parameterizations have been proposed and implemented in the past decades, for example, non-linear wave theories such as Second (or higher) Order Stokes (Stive, 1986; Dean and Perlin, 1986), Stream Function (Rienecker and Fenton, 1981) and the hybrid theory of Isobe and Horikawa (1982) that combines 3^{rd} Cnoidal and 5^{th} Order Stokes. These and other theories are compared in Dean and Perlin (1986). In general, the parameterizations derived from scaled physical experiments reproduce only skewness (velocity skewness) and acknowledge that asymmetry (acceleration skewness) is not accounted for (Isobe and Horikawa, 1982; Stive, 1986) and consequently predictions for shallower nearshore dynamics are rather inaccurate.

Cross-shore morphodynamic models of varying complexities account explicitly for physical processes coupled to sediment transport predictors in order to simulate nearshore dynamics. Wave non-linearities are incorporated through one of the aforementioned methods (e.g. Roelvink and Brøker, 1993; van Rijn et al., 2003). Although cross-shore models have mainly being applied to hindcast nearshore sandbar behaviour in short time spans (*O* hours-days), a few attempts to simulate mild energy conditions on longer time scales have been reported (van Rijn et al., 2003; Walstra et al., 2012). Here, the onshore net sediment transport only occurred when wave non-linear orbital velocities were included, for example with a stream function (Roelvink and Stive, 1989; van Rijn et al., 2003; Ruessink et al., 2007; Walstra et al., 2012) and with the skewness parameterization of Isobe and Horikawa (1982) (van Rijn et al., 2003; Grasmeijer, 2002). In these models the undertow and return currents are the main hydrodynamic contributors to offshore net sediment transport during storms and the short-wave non-linearity mainly contribute to the onshore transport during mild conditions

(Stive, 1986; Roelvink and Brøker, 1993; van Rijn et al., 2003). Whereas the skewness-based models are adequate for simulating sand bar migration in the shoaling and outer surfzone, their performance in the inner surfzone and near the shoreline, where skewness decreases while asymmetry increases, was poor, mainly due to the overestimation of sand transport towards the shoreline (van Rijn et al., 2003; Dubarbier et al., 2015). Recently, a parameterization including skewness and asymmetry was derived from comprehensive field data (Ruessink et al., 2012). The application of the Ruessink et al. (2012) parameterization in a cross-shore model (Dubarbier et al., 2015) demonstrated that neglecting the asymmetry led to poor performance. This could partly be compensated by enhancing skewness but resulted in unrealistically large deposition in the inner surfzone and shoreline displacement. On the other hand, the same model with skewness and asymmetry performed equally well for short-term surfzone sandbar migration without the unrealistic side-effects near the shoreline. Nevertheless, the performance of this parameterization has not yet been studied in the context of long-term morphological modelling.

Despite the acknowledged relevance in the cross-shore models, non-linearities of orbital velocities are not as well represented in process-based area morphodynamic models in depth-averaged (2DH) and three-dimensional (3D) configurations. These models are often intended to simulate complex coastal environments from deep water to the shoreline, including tidal inlets, tidal basins and estuaries that reproduce important features and dynamics between fluvial and coastal processes. By neglecting or oversimplifying the wave-orbital velocity shape, for example with linear wave theory (Warner et al., 2008; Villaret et al., 2013; Bertin et al., 2009) or skewness-only predictors (Nardin and Fagherazzi, 2012; Nienhuis and Ashton, 2016; Luijendijk et al., 2017; Nardin and Fagherazzi, 2018; Tonnon et al., 2018), we jeopardize the reliability of predicting the evolution of these complex environments especially in the long-term. The morphodynamic feedback system of morphology, sediment transport and hydrodynamics is then essentially preset to evolve to non-realistic equilibrium situations. In addition to the wave parameterization, 2DH models lack vertical processes, such as undertow and have relatively coarser grids when compared to purely cross-shore models. Therefore, these vertically distributed hydrodynamic processes in the cross-shore direction need to be (over)compensated for this limitation, which is commonly done by reducing the onshore sediment transport to a certain factor, by means of sediment transport linear calibration factors, to balance the lack of offshore component (Grunnet et al., 2004; Briere et al., 2011).

By (over)calibrating the sediment transport, a mismatch may arise along depth strata and between cross-shore and alongshore sediment transport rates and associated morphological timescales. As a consequence, studies had to focus on either cross-shore (e.g. Briere et al., 2011; Nardin and Fagherazzi, 2018) or alongshore processes (e.g. Grunnet et al., 2004; Luijendijk et al., 2017); or prioritize the lower-mid or upper shoreface morphological performance (van Rijn et al., 2003; Ruessink et al., 2007; Walstra et al., 2012). Consequently, a model calibrated to match alongshore transport rates can wrongly predict shoreline retreat or progradation and vice-versa. This is an important limitation for model studies of mixed environments, such as ebb deltas, tidal inlets and estuaries wherein tidal bars and shoals form through interaction of combined fluvial, estuarine and coastal waves and cur-

rents. As a result, limited attempts have been made in simulating long-term morphology in these conditions. Most models either focused on long-term simulations without waves or only accounting for low energetic wave conditions aiming sediment stirring (Storms et al., n.d.; Edmonds and Slingerland, 2010; Guo et al., 2015; van der Vegt et al., 2016; Braat et al., 2017; Geleynse et al., 2011) or short-term simulations (Grunnet et al., 2004; Bertin et al., 2009; Nahon et al., 2012; Nardin and Fagherazzi, 2012; Olabarrieta et al., 2014; Nienhuis et al., 2016; Nienhuis and Ashton, 2016; Tonnon et al., 2018; Luijendijk et al., 2017).

The hypothesis in this paper is that an important component of the overall nearshore sediment balance and morphological evolution in 2DH models derives from a more reliable parameterization of near-bed orbital velocities induced by wave skewness and asymmetry (Ruessink et al., 2007; Dubarbier et al., 2015). If implementation improves performance in long-term morphological modelling, then that would open up the possibilities to model mixed environments. Therefore, our aim is to compare long-term sediment transport and morphodynamic development in a 2DH area model with near-bed wave orbital velocities parameterized with a skewness-only method (Isobe and Horikawa, 1982) with a skewness and asymmetry formulation (Ruessink et al., 2012). We applied a comprehensive set of wave climates at two idealized coasts based on coastal sites in The Netherlands and USA, including locally generated short waves and swell conditions. Our assessment targets long-term nearshore profile equilibrium conditions in the cross-shore and the analogue response in the alongshore direction under varying parameterizations and sediment transport calibration scenarios. The morphological developments are compared with long-term measurements of cross-shore bed evolution.

4.2 Methods

To assess the morphodynamic performance of a skewness-only short-wave parameterization versus a skewness and asymmetry formulation, we implemented the Ruessink et al. (2012) parameterization into Delft3D which already contains, as default, the skewness-only Isobe and Horikawa (1982) formulation. Delft3D is an extensively applied morphodynamic model of finite differences, solving the momentum and continuity equations for unsteady shallow-water flow in depth-averaged or three-dimensional mode through the Navier-Stokes equation with hydrostatic pressure approximation (Deltares, 2017). The hydrodynamics are coupled with the SWAN (*i.e.* DELFT3D-WAVE) spectral wave model (Booij et al., 1999; Ris et al., 1999).

The equations from Ruessink et al. (2012) (further referred to as RUE) were embedded into the source code (Deltares, 2020, FLOW2D3D version 6.02.13.7658 from tag 7545) as an alternative to the currently operational Isobe and Horikawa (1982) method (referred to as IH), modified by Grasmeijer (2002) and van Rijn (2011). The near-bed orbital velocities are coupled with the TRANSPOR2004 (henceforth called VR04) sediment transport predictor (van Rijn et al., 2004; Deltares, 2017). We elected to use VR04 because it is well-calibrated on a wide range of environments computing current and wave-related sediment transport, including interaction between wave-current and intra-wave sediment transport and concep-

tually separates bed and suspended load for current and waves (van Rijn et al., 2004; van Rijn, 2007a; van Rijn, 2007b; van Rijn et al., 2007).

Below we describe the orbital velocity parameterization of IH and RUE, the sediment transport predictor, and the setup of the numerical models including the initial and boundary conditions and applied wave climate at Katwijk, The Netherlands and Duck, North Carolina, USA.

4.2.1 Parameterization of wave shape and orbital velocity

The near-bed orbital velocities are parameterized in IH and RUE based on the local root-mean-square wave height (H_{rms}), peak period (T_p) and water depth (h). The IH method after modifications from Grasmeijer (2002) and van Rijn (2011) computes the wave shape and skewed orbital velocities from a hybrid wave theory combining a fifth-order Stokes and third-order cnoidal wave theory derived from laboratory experiments. The RUE method computes skewness and asymmetry derived from the Ursell number (Ur), and the resulting wave shape follows from Abreu et al. (2010). The RUE parameterization applies a functional fit to compute Skewness (Sk) and Asymmetry (As) based on extensive field measurements in contrast with previous methods, including IH, based solely on limited physical experiments. The IH method does not explicitly compute Sk and As, therefore we applied simple skewness (R_u) and asymmetry (R_a) coefficients, based on predicted peak velocity and acceleration values, respectively

$$R_u = \frac{u_{on}}{u_{on} + |u_{off}|} \quad \text{and} \quad R_a = \frac{a_{on}}{a_{on} + |a_{off}|} \quad . \tag{4.1}$$

Here, u_{on} is the peak onshore and u_{off} offshore orbital velocity in m/s; a_{on} is the maximum onshore and a_{off} offshore a_{off} acceleration in m/s^2. Coefficients larger than 0.5 represent deviations due to non-linearities. Below we review the basic concepts of each formulation while detailed equations are provided in Appendix B.

Isobe Horikawa [IH]

The original formulation of Isobe and Horikawa (1982) parameterizes the wave shape and orbital velocities based on the offshore wave height and period, local water depth and bed slope without explicitly quantifying skewness. In order to be implemented in numerical models, this original formulation was adapted by Grasmeijer (2002), also based on physical experiments, to compute the peak orbital velocities u_{on} and u_{off} with local wave height and period, but without the bed slope dependence. In Delft3D-VR04 the adapted version of Isobe and Horikawa (1982) and Grasmeijer (2002) is implemented as default in order to calculate the intra-wave orbital velocity $u(t)$ within the wave period (van Rijn, 2011). In summary, we can describe the steps of IH parameterization as follows. First, based on H_{rms}, T_p, h, IH introduces an empirically derived non-linear parameter for calculating the maximum onshore

directed velocity u_{on}; and the maximum offshore velocity u_{off} is indirectly calculated based on the amplitude velocity U_w. From the relative ratio of u_{on} and u_{off}, the onshore (T_{for}) and offshore period (T_{back}) are estimated. The velocity profile is then derived separately for onshore ($0 < t < T_{for}$) and offshore-directed ($T_{for} < t < T$) flows from the intra-wave velocity profile $u(t)$:

$$u(t) = \begin{cases} u_{on} \sin\left(\pi \frac{t}{T_{for}}\right) & \text{for} \quad t < T_{for} \\ -u_{off} \sin\left[\frac{\pi}{T_{back}} (t - T_{for})\right] & \text{for} \quad t \geq T_{for} \end{cases} \tag{4.2}$$

Ruessink [RUE]

The RUE parameterization was derived from extensive field measurements of non-breaking and breaking waves for distinct wave climates and beach typologies (Ruessink et al., 2012). The RUE predictor uses the Ursell number (Ur) and empirically derived coefficients to estimate the Skewness (Sk) and Asymmetry (As). The Sk and As are then used to compute the non-linearity r and φ terms that are used in the intra-wave $u(t)$ relation of Abreu et al. (2010):

$$u(t') = U_w f \frac{\sin(\omega t') + \frac{r \sin(\varphi)}{(1+f)}}{1 - r\cos(\omega t' + \varphi)} \tag{4.3}$$

where $f = \sqrt{(1 - r^2)}$ is a dimensionless factor to match the amplitude of u and U_w, and ω is the angular frequency. In addition, t is modified into t' to ensure $u(0) = 0\ m/s$.

4.2.2 Sediment Transport Prediction

The sediment transport in van Rijn (2007a) and van Rijn (2007b) (VR04) is divided into four components: (1) current-related bed load ($S_{c,b}$); (2) current-related suspended load ($S_{c,s}$); (3) wave-related bed load ($S_{w,b}$); (4) wave-related suspended load ($S_{w,s}$). While we will focus mainly on the wave-related components ($S_{w,b}$) and ($S_{w,s}$), the orbital velocities do affect the current-related transports through the combined shear stress of currents and waves (Soulsby et al., 1993; van Rijn et al., 2004). Rather than providing a detailed review of the VR04 formulation, an overview is given here to guide our interpretations.

The general bed load predictor has similar formulation for waves $S_{b,w}$ and currents $S_{b,c}$:

$$\begin{aligned} S_b &= 0.5\, \rho_s\, d_{50}\, D_*^{-0.3} \left(\frac{\tau'}{\rho}\right)^{0.5} \frac{max(0, \tau' - \tau_{cr})}{\tau_{cr}} \\ &\text{being} \\ \tau' &= \frac{1}{2}\, \rho f'\, u^2 \end{aligned} \tag{4.4}$$

where S_b = instantaneous bed load transport [$kg/m/s$]; ρ_s = sediment density [kg/m^3]; ρ =

fluid density [kg/m^3]; f' = combined wave and current-related friction coefficient [$-$]; D_* = dimensionless particle size incorporating sediment and fluid density and viscosity [$-$]; d_{50} = median sediment grain size [m]; u = instantaneous velocity due to current and waves at reference height [m/s]; τ' = instantaneous grain-related bed-shear stress due to currents and waves [N/m^2]; τ_{cr} = critical bed-shear stress based on the Shields criterion [N/m^2]; For the intra-wave bed load component, S_b uses $u(t)$ derived from IH or RUE to compute the bed-shear stress within the wave period which is then integrated over the wave period to compose the wave-related bed load transport, *i.e.* $S_{b,w} = \int_{t=0}^{T} S_b \, dt$. The inclusion of a critical shear stress for the initiation of motion means that mobility varies with the degree of non-linearity. The VR04 predicts bed load transport in relation with flow velocity to a power of roughly 3 in high mobility, but much higher powers when the instantaneous shear stress (τ') barely exceeds the critical shear stress (τ_{cr}).

The suspended load transport due to waves included in Delft3D (van Rijn et al., 2004; van Rijn, 2007b; Walstra et al., 2007a) is calculated based on the parameterized maximum onshore (u_{on}) and offshore (u_{off}) orbital velocities rather than an intra-wave calculation. Furthermore, wave-induced streaming velocities are included and multiplied by the suspended sediment concentration (c) and a phase lag constant f_p, here 0.1

$$S_{s,w} = f_p \left(\frac{u_{on}^4 - u_{off}^4}{u_{on}^3 - u_{off}^3} + u_s \right) \int_a^{3\delta_s} c \, dz \tag{4.5}$$

where $S_{s,w}$ = suspended load due to waves [$kg/m/s$]; u_s = wave-induced streaming velocity near the bed; a = reference height [m]; δ_s = wave boundary layer thickness [m].

The current-related suspended load $S_{s,c}$ is computed by the advection-diffusion equation, using bed-shear stress and eddy viscosity to calculate reference sediment concentration by a relation coupled to the bed load, the concentration profile above the bed and flow velocities as the advection term (van Rijn et al., 2004). For calibration purposes, each transport component is multiplied by a user-specific value, with one being the default value.

4.2.3 Numerical Modelling

Numerical modelling in Delft3D was applied to two well-studied complementary coasts: (1) Katwijk - The Netherlands and (2) Duck, NC - USA. Those locations comprise long-term data of beach profiles and wave measurements in two different wave climates. Duck on the East Coast of USA represents oceanic wave conditions with swell and locally generated wind-waves, while Katwijk on the Central Dutch Coast, facing the semi-enclosed North Sea, has locally generated sea waves only. Rather than a direct and strict comparison with measured data, these contrasting cases are used to study model behaviours and long-term results. The most important indicator of model behaviour will be the long-term morphological development as a result of net sediment transport trends in comparison with the measured envelope of morphology over the past decades.

The simulations target the nearshore coastal evolution dominated by wave action on a timescale of decades. Over this time, the morphology will be considered in quasi-equilibrium

conditions with variations within a bed level envelope. The model will be evaluated on the tendency to develop towards a cross-shore equilibrium condition rather than unrealistic decadal rates of coastal accretion or erosion. In order to make the computational effort feasible, the measured wave climate was reduced to synthetic boundary conditions. In addition, the measured beach profiles were averaged over time and space for the initial bathymetric condition. Tides were included to provide water level oscillations that affect wave propagation and nearshore wave-induced currents. Below we describe the modelling scenarios, the initial beach profiles, wave climate and general model settings.

Modelling Scenarios

To unravel the differences and effects of orbital velocities parameterizations on hydrodynamics, sediment transport and long-term morphology we performed 20 model combinations between Katwijk and Duck (Table 4.1; 10 scenarios of IH and RUE). We first performed hydrodynamic simulations without morphological updates (constant bed level profile) for the average wave condition of each site (scenarios 1 and 7; see wave condition 7 in Table 4.2). Here we compared the intra-wave orbital velocities (wave shape), peak velocities u_{on} and u_{off} magnitudes and their difference (Δ *vel*), skewness (Ru) and asymmetry (Ra) coefficients at Katwijk and Duck. We then computed the annual equivalent sediment transport for cross-shore and alongshore directions incorporating the wave climate on a fixed bed for Katwijk and Duck (scenarios 2 and 8). Based on the annual cross-shore integrated sediment transport we defined calibration values, individually for Katwijk and Duck, aiming: (1) shoreline equilibrium by means of equal cross-shore integrated onshore and offshore transport magnitudes and (2) same net cross-shore transport magnitude for IH and RUE in addition of equal net bed load and suspended load within the methods. With default annual cross-shore sediment transport we can assess the sediment budget (balance) differences between IH and RUE and how far they are from predicting shoreline stability, when the onshore and offshore magnitudes should be equal to zero. In addition, we want to define calibration factors for sediment transport when IH and RUE would predict the same amount of onshore and offshore transport (and therefore shoreline stability) as well as bed load and suspended load, as they behave differently. In this way we can compare local differences in morphological evolution for the same amount of sediment transport, when only local sediment gradients differ between methods. Full morphodynamic simulations for the wave climate were performed with default and calibrated sediment transport values for Katwijk and Duck, both on an alongshore uniform bathymetry based on the measurements. In addition, we run a scenario with inverted calibration at Katwijk, when the IH parameterization runs with RUE sediment transport calibration factors and vice-versa. Finally, to assess the effects on the alongshore sediment transport, a scenario with calibrated sediment transport values was run with a coastal hump added on the Katwijk coast. For the hump scenario we choose to run only the calibrated scenarios in order to isolate cross-shore processes, as much as possible, when the hump diffuses based on alongshore sediment transport gradients. Here we assess the volumetric and cross-shore profile evolution of the hump and adjacent areas.

Table 4.1: Overall summary of performed numerical simulations. Wave conditions are described in Table 4.2 being wave 7 the single-averaged wave condition and wave climate refers to all schematized waves (Table 4.2); Default and calibration stand for sediment transport multiplication factors, being default equal to one and calibration values are presented in Table 4.3. All scenarios were performed for IH and RUE parameterizations.

Scenarios		Wave boundary	Bathymetry	Sed. transport	Morphology
1	**Katwijk 1**	single wave	uniform	off	off
2	**Katwijk 2**	wave climate	uniform	default	off
3	**Katwijk 3**	wave climate	uniform	default	on
4	**Katwijk 4**	wave climate	uniform	calibrated	on
5	**Katwijk 5**	wave climate	uniform	inv. calibrated	on
6	**Katwijk 6**	wave climate	hump	calibrated	on
7	**Duck 1**	single wave	uniform	off	off
8	**Duck 2**	wave climate	uniform	default	off
9	**Duck 3**	wave climate	uniform	default	on
10	**Duck 4**	wave climate	uniform	calibrated	on

Initial beach profiles

The initial bathymetry for the Dutch coast is a time-spatial averaged nearshore bed profile (Fig. 4.1a) obtained from the Dutch JARKUS database (Rijkswaterstaat, 2017) near Katwijk. The profiles were measured between 1965 and 2010 along 31 alongshore distributed profiles covering 15 km of coastline from the dunes up to approximately 18 m depth. The average profile has a slope of 1V:185H up to 2.3 m depth, steepening to 1V:63H up to the mean water line. The sediment grain size composition varies between 200 and 350 μm (van Rijn, 1995). A comprehensive morpho-sedimentary description of the Dutch coast is presented in Wijnberg and Terwindt (1995) and van Rijn (1995). Similarly, we averaged profiles from 1997 until 2008 (Fig. 4.1b) at Duck situated north of the Field Research Facility Pier. The beach profile at Duck is steeper than at Katwijk. The average profile has a slope of 1V:120H up to 2.4 m depth, steepening to 1V:25H up to the mean water line. The sediment grain size varies between 125 and 250 μm along most of the submerged profile with a second grain size mode of gravel-sized material near the shoreline (Stauble and Cialone, 1996). An extensive site and data description for Duck is provided in Trowbridge and Young (1989) and Gallagher et al. (1998). As can be seen in Figure 4.1b, the profile was linearly extended from 15 m depth up to the 17 m contour from where the wave data was retrieved. The cross-shore profile covers approximately 5 km at Katwijk and 3.8 km at Duck. From the measured envelopes in Figure 4.1, most morphological activity is constrained between the dunes and the 6 m depth contour at both sites.

The averaged profiles were extended seven kilometers in the alongshore direction creating an initial alongshore uniform bathymetry that suppresses alongshore gradients for the area 2DH models. To study effects of the wave parameterization on alongshore direction, a 3.7 Mm^3 coastal hump was included in further simulations in the Katwijk model setup (Fig. 4.1c; scenario 6). The hump resembles a beach nourishment extending from the dry beach up to approximately 5 meters depth. For analysis, the nearshore area is divided into 3 sections: The central area corresponds to the hump and the other two are the adjacent coasts to the North and South. The computed volumes considered all areas extending from the dry

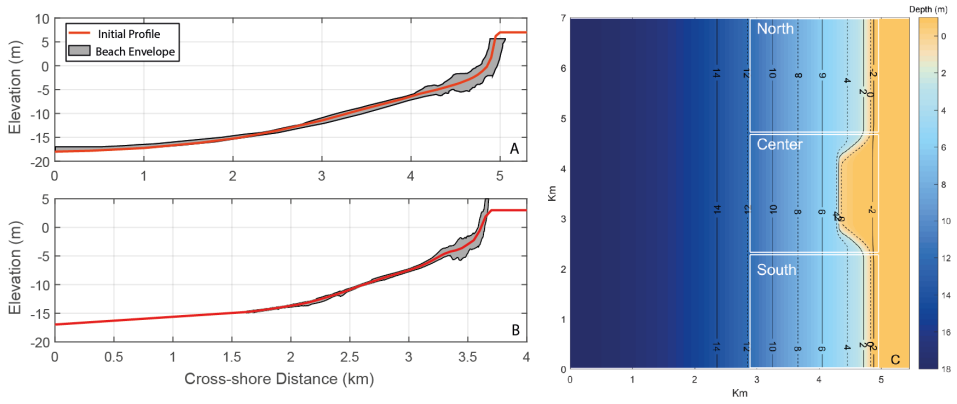

Figure 4.1: Initial time-space averaged modelling bathymetries and measured beach profiles represented as the overall beach envelope. Measured minimum and maximum coastal profile depths (gray) at Katwijk, the Netherlands (a), and Duck, USA (b). The smoothed average bed levels (red) correspond with the maps of uniform bathymetry in alongshore direction and were implemented into the numerical model. (c) Implementation of an idealized coastal hump into the Katwijk Dutch coastal profile.

beach into approximately 12 meter depth contour, enclosing the active beach profile, and therefore the majority of the sediment exchange happens via alongshore transport.

4.2.4 Wave climate

The wave conditions for the Dutch Coast were recorded by the IJmuiden 'Munitiestortplaats' directional buoy in the North Sea between 1990 and 2016. The wave measurements from Duck were recorded by a wave rider buoy (station wvrdr630) from 1997 to 2018. The wave directions were rotated 30° at Katwijk and 161° at Duck, respectively, to realign the waves with our idealized coast based on the local shoreline orientation (Fig. 4.2a,c). Therefore wave directions will be given in this new frame of reference, with 270° implying shore-normal wave incidence.

The wave climate at Katwijk consist of short period waves averaging 4.6 s with 11.7 s maximum. The maximum wave height reaches 7.6 m while the average is 1.32 m. The wave direction has two main components from SW (200°) and NW (310°) but also has a significant frequency of parallel and offshore going waves for 13% of the year. Duck has longer period waves up to 25 s and an average of 8.7 s. The maximum wave height reaches 8.12 m, averaging 0.99 m. The direction has one mode from 300° and limited offshore and parallel going waves summing 1% of the year.

For optimizing computational effort, the original time series were reduced into 13 representative waves following Walstra et al. (2013) and Benedet et al. (2016). The wave reduction consisted of 4 directions and 3 heights plus an average wave condition to replace the duration of offshore and parallel directed waves. The representative wave conditions were obtained by dividing the wave climate into 12 bins of equal energy E, being $E \sim H_s^2$. Then, the average wave period, direction and the total duration were calculated within each bin.

Consequently, one wave condition energetically represents a range (Fig. 4.2b,d), consisting of significant wave height, wave period, wave direction and duration. The reduced wave climate for Katwijk and Duck is shown in Table 4.2, with condition number 7 being the averaged condition to replace the recorded offshore and parallel going waves.

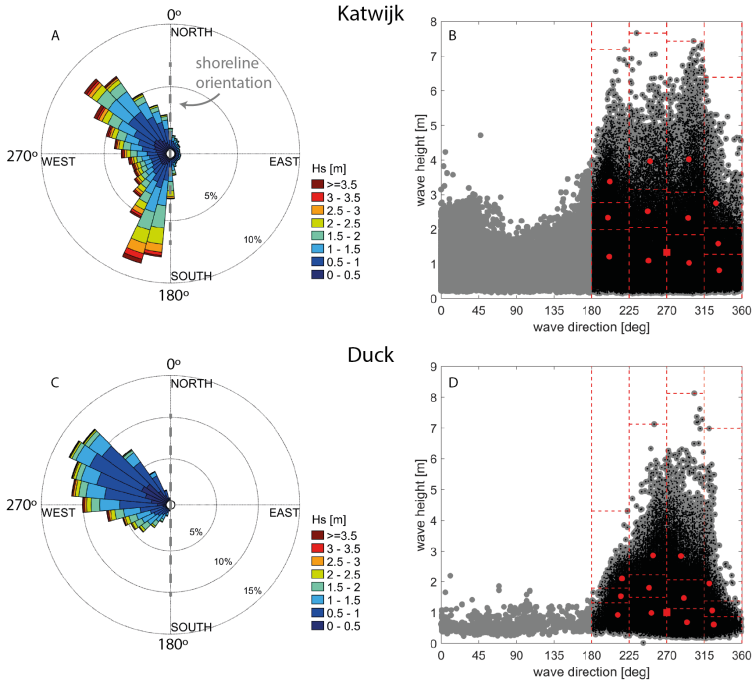

Figure 4.2: Measured and reduced wave climate at Katwijk and Duck. (a,c) Measured wave polar histogram for significant wave height (H_s); (b,d) and the reduction to wave bins for modelling. Data for Katwijk (a,b) recorded at the IJmuiden 'Munitiestortplaats' between 1990 and 2016. Directions were rotated 30° for application in the model domain. (c,d) Data for Duck collected near the FRF Pier from 1997 to 2018 after 161° rotation. (b,d) Measured wave heights (gray) were filtered to selected onshore-directed cases (black). Red lines divide each wave bin into equal energy and red dots are reduced wave conditions that represent the quadrant. The red square represents the average condition in the shore-normal propagation direction. Reduced wave conditions are presented in Table 4.2.

The 13 reduced wave conditions were organized as a constant alternating time-series sequence, following the order from Table 4.2, changing every hydrodynamic hour until its duration was exhausted. In this approach we are constantly changing the wave energy followed by wave direction. While the ordering of wave conditions is known to affect the dynamics of surfzone bars (Walstra et al., 2012; Walstra et al., 2013), the present focus is on equilibrium morphology and large scale sediment transport behaviour. This alternation process ensures that no wave condition perpetuates for too long driving the morphology into an alternative equilibrium.

Table 4.2: Reduced wave climate for Katwijk and Duck to 13 conditions of wave height (H_s), period (T_p), direction (*Dir*, rotated to the model domain) and normalized duration (%). Wave 7 is the average condition that replaces the offshore-directed and shore-parallel wave conditions.

Katwijk - NL					Duck - USA				
Wave	**Hs** m	**Tp** sec	**Dir** deg	**Duration** %	**Wave**	**Hs** m	**Tp** sec	**Dir** deg	**Duration** %
1	1.20	4.1	201	20	1	0.92	4.6	211	4
2	2.34	5.2	200	5	2	1.53	5.5	215	1
3	3.37	6.0	202	3	3	2.10	6.2	216	1
4	1.08	4.2	248	11	4	0.98	7.7	252	18
5	2.53	5.5	247	2	5	1.80	7.7	249	5
6	3.96	6.5	250	1	6	2.87	9.2	254	2
7	1.32	4.6	270	13	7	0.99	8.7	270	1
8	1.02	4.7	297	20	8	0.68	9.8	294	43
9	2.33	5.7	296	4	9	1.47	9.8	291	9
10	4.02	6.9	296	1	10	2.85	11.2	287	2
11	0.81	4.2	333	14	11	0.61	7.2	326	9
12	1.58	4.9	332	4	12	1.06	7.5	325	3
13	2.76	5.9	329	1	13	1.94	9.5	321	1

4.2.5 General Model Configurations

The numerical simulations are depth-averaged 2DH models with cross-shore resolution varying from 50 m offshore to 12.5 m towards the coastline and 50 m on the alongshore direction. The hydrodynamics are coupled with wave conditions computed with SWAN with online communication of bathymetry, waves, currents and water level. In combination with waves, the hydrodynamics for sediment transport are solved in Generalized Lagrangian Mean (GLM) mode to account for wave-induced processes, *e.g.* Stoke's drift (van Rijn et al., 2004).

The propagated wave conditions were coupled with flow every 30 minutes in order to consider the wave-current interaction, wave-induced currents, water level fluctuations due to tides and morphological bed evolution. Based on available tidal records, the tidal water level amplitude was set to 1.0 m at Katwijk and 0.5 m for Duck, both as 12 hour harmonic tides. To avoid undesired boundary effects, the alongshore domain encloses a 7 km long coastline with null gradient Neumann boundary conditions at the cross-shore boundaries.

After sensitivity analysis, not shown here, a constant morphological acceleration factor (morfac) between 10 and 20 was used to speed up the simulations performing in total 10 morphological years. The simulations 3 and 9 were performed with morfac equal to 10; the hump scenarios with morfac equal to 12; and models 4-6 and 10 with morfac equal to 20. These morfac values are similar to those used in other studies (e.g. Grunnet et al., 2004; Nardin and Fagherazzi, 2012; Nienhuis et al., 2016). Sediment transport was limited to depths greater than 0.3 m at Katwijk and 0.4 m at Duck based on the non-dimensional wave period condition $T_p\sqrt{g/h} < 40$, following Ruessink et al. (2007), to exclude swash zone processes. A single sand fraction of 250 μm was applied in all model runs. Other model settings are specified in the Supplementary material.

4.3 Results

4.3.1 Cross-shore Orbital Velocities

The cross-shore distribution of orbital velocities predicted with RUE and IH over the Katwijk and Duck profiles are shown in Figure 4.3a,b,f,g for the average wave condition (scenarios 1 and 7 in Table 4.1; wave 7 in Table 4.2). IH does not explicitly compute Sk and As. For direct comparison between methods we computed skewness (R_u) and asymmetry (R_a) coefficients based on velocity and acceleration, respectively (see eq. 4.1). Here IH consistently predicts higher skewness than RUE, and also predicts skewness in deeper water (Fig. 4.3d,i). For example, the skewness at Katwijk starts around 14 m depth for IH and 8 m for RUE. This effect is more pronounced at Duck where the wave period is larger. At Duck, IH is already skewed from the seaward boundary, at 17 m depth contour, while RUE shows linear behaviour up to 14.5 m depth. RUE predicts lower values of skewness seaward of the surfzone and develops asymmetry towards the surfzone, corresponding to 3 m depth at Katwijk and 6 m at Duck. The intervals asymmetry exceeds skewness correspond with the zone of wave breaking at 1.5 m and 2.5 m depth at Katwijk and Duck, respectively (Fig. 4.3e,j). On the other hand, IH has skewness-only, which increases strongly towards the waterline.

The main effects of the skewness predicted with IH into the orbital velocities and wave shape are twofold: (1) lower offshore directed velocities in comparison with the onshore velocities and (2) the shorter crest period marked by the zero contour line deviating from half of the normalized wave period. For RUE the sinusoidal linear shape persists longer towards the shoreline so that the onshore and offshore peak velocities are of similar magnitudes, deviating when skewness develops during shoaling process and again become nearly equal when asymmetry develops in the surfzone (Fig. 4.3c,h). The peak onshore velocity is similar for both methods except in the very shallow areas where RUE predicts higher magnitudes. This means that the onshore velocities are similar for IH and RUE and the lower prediction of offshore velocities by IH is the main difference concerning the peak velocities.

These effects result from how IH translates the non-linearity into the orbital wave shape. After computing the peak onshore and offshore velocities the wave period is split artificially based on the ratio between (u_{on}) and (u_{off}). The intra-wave velocity is then computed separately for each direction with a sine expression (eq. 4.2). This leads to a discontinuous wave shape for the intra-wave orbital velocity (Fig. 4.4). As a consequence, IH produces larger skewness than RUE, especially for longer period waves as demonstrated in Figure 4.3 at Duck.

4.3.2 Sediment Transport and Morphology on Alongshore Uniform Coasts

The orbital velocities are coupled to VR04 sediment transport via combined current and wave bed-shear stress. For the wave-related bed (eq. 4.4) and suspended load (eq. 4.5), the difference between onshore and offshore velocities is the main driver of cross-shore sediment transport and therefore we consider VR04 a skewness-based sediment transport predictor. For the bed load component, the critical shear stress enhances the non-linear behaviour in sediment transport near the beginning of motion due to the division of excess bed-shear stress by the critical shear stress.

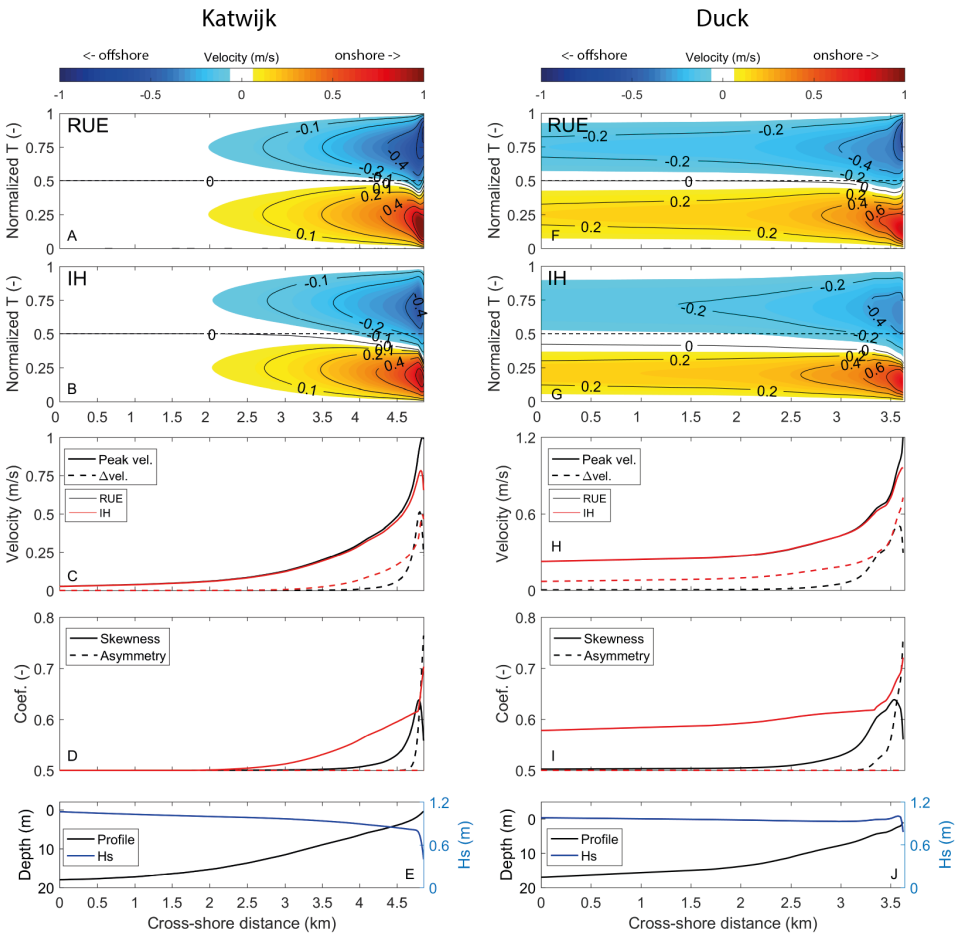

Figure 4.3: Hydrodynamic comparison between RUE and IH behaviour for the average wave condition (Wave 7) along the beach profiles of Katwijk (a-e left) and Duck (f-j right). Orbital velocities (positive onshore and negative offshore) within the wave period T for RUE (a,f) and IH (b,g). (c,h) Peak orbital velocity and the difference between onshore and offshore velocity amplitude $\Delta vel = |u_{on}| - |u_{off}|$, color-coded for RUE and IH. (d,i) Skewness and Asymmetry coefficients. (e,j) Beach profile and significant wave height.

Thus, the relation between flow velocity and sediment transport, in addition of critical shear stress of motion, creates a rather complex relation when adding non-linear oscillatory wave processes. To unravel this phenomena, Figure 4.5 compares the results of sediment transport (combined cross-shore and alongshore) between IH and RUE for each wave condition from Table 4.2 integrated over a tidal cycle. All IH simulations predicted more sediment transport than RUE. The sediment transport factor, defined as IH/RUE, varies from 1 to 3.1, except for the wave-related bed load transport ranging from approximately 3 to 12 with an outlier of 29. In general, the largest deviations between methods derive from small

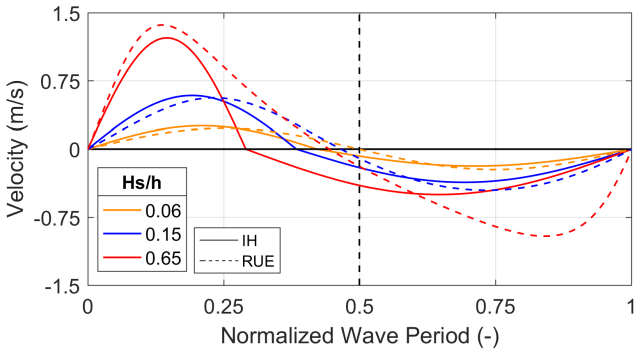

Figure 4.4: Intra-wave velocity profile (wave shape) computed at Duck with IH and RUE along different profile locations from deep (orange) to shallow (red) water represented by the ratio of wave height divided by water depth H_s/h. Positive velocities are onshore directed.

sediment transport values associated with low-energy frequent-duration wave conditions, specially for the wave-related bed load (Fig. 4.5a). To reinforce this trend, the observed outlier corresponds to the average wave condition at Katwijk ($Hs = 1.32\ m$; $Tp = 4.6\ s$) due to a relatively large difference in transport magnitude while the absolute values were small ($1.08x10^{-4}\ m^3$ for IH and $3.72x10^{-6}\ m^3$ for RUE). Therefore, the largest discrepancies between methods derived from situations near the beginning of motion instead of from more energetic (stormy) wave conditions. As these low energetic conditions are predominant in the yearly wave climate, they may result in large deviations for the annual sediment budget.

Cross-shore Sediment Transport

Next we computed the annual equivalent cross-shore sediment transport (scenarios 2 and 8 in Table 4.1) on the alongshore uniform coast applying the reduced wave climate at Katwijk and Duck. First we computed the annual bed load, suspended load and total transport of default sediment transport factors (Fig. 4.6a,b,e,f) and afterwards we defined calibration factors (Fig. 4.6c,d,g,h and Table 4.3) aiming stable nearshore cross-shore profile for the morphological simulations.

At both sites, with default sediment transport settings, the net cross-shore annual bed load (combined of current and wave) is onshore directed while the suspended load is offshore directed. As individual components, not shown here, the wave-related bed load ($S_{w,b}$) and suspended load ($S_{w,s}$) transports are onshore directed while the current-related bed load ($S_{c,b}$) and suspended load ($S_{c,s}$) are offshore directed. The IH simulations shows higher magnitudes for all sediment transport components. The higher onshore-directed bed load leads to an onshore-offshore sediment budget imbalance, which in this case will result in large shoreline accretion, mainly caused by the wave-related bed load component (Fig. 4.6b,f). The annual cross-shore integrated wave-related bed load transport is 4.62 times higher in IH than in RUE for Katwijk and 6.37 times higher for Duck. The wave-related suspended load is a factor of 1.29 and 1.64 higher for Katwijk and Duck, respectively. The choice of orbital ve-

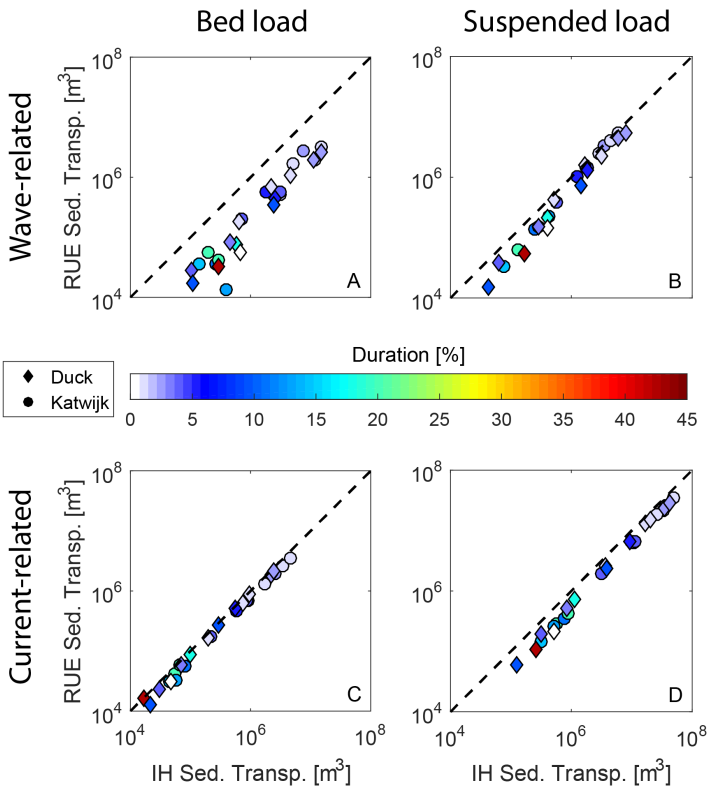

Figure 4.5: Sediment transport computed with default settings for individual wave conditions integrated over the cross-shore profile and tidal cycle for IH and RUE with colors representing the duration of each wave condition in the reduced wave climate. (a) wave-related bed load; (b) wave-related suspended load; (c) current-related bed load; (d) current-related suspended load. The dashed line represents a 1:1 reference.

locity parameterization also affects the current-related transports through the computation of sediment concentration from the combined wave-current shear stress; the current-related bed load was 1.41 times higher and the suspended load 1.37 times higher. After combining the four transport components, the total net cross-shore transport is onshore directed by a factor of 4.8 higher in IH than RUE at Katwijk and 7.8 at Duck.

Table 4.3: Sediment transport calibration factors for Katwijk and Duck for IH and RUE formulation. *w* stands for wave-related; *c* for current-related; *b* for bed load; and *s* for suspended load.

	Calibration Katwijk		**Calibration Duck**	
	IH	**RUE**	**IH**	**RUE**
Fw,b	0.155	0.720	0.112	0.720
Fw,s	0.154	0.200	0.123	0.199
Fc,b	0.709	1.000	0.875	1.000
Fc,s	0.272	0.375	0.228	0.360

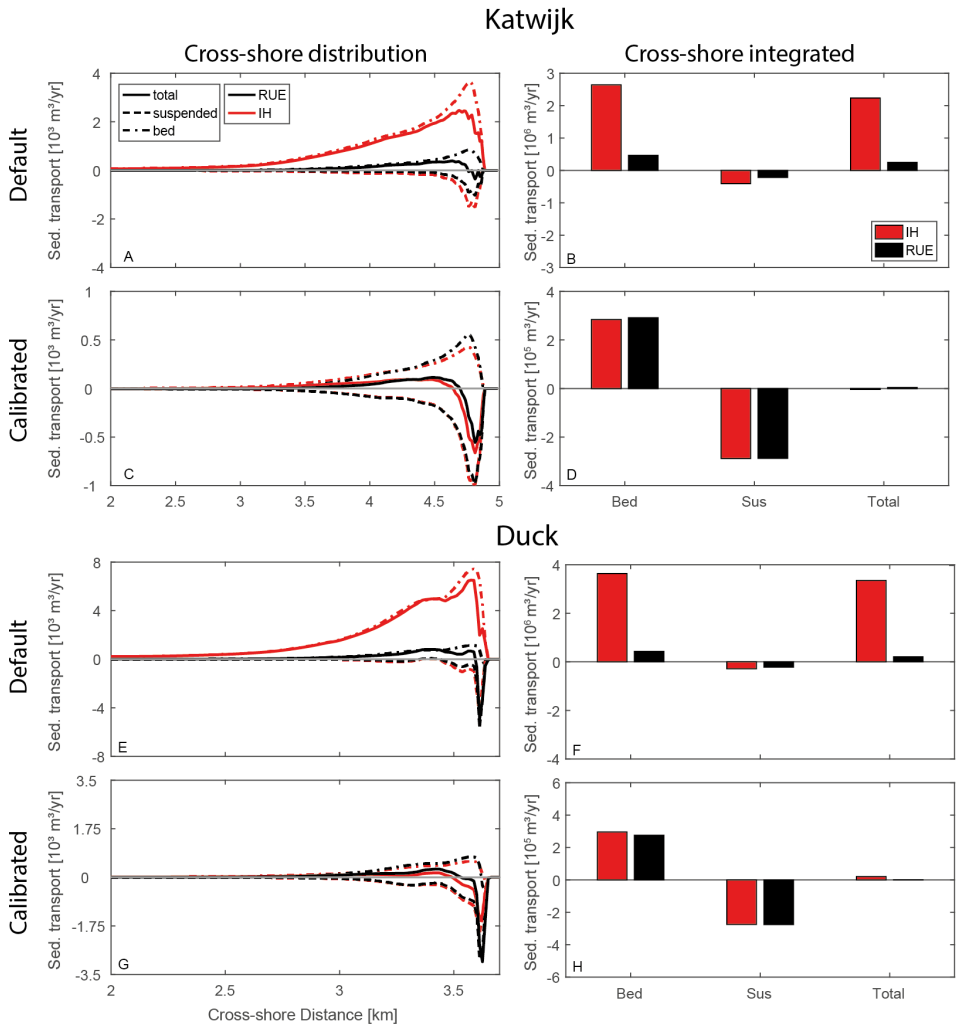

Figure 4.6: Annual cross-shore sediment transport at Katwijk (a-d) and Duck (e-h). Positive values are onshore directed. IH and RUE are color-coded with red and black. Note the difference in vertical axis scale between plots. (a,c,e,g) shows the cross-shore profile of sediment transport and (b,d,f,h) integrates the values in the cross-shore direction. Panels a,b,e,f shows sediment transport values for default sediment transport factors and panels c,d,g,h after calibration is applied (see Table 4.3).

Based on the annually cross-shore integrated sediment transport differences between IH and RUE, we performed a sediment transport calibration to be applied on the morphological models in addition of default value scenarios. Recapping, with this calibration procedure we want to achieve nearshore profile stability, with minimum shoreline translation, and equal total net cross-shore sediment transport between IH and RUE. First, we target the net total cross-shore transport to be zero for each method (*i.e.* IH and RUE). We started keeping

the current-related bed load of RUE equal to one, as it computes the least transport magnitudes (Fig. 4.5c), followed by correcting the wave-related bed load, wave-related suspended load and finally the current-related suspended load. This first iteration achieves the onshore-offshore balance of sediment and a second iteration was made to match the annual total transport between IH and RUE. Applying those calibration factors (see Table 4.3) resulted in equal annual cross-shore integrated magnitudes of bed load and suspended load with net total load nearly zero (Fig. 4.6d,h). Based on the necessary calibration factor to correct sediment transport, the largest differences are found in the wave-related bed load sediment transport, so that the $F_{w,b}$ was reduced to 11.2% and 15.5% of the original magnitude for IH at Duck and Katwijk, while RUE was kept at 72%. The $F_{w,s}$ was similarly reduced around 20% as the wave-related suspended load does not fully account for the intra-wave sediment transport and actually has similar behaviour in direction and magnitude as the wave-related bed load. Finally the $F_{c,s}$ was reduced between 23% and 37% to close the cross-shore sediment budget. After calibration, the cross-shore distribution of sediment transport shows similar shapes and gradients (Fig. 4.6c,g), except in the shallowest areas where we showed deviations starting from the hydrodynamics (Fig. 4.3). Therefore, local morphological variations are expected along the profile, especially in the surfzone and intertidal areas.

Alongshore Sediment Transport

The alongshore directed sediment transport rates were analyzed for Katwijk, only, in order to provide insights on the hump evolution simulated with the same settings. Both IH and RUE methods predict net northward sediment transport at Katwijk. For default sediment transport settings IH and RUE predict $1,320,000\ m^3/yr$ and $915,000\ m^3/yr$ (Fig. 4.7a,b). Thus, IH predicts $405,000\ m^3/yr$ (that is 1.44 times) more net northward sediment transport compared to RUE. The bed load sediment transport factors for waves and currents are 2.0-2.1 and the suspended loads 1.0-1.3. However, after applying the cross-shore based calibration (Table 4.3), IH results in much lower values for the net alongshore transport, namely 73% of reduction from the default value; and 56% of reduction for RUE (Fig. 4.7c,d). In volume, that represents a reduction of $968,200\ m^3/yr$ for IH after calibration while for RUE $517,000\ m^3/yr$. This means that the sediment transport calibration aiming coastal stability forces changes in the alongshore sediment transport with more than a factor of two for IH and slightly higher for RUE. This reduction of littoral drift may affect long-term morphological development, and the timescale thereof, along non-uniform coasts.

4.3.3 Alongshore Uniform Coastal Morphology

Ten morphological years of simulation were performed with default and calibrated transport factors (Fig. 4.8; scenarios 3,4,5,9,10 in Table 4.1). For the default sediment transport simulations at Katwijk, the wave-related transport appears from approximately 12 meters depth upwards. Between 12m and 5m IH erodes the bed creating net onshore sediment transport. As a result, the shallower areas and the shoreline became excessively obese and steep. Simulations with RUE also show net onshore transport, though less than IH, but hardly eroding deeper areas. In comparison to the measured bed profile envelope, IH prediction is outside the envelope from 9 meters depth up to the shoreline while RUE deviates only around the

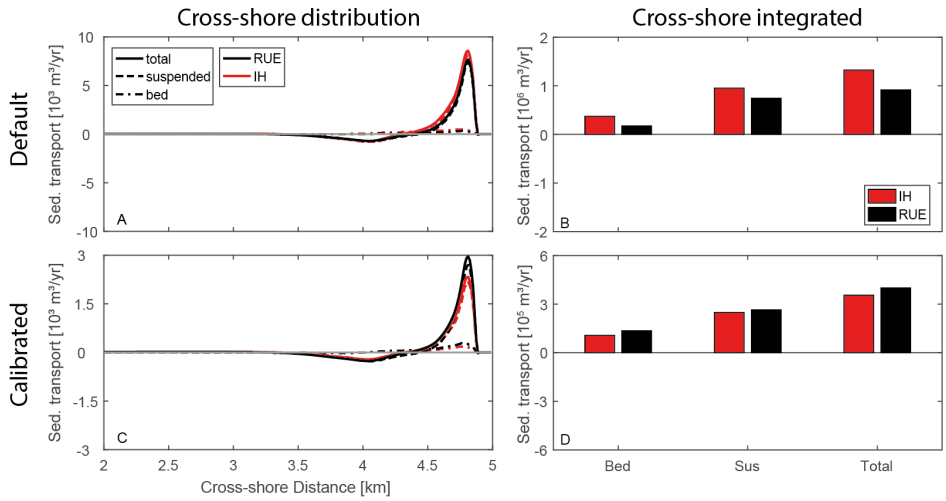

Figure 4.7: Annual alongshore sediment transport at Katwijk. Positive values are northward. Note different vertical axis scales. (a,c) cross-shore profile of net alongshore sediment transport. (b,d) Integrated the values in the cross-shore direction. Panels a,b show default sediment transport values and panels c,d show calibrated IH and RUE (see Table 4.3).

intertidal zone. From the measured profile envelopes we expected most morphological dynamics happening from 6 meters up to the shoreline, therefore, especially IH overestimated the profile changes.

Following calibration, both IH and RUE stayed within the envelope boundaries, with IH showing slightly more deposition in the intertidal shallow area. In addition, the calibration succeeded in balancing the onshore and offshore transport magnitudes towards a stable profile with minimum shoreline translation. The scenarios with RUE factors applied in IH and vice-versa (inverted calibration, scenario 6) show the largest morphological deviations. The RUE simulation with IH factors has the closest fit with the initial (equilibrium) profile which as a first glance suggests the best performance. However it is important to highlight that the extreme lower transport factors applied (see Table 4.3) for wave-related transport (around 10-15%) just shows lower morphological dynamics rather than being the best calibration. On the other hand, IH with RUE predicts the largest shoreline displacement (*i.e.* 290 meters) and large deposition on shallow waters up to 4 meters depth. This extreme case is the combination of high onshore transport rates due to wave-related bed load in addition of the reduced offshore transport caused by the smaller factor on the current-related suspended load. Similar response was observed for Duck (Fig. 4.8b) with a total shoreline displacement of 230 m with IH in comparison with 67 m with RUE for default scenarios. After calibration there is a divergence in the intertidal and subtidal areas up to 2 meters depth where IH results in a larger deposit. At Duck both methods resulted in more erosion on the lower shoaling zone and deposition on the upper shoaling zone and surfzone.

Despite the parameterization choice and calibration factor, there is a general and alike steepening of the shoreface in all simulations, excepted when the wave-related transport was drastically reduced in the scenario of RUE with IH calibration factors.

The combined interpretation of default, calibrated and inverted calibration unravels: (1) the wave-orbital motion and its parameterization highly affects the sediment transport in the nearshore and consequently the morphological development in this area; and (2) how much the (wrong) calibration factors can affect the morphological development, especially for IH that predicts larger onshore transport and therefore is more sensitive to small changes in calibration factors. The wave-related sediment transport is the main driver of nearshore sediment transport, which promotes only onshore sediment transport for the 2DH configuration. This trend ultimately results in disproportional shoreline progradation, when the offshore-directed current-related transport cannot balance this onshore component, in addition of causing shoreface steepening. In this perspective, IH with larger (in our case 4.6-7.8 times higher) onshore transport is more sensitive and prone to calibration, implying that small inaccuracies in calibration factors result in large profile and shoreline translation.

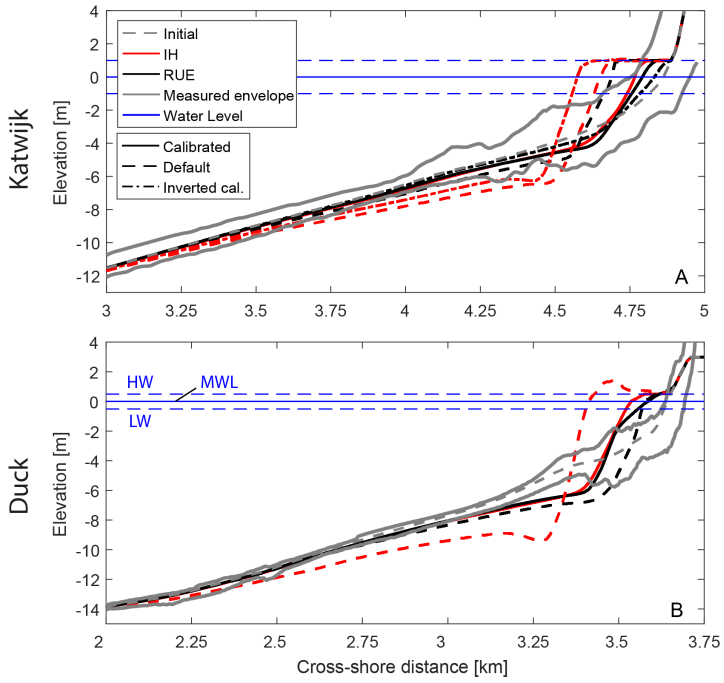

Figure 4.8: Cross-shore bed profiles at (a) Katwijk and (b) Duck after 10 morphological years. Katwijk (a) contains default, calibrated and inverted-calibration scenarios while Duck (b) default and calibrated. Initial and measured envelope are shown in gray, and water levels in blue. IH and RUE are color-coded with red and black.

Finally, we performed morphological simulations with a 'hump' (scenario 6 in Table 4.1) using the calibrated factors (Table 4.3) in order to exclude, as much as possible, cross-shore effects (*i.e.* erosion and deposition leading to shoreline translation) that were already extensively described in the alongshore uniform coast setup. As can be seen in Figure 4.9, erosion and shoreline retreat is concentrated within the hump central area. Most hump sediment is transported and deposited in the North adjacent area while the South benefits less due to the northward net sediment trend (Fig. 4.7).

The volumetric evolution follows pulses of fast diffusion when the more energetic waves occur in the time series followed by calmer period with slower decay (Fig. 4.9). In the Center, RUE predicts faster loss of sediment in comparison with IH. After 10 years, the hump with RUE decayed to 57% from its initial volume of 3.7 Mm^3 while IH decayed to 66%, representing a deviation of 336, 400 m^3 between the two methods.

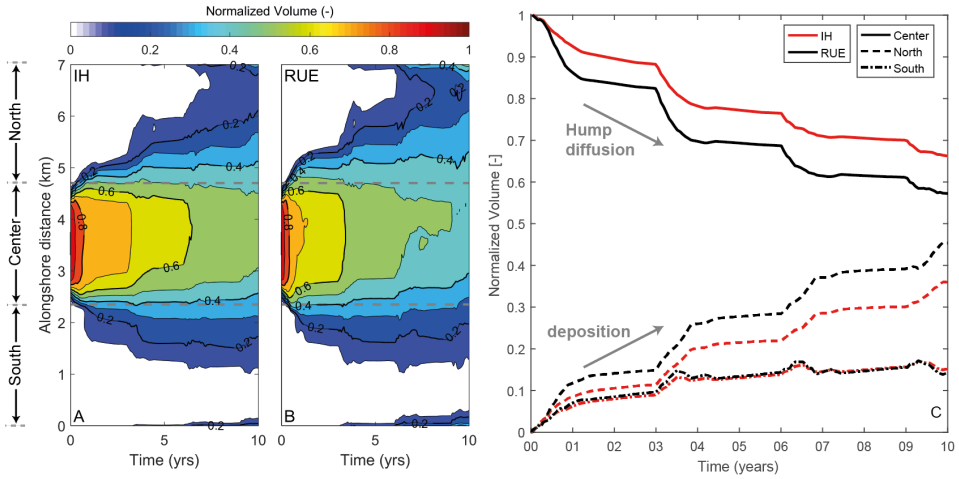

Figure 4.9: Volumetric diffusion of the coastal hump along the coast within 10 years. (a,b) Alongshore evolution of the normalized hump volume through time. (c) Normalized volume per zone, where Center is on the hump (indicated by dashed lines in a,b and also in figure 4.1c) and North and South are the adjacent areas from the hump. The temporal variability is due to the order of wave conditions.

The profile evolution after 10 years shows the retreat of the center profile, faster for RUE, while the North concomitantly responds with larger shoreline progradation when compared to the South (Fig. 4.10). In these scenarios, RUE predicts faster diffusion of the hump itself. This means, for example, that a beach nourishment would feed the adjacent downdrift areas faster, while lasting shorter, in comparison with IH predictions. Therefore, the parameterization choice affects the timescale of alongshore morphological processes. In general, the profiles evolved towards the measured envelope in a trend to restore the alongshore uniform dynamic equilibrium when the alongshore transport gradients tend to zero. Despite the introduction of this large shoreline perturbation, the final cross-shore profile (Fig. 4.10) did

not differ in shape from the alongshore uniform case (Fig. 4.8a), which is a further indication that the final morphology is indeed a robust equilibrium condition for the chosen wave climate, calibration and orbital velocity parameterization.

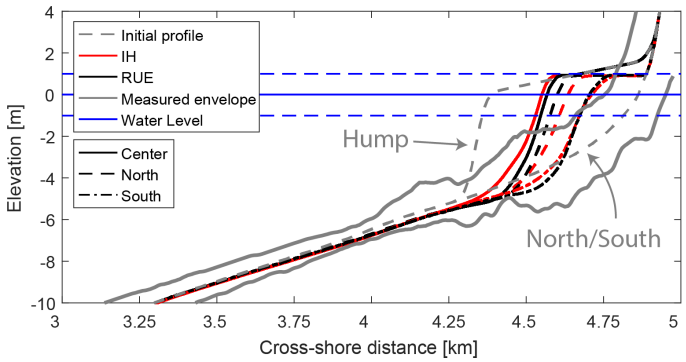

Figure 4.10: Cross-shore profiles over the hump and adjacent areas at Katwijk after 10 morphological years. Center presents the hump area while North and South are the adjacent areas from the hump (see figure 4.1). Measure profile envelope (solid lines) and initial model bed levels (dashed lines) are depicted in gray.

4.4 Discussion

The near-bed orbital velocities parameterizations differ in predicting wave shape transformation in shallow water and profoundly impact the resulting long-term sediment transport and morphological evolution. Below we discuss the main implication of parameterization choice.

4.4.1 Long-term morphodynamic evolution

The main consequences of higher onshore directed sediment transport by IH are twofold: (1) erosion of deeper nearshore areas where waves were not expected and observed to cause such effect (Figs. 4.8, 4.11) and (2) overfeed of the shallow upper beach profile. Here, the first effect was caused by non-linearities (skewness) starting earlier (deeper) in the wave propagation path (Fig. 4.3) resulting in a onshore directed gradient that pushes the sediment towards the shoreline (Fig. 4.6). This phenomena combined with incorrectly increasing skewness in the surfzone (Fig. 4.3) results in larger shoreline progradation (Fig. 4.8) due to excessive deposition, beyond the measured profiles and volumes, and imbalance between onshore and offshore directed transport (Figs. 4.6, 4.11). This excess of onshore sediment transport was larger for the longer period waves of Duck, reaching a factor of 7.8 when considering the annual sediment budget, which translated into unrealistic shoreline progradation and profile evolution (Fig. 4.8b). With default settings, RUE parameterization also overestimated onshore transport, however to less extent in comparison with IH.

The main reason for unrealistic net onshore sediment transport is the combination of the wave shape parameterization and the importance of the threshold for the beginning of sedi-

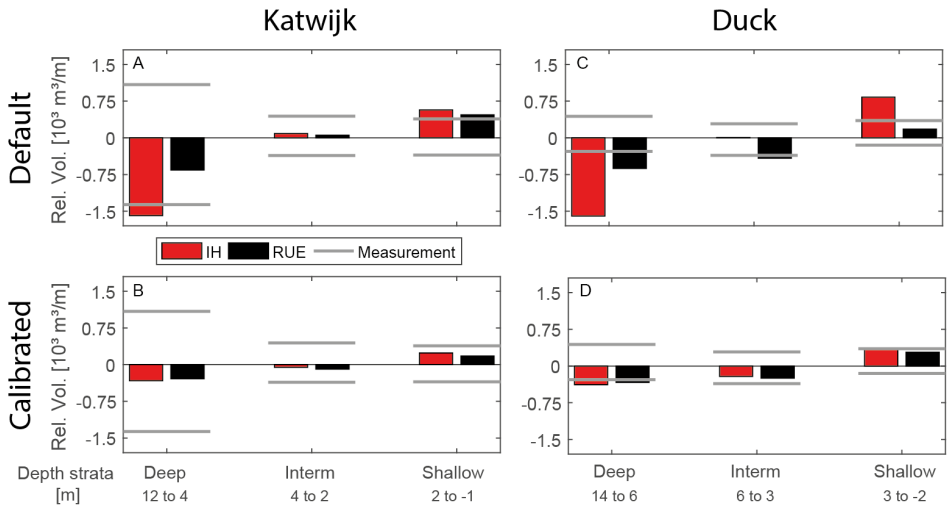

Figure 4.11: Profile volume after 10 years relative to the initial profile divided in depth zones. Positive values show deposition. Pannels a,b (left) are results from Katwijk and c,d (right) from Duck; a,c (top) are results for default sediment transport and b,d (bottom) for calibrated scenarios. The gray lines represent the minimum and maximum measured volumes as a reference.

ment motion in the lowest wave classes. The skewness-only IH method predicts larger skewness and sediment transport in comparison with the skewness-asymmetry RUE predictor. The higher sediment transport factors (*i.e.* IH/RUE), especially for the wave-related bed load component, correlates with lower steepness and low energy waves (Fig. 4.12), including the outlier (*i.e.* factor of 29) represented by the average wave condition of Katwijk. In Figure 4.12 we defined wave power as $Power = \frac{\rho g^2 H_s^2 T_p}{32\pi}$ in Watts and wave steepness as $Steepness = H_s/L$. The largest discrepancies between the two methods thus derive from situations near the beginning of motion for the bed load component (eq. 4.4) when the sediment transport is strongly non-linear, in this case, higher than a power of 3 for VR04. These low energetic conditions have a larger duration (Fig. 4.5) in comparison with the high-energy stormy events and are the dominant wave conditions in the wave climate (Table 4.2). Therefore, one can expect sediment transport deviations within a factor of 3-12 when simulating morphology with a wave climate or even higher when including an individual wave condition only, which is commonly of small-intermediate wave energy (e.g. Edmonds and Slingerland, 2010; Geleynse et al., 2011; Nahon et al., 2012; Nardin and Fagherazzi, 2012; Olabarrieta et al., 2014; Nienhuis and Ashton, 2016; Nienhuis et al., 2016; van der Vegt et al., 2016; Braat et al., 2017).

After applying calibration factors on the sediment transport, the overall equilibrium profiles and volume changes with IH and RUE were fairly similar (Figs. 4.8, 4.11). Nonetheless there are discrepancies in deeper and especially shallower areas. The overfeeding near the shoreline was also observed for other skewness parameterizations methods in cross-shore models (e.g. van Rijn et al., 2003; Ruessink et al., 2007; Dubarbier et al., 2015). Meanwhile,

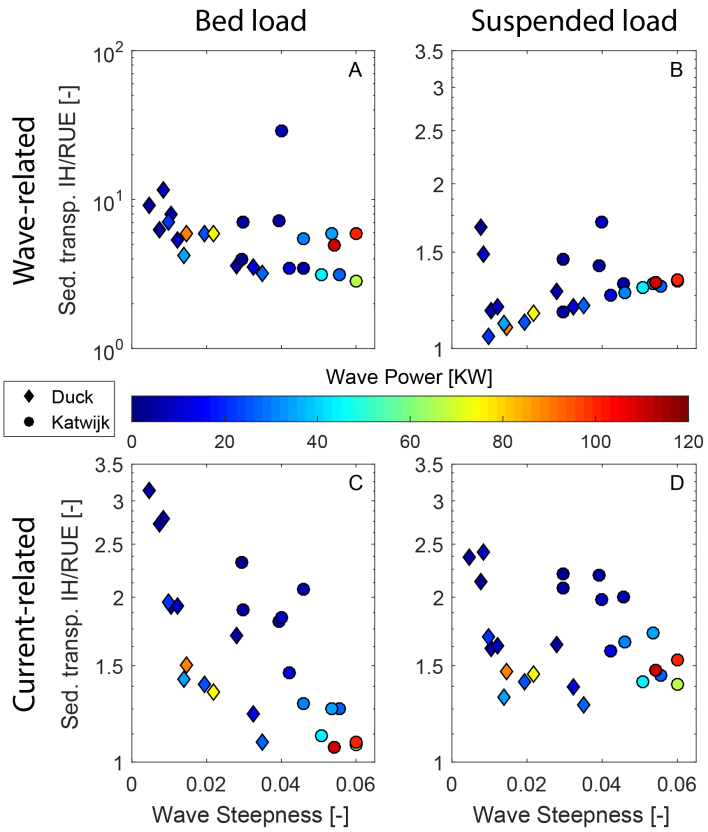

Figure 4.12: Tidally integrated sediment transport factors of IH/RUE parameterizations against wave steepness at Katwijk and Duck, with colors representing the wave power for each wave case from the climate (Table 4.2). (a) wave-related bed load; (b) wave-related suspended load; (c) current-related bed load; (d) current-related suspended load.

the shoaling zone, where skewness dominates, showed closer results. However, to achieve these conditions, the wave-related sediment transport for IH had to be reduced to 10-15% from the default values. Such reduction, although extreme, is not an exception when compared to recent studies (Nienhuis et al., 2016; Nienhuis and Ashton, 2016; Grunnet et al., 2004), which raises serious doubts about the validity of IH to coastal environment applications in combination with general sediment transport predictors (e.g. van Rijn, 2007a; van Rijn, 2007b; Bailard, 1982). Based on the assumption that 2DH models have to compensate for the lack of offshore directed transport, with IH we are implicitly considering that 85-90% of transport is offshore directed due to return currents, for example. On the other hand, with RUE, when we applied a correction of 70%, we are compensating for 30% of offshore directed transport. The latter figure better represents an average condition between calm and storm conditions, while the 85-90% of IH represents storm conditions when undertow is dominant over short-wave non-linearity (Stive, 1986; Gallagher et al., 1998; van Rijn et al., 2003).

The main adverse consequence of (over)compensating the sediment transport aiming to counteract shoreline translation is the drastic reduction of alongshore transport, in the order of 73% in our case with IH. This highlights the current limitations in properly reproducing overall morphology and time-scales in one model. Reducing the net alongshore transport by a factor of 0.73 (*i.e.* $968,000\ m^3/yr$) represents 385% of the annual net alongshore transport computed by van Rijn (1995), based on $200,000\ m^3/yr$ estimation for the central Dutch Coast. This means that in applications of IH, one could either realistically simulate the alongshore process or the cross-shore process but not the combination. This limitation further hampers the hindcast and forecast of more complex environments, like tidal basins and inlets which work in strict balance and feedback between waves, tides and fluvial processes in three dimensions.

4.4.2 Limitations and perspectives for wave-driven sediment transport prediction

While our results derive from the Delft3D model, we believe that the RUE parameterization would also improve other morphodynamic numerical models, not restricted to 2DH applications, as it corrects a fundamental mismatch in wave hydrodynamics, which is common to other 1D-2DHV-3D morphodynamic models. Skewness-only parameterizations proved to be able to reproduce beach recovery, after storms, in specific cross-shore 1D/2DV models (see compilation in van Rijn et al., 2003). However, as demonstrated in Dubarbier et al. (2015), the performance near the shoreline is the result of overcompensation of skewness-related transport, which has been used in the past to compensate for the lack of asymmetry effects in sediment transport functions. Here we observed a similar issue in the comparison of hydro-morphological results with IH versus RUE in a model-to-model approach and validation of results with measured beach-envelopes. Therefore, it is relevant to consider the origin and physical basis of each parameterization. RUE derived from nearshore field measurements, including the Central Dutch and Duck coasts (Ruessink et al., 2012), while IH and its further adaptations were based on scaled lab experiments (Isobe and Horikawa, 1982; Grasmeijer, 2002) intended to reproduce wave-skewness. Therefore, we can argue that RUE provides better estimations of near-bed orbital velocities than IH, especially for our case-studies in Katwijk and Duck as shown by our hydrodynamic and morphological results. The important improvement is that these effects need no longer to be compensated by extreme calibration factors on the sediment transport, which affects alongshore transport as well, but addresses the hydrodynamics of orbital velocities. Consequently, the approach in this paper is suitable for large-scale, long-term 2DH modelling but still limited for predicting coastal beach profiles, as all scenarios predict rather steep and convex shoreface profiles (Fig. 4.8), which we attribute to the lack of (quasi)3D-vertical processes combined with the dominant onshore-directed sediment transport driven by waves, similarly to observations from van Rijn et al. (2003) and Grunnet et al. (2004).

The IH predictor overestimates sediment transport mainly for the wave-related bed load component (Figs. 4.6, 4.12). A consequence is that, IH also promotes morphological diffusion due to bed slope gravitational effects. The bed slope effects on sediment transport and morphological development strongly determine the results for situations with currents-only as demonstrated in Baar et al. (2018b) and Baar et al. (2018a). With the overestimated bed

load contribution of waves, we expect stronger diffusion affecting the very shallow areas represented by shoals, bars and channels. The down-slope transport acts as a natural damping mechanism of morphological perturbations, however, its overprediction leads to unnaturally flat morphology. This damping effect was also explored by Dubarbier et al. (2015) and Dubarbier et al. (2017) for nearshore sandbars where increasing the downslope transport component decreased the growth of nearshore sandbars in their model.

The results generalize to many models and general sediment transport predictors that do not account for asymmetry-driven sediment transport (e.g. van Rijn et al., 2004; van Rijn, 2007b; Bailard, 1981). On the other hand, specialist, coastal-oriented sediment transport predictors such as Dubarbier et al. (2015) and van Thiel de Vries (2009) incorporated asymmetry-driven sediment transport, but these are strongly dependent on user-defined calibration due to the lack of a robust physical relation (Brinkkemper, 2018). Moreover, such coastal-oriented formulations are poorly tested and arguably unsuitable for fluvial processes that are important in the fluvial-tidal transition that the general transport predictors can cover. Thus, further research should focus on robust incorporation of asymmetry-driven sediment transport into general and broadly applicable morphodynamic models, while the present advance opens up the possibility of long-term morphological modelling of coastal systems where cross-shore and alongshore transport are of similar importance.

4.5 Conclusions

The parameterization of wave-induced near-bed orbital velocities highly affects the long-term (year to decades) prediction of the nearshore morphology due to its non-linear relations with sediment transport. The comparison of the Isobe Horikawa (IH) (Isobe and Horikawa, 1982) skewness-only parameterization versus the skewness and asymmetry method of Ruessink (RUE) (Ruessink et al., 2012) within the Van Rijn (VR04) transport equations (van Rijn et al., 2004) shows that a better representation of wave shape and near-bed orbital velocities leads to overall more realistic morphodynamic predictions.

The IH parameterization predicts larger skewness and onshore-directed sediment transport in comparison with the RUE method. Depending on the wave condition, the tidally integrated net transport with IH was between 3 and 12 times larger than with RUE, with an outlier of 29. The largest differences were observed for calm wave conditions, which are dominant in the wave climate, further enhancing the difference between the two methods in the yearly sediment budget. Thus, with default sediment transport settings, IH simulations led to an overfeeding of shallow areas while eroding the deeper portion of the profile. RUE simulations with default settings also overpredict onshore directed transport in the shoaling and surfzone, however, to a lesser extent. After applying calibration factors on the sediment transport components, to ensure shoreline stability by means of equal yearly net onshore and offshore sediment transport, both IH and RUE predicted profiles within measured beach envelopes at two sites selected, *i.e.* Duck, NC, USA and Katwijk, NL. However, IH wave-related sediment transport needed to be reduced to 10-15%, which in turn affected the alongshore transport rates by 73%, representing 385% of the annual littoral drift of the Dutch Coast.

For the same conditions, RUE simulations were reduced to 72% in order to match the beach envelopes and consequently had a lower impact on the alongshore sediment transport (56%).

Thus, by improving the parameterization of near-bed wave orbital motion there is less need to (over-)calibrate sediment transport. The skewness-asymmetry parameterization also proved to be robust, in the sense that predictions were less sensitive to variations in the user-defined calibrations factors. Therefore, RUE parameterization results in a closer coupling of cross-shore and alongshore sediment transport in the nearshore, which improves the long-term hindcast and forecast of complex coastal and estuarine environments.

Acknowledgements

Supported by ERC Consolidator agreement 647570 to MGK. Code development was supported by Deltares and we gratefully thank Dirk-Jan Walstra for the arrangements. We acknowledge Rijkswaterstaat and USACE-FRF for making field data available. Authors appreciated the fruitfully discussions and model assistance from Bart Grasmeijer and Pieter Koen Tonnon. Delft3D source code is freely distributed and available at the Deltares (SVN) repository. The authors encourage the compilation and usage of this version. The supplementary material contains the SVN path along with specific instructions to activate the options between IH and RUE parameterization. Please contact the corresponding author for further technical information and consult Delft3D-Deltares web-page for compiling and general model instructions.

Chapter 5

Vegetation reconfigures barrier coasts and affects tidal basin infilling under sea level rise

Worldwide, many tidal basins associated with barrier coasts have infilled over the past millennia due to the combination of sediment supply, wave-tidal sediment transport, and eco-engineering effects of vegetation. However, the biogeomorphological interactions between saltmarsh and the morphodynamics of an entire coastal barrier system are poorly understood, especially under sea level rise (SLR). Here we study the evolution of a barrier coast for combinations of mud availability, presence of vegetation and SLR. We developed a novel biogeomorphological model of an idealized barrier coast enclosing a tidal basin with sandy-clayey sediments that was subjected to tides and waves for a century. The morphodynamic Delft3D model was coupled to a vegetation code which accounts for the dynamics of marsh-type vegetation. Initially, vegetation contributed to reducing the tidal prism while sediment was imported. However, with SLR this trend was reversed and the tidal basins started to export sediment for vegetated runs after about 50–60 years while the unvegetated scenarios continued to infill in pace with the SLR. The sediment export was caused by cascading biomorphodynamic feedback effects triggered by vegetation which modified channel and shoal dynamics. Even under higher mud supply, the SLR resulted in vegetation collapse. The hypsometries, similar to natural systems, showed that vegetated systems converge to an alternative stable state condition. We conclude that, the long-term resilience of the tidal basin associated with sediment infilling under SLR can be reduced by cascading large-scale effects of vegetation on the morphodynamics of barrier coasts.

Published as: Boechat Albernaz, M., Brückner, M., van Maanen, B., van der Spek, A., Maarten G. Kleinhans (2023) Vegetation reconfigures barrier coasts and affects tidal basin infilling under sea level rise *Journal of Geophysical Research: Earth Surface*, 128, https://doi.org/10.1029/2022JF006703

5.1 Introduction

Tidal basins and associated saltmarshes along barrier coasts are important marine-terrestrial interface environments that provide valuable ecosystem services including coastal protection (Barbier et al., 2011; Zhu et al., 2020) and shelter for harbours. In this article, 'barrier coasts' refer to systems composed of mainland-backed tidal basins enclosed from the ocean by barrier islands and spits while connected to the open sea via inlets (Figure 5.1). Inlet geometry is controlled by waves and littoral drift, which work to narrow and close inlets, and tidal forces, which strive to maintain the connection (De Swart and Zimmerman, 2009). The inlets are bracketed by ebb- and flood-tidal deltas that provide sediment storage and protection against storms for the shallow areas rich in marine and terrestrial ecology (De Swart and Zimmerman, 2009; Moore et al., 2018). The morphological evolution of the barrier coast is driven by the combination of sediments transported by tides and waves (Davis and Hayes, 1984; Boyd et al., 1992; De Swart and Zimmerman, 2009). The combined effects of tides and waves promote water and sediment exchange between the open coast, tidal-deltas and the inner basin. These hydrodynamic forces combined with sediment transport processes exert a major control on the formation of channels, the ebb-flood delta and on the inlet dimension and thus shape the entire barrier coastal system (De Swart and Zimmerman, 2009).

Many tidal basins worldwide were formed during sea level rise in the early and middle Holocene (Boyd et al., 1992; FitzGerald and Buynevich, 2003; de Haas et al., 2018). Tidal basins receive sediments from a combination of coastal and fluvial supplies. While a high fluvial supply can be present for estuaries, the fluvial supply in tidal basins can be absent or negligible when the open coast is the main source of sediments. The coastal sediment supply derives from the advection of mud, littoral drift of sand and ebb delta dynamics. Under increasing sediment demand, for example due to sea level rise, the basin needs more sediments to keep up with the increase in accommodation space. Sediments can be supplied by the ebb delta in the short-term while in the long-term the offshore and the updrift coast, including the barrier itself, are the main sources (Beets and van der Spek, 2000). Mud and sand show different behaviours. Non-cohesive (coarser) sandy sediments are transported as bed and suspended load and they respond strongly to the flow velocities due to the non-linear relation of flow velocity and sediment transport (van Rijn, 2007a). Cohesive muddy (finer) fractions are transported as suspended load and their deposition is strongly related to the duration of rising-falling tides and the slack-water periods that allow for sedimentation. Sandy material is supplied by tidal and wave-related sediment transport from the adjacent barriers and ebb-tidal delta. Mud and fine suspended material advected from offshore and stirred from shallow areas within the basin are transported by wave-tidal currents. Part of these sediments are bypassed to the downdrift coast via the inlet, ebb delta and from offshore, while another part remains inside the basin (Bruun and Gerritsen, 1959; FitzGerald, 1996; FitzGerald et al., 2000; Elias et al., 2019; Lenstra et al., 2019). The balance between imported and exported sediments is influenced by the tidal asymmetry, the shape and length of the basin, intertidal volume storage, the antecedent hypsometry (bed elevation distribution of channels and shoals) and the presence of vegetation (Friedrichs and Aubrey, 1988; van Maanen et al., 2013; Stark et al., 2017).

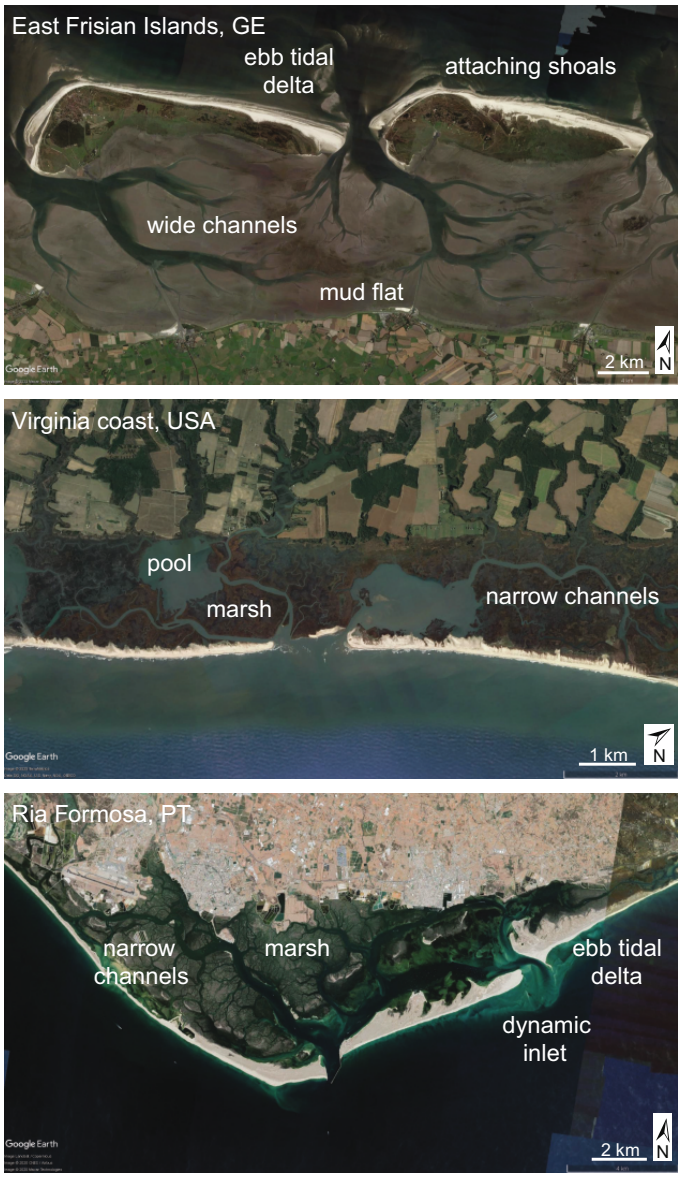

Figure 5.1: Examples of tidal basins and biogeomorphological elements. The East Frisian Islands in the (German) Wadden Sea barrier coast (53°43′36.01″N, 7°40′46.95″E) consists mainly of mud flats and relatively wide and sandy channels. The coastal barrier of Virginia (37°26′21.95″N, 75°45′1.60″W), USA presents narrow channels and abundant marshes with the presence of larger deeper areas (pools) in between marsh areas. The Ria Formosa in Portugal (36°59′37.52″N, 7°53′11.35″W) has wider main channels crossing the marsh lands behind the multiple inlet barrier coast systems. (Source: Google Earth)

The net sedimentation (infilling) is therefore a result of the hydrodynamics, sediment transport and eco-engineering effects of vegetation. Eco-engineering means the capacity

of vegetation to alter flow and sediment transport processes on biomorphodynamics. Paleogeographical reconstructions of the Netherlands show that middle Holocene back-barrier systems were filled in by reed peat (Vos, 2015) and transformed into a coastal plain when the sea level rise rate decelerated from ca. 5 mm/yr to less than 2 mm/yr (Hijma and Cohen, 2019). This suggests a long-term sustained feedback of vegetation promoting sedimentation and consequently tidal basin filling (de Haas et al., 2018). Modelling studies mostly support that vegetation retains more sediment and contributes to the local increase of bed levels (e.g. Kirwan and Murray, 2007; D'Alpaos, 2011; Fagherazzi et al., 2012), and that for sea level rise exceeding the sedimentation due to sediment supply, the vegetation can collapse, exacerbating the drowning (Kirwan et al., 2010; Schuerch et al., 2018). Other studies suggest that large patches of vegetation reduce flow velocities, local sediment supply and sedimentation away from the feeder channels (D'Alpaos et al., 2007; Boechat Albernaz et al., 2020; Brückner et al., 2020). Mud and vegetation tend to confine channels (i.e., smaller width to depth ratio) which favors ebb-dominance (Friedrichs and Aubrey, 1988; Bij de Vaate et al., 2020). Depending on the local small-scale characteristics, adjacent channels and shoals can be flood or ebb dominant, whereas on average the channels are ebb dominant and shoals flood dominant (van Veen et al., 2005) due to the balance between friction and inertia. Shallow shoals and intertidal flats also allow for the settling of vegetation (assuming that the underlying environmental conditions are also satisfied), which in turn alters the hydrodynamics and sediment transport in the morphodynamic feedback loop (Wright and Thom, 1977; Boyd et al., 1992).

Tidal basins depend on sediment fluxes to/from the littoral zone, and the evolution of each sub-system affects the interaction between the parts (Robbins et al., 2022). The resulting sediment transport in and out from the basin depends on the wave-tidal dynamics that, in turn, depend on the tidal basin and ebb-flood delta properties, including effects of vegetation. The working hypothesis is that the tidal basin development is the result of interactions between the littoral sandy processes, the mud dynamics and vegetation. As such, the sediment fluxes cannot simply be assumed or imposed at the basin boundary (e.g. inlet) but are the dynamic result of coastal processes interacting with the tidal basin.

The combined effects of vegetation changing local sedimentation, channel configuration, tidal penetration and distal sedimentation suggests a need to evaluate the conditions under which vegetation promotes a negative feedback (increasing infilling towards a steady state) or a positive feedback (erosion and drowning) on the basin evolution, regardless of the sediment supply. These coupled mechanisms have not yet been investigated with more comprehensive hydro-biomorphodynamic models, while the negative feedback was inferred from paleogeographical reconstructions (de Haas et al., 2018).

In such a complex open biogeomorphic system, it is an open question under which conditions a steady state, or equilibrium, occurs. Research on barrier coasts and tidal basins started with field-derived equilibrium conditions attributed for example to inlet dimensions and tidal prism (Escoffier, 1940; O'Brien, 1967; Escoffier, 1977; Powell et al., 2006; Huismans et al., 2022), or the volume of ebb and flood delta related to basin dimensions (Walton and Adams, 1976; Dronkers, 1998; Powell et al., 2006). This data-driven approach is valuable when studying observation-rich systems that are in a steady state. However, they provide less insight about the underlying physical processes, especially under changing boundary condi-

tions (Ranasinghe, 2020). Numerical and analytical models have been applied to overcome these limitations as they can test alternative scenarios including changes in hydrodynamics and sediment supply. However, comprehensive process-based models, such as Delft3D (Lesser et al., 2004) and TELEMAC (Villaret et al., 2013) are complex and computationally intensive, especially with wave-driven sediment transport. For these reasons, morphodynamic models until now were able to perform either short timescale simulations (*O*-years) or needed to be simplified (e.g., no waves, single sediment fraction or neglect the coast and inlet) to simulate long-term morphodynamics (*O*-decades). Only lower complexity models were able to reach the time-space scales of full barrier coast development (De Vriend, 1991a; Elias et al., 2019; Ranasinghe, 2020). Furthermore, the effects of eco-engineering vegetation species (Brückner et al., 2020) and eco-engineering benthic species (Brückner et al., 2021), often disregarded in models, have large eco-morphodynamics effects. In summary, we currently rely for our long-term predictions on *a priori* equilibrium modes or simplified models (D'Alpaos et al., 2007; Kirwan and Murray, 2007; De Swart and Zimmerman, 2009; D'Alpaos, 2011; Fagherazzi et al., 2012; Townend et al., 2016; Mariotti and Canestrelli, 2017b; Leuven et al., 2019; Xu et al., 2019; Nardin et al., 2020; Ranasinghe, 2020).

In view of the raised questions and ongoing global climate change, there is an urgent need for understanding how barrier coasts will respond to natural and human induced relative sea level rise, and changes in sediment supply (e.g. Syvitski et al., 2005; Dunn et al., 2019; Eslami et al., 2019; Nienhuis et al., 2020). The starting point in this paper is the hypothesis that the interaction between sediment supply and vegetation determines the evolution of barrier coasts under rising sea level. We expect that the local morphodynamic feedback between sediment transport and vegetation on the formation of channels and shoals exerts an important control on the basin-scale evolution.

In order to test our hypotheses and unravel the main underlying mechanisms behind barrier coast evolution and basin infilling, we developed a novel large-scale biomorphodynamic model consisting of an entire idealized barrier coast system with a dynamic vegetation module that interacts with the hydro-morphodynamics. The domain encompasses a tidal basin with a single inlet within an alongshore uniform coast. The model is the first process-based (i.e. hydrodynamics resolving model coupled to detailed sediment transport formulations) biomorphodynamic model that includes comprehensive wave climate, morphological tidal constituents including overtides, a sediment composition from sand to clay, and dynamic vegetation. Our scenarios cover a century of biomorphodynamics under sea level rise for a range of concentrations of offshore mud supply. In total we simulated 8 scenarios with and without vegetation, with different clay concentrations between 15 and 60 mg/L and reference scenarios without sea level rise.

5.2 Methods

The morphodynamic simulations were performed in a depth-averaged (2DH) configuration of Delft3D (Deltares, 2020, modified from tag 7545) in which the parameterization of near bed wave orbital velocities were modified according to Boechat Albernaz et al. (2019). This modification improved the shallow wave-induced sediment transport and the resulting

coastal morphology. Most importantly, this improvement allowed the modelling of coastal sediment transport with a more realistic coupling between the cross-shore and alongshore sediment transport fluxes and consequently a better overall sediment balance (see Boechat Albernaz et al., 2019). The Delft3D model is an extensively applied morphodynamic model for finite difference solving of the momentum and continuity equations for unsteady flow in depth-averaged mode through the Navier-Stokes equation with hydrostatic pressure approximation (Deltares, 2017). Waves were simulated with embedded Delft3D-WAVE (i.e. SWAN spectral wave model, see Booij et al., 1999; Ris et al., 1999) online coupled (i.e. two-way interaction) to the FLOW module which computes wave-current hydrodynamics, sediment transport, effects of vegetation and morphological evolution (Lesser et al., 2004; Deltares, 2017).

We applied the VR04 sediment transport predictor (van Rijn et al., 2004; van Rijn, 2007a; van Rijn, 2007b; van Rijn et al., 2007), improved according to Boechat Albernaz et al. (2019) for the computation of near-bed wave orbital velocities. We choose the VR04 predictor because it is well-calibrated for wave- and current-driven sediment transport, includes wave-current interaction and intra-wave sediment transport, and conceptually separates bed and suspended load for currents and waves. The mud fractions are treated as cohesive sediments and the deposition and erosional fluxes are computed according to Partheniades-Krone formulation (Partheniades, 1965) based on user-defined critical shear stresses for erosion and sedimentation. The critical shear stress for erosion was set to 0.5 N/m^2 and the sedimentation threshold to 1000 N/m^2 (the high value means that it always allows for sedimentation), both default values. For simulating the eco-morphodynamic effects of vegetation (eco-engineering species) we online coupled (i.e. two-way interaction) Delft3D to a dynamic vegetation module adapted from Brückner et al. (2019) that computes vegetation settlement and mortality derived from the hydro-morphodynamic development. In turn, the vegetation alters the hydro-morphodynamics through vegetation density-dependent roughness and drag (Baptist et al., 2007), which completes the feedback loop. The model was inspired by the sediment-dominanted coastal systems of the North Sea, where the accumulation of organic material can be neglected. In view of the model complexity and the imposed spatial limit of the tidal basin, the succession of vegetation and peat builders (i.e. found further landward) were neglected.

Below we detail the relevant model settings, including the initial and boundary conditions, and the dynamic vegetation characteristics.

5.2.1 Model domain

The model domain was broadly inspired by the East Frisian Wadden Sea (see Figure 5.1 and Fitzgerald et al., 1984) and consists of a 20 by 5.5 km idealized coast connected to a basin of 1 m depth and 4.4 by 7.7 km dimensions via a single 1 km wide inlet enclosed by coastal barriers (Figure 5.2). These dimensions, specially the shallow basin with 1 m depth, represents a developed state of a backbarrier basin filled with clastic sediments, where intertidal areas can form and vegetation can settle. In order to perform simulation of a near-equilibrium condition between the coastal profile, tides and wave climate, the coastal domain has a time-

spatial averaged profile from the Dutch coast on the North Sea, and the tides and wave climate were schematized based on long-term measurements on the North Sea.

The coastal bathymetry was calculated from an alongshore uniform profile derived from a time-spatial averaged nearshore bed profile obtained from the Dutch JARKUS database (Rijkswaterstaat, 2017) on the Holland Coast near Leiden-Katwijk, the Netherlands. The profiles were measured between 1965 and 2010 along 31 alongshore distributed locations covering 15 km of coastline from the dunes up to approximately 15 m depth. The average profile has a slope of 1V:185H up to 2.3 m depth, steepening to 1V:63H up to the mean water line (as in Boechat Albernaz et al., 2019). A comprehensive morpho-sedimentary description of the Dutch coast is presented in Short (1992), Wijnberg and Terwindt (1995), and van Rijn (1997).

We included four sediment fractions, i.e. 200 and 125 μm sand, silt and clay, in order to represent the different environments from the wave-exposed coast to the protected and vegetated mud flats (Figure 5.1). Each sediment fraction was individually recorded by the stratigraphic bed module from Van Kessel et al. (2012) to allow different sediment mixtures and the effect of differential bed composition on sediment transport rates for each sediment fraction. The module tracks and stores the bed composition with a user-defined vertical resolution, here 0.1 m, and the sediment transport is computed for the active top-layer on the basis of the top sediment mixture. The sediment supply was defined at the open sea boundaries as equilibrium concentration supply for the sand fractions, while clay was supplied as user-defined concentrations varying between 15 and 60 mg/L (within measured range of e.g. van Kessel et al. (2011) and Kleinhans et al. (2005)) according to the modelling scenarios (see Figure 5.3). Note, however, that the open sea boundaries are far away from the tidal inlet, so that the sand concentrations at the inlet are entirely determined by the dynamic interactions within the littoral zone.

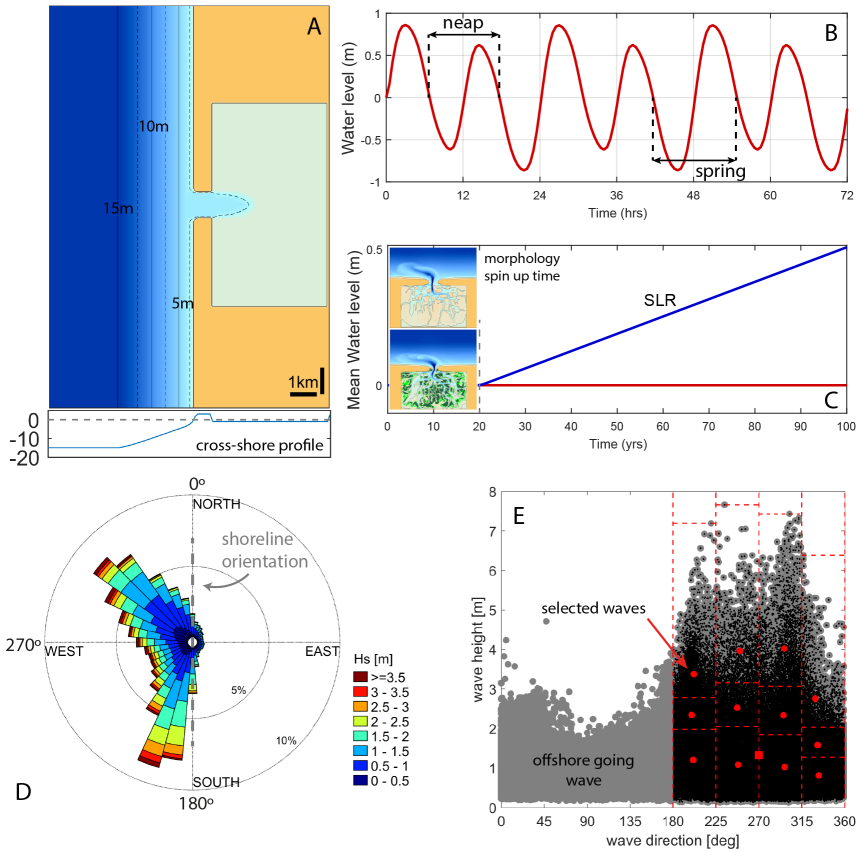

Figure 5.2: Delft3D model layout and boundary conditions. (a) plan view of initial model domain and cross-shore profile. The alongshore domain was reduced for visualization purposes; (b) morphological tides; (c) implementation of sea level rise including inserts of model examples after the spin up time of 20 years; (d) Wave polar histogram for significant wave height (H_s); (e) and the reduction and schematization to wave bins for modelling. The wave data was recorded at the IJmuiden 'Munitiestortplaats' between 1990 and 2016. Directions were rotated by 30º for application in the model domain with the same relative angle. Dots indicate selected wave conditions and the square indicates the time-averaged condition.

5.2.2 Tides, wave climate and sea level rise

The tidal boundary conditions were inspired by the North Sea records. The model has alongshore propagating morphological tides (Latteux, 1995; Cayocca, 2001; Lesser, 2009) with 0.75 m M2 amplitude, 0.075 m M4, 0.035 m M6 components and a generic diurnal (i.e. 24 hours) component of 0.2 m to create spring-neap cycles. All tidal components were rounded to integer hours.

The wave conditions of the Dutch Coast were recorded at, and summarized for, the IJmuiden 'Munitiestortplaats' directional buoy in the North Sea between 1990 and 2016 (Boechat Albernaz et al., 2019). The wave directions were rotated 30º to realign the waves with our idealized coast based on the local shoreline orientation (Figure 5.2d). The wave climate consist

of short-period waves averaging 4.6 s with 11.7 s maximum. The maximum wave height reaches 7.6 m while the average is 1.32 m (square in Figure 5.2e). The wave direction has two main components from SW (200°) and NW (310°) but also has a significant frequency of parallel and offshore going waves for 13% of the year.

The wave record was reduced and schematized into 13 representative wave conditions to optimize the computational effort following Walstra et al. (2013) and Benedet et al. (2016). The wave reduction consisted of 4 directions and 3 heights plus an average wave condition for the duration of offshore-directed and shore-parallel waves. The representative wave conditions were obtained by dividing the wave climate into 12 bins of equal energy E, being $E \sim H_s^2$. The wave period, direction and the total duration were calculated as the average within each energy bin. Consequently, one wave condition energetically represents a range, consisting of significant wave height, wave period, wave direction and duration. The reduced wave climate is shown in Table 5.1, with condition number 7 being the averaged condition to replace the recorded offshore and parallel going waves.

The wave conditions were implemented as 13 independent model cases which were run in parallel while sharing the bed level every timestep (12 seconds). At each merge event, the new bathymetry was calculated as the sum of morphological changes across the 13 models. To weigh the differing occurrence of each wave condition, we multiplied the morphological change by individual morphological acceleration factors (i.e. morfac, see Roelvink, 2006; Ranasinghe et al., 2011) from Table 5.1 that were derived from the duration of each wave bin. This approach means that less energetic but persistent wave conditions have a higher morfac while the more energetic (stormy) conditions are performed with a lower morfac, which represents the sporadic stormy conditions. This parallel mode, known as 'mormerge' (called "parallel online approach" in Roelvink, 2006), allows for the usage of more parallel computational resources while also improving the model stability (Roelvink, 2006). This parallel technique also mitigates artificial effects of ordering the wave conditions that can affect the dynamics of bars (Walstra et al., 2012; Walstra et al., 2013), which is important for the sediment bypassing and for the formation of channels and ebb delta sandy bars (FitzGerald et al., 2000; Elias et al., 2019). To further enhance model stability and avoid bias towards one tidal condition, the tidal signal of each case was shifted in phase such that the ebb and flood conditions with higher morfacs happen simultaneously in different model cases, and therefore minimize the net change within the tidal cycle (Roelvink, 2006). With this model approach, we capture the net long-term morphological evolution, rather than episodic events, with more efficiency for the timescale of one century.

Sea level rise commenced after 20 years of morphological development to allow for a similar incipient tidal basin, ebb delta and vegetation pattern for all scenarios. Sea level rise was implemented as a linear water level rise of 0.5 m per 100 years (i.e. 5 mm/yr), considering the total simulation time. This value was inspired by the Holocene evolution of tidal basins in the western Netherlands. These transgressive basins formed before 7500 BP under high sea level rise rates, migrated landward and filled in from 5000 BP onwards under a decelerating rate of relative sea level rise (RSLR) combined with abundant supply of sediment (Beets and van der Spek, 2000; Meijles et al., 2018; de Haas et al., 2018). The rate of RSLR during the phase of basin expansion was 5 mm/yr and higher, and dropped to less than 2 mm/yr dur-

Table 5.1: Model scheme with 13 'mormerge' cases (see text) with wave height (H_s), period (T_p), direction (Dir, rotated to the model domain) and normalized duration (%), tidal phase shift and morphological factors (morfac). Each of these conditions are merged into one shared bed level for all cases every timestep.

Case	H_s m	T_p sec	Dir deg	Duration %	Morfac -	Tide phase (deg)
1	1.2	4.1	201	20	97.67	0
2	2.34	5.2	200	5	25.73	45
3	3.37	6	202	3	12.40	297
4	1.08	4.2	248	11	53.13	315
5	2.53	5.5	247	2	9.79	243
6	3.96	6.5	250	1	3.99	117
7	0.8	3.5	270	13	64.36	90
8	1.02	4.7	297	20	99.15	180
9	2.33	5.7	296	4	19.01	135
10	4.02	6.9	296	1	6.41	324
11	0.81	4.2	333	14	70.51	270
12	1.58	4.9	332	4	18.46	225
13	2.76	5.9	329	1	6.06	63

ing the phase of basin infilling (Hijma and Cohen, 2019). The applied rate of 5 mm/yr thus marks the transition from basin expansion to basin infilling. In addition, the 5 mm/yr rate of RSLR is also in line with the IPCC's projected climate scenario under RCP4.5 (Representative Concentration Pathway), which predicts 0.52 m of sea level rise for the Dutch Wadden Sea area by the end of this century (Vermeersen et al., 2018). This value is bracketed by RCP2.6 and RCP8.4, which predict 0.43 m and 0.84 m of global sea level rise by the year of 2100, respectively (Oppenheimer et al., 2019). However, higher values of RSLR in the order of 5 mm/yr or higher are expected locally due to the added effects of, for example, subsidence and extraction of water and gas from the subsoil e.g. Minderhoud et al., 2020; van Dobben et al., 2022. Therefore our choice of the SLR rate represents the past transition from transgression in the Dutch coastal systems towards infilling (Vos, 2015), but is also in line with the future projections of relative sea level rise of for example the Netherlands which also accounts for subsidence.

5.2.3 Dynamic vegetation model

To investigate the effects of saltmarsh-type vegetation on the morphodynamics and related infilling processes, we implemented in the model a generic saltmarsh species, similar to Brückner et al. (2019), that represents common saltmarsh compositions in the northwestern Europe. At each ecological time-step coupling (defined at every neap-spring tidal cycle, i.e. 24 hours), the results of the Delft3D hydro-morphodynamics (i.e. inundation period, flow velocity and bed level changes) were fed into the dynamic vegetation model to calculate the new vegetation composition based on rules that determine the establishment and mortality. To correctly account for the inundation period and velocities, the vegetation module was coupled to the results of the case 7 (Table 5.1), which represents the average wave condition. The new vegetation coverage and properties were then applied to all cases. Below

we describe the main parameters, and more details on the dynamic vegetation model are provided in Brückner et al. (2019).

To translate the vegetation effects into the hydro-morphodynamic model, we applied the Baptist predictor (Baptist et al., 2007) to calculate the effects of vegetation on hydraulic roughness and flow drag force. This combination allows for a more realistic sediment transport computation when compared to roughness-only methods which leads to the overprediction of sediment transport rates due to the increase of the bed shear stress.

The dynamic vegetation model included settling and mortality rules conceptually similar to those in the literature (Kirwan and Murray, 2007; D'Alpaos, 2011; Fagherazzi et al., 2012; Marani et al., 2013; Oorschot et al., 2016; Brückner et al., 2019) for mature vegetation. The interaction between vegetation and waves was not accounted for in our models as the wave action inside the basin, where vegetation is present, is negligible. Due to the long time-scale of the model, the vegetation growth phase was neglected as the ecological time step in morphological time is larger than the plant growth timescale. Therefore, settling was applied for mature plants with a specific plant height of 2 *m* as emergent vegetation, a root length of 1 m, a stem diameter of 2 cm and a stem density of 400 stems/m^2 (Yamasaki and Tange, 1981; Leonard et al., 2002; Bouma et al., 2013). The initial coverage was set to a fraction of 0.25 (i.e. at each settling event the vegetation can settle at 25% of the grid cell), and can reach up to 1.0 representing the maximum coverage at one grid cell. At each coupling the vegetation can recolonize suitable numerical cells as long as the maximum total fraction of 1 in the cells is not exceeded. The vegetation fraction implicitly accounts for the effect of plant biomass in the hydrodynamics via the Baptist predictor. The mortality induced by flow velocity, desiccation and inundation stress linearly reduces the vegetation fraction in a cell. In addition, bed level changes that exceed the plant size immediately remove the entire fraction representing either complete burial for sedimentation larger than the plant height or removal for erosion deeper than the root length.

Vegetation settles in grid cells with an initial fraction representing patch-density rather than individual plant-density and therefore implicitly accounts for rhizome growth of e.g. *Spartina anglica* and plant dispersion. New fractions can added in suitable cells at every coupling time-step, which represents lateral expansion and seedling establishment and leads to saltmarsh growth such as observed in nature (Marani et al., 2007; Fagherazzi et al., 2012; Brückner et al., 2019; Schwarz et al., 2022). The mortality is a portion of the initial fraction, which allows for constant die-off rates independent of the plant fraction present. This strategy leads to dense vegetation higher up the marsh while lower densities populate the more stressful locations (Brückner et al., 2019). The vegetation model does not include organic accumulation, which is, in the sediment-dominant systems considered here, only important landward of the tidal basins covered in the model. Here we considered mortality values typical for *Spartina anglica*, *Phragmitis australis* and *Scirpus maritimus* (Leonard et al., 2002; Bouma et al., 2013; Yamasaki and Tange, 1981). Succession of species at higher elevations was ignored. The causes of mortality were implemented as dose-effect relationships (Brückner et al., 2019) as follows:

1. Uprooting from 0.25 to 0.35 m/s

2. Inundation period between 0.70 and 0.95 [-]
3. Desiccation period between 0 and 0.1 [-]

5.3 Results

5.3.1 Tidal basin morphodynamics

Our results show strikingly different morphodynamic end-members between the vegetated and unvegetated scenarios (Figure 5.3). The reference runs without SLR (models 1 and 5 in Figure 5.3) demonstrate that vegetation increases the number of channels and distributaries inside the basin. Also, without vegetation the northern coastal barrier migrates southward (alongshore) 1.3 km (i.e. 13 m/yr migration rate) and confines the inlet, while the scenario with vegetation develops a more stable and wider inlet (Figure 5.4). In the absence of vegetation, a single main channel develops inside the basin and migrates southward accompanying the inlet migration, whereas vegetation creates more equally distributed and stable channels landward of the inlet.

All scenarios initially evolve with reducing tidal prism through the inlet (Figure 5.5a). However, while unvegetated basins continue reducing the tidal prism while importing sediments, the vegetated scenarios revert to a trend of increasing tidal prism, enlargement of the inlet cross-section (Figure 5.5b) and export of sediments (Figure 5.5c). This sediment export trend causes the growth of the ebb-tidal delta (Figure 5.5d) while the vegetation cover declines for the sea level rise scenarios (Figure 5.5e) as the vegetation cannot keep up with the increasing environmental pressure. The vegetation coverage was only stable with constant sea level. The accommodation space, calculated from the volume of water inside the basin, stays constant for most scenarios (Figure 5.5f), except for the combinations of sea level rise and vegetation (models 6-8). The constant and stable accommodation space indicates a steady state condition between the creation of space driven by the sea level rise and the sediment infilling. The combination of sea level rise with various mud concentrations does not modify the general evolution of the unvegetated scenarios (models 2-4) when the basin imports more sediments to keep up with the increase of accommodation space. However, the corresponding scenarios with vegetation (models 6-8) show large deviations from the reference scenario (model 5). The accommodation space and tidal prism evolution of the vegetated reference scenario (model 5) is rather stable and of similar pattern as the unvegetated scenarios. The sea level rise in combination with vegetation results in under-filled basins and subsequent vegetation mortality in the late evolution stages. The increase in mud concentration, for example in scenario 8 with 60 mg/L, results in more shoals and vegetation patches (see Figure 5.3) in comparison with scenario 6 and 7 (with 15 and 30 mg/L of mud, respectively). Nonetheless, the increase of mud supply is not sufficient to counteract the general vegetation collapse and drowning trend.

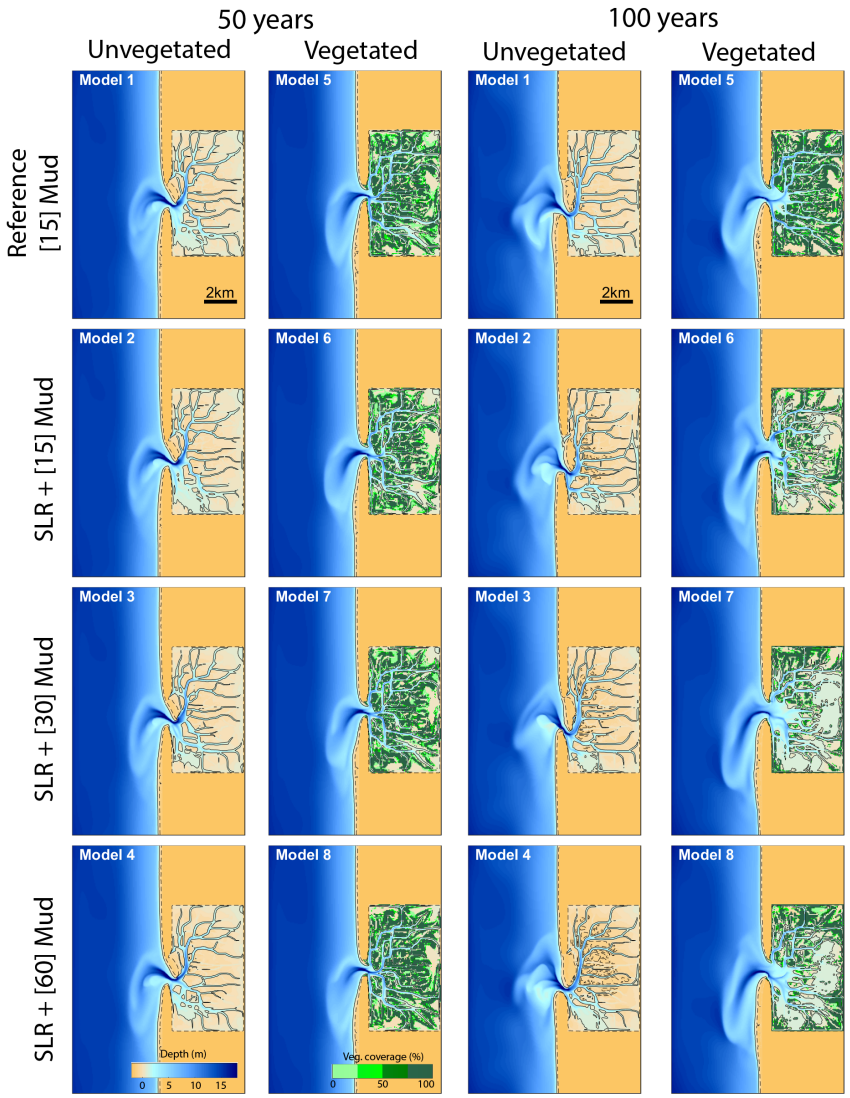

Figure 5.3: Maps of bed levels and vegetation coverage after 50 and 100 years of morphological evolution. Contour lines represent -0.8 and 0.8 m which approximate the intertidal areas.

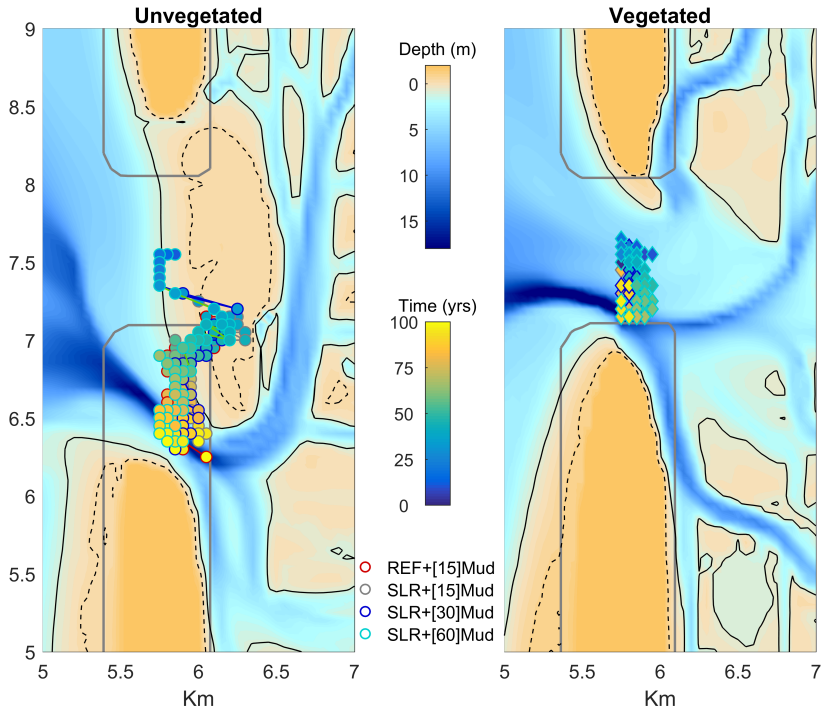

Figure 5.4: Inlet migration along 100 years represented by the position of the thalweg in the inlet cross-section. The gray contour line represent the zero meter depth at the initial time. The black contours are the -0.8 and 0.8 m which approximate the intertidal areas after 100 years.

The vegetation in the basin triggers a cascade of positive feedbacks that lead to net erosion followed by vegetation mortality and basin drowning. The cascading feedbacks develop as follows: (1) an increase of the average depth of the shoals and channels (Figure 5.6), as shoals did not keep up from the beginning of SLR (25–30 years), while the main channels got deeper after 40 years (due to vegetation and due to increasing tidal prism, see below), (2) a shift from sediment import to export around 50–60 years as the increase of flood storage led to ebb-dominance (Figures 5.5 and 5.7), (3) sediment starvation and erosion of the distal (landward) reaches of the basin, despite connection to tidal channels, which resulted in vegetation mortality and the formation of deepening ponding areas around 80 years (Figures 5.3 and 5.7). Conversely, the basin without vegetation continuously imports sediments and grows higher shoals.

The long-term erosional trend associated with sea level rise in vegetated basins (Figure 5.7) suggests that the local eco-engineering effects of saltmarsh plants can lead to system-scale drowning. Initially, sparse vegetation allows for local sediment trapping, with a typical pattern of onshore-directed transport on the tidal flats and further landward in the channels, and offshore-directed transport in the deeper channels (Figure 5.7b at 20 years). The larger vegetation patches reduce sedimentation on the distal tidal flats, compared to the unvege-

tated cases. Moreover, the increased friction on shoals and intertidal areas combined with deeper channels increase flood storage and cause a change to ebb-dominance and consequently net sediment export and drowning under sea level rise. Important to note that the combination of vegetation and SLR results in the lack of steady state. Without SLR the vegetated basin reaches a steady state even with relatively low mud supply (i.e. 15 mg/L) and without vegetation the basin infills under SLR irrespective of the offshore mud supply. One could argue that scenario 5 (vegetation + no SLR + [15] mg/L) also shows a sediment export trend, similar to the vegetated scenarios under SLR that lead to drowning. However, the export of sediments in scenario 5 strongly decreases its rate after 80 years, which indicates a convergence to a steady state condition. Furthermore, the accommodation space and tidal prism of scenario 5 are rather stable, and of similar trend and magnitude of the unvegetated cases that likewise reached steady state. On the other hand, the sharp increase in both tidal prism and accommodation space for the scenarios 6-8 indicate that the barrier tidal basin is not in steady state when combining SLR and vegetation.

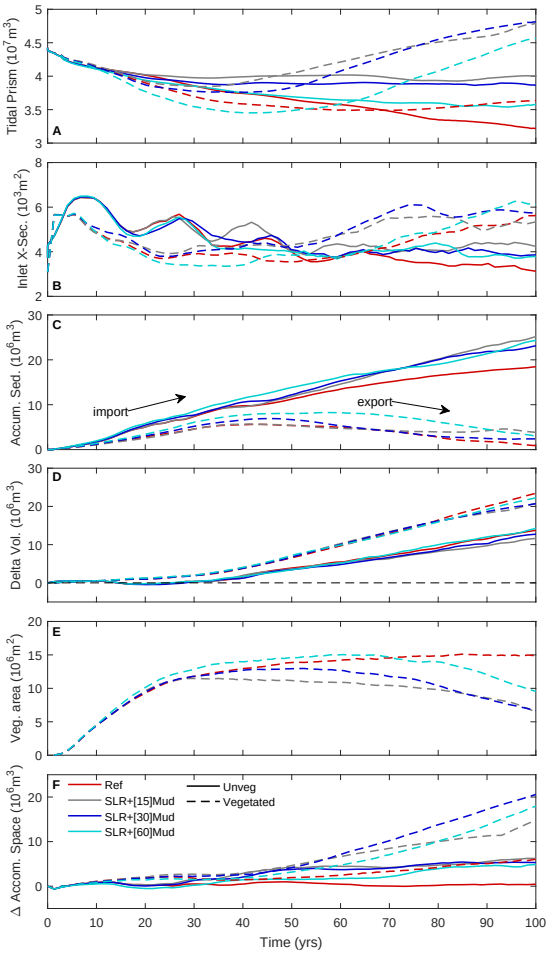

Figure 5.5: Time series of barrier coast evolution including (a) tidal prism, (b) inlet cross-section area, (c) cumulative sediment flux through the inlet, (d) volume growth of the ebb-tidal delta, (e) vegetation coverage area and (f) the evolution of the accommodation space with respect to the initial condition.

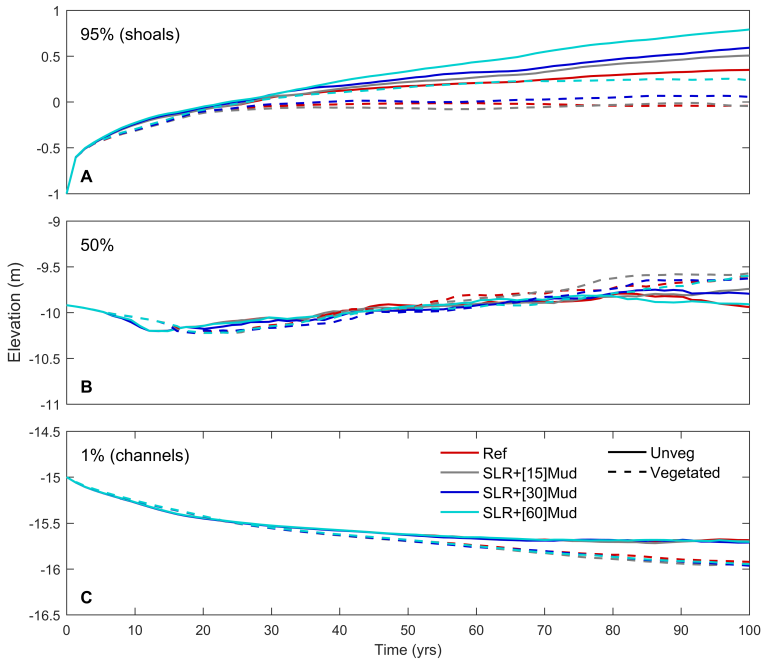

Figure 5.6: Timeseries of bed elevation distribution of the inner basin depicted as (a) the 95^{th} percentile representing the higher shoals, (b) the median elevation and (c) the 1^{st} percentile representing the main channel depth. The elevation is relative to MSL at the beginning of the simulation.

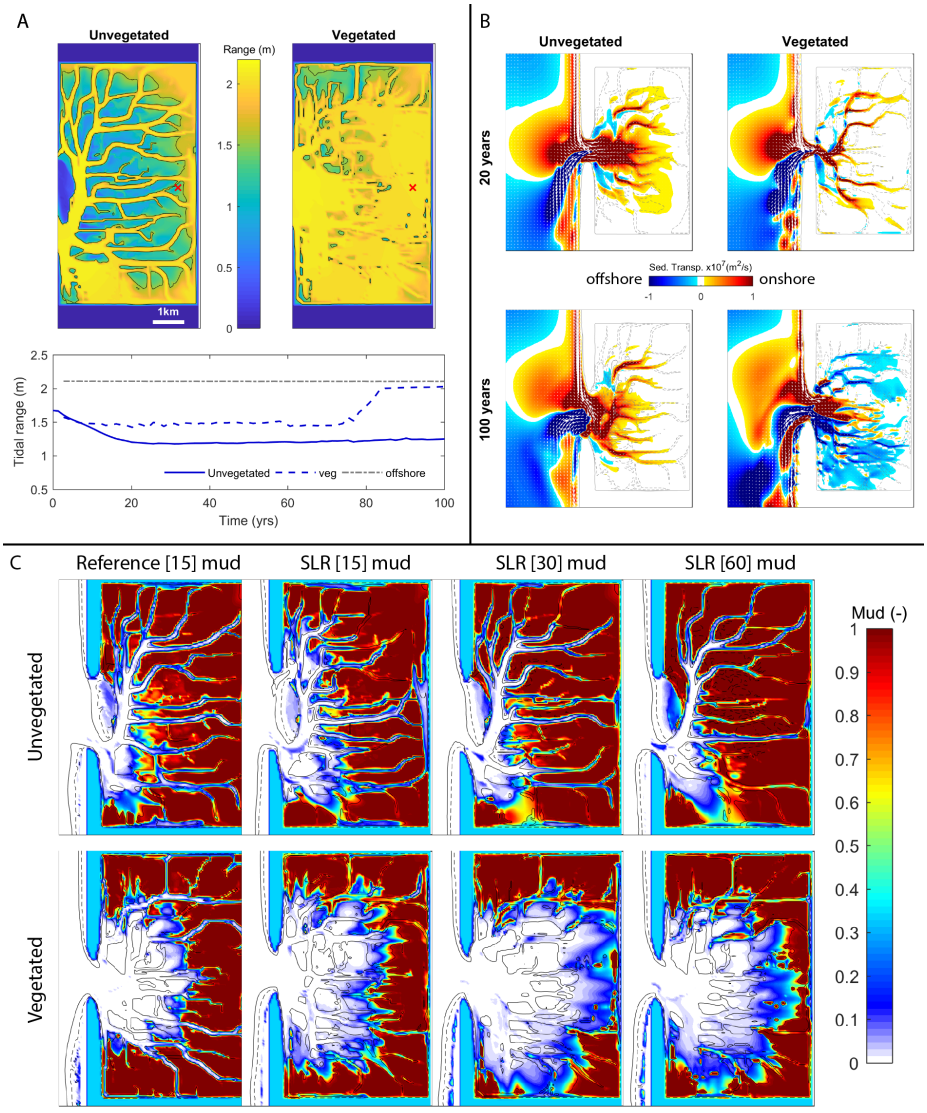

Figure 5.7: Import and export of the backbarrier basin. (a) Map of tidal range after 100 yrs for the scenarios with SLR and 30 mg/L clay concentration. Lower panel shows the time series of tidal range on the red cross location in the maps. (b) Sediment transport integrated over a spring-neap tidal cycle from the scenarios with SLR and 30 mg/L of clay. The colors represent the E-W directed net sediment transport where positive means import (flood-directed) to the basin. The arrows denote the net sediment transport vectors and the contour lines are -0.8 and 0.8 m depth, indicating approximately the intertidal areas. (c) Maps of relative mud fraction distribution against sand after 100 years.

5.3.2 Transition from infilling to drowning

The question is what controls the system-scale infilling or drowning of the tidal basins under the imposed sea level rise. The change from import (flood-dominance) to export (ebb-dominance) with ongoing sea level rise takes place before the vegetation starts to collapse. Figure 5.8a shows that first the tidal basin changes from importing to exporting sediment, induced by the eco-engineering effect of vegetation, and later the vegetation coverage starts to decrease due to erosion (uprooting) and drowning (longer inundation periods). In other words, vegetation mortality results from initial erosion, then later drowning. The only exception is with low mud supply (15 mg/L) when the erosion and vegetation mortality happen simultaneously.

The presence of vegetation reduces the basin dynamics (Figure 5.8b), defined as tidal prism (i.e. tidal discharge through the inlet) divided by accommodation space (i.e. total water volume in the basin), when compared to the non-vegetated analogue scenarios. That means a decrease of tidal prism relative to the accommodation space which translates in more water retention, larger flood storage and therefore ebb dominance. However, the non-vegetated scenarios show a persistent infilling trend, whereby the higher the mud content, the higher the infilling rate. Conversely, vegetation effects reduce the infilling independently of mud concentration. Figure 5.8b shows that scenario 8 (vegetation + SLR + [60]mg/L) has an incipient infilling trend, but reverts to the same lower infilling rate as the other scenarios. Scenario 7 with intermediate mud concentration (vegetation + SLR + [30]mg/L) resulted in negative infilling, meaning a negative sediment balance after 100 years, which is also shown in Figures 5.3 and 5.7. Scenario 5 (vegetation + no SLR + [15]mg/L), although showing similar sediment export trend, indicates a strong decrease in the rate of sediment export in the last decades while the vegetation coverage is still stable and maximum compared to the other scenarios.

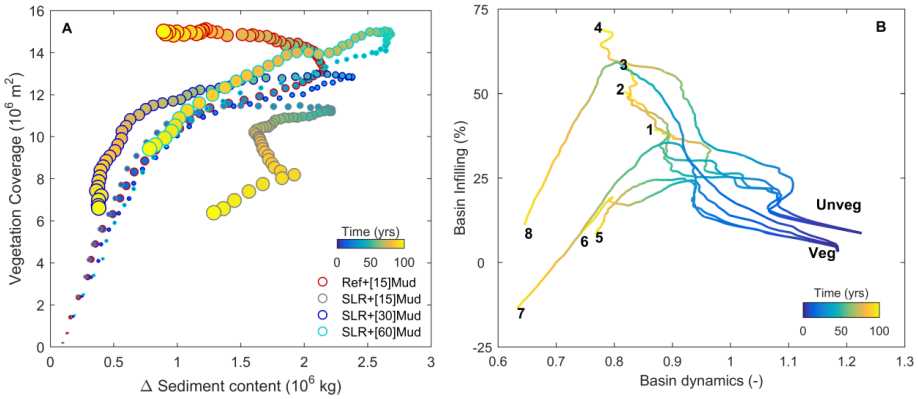

Figure 5.8: Backbarrier infilling. (a) Plot of vegetation coverage versus the sediment mass of the tidal basin relative to the initial condition. Color denotes time and the dot sizes are proportional to the normalized accommodation space. (b) Plot of basin dynamics defined as tidal prism divided by accommodation space versus basin infilling which consist of basin volume divided by the initial accommodation space. The numbers refer to the model scenarios depicted in Figure 5.3.

In summary, from our set of models we observe a cascade of biomorphodynamic events that in the long-term resulted in distinct end-members (Figure 5.3) of the coastal barrier system following basin development and vegetation settling with sea level rise. The unvegetated basins were able to infill with sediments under all scenarios of sediment supply and sea level rise towards a steady state regarding tidal prism and accommodation space. Conversely, our vegetated basins only achieved a steady state without sea level rise. The increase of accommodation space induced by sea level rise followed an increase in tidal prism that could not be compensated by sedimentation. In fact, the basin developed ebb-dominance which resulted in net erosion and vegetation mortality, which represents a positive feedback towards erosion and drowning.

5.4 Discussion

Our novel set of models show that vegetation changes the morphodynamic feedbacks of the coastal barrier and that under sea level rise the basin drowns and the marsh coverage declines irrespective of the sediment supply. Now we discuss the different (quasi-) steady states, how our model results relate to past and modern natural environments, and how our results enlighten future adaptations in face of climate change and sea level rise.

5.4.1 Multiscale biomorphodynamic interactions and steady states

Previous works showed that vegetation dissipates hydrodynamic energy e.g. van Wesenbeeck et al., 2022 and consequently increases sedimentation e.g. D'Alpaos et al., 2007; Fagherazzi et al., 2012; Nardin et al., 2018; Contti Neto et al., 2022. This mechanism is supposed to stabilise landscapes and to allow for vertical bed level accretion to keep up with sea level rise (Kirwan et al., 2016), suggesting that restoration of wetlands is an invariable nature-based solution for coastal protection (Schuerch et al., 2018). This contrasts with the main findings of this study. Our results show that the long-term biomorphodynamic interaction of vegetation and sea level rise may lead to net erosion, vegetation mortality and final basin drowning, while without vegetation the basin may keep up with sea level rise.

Vegetation initially reduces the basin dynamics Boechat Albernaz et al., 2020, similar to and sedimentation takes place near feeder channels, which suggests that vegetation promotes fast infilling and reduction of accommodation space. However, similarly to D'Alpaos et al. (2007), Boechat Albernaz et al. (2020) and van Dobben et al. (2022), we showed that large patches of vegetation limit the conveyance of sediments, including mud, further from the feeder channels. This results in vegetation confining flow and sediment transport to channels, which was also observed in coastal (Schwarz et al., 2018; van Dobben et al., 2022) and fluvial systems (Kleinhans et al., 2018). However, our models show that these local effects of vegetation have a basin-scale implication in the long-term. The long-term and large-scale morphodynamic effects of vegetation are to change the tidal dynamics through depth distribution (Figure 5.6a) and flood storage within the basin (Friedrichs and Aubrey, 1988) and consequently the sediment balance (Figure 5.5c and Figure 5.7b) of the entire basin.

Previous studies found that the tipping point for marsh survival and basin infilling are related to ratios of the sediment supply and sea level rise rates, e.g. Kirwan and Murray (2007),

Kirwan et al. (2010), D'Alpaos (2011), and Fagherazzi et al. (2012). However, unlike previous saltmarsh models, with enforced sediment concentration at the inlet boundary (e.g. Kirwan and Murray (2007) and Mariotti and Canestrelli (2017b)), our model has a dynamic and free-evolving coastal zone where the wave-tidal conditions interacting with the nearshore and ebb-tidal delta to determine the sand-mud concentrations and the sediment budget (including sediment bypassing) of the basin. As a result, we were able to unravel a new and system-scale biomorphodynamic feedback where vegetation combined with SLR triggers a cascade of effects towards drowning that could not be counteracted by increasing sediment (mud) availability. These feedbacks eventually led to erosion and basin drowning under sea level rise even before the vegetation started to decline. Moreover, the basin drowning could not be counteracted by increasing the supply of mud as the basin develops a net sediment export behaviour. The long-term erosive trend resulted in the growth of subtidal flats, also called "pools" see Figure 5.1 and Mariotti, 2020 as a consequence of the habitat loss. The unvegetated cases with the same conditions developed to a steady state between accommodation space and infilling. These findings demonstrate that the basin infilling and steady state is a result from the multiscale biomorphodynamic interaction related to the spatial connectivity of sediment pathways within the barrier coast (Elias et al., 2019; Pearson et al., 2020). In other words, the dynamics between the coastal area and the basin biomorphodynamics are determinant for the tidal basin and marsh survival.

This leads to the question whether these alternative equilibrium states are observed in natural systems. Figure 5.9 shows the depth distributions of natural tidal basins and modelled tidal basins, subdivided in vegetated and unvegetated conditions. From the natural systems, we observe the sharp predominance of inter- subtidal flats (leptokurtic distribution) and shallower wider channels on the unvegetated German and Dutch (Ameland) Wadden Sea Fitzgerald et al., 1984; Elias et al., 2019, Figure 5.1 and. Conversely, the vegetated systems see Hein et al., 2012; Carrasco et al., 2018; Nardin et al., 2018; Donatelli et al., 2020, in general, present a wider depth distribution (platykurtic) or even bi-modal distribution (e.g. see VCR in Figure 5.1) of deeper and narrower channels, and a wider depth range between supra and subtidal flats including the higher (vegetated) shoals. This comparison strongly suggests that vegetation affects the depth distribution of channels, shoals and flats, and that the alternative stable states exist in nature, similar to Marani et al. (2013). This does not exclude the possibility that other causes determine system development, equilibrium conditions and the presence and absence of vegetation. Nonetheless, our models support that the existence of different equilibrium states may manifest solely upon the presence-absence of vegetation while all other boundary and initial conditions are the same.

The tidal basin evolution and its response to changes in conditions, such as SLR or marsh decline, also relates to the larger-scale coastal barrier behaviour. Over long timescales (*O*-centuries to millennia) a barrier coast may adjust the accommodation space of the tidal basin via the translation of the barrier (i.e. regression or transgression) (van der Spek and Beets, 1992; Vos, 2015; FitzGerald et al., 2018). The FitzGerald et al. conceptual model (see Figure 22 in FitzGerald et al. (2018)) shows that marsh decline follows an increase in the tidal prism, accommodation space and the growth of the ebb- flood-deltas. However, at a later stage, the barrier tends to migrate landward (i.e. barrier transgression) which reduces the accommo-

dation space. Our models, despite the fact that they cannot simulate barrier migration, show similar response regarding the marsh collapse and the tidal prism growth. However, in our models the marsh decline results from tidal prism growth and increasing erosion that started decades before the vegetation decline.

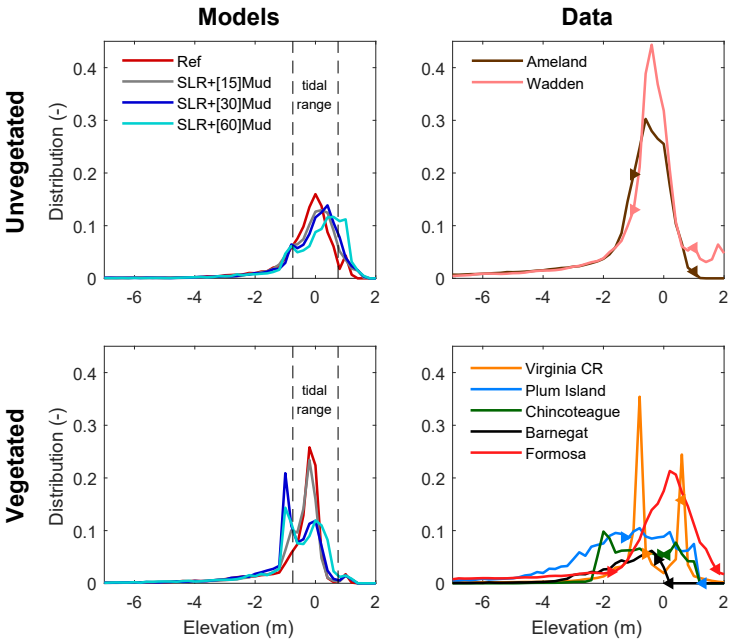

Figure 5.9: Bed elevation distribution of tidal basins from our models and natural systems. The arrow heads indicate the natural tidal range (right panels). Data from DGT (2011), Richardson et al. (2018), Donatelli et al. (2020), and Sievers et al. (2020) plotted relative to MSL.

The revealed multiple equilibrium states and complex multiscale feedback mechanisms controlling vegetated and unvegetated tidal basins connected to the barrier coast points at the risk of using simplified models or empirical equilibrium relations to predict their morphological evolution. The empirical equilibrium relations (e.g., inlet cross section versus tidal prism) or models with boundary conditions imposed inside the barrier coast (e.g., at the inlet) are insufficient to predict long-term effects of sea level rise on barrier coasts. As we showed, the complex barrier coast multiscale feedbacks and sediment pathways are crucial in predicting the ebb tidal delta and the inlet geometry and the resulting sediment fluxes across the inlet, which are indispensable to understand the system-scale response of barrier coasts to SLR and sediment supply. A comparison of our model results and existing classical relationships between tidal prism and cross-sectional area of the inlet (Figure 5.10) shows that the reference runs without sea level rise have a much steeper trend than the empirical relationships, and in fact do not fully converge on any of them. Moreover, the final situation (top inset in Figure 5.10) after a century differs much between the runs, with vegetated

runs evolving towards larger cross-sectional inlet areas than unvegetated runs, even without sea level rise. The models without sea level rise, for which the simple equilibrium relationships were derived, have different stable states due to the presence or absence of vegetation, in agreement with observations (Marani et al., 2013; van Belzen et al., 2017; Schuerch et al., 2018). To reveal those systemic connections across the sub-domains of a barrier coast the modelling of the entire barrier coast is required.

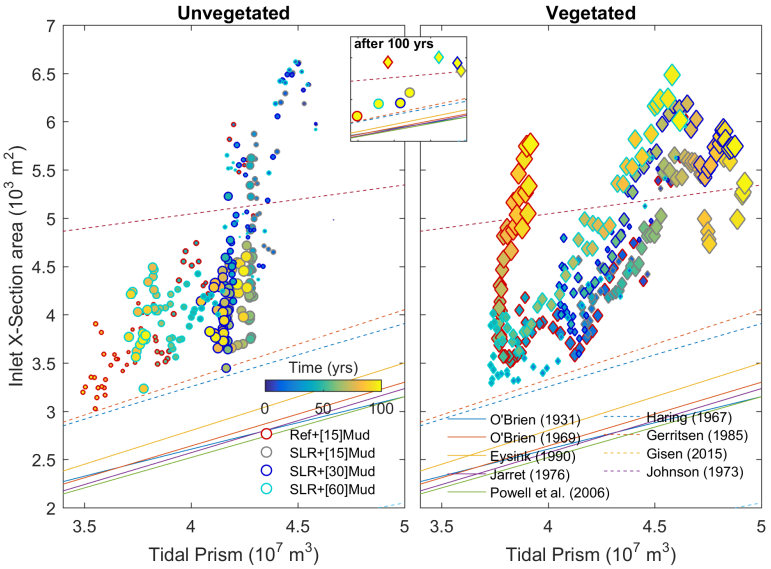

Figure 5.10: Inlet cross-sectional area versus tidal prism for the unvegetated and vegetated model runs, showing that neither the equilibrium nor the changes under sea level rise follow the trends predicted by relationships from literature in Leuven et al., 2018b. Dot sizes are proportional to the normalized accommodation space. Inset shows the final condition at the end of each model run.

5.4.2 Past and future evolution of barrier coasts

The model results of basin evolution under SLR and the biomorphodynamic feedbacks are consistent with the paleorecords of the mid-Holocene Dutch coastal plain that inspired this research. In our models with sea level rise on a late stage of infilling (i.e. mature infilled basin), the vegetation perished and lost its infilling effects for a sea level rise rate of 0.5 m per century, despite the littoral (sand) and offshore (mud) supply of sediment. The vegetated basin under SLR could not attain a steady state condition with respect to tidal prism and accommodation space (Figure 5.5 and 5.8b). Such (quasi-) steady state condition was only attained without sea level rise for both vegetated and unvegetated scenarios, and for the unvegetated scenarios with sea level rise. We expect that lower SLR rates would show similar behaviour to our 'no SLR' scenarios. Along the present-day Holland Coast, unvegetated backbarrier basins formed between the present-day cities of The Hague and Alkmaar around 7500 yr BP. These barrier systems formed under a sea level rise rate of approximately 0.3-0.5 m per century, while vegetation began to expand around 5000 yr BP when the sea

level rise rate declined to 0.1-0.05 m per century (Vos, 2015; de Haas et al., 2018; Hijma and Cohen, 2019; Pierik et al., 2023). The paleogeographical reconstruction of the basin around Leiden-Katwijk in the Old Rhine area from Pierik et al. (2023) showed that vegetation settled on the margins of the tidal basin under higher sea level rise rates and expanded towards the mouth as the rate of sea level rise declined. The decline in RSLR rate together with the substantial fluvial sediment supply from the Rhine river promoted the infilling of the basin that allowed for the settlement and expansion of vegetation.

Regardless of predicting a precise SLR rate for the vegetation collapse (which is not our intention with the schematised model setup and the few runs with limited SLR scenarios), our results highlight the possible fate of coastal barrier systems under sea level rise, which is projected at 0.43 m rise until 2100 for RCP2.6 and 0.84 m until 2100 for RCP8.4 (Oppenheimer et al., 2019). Considering the predicted range of SLR, the reconstruction of the past Holocene Dutch coast and modern marsh research (FitzGerald et al., 2021) suggest that supra and intertidal areas will likely be reduced under RSLR rates in the order of 5mm/yr. In this scenario, the vegetation coverage will also decline due to drowning, similar to the model results. The loss of supra- and intertidal areas, and vegetation is especially valid for embanked and diked areas where the retreat and the landward expansion of the natural system is limited or impossible. If the past SLR rates and sedimentation was indeed the key limiting factor for vegetation expansion, then a strategy of nature restoration for increasing land-surface elevations may only work in sediment-rich environments, such as river estuaries see Pierik et al., 2023, while tidal basins may not be able to counteract drowning induced by RSLR. It is important to note that organic accretion promoted by vegetation, not incorporated in our models, but present in other model studies, e.g. (Fagherazzi et al., 2012), peat and soil formation is further subject to higher compaction rates in comparison with sand and mud. The higher soil compaction rate of organic-rich layer is mainly induced by the weight of clastic sediments, organic decay and also from drying out when the water table is lowered by natural or human processes (Pierik et al., 2018; Minderhoud et al., 2020). That said, vegetation and organic accretion can be seen as a comparatively fast short-term mechanism of infilling (Lorenzo-Trueba et al., 2012) but perhaps not a long-term solution for land rising. Conversely, sand and mud clastic deposits are less subjected to compaction and less prone to be altered by decomposition and decay in comparison with the organic matter.

The collapse of vegetation observed in our models, irrespective of varying sediment supply, and the indications of an initiation of collapse in field sites e.g. Baptist et al., 2016; FitzGerald et al., 2021; van Dobben et al., 2022, raise the question of whether the modelled salt-marsh vulnerability to sea level rise is oversensitive to model assumptions and short-term field measurements or if it is genuinely a fragile ecosystem that would indeed perish under accelerated sea level rise conditions (Kirwan and Megonigal, 2013). For example, our models do not incorporate organic soil growth or multiple marsh species (D'Alpaos et al., 2007) that would likely increase the marsh resilience and the ability of sedimentation and bed level rise (FitzGerald et al., 2018). However, our results can be seen as conservative estimates to be compared to sediment-dominated natural systems. Yet, this type of collapse can hardly be explored from paleogeographical records as there are no available record of eroded systems, let alone one where vegetation collapse was followed by erosion. Despite the lack of

long-term detailed paleorecords, the collapse of vegetation and its effects have been observed and projected in natural systems for the coming decades. For example, at the well-studied marsh of Plum Island in the USA, the marsh area is forecast to reduce dramatically by 2050 (FitzGerald et al., 2021). The projection of marsh reduction in FitzGerald et al. (2021) points that the Plum Island marsh (dominated by organic accretion) may lose a great portion of its high marsh in the coming decades under the RCP4.5 scenario. Part of the high marsh will possibly turn into low intertidal marsh which in turn increases the tidal prism that, similar to our models, could drive the whole marsh system towards a collapse. Our models show that the increase of flood storage and tidal prism can be an earlier trigger for erosion and marsh decline. Likewise, the Venice Lagoon in Italy shows a complex distribution of elevation-dependent saltmarsh states (Marani et al., 2013), all of which collapse under sea level rise rates between 0.39–0.59 m per century (Marani et al., 2007; Carniello et al., 2009; Marani et al., 2013). In contrast, unvegetated systems (or mostly unvegetated) such as the Dutch Wadden Sea are recognized to be able to cope with SLR rates up to 4-5 mm/yr due to a net import of sediments (van Dobben et al., 2022; Huismans et al., 2022).

The evolution of tidal basins is intricately connected to other elements of the barrier coast such as the adjacent sandy coasts, inlet and ebb delta (van der Spek and Beets, 1992; Elias et al., 2019; Lenstra et al., 2019; FitzGerald et al., 2000; Pearson et al., 2020; FitzGerald et al., 2021; Robbins et al., 2022). The underfilled state of our vegetated tidal basins in comparison with the vegetation-bare basins means that vegetated tidal basins need less sediments to reach (quasi-) steady state. Therefore, more sediments, especially sand, are available to the adjacent coast and to the ebb-tidal delta. The vegetated scenarios after 100 years promoted larger ebb-tidal deltas in the order of 10 million cubic meters of sand and fed the downdrift coast with 20 million cubic meters of sediments in comparison with the unvegetated scenarios. Similarly, the main channels in our vegetated basins are approximately 0.5 meter deeper on average (Figures 5.6 and 5.5). These changes promoted by vegetation mean better navigability for harbors and more sustainable downdrift coasts in terms of sediment availability. The lower trapping of sediments in the basin, which no longer acts as a sink of sediments, promotes more sediment bypass to the downdrift coasts. These eco-engineering effects of marshes, therefore, translate into societal benefits within the basin but also beyond the barrier coast domain. These benefits enclose, for example, less need of extensive dredging, mitigation of downdrift structural coastal erosion that minimize the need of beach nourishments to try and avoid the coastal squeeze and having to abandon coastal plains (Siders et al., 2019). Therefore, apart from the intangible value of vegetation, the biomorphodynamic effects of a healthy tidal basin have positive implications on the barrier system as a whole. Yet, the collapse of coastal vegetation, such as saltmarshes and mangroves, due to accelerated sea level rise and climate change, may not only trigger losses in important ecosystem services, but also changes in the morphodynamic equilibrium state towards an unknown alternative state that mostly likely differ from the analogue unvegetated state due to hysteresis (Kleinhans et al., 2018).

5.5 Conclusions

Our set of biomorphodynamic models of an entire barrier coast system with a vegetated backbarrier tidal basin show that vegetation drives the tidal basin morphodynamics to an alternative steady state condition in comparison with unvegetated scenarios under otherwise the same conditions. The local vegetation effects on hydrodynamics and sediment transport first reduces shoal growth while deepening the channels, which later cascades to a basin-scale transition from flood-dominant to ebb-dominant conditions and consequently a tipping from net import to net export of sediments.

The contrasting morphodynamic evolution between unvegetated and vegetated basins has major implications in the scenarios with sea level rise. Here, the vegetated scenarios, despite abundant sediment (mud) supply, could not keep up with the increasing sea level. The export of sediments combined with increasing water levels leads to an increase in tidal prism, erosion and vegetation mortality. Vegetation mortality and the formation of subtidal flats (ponds) causes a further increase of tidal prism as a positive feedback mechanism towards basin drowning. Large-scale vegetation mortality ensued and the system drastically changes to a new, drowned stable state. Conversely, the unvegetated scenarios persistently import sediments under sea level rise that compensates for the increase in accommodation space.

These findings highlight the potential consequences for natural systems that cannot keep up with the increasing climate and sea level rise pressure. While vegetation has been argued to invariably enhance sedimentation to keep up with sea level rise, our results suggest that in the long-term, vegetation can reduce sedimentation in tidal basins. This counter-intuitive and novel insight derives from a cascade of biomorphodynamic effects and feedbacks that revert the initially intertidal importing system to an export intertidal and subtidal state.

From a societal-economical perspective, the vegetated systems result in deeper channels and need less sediments to achieve a steady state condition. This implies that more sediments are available to the coastal system. This means less need for dredging of navigation channels and also less need for nourishment of the downdrift coast. Moreover, marshes and coastal vegetation should be preserved but should not be seen as a direct measure for sedimentation that can be indiscriminately applied in future adaptations to sea level rise. Rather, human interventions will need to account for the complex biomorphodynamics that determine the fate of tidal basins and barrier coasts.

Acknowledgements

Supported by ERC Consolidator grant 647570 to MGK. The computer resources were further supported by NWO-SurfSARA project 17635, and the Geosciences Eejit cluster at Utrecht University. The authors acknowledge the assistance from Edwin Sutanudjaja (UU), Lukas van de Wiel (UU) and Maxime Moge (SurfSARA) to compile and run Delft3D in the HPC Linux clusters, and João Dobrochinski (Deltares) for the guidance with the Mormerge parallelization. We thank the reviewers, including Brad Murray, for their commitment and engagement to our article through constructive and challenging comments that highly improved the final article. We are thankful to Harm Jan Pierik for the fruitful geological discussions. We further acknowledge Ana Rita Carrasco and Óscar Manuel Fernandes Cerveira Ferreira from Universidade do Algarve for sharing recent complementary bathymetric data from the Ria Formosa, PT.

Delft3D steering settings from our reference scenarios (model 1 and model 5) and main model results are available at the repository YODA (Boechat Albernaz, 2022). Delft3D source code is freely distributed and available at the Deltares (SVN) repository from Boechat Albernaz (2019). The vegetation module is also available at Brückner (2020) based on Brückner et al. (2019). Data from natural systems (see Figure 5.9) were obtained from DGT (2011), Richardson et al. (2018), Donatelli et al. (2020), and Sievers et al. (2020).

Chapter 6

Biogeomorphodynamics: a discussion

6.1 Introduction

In this thesis I applied numerical models in order to test hypotheses inspired by the paleogeographical reconstructions of the Dutch delta during the Holocene. The biogeomorphodynamic numerical models were idealized in a way to represent no specific site but rather a larger collection of natural analogue sites. In this way, I was able to compare the model results with several natural fluvial, estuarine and coastal systems. Here we can learn both from how the models matched the observations, and therefore reproduced nature to some extent, but also, when the models did not reproduce nature or deviated from empirical relationships.

Modelling the long-term evolution of large-scale environments with comprehensive models and processes, such as tides, waves and fluvial discharge and taking into account sand-mud mixtures and biota altogether was a technical challenge by itself that first required the improvement of numerical models, here the Delft3D morphodynamic model. Therefore, the first part of this synthesis covers the model developments presented in Chapters 2 and 4, which refers to hypotheses 1 and 2. With the improved models set to run in HPC clusters and desktop computers, I was able to study and unravel novel mechanics and processes that shaped levees, crevasses, inlets, tidal basins and consequently entire estuaries and barriers coasts including the effects of vegetation at the scale of kilometers over centuries. These findings are covered in the Chapters 3 and 5 (hypotheses 3–5) with a view on the implications related to geological reconstructions.

Here in the synthesis, I devote special attention to the model improvements, the effects of vegetation on the morphodynamics and to the implications of varying boundary conditions such as tides, fluvial discharges, sea level rise and sediment supply (in both past and future context) and how natural and human-induced environmental changes can modify and perhaps steer the fate of entire fluvial-coastal systems.

Finally, I formulate recommendations for future work based on unanswered questions but also on new questions that emerged from this research.

6.1.1 Model improvements

The long-term evolution of coastal-fluvial landscapes in numerical models is strongly controlled by the parameterization of the transverse bed slope sediment transport and the near-bed wave orbital velocities (hypotheses 1 and 2), as shown in Chapters 2 and 4. Both parameterizations in the long-term affect the local and system-scale morphodynamics through a series of cascading feedbacks. Only when these processes were properly steered, the large-scale model presented in Chapter 5 was able to simulate more natural looking channels, shoals, inlet migration and the offshore shoals and ebb delta. Similarly, levees from Chapter 3 only

grew with the inclusion of several sediment fractions in combination with appropriated bed slope effects.

Chapter 2 demonstrates that the choice of sediment transport predictor, here Van Rijn et al. (2004) and Engelund and Hansen (1967), coupled to the transverse bed slope parameterization of Koch and Flokstra (1981) and Ikeda (1984) determines the pattern and magnitude of sediment transport that consequently modifies the landscape. Therefore, hypothesis 1 was verified as positive. It turns out that the combination of different choices lead to realistic predictions of either sediment transport, slopes or overall morphology. The type of environment, such as depositional or erosional, also influences the model behavior (see Chapter 2). Until now, conclusions about transverse bed slope parameterizations that produced reasonable morphology were usually based on only one environment, such as estuarine (e.g. van der Wegen and Roelvink, 2012) or deltaic (e.g. Van der Vegt et al., 2016). The model results in Chapter 2 unraveled that the transverse bed slope parameterization coupled to the sediment transport predictor determines the potential of sediment deflection and morphological diffusion by eroding higher grounds (shoals) while depositing in deeper areas (channels). The morphological diffusion effect is stronger for the sediment predictor of Engelund-Hansen (EH) that computes total transport, i.e. no differentiation of bed load and suspended load. Furthermore, EH predicts, in general, more sediment transport compared to Van Rijn (VR), and therefore, more sediment is deflected down the slope. Conversely, VR predicts less total sediment transport than EH, apart of sorting out bed load and suspended load from which only the bed load is subjected to bed slope effects. As a consequence, VR tends to carve deeper channels due to the stronger nonlinearity of sediment transport in response to local flow. In numerical models the choice of transverse bed slope method and the applied magnitudes need to also artificially compensate for models weaknesses derived from the computation and numerical discretization of sediment transport, but also from grid-dependent diffusion. The interrelation of transverse bed slope parameterization, sediment transport predictor and numerical artifacts results in the need for large deviations in settings from the actual magnitude of slope effects observed in physical experiments (Baar et al., 2018b). The lack of a clear a priori definition of parameters to be applied in morphodynamic models poses an extra challenge for modelling long-term morphodynamics.

Similarly, the parameterization of the near-bed orbital velocities from Chapter 4 also showed local and large-scale effects on the sediment transport and on the long-term evolution of coastal systems, both on the open coast and within the tidal basin (Chapter 5). Therefore, hypothesis 2 was confirmed. Until now, it was challenging to obtain coastal equilibrium in two-dimensional numerical models due to the need to balance the onshore and offshore directed transport. Balancing the onshore-offshore sediment transport within the beach profile is further challenging due to lack of 3D and vertical circulations patterns present in the nearshore such as the undertow. The classical wave parameterizations were often derived from scaled physical experiments that reproduced only velocity skewness while neglecting velocity asymmetry (also called acceleration skewness), see e.g. Dean and Perlin (1986) and Stive (1986). Furthermore, the parameterization of Isobe-Horiwaka (Isobe and Horikawa, 1982) (IH), largely applied in numerical models such as Delft3D (see Grasmeijer, 2002), proved to overestimate skewness and the onshore transport while neglecting asymmetry (see

e.g. van Rijn et al. (2003), Dubarbier et al. (2015) and Chapter 4). The overprediction of the onshore directed sediment transport results in overfeeding of the shoreline which then builds out the coastal profile (shoreline progradation) and develops steeper slopes compared to nature in the nearshore area. Often, to counteract this artificial effect, modelers are forced to overcalibrate (i.e. applying calibration parameters beyond their expected range) their models (e.g. Nienhuis et al., 2016; Nienhuis and Ashton, 2016; Grunnet et al., 2004) focusing on either the cross-shore or alongshore transport, hampering the prediction of the overall morphology. This shortcoming has limited our ability to model complex environments such as barrier coasts and back-barrier basin where both cross-shore and alongshore sediment transport are important (Lenstra et al., 2019). Chapter 4 showed that the new parameterization from Ruessink et al. (2012) (RUE) based on field data that includes both velocity skewness and asymmetry better reproduced the wave shape and consequently the long-term coastal development. It is important to note that the morphodynamic improvements associated with the RUE parameterization are mainly related to the better prediction of the wave skewness as the sediment transport formulations in Delft3D, e.g. the VR04 (van Rijn et al., 2004), only calculate transport via velocity (skewness) while the sediment transport related to asymmetry (acceleration) is absent. Nonetheless, with the application of this new parameterization in Delft3D, we were able to achieve more natural (equilibrium) coastlines with more realistic cross-shore and alongshore sediment transport. The new orbital velocity parameterization opened up the possibility to simulate complex environments in the long-term, as we demonstrate in further applications, such as in Chapter 5.

I also found a link between the transverse bed slope problem (Chapter 2) and the wave-driven sediment transport problem (Chapter 4). The trend of the Van Rijn (VR) sediment transport predictor to promote deeper incision and one-cell channels (Figure 1.3c) observed in current-only models is less pronounced in combination with wave-current sediment transport. Chapter 4 shows that especially the combination of VR with the orbital parameterization of Isobe-Horikawa (IH), default option in Delft3D, artificially overestimates the bed load component, and therefore promotes excessive morphological diffusion via the bed slope mechanism (Figure 1.3b) that diffuses channels and shoals and therefore hampers the long-term modelling of tidal basins. These contrasting mechanisms partially explain the mismatch between transverse bed slope values derived from experiments and the values applied in numerical models, see Chapters 2, 4 and Baar et al. (2018b).

By combining the knowledge and model improvements gained with both transverse bed slope effects and wave parameterization (Chapters 2 and 4), it was possible to build novel models that for the first time were able to spontaneously create fluvial-tidal levees (Chapter 3) and develop a barrier coast and tidal basin with all of its elements such as ebb-tidal delta, shoals, spit migration and inner basin channelisation and infilling over a century (Chapter 5). With these models, the development of environmental conditions for eco-engineering vegetation also became within reach of the numerical model capabilities. Eco-engineering plant species were implemented on the basis of Oorschot et al. (2016) and Brückner et al. (2019) to enrich the predictions of the biogeomorphodynamics where vegetation also plays an important role in shaping the landscape. The biogeomorphodynamic models developed during

this project helped to better understand the past conditions observed in paleogeographical reconstructions as well to help predicting the future evolution of coasts and estuaries.

6.1.2 Hypothesis testing and novel insights

With the biogeomorphodynamic models, the remaining hypotheses 3 to 5 were tested, including the frequently voiced hypothesis that vegetation (invariably) helps sedimentation and infilling especially when sediments are scarce (hypothesis 5). Several scenarios of landscape evolution were explored under various boundary conditions and sediment availability, with and without vegetation, in two contrasting environments: a fluvial-tidal estuary in Chapter 3, and a barrier coast (wave-tidal) system in Chapter 5. The fluvial-tidal estuarine setup focused on the landscape evolution where levees were able to freely form and evolve under combinations of fluvial and tidal discharges and different eco-engineering species, namely reeds and trees. The wave-tidal setup consisted of a comprehensive sand-mud barrier coast system with marshes under the influence of wave climate, tides and sea level rise. Both set of models were largely inspired by the paleogeographical evolution of the Dutch coast during the Holocene (Figure 1.2) where all those elements interacted to build and transform the landscape.

The fluvial-tidal model of a floodbasin enclosed by coastal barriers and connected to upstream river in Chapter 3 showed that levees were able to form, grow and evolve under various combinations of fluvial and tidal conditions. Levees were built by intermediate grain sizes between the coarser channel sands and the finer muddy floodplain. Without the intermediate grain sizes, no levees were formed under otherwise the same hydrodynamic boundary conditions. Levees were narrower, higher and no crevasses were able to form when reeds (i.e. dense vegetation) were abundant in the floodbasin. Conversely, trees (i.e. sparse vegetation) promoted wider levees and more crevasses along the connection between the upstream river and the coast. It is conceivable that the combination of trees with other species would cause intermediate effects. Tides and fluvial floods enhanced the formation of crevasses and larger levees. Therefore, as hypothesized (hypothesis 3), the levees, crevasses and floodbasin are controlled by the fluvial-tidal conditions in combination with sediment supply and vegetation. Besides these end-member states in the levee morphology, the combination of fluvial-tidal discharges and different eco-engineering species highly modified the long-term fate of the overall landscape. The dense vegetation damped the tidal flow energy within the basin and ultimately the levee expansion connected the fluvial upstream system to the downstream coastal barrier. This connection completely ended the tidal influence (in terms of water level fluctuations and flow velocity) on the basin and turned the former tidal basin into a narrower estuary with lagoons on its side flanks. This set of model scenarios represents stages in the observed development of the Old Rhine estuary where the main branch of the River Rhine used to discharge during the mid-Holocene. The model results showed that the transformation from tidal basin to estuary could be solely driven by the growth of vegetation, while the offshore tidal conditions remained rather constant. Here, the vegetation damped the tidal influence and allowed the levees to connect with the coastal barrier. Without the tidal influence, the basins changed to a freshwater (or low salinity) lagoon, which further allowed the formation of peat that helped to infill the landscape. The models also showed

that crevasses, responsible for distal infilling, were absent when reeds were dominant, while abundant crevasses were able to form when trees were dominant in the floodbasin. Similarly, the Old Rhine had a transition from back-barrier basin to an estuary (de Haas et al., 2018) where levees were able to grow and the transition from reeds to trees helped to create crevasses systems along the fluvial-tidal domain. Ultimately, the Old Rhine floodbasin was infilled by sediments and peat (van Dinter, 2013; Pierik et al., 2017b; Pierik et al., 2023), as we see in the landscape of the area between Utrecht and Katwijk nowadays.

The wave-tidal model of a coastal barrier enclosing a backbarrier (non-)vegetated basin (Chapter 5) showed at first that the long-term evolution of the barrier coast comprised an intrinsic and tight dependency between the morphological units, such as the open coast, ebb-delta, inlet and tidal (backbarrier) basin. This finding verifies hypothesis 4 that the coastal barrier evolution is a product of all sub-environment units interacting altogether. These units interact through complex multi-scale feedbacks that control the overall long-term evolution of the system. The model results showed contrasting morphological end-member and equilibrium states between vegetated and unvegetated basins with sea level rise and otherwise constant boundary and initial conditions among all scenarios. The dense (marsh) vegetation changed the local channel and shoal configurations which in turn controlled the overall ebb-flood dominance and consequently the import and export of sediments. Vegetation narrowed and deepened the channels while also increasing friction on the higher vegetated grounds (e.g. shoals and bars). These effects of vegetation on friction and on bank stability are well-known from both nature and other modelling studies. However, we unravelled that these effects generate cascading multi-scaled effects on the large-scale and long-term evolution on the entire barrier coast system. Instead of retaining more sediments, as expected, vegetation promoted the export of sediments towards the open coast through its long-term effects on the morphodynamics. These findings falsify hypothesis 5 as in fact the long-term effect of vegetation was to decrease sedimentation under sea level rise. The net sediment export combined with sea level rise (i.e. increase of accommodation space) caused vegetation collapse and basin drowning. Conversely, the unvegetated basins predominantly evolved with muddy (lower) flats and wide and shallower channels that were flood-dominant and therefore favored the import of sediments and could keep up with the imposed sea level rise.

The effects of vegetation on the biogeomorphodynamics can be observed from both fluvial-tidal and wave-tidal models. The models of the river-dominated basins and the wave- and tide-dominated basins showed the strong effect of vegetation in controlling the long-term evolution of coastal landscapes. The vegetation, considered here as an internal condition rather than a boundary condition, changed the long-term evolution of the entire landscape. In the set of levee models, different types of vegetation promoted (in the case of trees) or inhibited (reeds) the formation of crevasses. Ultimately, dense vegetation dampened the tides in the floodbasin facilitating the levee extension up to the coastal barrier. That connection fully isolated and ended the tidal influence inside the floodbasin–an effect that is usually attributed to tidal-fluvial boundary conditions. Startlingly, Chapter 3 demonstrated that solely vegetation could steer this change. Moreover, vegetation in the barrier coast model (Chapter 5) changed the ebb-flood dominance and again steered the fate of the backbarrier into a different end-member when compared to the analogue unvegetated case with otherwise

the same boundary and initial conditions. The long-term, counter-intuitive effect of dense (marsh) vegetation was to decrease the net infilling of sediments when compared to the analogue non-vegetated scenario. These findings bring important insights about the long-term effects of vegetation on the biogeomorphodynamics. Commonly, vegetation effects on morphodynamics are considered only locally, via local sedimentation within vegetation patches, or as a passive agent on the landscape that will only survive or die-off while having little control on the landscape evolution. The models in this thesis show that in fact vegetation can steer large-scale morphodynamics changes that insofar have been attributed to changes in abiotic boundary conditions such as sea level fluctuations, tides, waves and sediment supply. The principle of equifinality (i.e. multiple conditions can lead to the same result) is still a challenge when interpreting geological-paleogeographical data towards a reconstruction, however we unravelled new insights that may help to enrich future paleogeographical reconstructions.

6.1.3 Long-term predictions and biomorphodynamic equilibrium states

Climate, metocean conditions and coastal environments are constantly changing under natural and human-induced forces. Several coastal plains and deltas around the world are eroding (retreating) as a combination of relative sea level rise, including subsidence, and lower sediment supply (Syvitski et al., 2005; Dunn et al., 2019; Eslami et al., 2019; Nienhuis et al., 2020). To predict the response of future adaptation to these changes, we first need to understand past developments and improve our knowledge and tools. One important question for long-term biogeomorphodynamic predictions is whether equilibrium states exist and to which extend they are valid. Just as an example: the convergent shape of an infilled estuary with elevated floodplains (e.g. Savenije, 2015) is a general equilibrium condition or a special equilibrium condition? In other words, how far the equilibrium states hold under changing conditions and forces such as climate, metocean and environmental changes? Some systems maintain a more defined and predictable equilibrium state, for example cases under topographic forcing of headlands and outcrops, such as embayed beaches and estuaries constrained in valleys (Townend et al., 2016). In the coastal zone, a forced equilibrium exist, for instance in headland pocket beaches where the sediment exchange is limited and the sand transport is mainly driven by waves (Hsu and Evans, 1989) in the alongshore direction as the cross-shore dynamics also follows a dynamic equilibrium in the long-term (Dean, 1977). The equilibrium condition of pocket beaches, with respect to the shoreline position, suggests that relatively closed systems with fewer degrees of freedom allow for more simplistic equilibrium approaches such as the Hsu and Evans (1989) parabolic shape to predict the equilibrium shoreline position (González and Medina, 2001). Similarly, the hydraulic geometry of rivers is rather well predicted based on classic equilibrium conditions (Gleason, 2015). However, estuaries and tidal basins are rather complex open systems with multiple open boundaries and evolve under a combination of independent hydrodynamic drivers, sediment supply, inherited geology and eco-engineering species that do not necessarily converge or return to some well-defined equilibrium or steady state condition (see Figure 5.10) as shown in this thesis.

The geomorphological predictors based on equilibrium states, such as the relations between the tidal prism and asymmetry and cross-sectional area of tidal inlets and ebb-delta volume and tidal flats (O'Brien, 1967; Dronkers, 1986; Escoffier, 1977) carry many assumptions and hidden conditions in their coefficients and mathematical shape of the relations (D'Alpaos et al., 2010). These so-called calibration values are therefore site and time dependent. For example, the free coefficients of hydro-morphological relations hide conditions of friction, inertia and sediment supply that are difficult to be taken into account when the system is under change due to sea level rise, sediment supply shortage or changes in vegetation. These predictors have been used, for example, on the adaptation of the Lauwerszee in the Dutch Waden Sea (Wang et al., 2009) after human interventions that closed part of the tidal basins with dikes. The complexity of the biogeomorphodynamics feedbacks in coastal systems suggest that a change in one or multiple conditions leads to a morphological development, permanently away from the past state (e.g. Zhou et al., 2017). The models from Chapter 3 and 5 show that a set of scenarios with exactly the same initial and constant or steady state boundary conditions but different internal processes due to the presence-absence of different vegetation species (Figure 1.4) leads the morphological evolution to different end-members, either in a steady state (equilibrium) condition or not. Especially the long-term effects of vegetation on the morphodynamics are most commonly absent or neglected in studies even though they change friction, tidal prism, channel-shoal and inlet dimensions, all with important long-term and multi-scaled effects on the geomorphology. More importantly, under climate change and human pressure, the biota assemblage is likely to change in the near future because of variations in temperature, precipitation, salinity and nutrients, and in that case, also the biogeomorphodynamics. In brief, the simple assumption of equilibrium morphology as a function of boundary conditions may be often problematic and risky, especially under changing natural and human-induced conditions.

Apart from the natural processes, human-induced subsidence from gas-water-salt extraction (e.g. van der Spek, 2018), and dredging and sand mining (Eslami et al., 2019) are also playing an important role on the fate of some coastal environments. The effects of sand mining have been studied at the Dutch delta (Cox et al., 2021) and Mekong Delta (Eslami et al., 2019; Eslami et al., 2021) and they vary from salinization (salt water intrusion) to sediment shortage for the entire fluvial-coastal system that enhance landscape drowning and coastal erosion. Coastal erosion is also induced and enhanced by sediment mining, upstream dams, breakwaters and groynes, and the suppression of natural vegetation such as mangrove forests (Xie et al., 2020) that act as a natural protection against storms and erosion.

Nature-based initiatives often promote the introduction of vegetation to enhance coastal protection, sediment retention and land level rise. The models presented here bring important insights with respect to the long-term effects of vegetation and sediment supply on the geomorphology. For example, without key sediment fractions, no levees developed (Figure 3.6) in the model even though all other conditions were suitable for levee formation. In turn, levees and crevasses are important features controlling the distribution of water and sediments into lowlands and floodplains. Vegetation also has important controls on the landscape. Vegetation itself can immediately and locally increase sedimentation. However, dense and large patches of vegetation decrease sedimentation further inland and away

from the main channel or sediment source. Ultimately, the backbarrier model in Chapter 5 showed that vegetation combined with sea level rise promoted a long-term cascading effect that changed the sediment infilling behavior of the basin, from importing to exporting. As a consequence, the vegetated basin could not keep up with sea level rise while the analogue unvegetated basin was able to infill and reached a steady state condition in terms of accommodation space and tidal prism. This counter-intuitive effect of vegetation has consequences for the design of interventions such as by sediment management strategies. Vegetation, as shown here, is not an invariable solution for increasing sedimentation and counteracting drowning due to sea level rise and sediment shortage. Therefore, we must take into account these biogeomorphodynamic feedback effects while planning future interventions, especially regarding the long-term effects of sediment starvation and the change of vegetation.

Under the imminent need to plan future adaptations facing for example sea level rise and sediment shortage, we must rely on better tools and knowledge to be able to mitigate negative effects and to improve the sustainability of human use of natural space. Here in this thesis, I showed that it is feasible and important to model complex biogeomorphodynamics of large spatial (***O***-kilometers) and long time (***O***-centuries) scales to improve, together with the robust semi-empirical models, the qualitative and quantitative predictions of the evolution of fluvial-coastal landscapes.

6.1.4 Food for thought

In this thesis I pushed at two distinct forefronts in the field of biogeomorphodynamics: improvements of modelling tools, and knowledge about the long-term biogeomorphodynamic processes of coastal-fluvial systems. On both fronts progress was made on this journey. This section intends to spark new, and perhaps societally relevant discussions and ideas for new research.

Regarding the model improvements, we still lack several processes, and further knowledge is needed of the natural world to narrow the gap between model results and nature. For example, the bed slope effects in numerical models are still detached from physics as they need to compensate for other model weaknesses. Currently, the choice and calibration of bed slope effects also needs to act as a morphological diffusion term to compensate for grid resolution, the staggered grid properties, the choice of sediment transport predictor and the condition of dominant erosion or deposition. Specifically, the choice of bed slope effect has a very strong control on the long-term geomorphology (Chapter 2 and Baar et al. (2019)). Furthermore, it is unclear how much the bed mobility of sand-mud mixtures controls the sorting of sediments and the effects thereof on the morphological development. Before the implementation of the new wave-driven sediment transport from Chapter 4 combined with the adjustment bed slope effect (Chapter 2) and the use of multiple size-fractions, both the levee and the tidal basin models showed rather flat and diffusive morphologies, or unrealistic extreme incision (Figure 1.3). Clearly, the model improvements are great, but what else are we missing to properly couple the bed slope effects to physics while leaving out numerical and model artifacts?

The formation of peat following vegetation development is another relevant model limitation in long-term mophodynamics. Peat infilled a great part of the Dutch landscape, but

also compacted considerably when overtopped by levee (sandy) sediments or when the water table was (artificially) lowered (Vos, 2015; Pierik et al., 2017a). Similarly, floodplain mud consolidates on time scales that the numerical models are now able to cover. However, peat dynamics and mud compaction processes are still absent or oversimplified in most numerical models available in the literature due to their complexity, our limited quantitative knowledge on this topic (Fagherazzi et al., 2012) and high computational cost (Winterwerp et al., 2018).

The inclusion of the eco-engineering effects of vegetation on morphodynamics is rather novel for process-based models such as Delft3D (e.g. van Oorschot et al., 2017; Brückner et al., 2021). While the results presented here are insightful, the ecological dynamics of biota incorporated in the vegetation module in the present model runs are primitive compared to the natural complexity. In nature, a species can disperse, settle, grow and die in many different ways, while here the models only accounted for a few abiotic causes of mortality, e.g. flow velocity, inundation period and erosion-deposition. The vegetation module also did not account at all for dispersion mechanisms and factors determining the growth. In reality, the colonization starts with a species being available and dispersed to the area (i.e. importance of the species reproduction and early-stage strategies for dispersion), having enough nutrients and (a)biotic conditions for surviving and growing. Competition, predation and facilitation add another level of complexity that would require an ecological model itself to predict a species distribution and interaction-dependent growth in the morphodynamic model, such as initiated in Brückner et al. (2021). Furthermore, the same group of species, for example benthic tube-builders, can have opposite effects depending on conditions (de Smit et al., 2021). On the one hand they promote more sediment erosion and resuspension via the increase in roughness with their tubes and because they convey mud from the substrate to the surface as they forage. On the other hand, their tubes, secretion and sediment mixing (mixing of sand-mud layers) add apparent cohesion to sand-mud particles. The combination of the opposed effects on the critical shear stress for erosion makes this an important but rather uncertain free parameter in most numerical models. For now, the approach of eco-engineering species represented by functional groups of stabilizers and destabilizers distributed over a certain range of abiotic conditions and environments is (as good as possible) a practical manner for further development of the field of biogeomorphodynamics.

Regarding the novel knowledge about the biogeomorphodynamics of natural systems and the driving mechanisms that shape coastal and fluvial environments, we gained valuable insights especially on the long-term feedbacks of vegetation into the morphodynamic loop. Here, one important question for future research is in which stage or part of the development cycle our natural systems are. For example: what are the long-term trends of the Wadden Sea (NL/DE), the Ria Formosa (PT), the USA East-Coast barriers and the Venice Lagoon (IT), and many other systems worldwide, in terms of evolution phases? Are they in a steady state or near collapse, and how can we know that (in advance)? Especially the model results from Chapter 5 show that basin drowning may start years-decades before the vegetation starts to decline. It thus implies that drowning is a "silent", difficult process to observe until it is perhaps too late for counteracting measures. A few studies have been conducted for individual saltmarsh patches (e.g. D'Alpaos et al., 2007) but not on entire environments. The fewer exceptions are the Plum Island study by FitzGerald et al. (2021) and the Wadden Sea studies

by Wang et al. (2012) and Wang et al. (2018). FitzGerald et al. (2021) was one of the first to empirically demonstrate the alarming and probable ongoing collapse of a marsh that is not keeping up with the environmental pressures. For the Dutch Wadden Sea, Wang et al. (2018) analysed the sustainability of the barrier system mainly in terms of sediment budget, showing that the shallower and sediment-rich eastern part of the Dutch Wadden Sea may keep up with higher sea-level rise rates in comparison with the Western portion. But why does the Wadden Sea not have abundant vegetation and is this absence a cause for it remaining open in contrast with the western coast of the Netherlands (that closed up in the mid-late Holocene), or is remaining open a consequence of different environmental conditions? The model results show that a barrier coast *without* vegetation, such as the Wadden Sea, is a great sink of sediments. In the Western part of the Wadden Sea, this sink behaviour was enhanced especially by the closure of the IJsselmeer and the large embankment of the coast by dikes. On the other hand, are the vegetated systems such as the Venice Lagoon and the USA back-barriers with their vegetation decline in an early stage of drowning? And if yes, what happens if the marsh erodes and disappears from the basins? Is it possible that they start capturing more sediment, if available or supplied? These questions are of extreme importance for society and future management and policy strategies regarding dredging, ports, fisheries, water and sediment intake and coastal protection. Nature-based restorations are conducted by promoting settling of sea grass, marsh species and bivalves (e.g. mussels and oysters) in order to counteract erosion and drowning. Here it is important to distinguish and identify the differences between restoring species that disappeared from the area in the near past, and therefore a desirable type of restoration, from introducing new or long-term vanished species that are not part of the ecosystem anymore. The latter can have large impacts on the morphodynamics as we demonstrated with the vegetated models, not to mention the ecological and perhaps economical impacts due to the changes in the natural equilibrium. The set of vegetation models presented here show the importance of assessing the long-term effects of biota in the biogeomorphodynamics (that were not trivial), among other relevant impact assessments.

Examples of combined vegetation collapse with their implications on the morphodynamics are virtually absent from paleogeographical records in the literature. Partially because one can hardly identify in the paleorecord a large-scale vegetation die-off together with its consequences in the landscape change from geological-paleogeographical record as they are often in an erosional hiatus in the records. Paleoreconstruction studies based on palynology, paleo-botany, diatoms and foraminifera are potentially able to identify large scale and abrupt changes in biota composition from the strata. In few cases, such a biota change has been correlated with abrupt changes in sedimentary successions, e.g. Pierik et al. (2023). However, as mentioned in this thesis, the problem is often to identify triggers and cause-consequence relationships between the sedimentary record and the biota, in addition of the equifinality problem. Here, the models and the approach presented in this thesis can help understating the biogeomorphodynamic processes that shaped the past landscapes. This combined approach, such as in Pierik et al. (2023), between biogeomorphodynamic modelling and geological reconstructions studies are key to unravel what happens with estuaries and coastal environments in the past, also under climate and sea level changes.

The long-term models developed here had the key premise of being free to evolve as the implemented physics dictated. There were no forced equilibria or limits to erosion and sedimentation. The question that remains open is: is there a morphodynamic equilibrium for tidal basins and estuaries in the time scale of decades-centuries? With the degrees of freedom of a wave-fluvial-tidal environment with multiple sediment fractions and vegetation interacting in different time-space scales, our idealized models suggest that there is hardly a clear equilibrium state after decades-centuries due several cascading feedback effects with multiple time-spatial scales acting altogether. Instead, multiple different steady states are possible, in part depending on the initial conditions and the boundary conditions. Other systems with fewer variables (and therefore less degrees of freedom) such as embayed beaches and rivers suggest that there is a more clear dynamic equilibrium for which empirical tools are more applicable. Such empirical equilibrium relationships are simple and robust, but limited by their equilibrium assumptions. Conversely, numerical models are complex and can simulate scenarios beyond its assumptions as far as the physics are valid. However, long-term predictions with such non-equilibrium driven morphological models can lead to uncertainties, and the often performed model validations for short-term simulations are commonly unfeasible for these longer time scales. Nonetheless, small deviations along the numerous timesteps (i.e. few seconds) upscaled to centuries within the morphodynamic feedbacks can lead to large deviations. Currently, the best approach is to cross-check the results among several methods and sources including geological reconstructions, and to analyze the model results critically to interpret the outcome given the known limitations and assumptions.

6.1.5 Conclusions

The model developments concerning the parameterization of transverse bed slope (TBS) sediment transport and the sediment transport driven by near-bed wave orbital velocities proved to improve long-term morphodynamic simulations in the sense that the simulated morphological development is now more realistic compared to nature. Although, the TBS values applied in numerical models, in general, still deviate from the empirical values derived from physical experiments. This discrepancy is likely due to the fact that the TBS needs to compensate for other model artifacts such as grid-size (dependency) and erosion-sedimentation processes. The choice of TBS varies with the sediment transport formulation, the grid size and the dominance of erosion or sedimentation. Furthermore, when coupling to wave-related sediment transport, the TBS also needs to be changed (mainly lowered) to account for the higher mobility condition induced by waves. In summary, the TBS is important for long-term morphology, however, it needs to be calibrated for every model setup.

The parameterization of near-bed orbital velocity from RUE showed better results in terms of onshore-directed but also alongshore sediment transport in open coasts when compared to the IH. The RUE parameterization takes into account both wave-induced velocity skewness and asymmetry, which when coupled to the skewness-based VR04 sediment transport predictor, resulted in more realistic coastal profiles compared to data from Katwijk (NL) and Duck (USA). Furthermore, when this parameterization was applied to the more complex case of a barrier island, the model showed dynamic ebb-tidal deltas that grew, migrated and

even merged with the downdrift coast. These ebb-tidal delta dynamics and the overall inlet development were not possible with the previous (default) version of Delft3D with IH.

The application of the biogeomorphodynamic model to a tidal-fluvial basin inspired by the Old Rhine paleoreconstructions showed that vegetation played a major role in transforming the coastal landscape. Furthermore, the results were able to unravel the fluvial-tidal, sediment supply and vegetation controls in building levees and crevasses that infilled the landscape. The dense reed vegetation in the floodbasin reduced the floodbasin sedimentation and the levee width but, more importantly, it inhibited the formation of crevasses that could have conveyed sediment to the floodbasins. Conversely, trees (sparse vegetation) enhanced the formation of crevasses. Furthermore, the set of models showed that vegetation alone was able to reduce the tidal effect in the floodbasin while enabling the seaward expansion of levees. The seaward levee expansion continued until the levees connected to the coastal barrier, closed off the floodplains and thus transformed the tidal basin into an estuary. Essentially, this shows that the transition of the Old Rhine from a tidal basin to an estuary could be solely driven by the settling of reeds (followed by later peat formation) with all other boundary conditions (offshore tides and fluvial discharge) being equal.

The back-barrier basin model responded strongly to the presence of marsh vegetation in a similar way. The vegetation in the tidal basin changed the local configuration of channels and shoals, which triggered a cascade of effects beyond the vegetation patches that changed the sediment import-export balance of the basin. The unvegetated basins, regardless the magnitude of the offshore supply of mud, imported sediments and kept up with sea level rise. Conversely, the vegetated basins showed a net export of sediments after the marsh establishment. Without sea level rise, the basin reached a steady-state (equilibrium). However, with sea level rise and varying supply of offshore mud the export of sediment led to basin drowning and extensive marsh mortality. This suggests that, in contrast with most literature, vegetation may not invariably contribute to the infilling that potentially counters sea level rise.

Of course, all models are wrong and nature is not. Scientific exploration of nature requires understanding the limitations of our tools and scientific knowledge builds on expert critical judgment of model outputs. I believe that such expert knowledge is also needed to help find better ways to co-exist with nature as good guests.

Appendix A

Supplementary information from: Critical dependence of morphodynamic models on empirical downslope sediment transport

Supplementary Figures

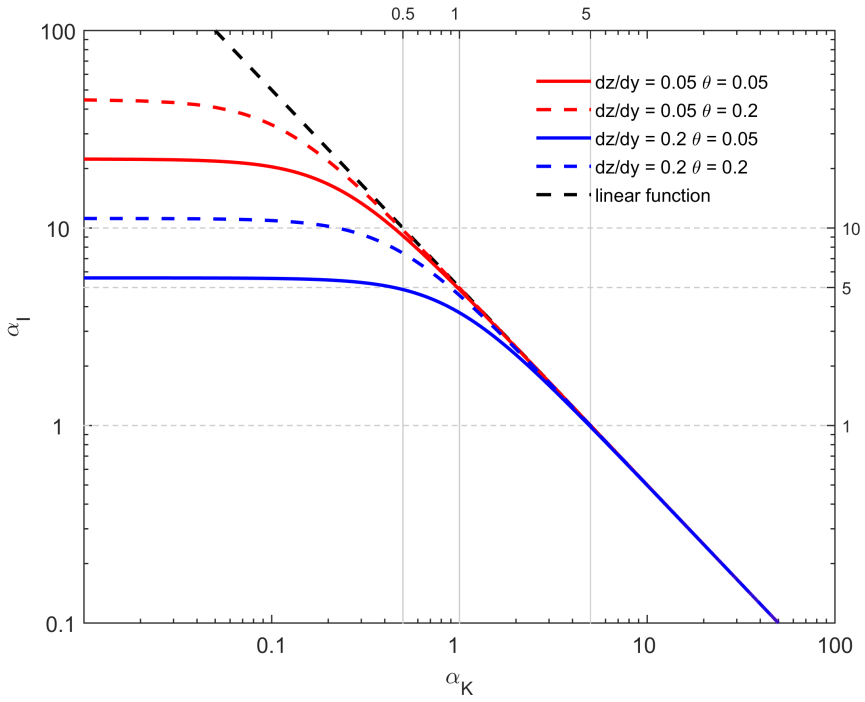

Figure A.1: Supplementary Figure 1: Relation between α_I and α_K, the input parameters of the two main options to calculate sediment transport on transverse bed slopes in the morphodynamic model Delft3D, when assuming equal downslope sediment transport (Eq A.7). Colored lines indicate combinations of transverse slope and sediment mobility, with a critical sediment mobility of 0.04. Gray lines indicate values for the α_I and α_K used in the delta model (Supplementary Figure A.6). Adapted from Baar et al., 2018b

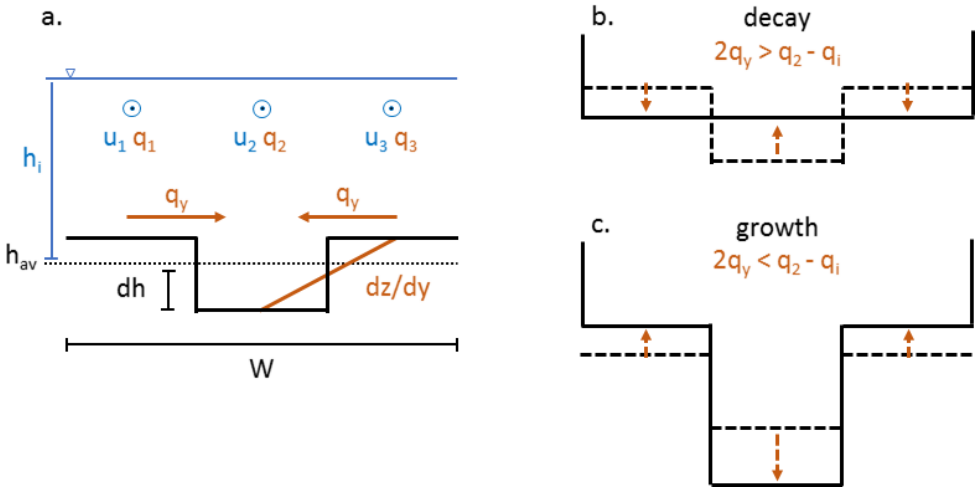

Figure A.2: Supplementary Figure 2: Concept of the analytical model. The cross-section is three grid cells wide with a bed level difference between the middle grid cell and the surrounding cells as an initial perturbation. The numerical channel is also based on this concept. a) Definition of the flow velocity and transport vectors, channel width (W), initial channel depth (h_i), bed level difference (dh), and transverse slope (dz/dy). b) The perturbation decays when transverse sediment transport is larger than the difference between incoming and outgoing sediment transport. The middle grid cell will accrete, while the surrounding cells will erode till the average bed level. c) The perturbation grows when transverse sediment transport is smaller than the difference between incoming and outgoing sediment transport. The middle grid cell will incise further, while the surrounding cells will accrete.

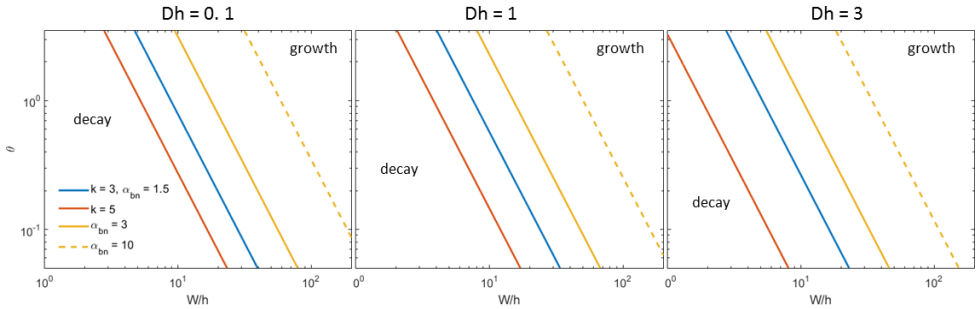

Figure A.3: Supplementary Figure 3: The trend in equilibrium width-to-depth ratios with increasing sediment mobility, for three different depths of the initial perturbation (dh), resulting from the analytical model. Colors indicate the non-linearity of sediment transport (k). Solid lines indicate default slope effect (α_I = 1.5), dashed lines indicate an increased slope effect (α_I = 10). Width-to-depth ratios to the left of these lines will result in a decay of the initial perturbation, while ratios towards the right will result in a growth.

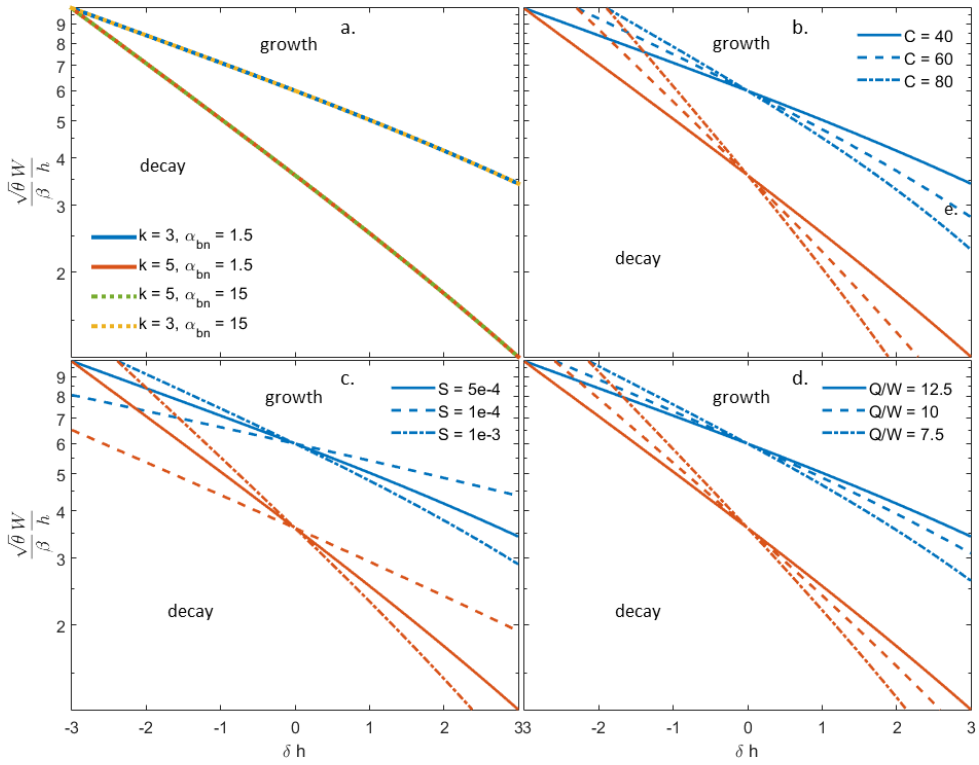

Figure A.4: Supplementary Figure 4: Channelization factor resulting from the analytical model, plotted against the depth of the initial perturbation. Width-to-depth ratios lower than these lines will result in a decay of the initial perturbation, while higher ratios will result in a growth.

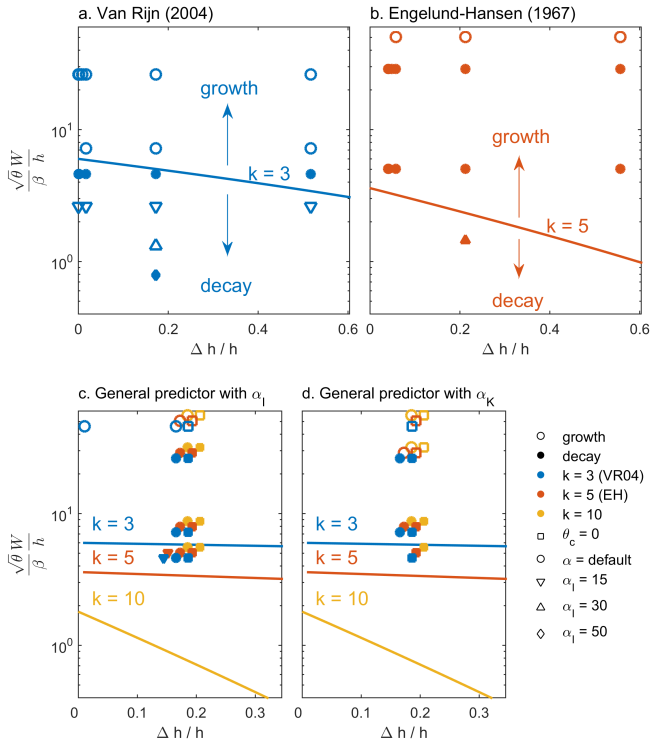

Figure A.5: Supplementary Figure 5: Comparison between the behavior of the analytical model (lines) and the numerical channel (symbols) with (a) the VR sediment transport predictor, (b) the EH sediment transport predictor, (c) the general transport predictor with the IK slope parameterization, and (d) the general transport predictor with the KF slope parameterization. The analytical model predicts the width-to-depth ratio (W/h) for a certain non-linearity of sediment transport (power k on shear stress) at which incision and downslope sediment transport are in balance. The channelization factor ($W/h\sqrt{\theta}/\beta$) is plotted against the relative depth of the initial perturbation ($\Delta h/h$). The perturbation in the numerical models either grows (open symbol), or decays (filled symbol). Colors represent non-linearity of the sediment transport predictor and symbols represent the magnitude of the slope effect based on the IK slope parameterization, or in case of the general transport predictor the absence of a critical sediment mobility.

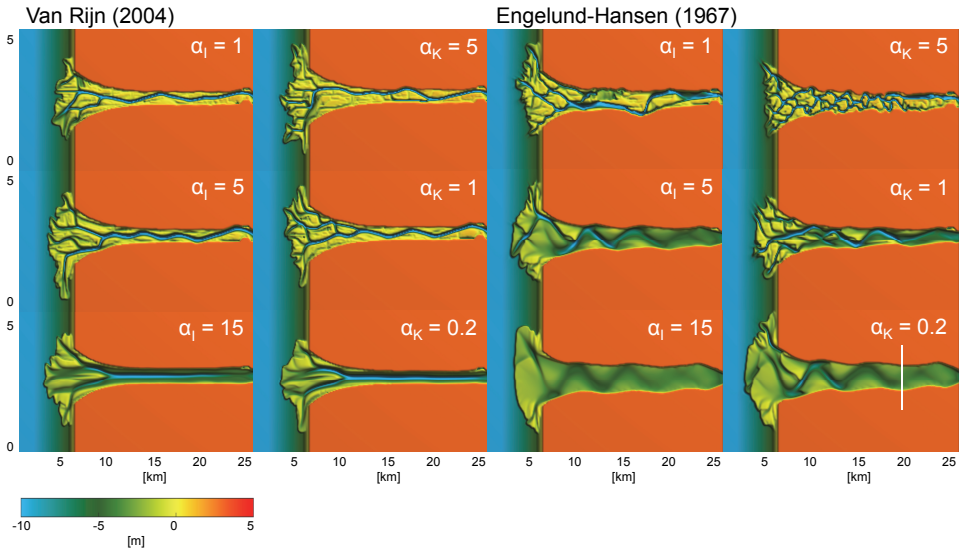

Figure A.6: Supplementary Figure 6: Morphology of 12 delta model runs after 1000 years for combinations of slope effect and sediment transport predictors. Maps on the horizontal axis have an equal slope effect, with slope effect increasing downwards. The α_I is the input parameter of the method of Ikeda, while the α_K is the input parameter of the method of Koch and Flokstra. The models in the first two columns were run with the VR sediment transport predictor, while the models in the last two columns were run with the EH predictor. The average sediment transport rates plotted in Supplementary Figure A.10 were computed for all model runs over a cross-section at 20 km, represented by the white line in the bottom right panel.

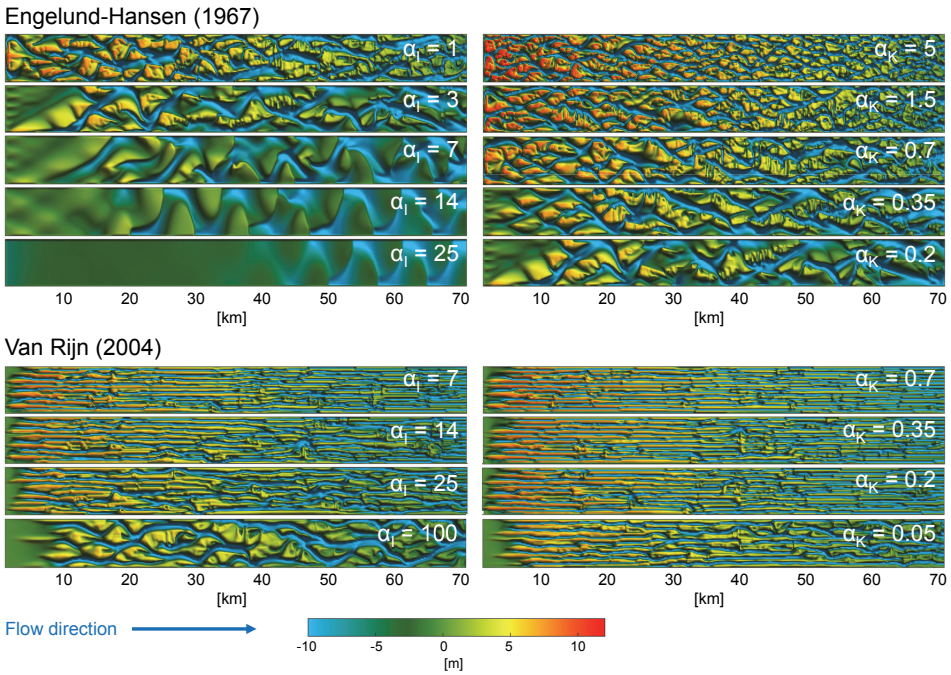

Figure A.7: Supplementary Figure 7: Morphology of 18 braided river model runs for all combinations of slope effect and sediment transport predictors. Models on the horizontal axis have equal slope effect, which increases downwards for each transport predictor. The α_I is the input parameter of the method of Ikeda, while the α_K is the input parameter of the method of Koch and Flokstra, both with defaults of order 1.

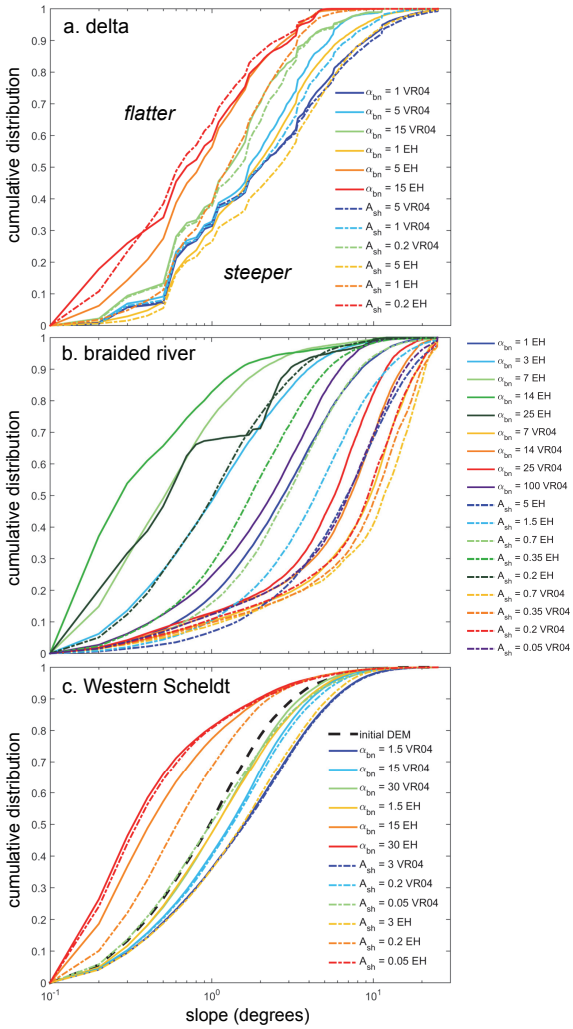

Figure A.8: Supplementary Figure 8: Cumulative slope distributions of (a) the delta model runs, (b) the braided river model runs, and c) the Western Scheldt model runs. Solid lines are results with IK and dashed lines are results with KF. Colors indicate equal transverse sediment transport magnitudes and the same sediment transport predictor. The black dashed line in the Western Scheldt plot represents a measured bathymetry used as input.

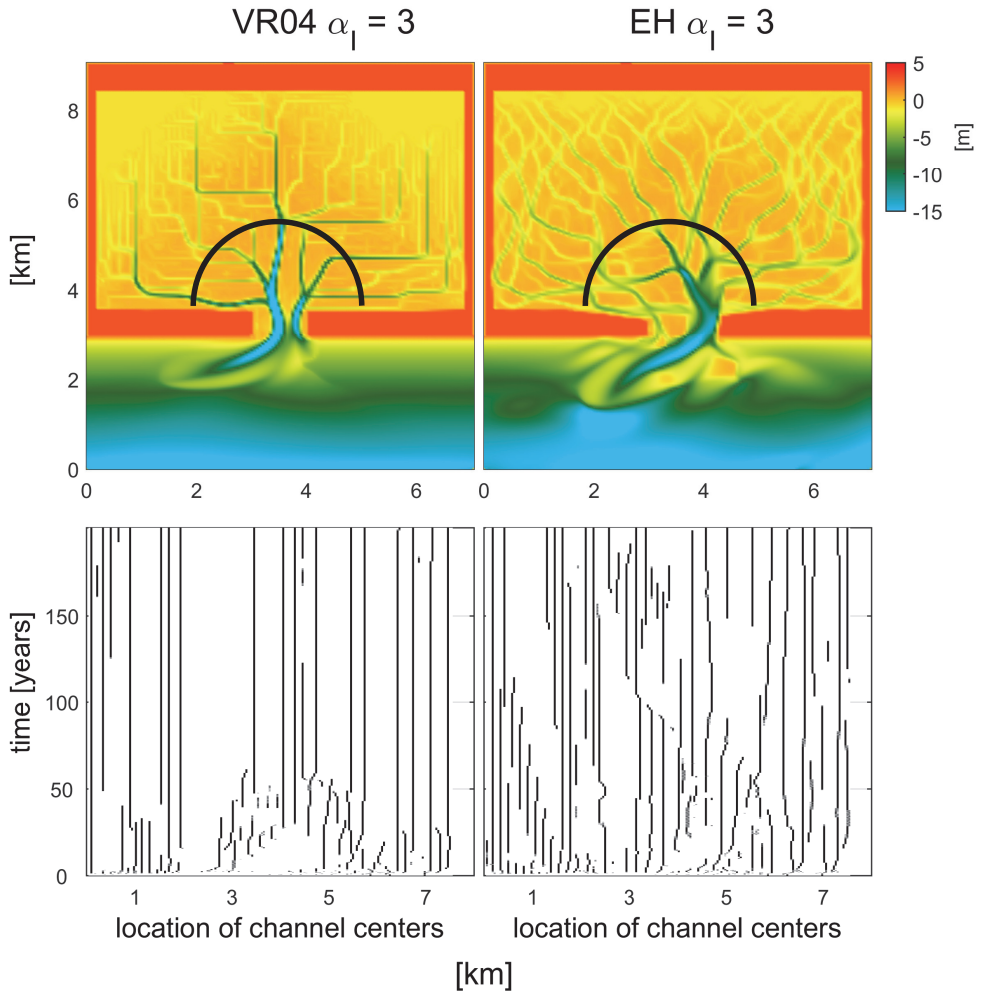

Figure A.9: Supplementary Figure 9: Difference in morphology between the tidal basin model with either the sediment transport predictor of Van Rijn or Engelund-Hansen. The lower two panels show the locations of the channel centers over time at the cross-section that is indicated with the black circle in the upper two DEMs. The slope parameter is constant and modeled with the IK slope parameterization.

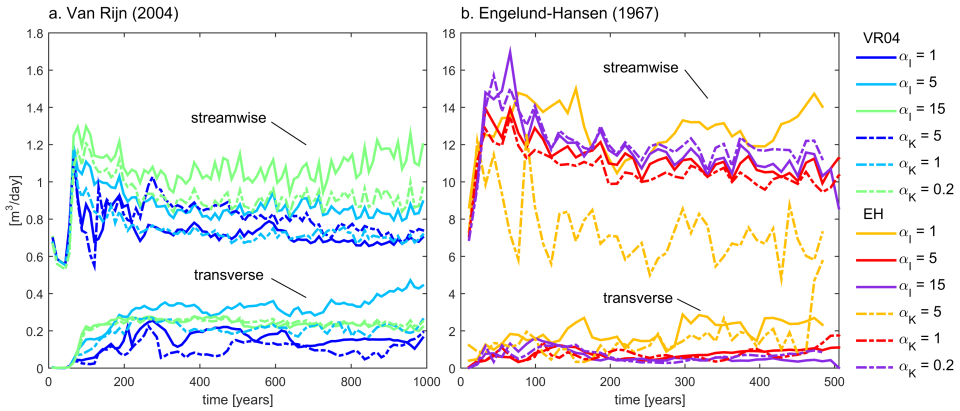

Figure A.10: Supplementary Figure 10: Total sediment transport over a transect at km 20 in the river part of the delta model, integrated over the active channel width. (a) Streamwise and transverse sediment transport over time for all models with the VR sediment transport predictor, and (b) for all the model runs with the EH predictor. Note different vertical scales. Solid lines represent model runs with the IK method to calculate downslope sediment transport, while the dashed lines represent the models with the KF method. Lines with the same colors represent corresponding slope effects and sediment transport predictors.

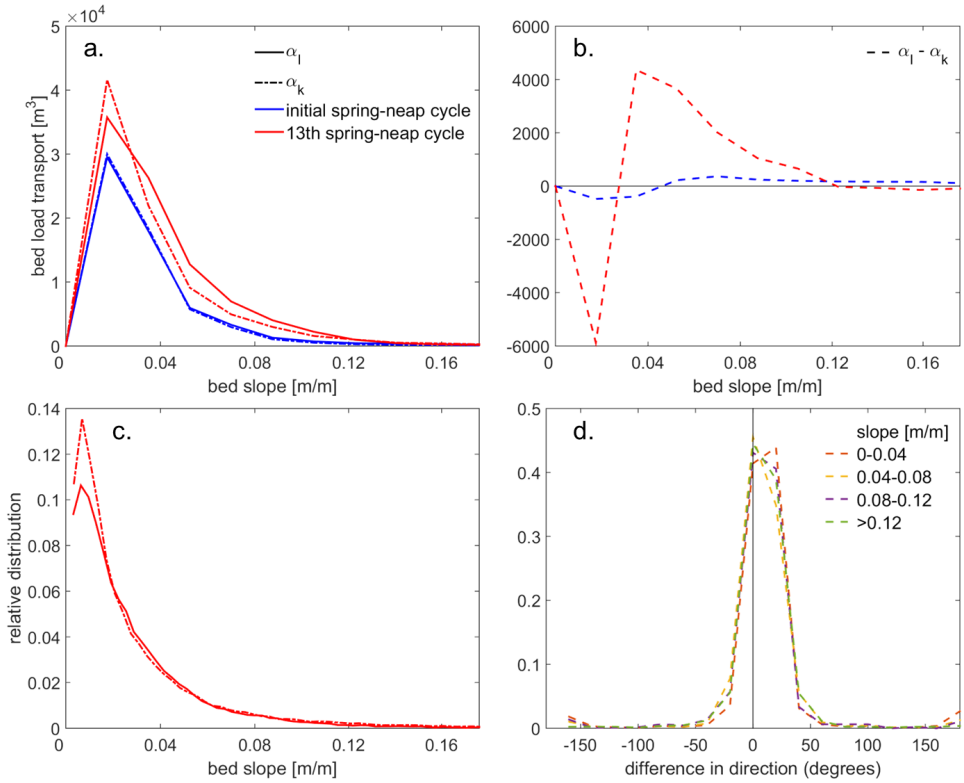

Figure A.11: Supplementary Figure 11: (a) Total amount of sediment transported on specific bed slopes for the Western Scheldt models with different slope parameterizations, at the beginning and at the end of the model run. (b) The difference in sediment transport between both slope parameterizations on specific bed slopes. (c) relative distributions of bed slopes in both Western Scheldt models. (d) Difference in direction of sediment transport between the models with different slope parameterizations. This distribution shows the relative abundance of these differences for all grid cells in the model.

Supplementary Notes

Supplementary Note 1

To understand the implementation of the bed slope effect in Delft3D and how it interacts with sediment transport predictors, we first explain the calculation of streamwise sediment transport. In this study, we focus on the difference between the Van Rijn (Van Rijn et al., 2004) and Engelund-Hansen (Engelund and Hansen, 1967) sediment transport predictor and their influence on the balance of incision and downslope sediment transport. Furthermore, we briefly compare these results with a general sediment transport predictor, where the non-linearity of sediment transport and the addition of a critical shear stress can be specified by the user. Henceforth, we refer to the predictor of Van Rijn as VR, and to the predictor of Engelund-Hansen as EH.

VR makes a distinction between bed load and suspended load transport, by imposing a reference height, below which sediment transport is treated as bed load and everything above this height is treated as suspended load. Gravity only acts on the bed load, which is calculated as follows:

$$q_b = 0.5\rho_s d_{50} D_*^{-0.3} \left(\frac{\tau}{\rho}\right)^{0.5} \frac{\tau - \tau_{cr}}{\tau_{cr}} \tag{A.1}$$

where q_b = bed load sediment transport rate per meter width [$m^2 s^{-1}$], ρ_s = sediment density [kg m^{-3}], ρ_w = water density [kg m^{-3}], D_{50} = median grainsize [m], D_* = dimensionless particle size, τ = shear stress [N m^{-2}], ρ = density [kg m^{-3}], τ_{cr} = critical shear stress based on the Shields criterion [N m^{-2}]. As a result, the sediment transport rate is related to flow velocity to the power of 3, which determines the non-linearity of the sediment transport predictor. However, since this predictor also includes a critical flow velocity, the relation between flow velocity and sediment transport will be more non-linear near the beginning of motion.

EH is a total load predictor (q_t), and unlike VR, it does not include a critical velocity or critical shear stress:

$$q_t = \frac{0.005\alpha u^5}{\sqrt{g} C^3 \frac{\rho_s - \rho_w}{\rho_w} D_{50}} \tag{A.2}$$

where α = a calibration coefficient in the order of 1. Here, the sediment transport rate is related to flow velocity to the power of 5.

The general sediment transport predictor in Delft3D is based on the predictor of Meyer-Peter Mueller (Meyer-Peter and Müller, 1948):

$$q_t = \alpha D_{50} \sqrt{\frac{\rho_s - \rho_w}{\rho_w} g D_{50}} \theta^b (\theta - \theta_c)^c \tag{A.3}$$

where b and c are user defined parameters, which determine the non-linearity of the sediment transport predictor and the addition of a critical sediment mobility. The sediment mobility θ, a dimensionless form of the bed shear stress, reads:

$$\theta = \frac{u^2}{C^2 \frac{\rho_s - \rho_w}{\rho_w} D_{50}} \tag{A.4}$$

When the magnitude of the bed load or total load sediment transport is calculated parallel to the flow velocity, the direction and magnitude of the transport vector is adjusted for bed slopes. For transverse slopes, the two commonly used parameterizations are the predictor of Koch and Flokstra (KF, ISlope = 3) and Ikeda (IK, ISlope = 2). The main difference between both options is in the calculation of the transport vector (Fig. 2.2 in main text). For KF the direction of sediment transport is corrected for transverse gradients by rotating the transport vector based on the user-defined factors α_K and β_K:

$$tan(\psi) = \frac{1}{\alpha_K \theta^{\beta_K}} \frac{\partial z_b}{\partial y} \tag{A.5}$$

For IK an additional transport vector is calculated perpendicular to the flow direction, based on the input parameter α_I:

$$q_n = q_s \alpha_I \sqrt{\frac{\theta_c}{\theta}} \frac{\partial z_b}{\partial y} \tag{A.6}$$

where q = sediment transport load [$m^2 s^{-1}$] in the streamwise (s) or transverse (n) direction, and $\frac{\partial z_b}{\partial y}$ = transverse slope [m m^{-1}].

As a result, the IK method increases the direction and total magnitude of sediment transport when a transverse slope is present, while for KF only the direction is changed. Another difference is that the IK method uses a critical shear stress, which is absent in the KF method. The default value of α_I in Delft3D is set to 1.5, while the parameter α_K is not defined in the model, but should be 1.5 according to Koch and Flokstra. The method of calculating the sediment transport vector in both slope options therefore has major implications for calibrating models with the transverse slope parameter. By increasing the α_I in the IK method by a factor of ten for example, the amount of downslope sediment transport is also increased by a factor of ten, which increases the total sediment transport significantly (Fig. 2 in main text). With the KF method sediment transport is not increased, but here, decreasing the α_K to values reported in literature (Schuurman et al., 2013; Oorschot et al., 2016; Braat et al., 2017) could easily result in more downslope sediment transport than streamwise sediment transport.

It is possible to compare the effect on resulting morphology of using different slope predictors by requiring either the magnitude or the direction of transverse sediment transport to be equal. When assuming an equal magnitude, the method of KF needs to be corrected for a given slope and sediment mobility. Using Equation A.5 and Equation A.6 with a β_K of 0.5 it follows that:

$$\alpha_I = \left(\alpha_K \sqrt{\theta_c + \frac{\theta_c}{\alpha_K^2 \theta} \left(\frac{dz}{dy} \right)^2} \right)^{-1} \tag{A.7}$$

The resulting relation between α_I and α_K is plotted in Supplementary Figure. A.1 for four combinations of transverse slope and sediment mobility. When assuming equal direction of sediment transport, it follows that:

$$\alpha_I = \left(\alpha_K \sqrt{\theta_c}\right)^{-1} \tag{A.8}$$

which is shown as the linear solution in Supplementary Figure A.1.

Supplementary Note 2

To help identify the cause of the overdeepening of channels in numerical models, we compare the balance between incision and transverse sediment transport in a straight river channel in Delft3D with an analytical model of a channel cross-section with the same characteristics. Since we only consider a cross-section, the streamwise sediment transport is in balance with the constant flow conditions and the model does not account for deposition along a river reach. The analytical model consists of three grid cells in cross-section, with an initial bed level difference between the middle cell and the surrounding cells, representing a disturbance that either decays or grows by incising further (Supplementary Figure A.2). The aim of this model is to find the equilibrium width-to-depth ratio at which incision is equal to transverse sediment transport, and how this ratio depends on flow conditions, sediment transport processes, and size of the disturbance.

The model first calculates upstream flow characteristics and corresponding sediment transport rate based on the input parameters, which are a constant Chézy coefficient for friction (C), channel slope (S), grain size (D_{50}), the non-linearity of the sediment transport predictor (k), and a height difference (dh). We assume a constant specific discharge such that the relation between channel width (W) and discharge (Q) is linear:

$$Q = aW \tag{A.9}$$

The upstream flow velocity (u_i) and water depth (h_i) are calculated by iteration, using the following equations for flow velocity:

$$u_i = C\sqrt{h_i S} \tag{A.10}$$

$$u_i = \frac{a}{h_i} \tag{A.11}$$

The upstream sediment transport rate (q_i) is based on the same general sediment transport predictor as in Delft3D:

$$q_i = \alpha D_{50} \sqrt{\frac{\rho_s - \rho_w}{\rho_w} g D_{50}} \theta_i^{\frac{k}{2}} \tag{A.12}$$

Then, flow characteristics and sediment transport fluxes are calculated for the cross-section under consideration, based on the height difference between the middle grid cell (h_2) and

the outer two grid cells (h_1, h_3) (Supplementary Figure A.2a). It is assumed that the average water depth at the cross-section is equal to the initial water depth, which leads to:

$$h_1 = h_3 = h_i - 0.5dh \tag{A.13}$$

$$h_2 = h_i + dh \tag{A.14}$$

The sediment transport rate for each cell is then calculated with Equations A.4, A.10 and A.12, but with the specific water depths. The sediment transport rate towards the middle cell as a result of the transverse slope (q_n) is based on the method of Ikeda:

$$q_n = q_1 \frac{\beta}{\sqrt{\theta}} \frac{1.5dh}{\frac{W}{3}} \tag{A.15}$$

where β = transverse slope parameter, which is based on α_I from Equation A.6. The transverse slope is defined as the height difference between two cells divided by the width of one grid cell, which is the same method as in Delft3D.

A balance between incision and downslope sediment transport is assumed when the difference between the upstream sediment transport and the sediment transport rate for the middle grid cell is equal to the total downslope sediment transport:

$$2q_n = q_2 - q_i \tag{A.16}$$

When the transverse sediment flux is larger, there is sedimentation and the perturbation will likely decay (Supplementary Figure A.2b), while when the transverse sediment flux is smaller, the grid cell is incised and the perturbation will grow (Supplementary Figure A.2c). Using Equations A.4, A.10 and A.12 it follows that:

$$W_{eq} = \frac{h_1^{k/2}}{h_2^{k/2} - h_i^{k/2}} \frac{9\beta dh}{\sqrt{\theta}} \tag{A.17}$$

where W_{eq} = width of the channel when incision is equal to the transverse sediment transport. The equilibrium width-to-depth ratio is now a function of the size of the disturbance, sediment mobility and the non-linearity of sediment transport. All other parameters influence this equilibrium by changing the sediment mobility. In further analyses we first assume a constant channel slope of 0.5 mm m^{-1}, a Chezy coefficient of 40 $\sqrt{m}/s^{-1}$, a ratio between channel width and discharge of 12.5, and a grain size of 0.5 *mm*.

With increasing sediment mobility, the equilibrium width-to-depth ratio decreases exponentially (Supplementary Figure A.3), which means that at higher sediment mobility a channel is more likely to incise. A higher non-linearity of the transport predictor causes a higher sediment transport rate, and therefore results in more incision and a lower equilibrium width-to-depth ratio at any sediment mobility. Increasing the transverse slope parameter has the opposite effect, since more sediment is transported downslope which counteracts incision. Increasing the depth of the initial perturbation also decreases the equilibrium

width (Supplementary Figure A.3), since deeper channels attract more flow and therefore need more downslope sediment transport to counteract this. However, this influence is less than changing the bed slope effect or the non-linearity.

To be able to show the effects of height of the perturbation and the other parameters that influence sediment mobility, the width-to-depth ratio is multiplied by the square root of the sediment mobility divided by the slope parameter, which is the ratio that describes the slopes of the graphs in Supplementary Figure A.3. We call the resulting parameter the channelization factor, since it describes the balance between the tendency to enhance perturbations determined by the width-to-depth ratio, and the bed slope effect that counteracts incision. This balance thereby controls the formation of channels. As a result, Supplementary Figure A.4a shows how models with varying slope effect and sediment mobility collapse when plotting this factor against height of the perturbation. Again, a higher non-linearity of sediment transport results in a growth of the perturbation at lower width-to-depth ratios. Higher Chezy values, and thus lower friction, also results in a growth of the perturbation at lower width-to-depth ratios when increasing the depth of the perturbation, but less dramatically. However, negative perturbations, i.e. when the middle grid cell is higher than the surrounding cells, need higher width-to-depth ratios for the perturbation to grow. Increasing the channel slope or decreasing the ratio between discharge and channel width shows the same trend.

Since the analytical model identifies the equilibrium channelization factor, perturbations in numerical models plotted below this line should theoretically decay, while models plotted above the line should have growing perturbations (Supplementary Figure A.5). With the default value for the slope effect (α_I = 1.5), the VR models corresponded reasonably well with the analytical model, since the transition from a dampened system towards a channel where the perturbation grows is around the theoretical equilibrium line (Supplementary Figure A.5a). There was no effect of the depth of the initial perturbation in the numerical model. However, with increased slope effect, the numerical models significantly deviated from the analytical model. Here, the numerical model with wider channels required a disproportionately larger slope effect to dampen the initial perturbation (more than 30 times higher than the default factor as opposed to 4 times the default in the analytical model). On the other hand, the initial perturbation in models with the models with the EH predictor immediately decayed (Supplementary Figure A.5b), until the channel has a width-to-depth ratio around 36, which is more than 15 times higher than the theoretical model. This behavior was very similar to that of the models with the general predictor (Supplementary Figure A.5c,d). Even when sediment transport is related to flow velocity to the power of 10, perturbations did not start to grow at a lower width-to-depth-ratio, while this was expected based on the analytical model. The two slope parameterizations differed only slightly and removing the critical sediment mobility from the generic transport predictor had no effect on equilibrium morphology. These results demonstrate a stronger tendency to incise in the numerical model with VR than expected from theory, and a weaker tendency to incise in numerical models with EH.

Supplementary Note 3

The fifth set of models is a detailed case study of the topographically forced Western Scheldt estuary in the Netherlands, to test the sensitivity of a calibrated model with two different slope parameterizations in comparison with measured bathymetry. This topographic forcing is typical for many natural and engineered systems and is important because it limits free bar and pattern formation, rendering models less sensitive in large-scale pattern to chosen parameterizations. Here, we focused on differences in local sediment transport dynamics in two model runs with different slope predictors that showed the same large-scale morphology in view of the need to predict sediment transport rates for fairway maintenance dredging. After 10 years of morphological development, these models reproduced the cumulative slope distributions that were closest to the actual morphology of the Western Scheldt that was used as input (Supplementary Figure A.8c). The models had a strong slope effect, namely an α_I of 30 and an α_K of 0.05, which again shows that a higher than physical slope effect is needed when calibrating the Western Scheldt model on existing morphology.

While large-scale morphology is similar between both models after ten years (Supplementary Figure A.8d), the dynamics differ in local sediment transport. The model with the IK method has higher bed load transport rates on steeper slopes, while the model with the KF method has higher transport rates on lower slopes (Supplementary Figure A.11). Furthermore, there is a significant difference in direction of the transport vectors in more than half of all grid cells in the model (Supplementary Figure A.11d), which is independent of slope. These differences in direction and magnitude imply locally channels can be orientated differently and location and speed of bank erosion will differ. For fairway maintenance dredging this means that predicted time scales can significantly differ when models are calibrated with a different slope parametrization on the same measured morphology.

Appendix B

Parameterizations of orbital velocities

Parameterizations of orbital velocities

Isobe Horikawa (IH)

The equations of IH presented here were based on the Delft3D source code and van Rijn et al. (2004) and van Rijn (2011). As a first step, the velocity amplitude U_w is estimated based on linear wave theory applying local wave conditions: wave height (H_{rms}), period (T) and local water depth (h)

$$U_w = \frac{H_{rms}\,\pi}{T\,\sinh(kh)} \tag{B.1}$$

where, k is the wave number calculated from the dispersion relation: $w^2 = gk\,\tanh(kh)$; g is the gravity acceleration and w the angular frequency. Then, the maximum velocity amplitude U_{max} is computed according to

$$U_{max} = 2U_w\left[-0.4\left(\frac{H_{rms}}{h}\right)+1\right] \tag{B.2}$$

From the velocity amplitude, the maximum onshore (U_{on}) and offshore (U_{off}) directed velocities are calculated following

$$\begin{aligned} u_{on} &= U_{max}\,(0.5+(r_{max}-0.5)\,\tanh\left(\frac{r_a-0.5}{r_{max}-0.5}\right) \\ u_{off} &= U_{max}-u_{on} \end{aligned} \tag{B.3}$$

where,

$$r_a = \begin{cases} -5.25-6.1\,\tanh\left(A_1\,\frac{U_{max}}{\sqrt{(g/h)}}-1.76\right) & \text{if} \quad r_a \geq 0.5 \\ 0.5 & \text{if} \quad r_a < 0.5 \end{cases} \tag{B.4}$$

$$A_1 = -0.0049\,(T\sqrt{g/h})^2 - 0.069\,(T\sqrt{g/h}) + 0.2911$$

and,

$$r_{max} = 0.62 < -2.5\,(h/L) + 0.85 < 0.75 \tag{B.5}$$

Then, the duration of onshore (T_{for}) and offshore (T_{back}) directed velocities are calculated in

$$T_{for} = \frac{u_{off}}{u_{on} + u_{off}} T$$
$$T_{back} = T - T_{for} \tag{B.6}$$

And finally the onshore $u_{on}(t)$ and offshore $u_{off}(t)$ directed velocities are computed with t varying from 0 to wave period T according to

$$u(t) = \begin{cases} u_{on} \sin\left(\pi \frac{t}{T_{for}}\right) & \text{for} \quad t < T_{for} \\ -u_{off} \sin\left[\frac{\pi}{T_{back}} (t - T_{for})\right] & \text{for} \quad t \geq T_{for} \end{cases} \tag{B.7}$$

Ruessink (RUE)

The Ruessink method description is based on Ruessink et al. (2012). The method starts with the calculation of Ursell number (Ur) as

$$Ur = \frac{3\sqrt{2}\, H_{rms}}{8} \frac{k}{(kh)^3} \tag{B.8}$$

Based on the Ursell number the total non-linearity (B) and the phase (Ψ) are computed as the following

$$B = p_1 + \frac{p_2 - p_1}{1 + \exp \frac{p_3 - \log(Ur)}{p_4}} \tag{B.9}$$

$$\Psi = -90^\circ + 90^\circ \tanh\left(\frac{p_5}{Ur^{p_6}}\right) \tag{B.10}$$

where: $p_1 = 0$; $p_2 = 0.857$; $p_3 = -0.471$; $p_4 = 0.297$; $p_5 = 0.815$; $p_6 = 0.672$;
With the total non-linearity and phase, the skewness (Sk) and asymmetry (As) are calculated with

$$Sk = B \cos(\Psi) \tag{B.11}$$

$$As = B \sin(\Psi) \tag{B.12}$$

Then a new non-linearity (r) and phase (φ) are derived from B and Ψ as in

$$b = \frac{\sqrt{2B^2}}{\sqrt{9 + 2B^2}}$$
$$r = \frac{2b}{1 + b^2} \tag{B.13}$$

$$\varphi = -\tan^{-1}\left(\frac{A}{S}\right) - \frac{\pi}{2} = -\Psi - \frac{\pi}{2} \tag{B.14}$$

The amplitude of orbital velocities U_w is obtained following equation B.1. Finally, $u(t)$ is calculated based on the velocity amplitude, total non-linearity and phase, as demonstrated in

$$u(t') = U_w f \frac{\sin(\omega t') + \frac{r\sin(\varphi)}{(1+f)}}{1 - r\cos(\omega t' + \varphi)} \tag{B.15}$$

where, $f = \sqrt{(1 - r^2)}$ is a dimensionless factor to match the amplitude of u and U_w. In addition, t is modified into t' to ensure $u(0) = 0$.

$$t' = t - \left[\frac{1}{\omega}\arcsin\left(\frac{r\sin(\varphi)}{1+f}\right)\right] \tag{B.16}$$

References

Abreu, T., P. A. Silva, F. Sancho, and A. Temperville (2010). Analytical approximate wave form for asymmetric waves. *Coastal Engineering* 57.7, pp. 656–667. DOI:HTTPS://DOI.ORG/10.1016/J.COASTALENG.2010.02.005.

Adams, P. N., R. L. Slingerland, and N. D. Smith (2004). Variations in natural levee morphology in anastomosed channel flood plain complexes. *Geomorphology* 61.1, pp. 127–142. DOI:HTTPS://DOI.ORG/10.1016/J.GEOMORPH.2003.10.005.

Baar, A. W., M. Boechat Albernaz, W. M. van Dijk, and M. G. Kleinhans (2019). Critical dependence of morphodynamic models of fluvial and tidal systems on empirical downslope sediment transport. *Nature Communications* 10 (1). DOI:10.1038/s41467-019-12753-x.

Baar, A., M. B. Albernaz, W. van Dijk, and M. Kleinhans (2018a). The influence of transverse slope effects on large scale morphology in morphodynamic models. *E3S Web Conf.* 40, p. 04021. DOI:10.1051/E3SCONF/20184004021.

Baar, A. W., J. de Smit, W. S. J. Uijttewaal, and M. G. Kleinhans (2018b). Sediment Transport of Fine Sand to Fine Gravel on Transverse Bed Slopes in Rotating Annular Flume Experiments. *Water Resources Research* 54.1, pp. 19–45. DOI:10.1002/2017WR020604. eprint: https://agupubs.onlinelibrary.wiley.com/doi/pdf/10.1002/2017WR020604.

Bailard, J. A. (1981). An energetics total load sediment transport model for a plane sloping beach. *Journal of Geophysical Research: Oceans* 86.C11, pp. 10938–10954. DOI:10.1029/JC086IC11P10938. eprint: https://agupubs.onlinelibrary.wiley.com/doi/pdf/10.1029/JC086iC11p10938.

Bailard, J. A. (1982). Modeling on-offshore sediment transport in the surf zone. *18th International Conference on Coastal Engineering*, pp. 1419–1438.

Baptist, M., V. Babovic, J. R. Uthurburu, M. Keijzer, R. Uittenbogaard, A. Mynett, and A. Verwey (2007). On inducing equations for vegetation resistance. *Journal of Hydraulic Research* 45.4, pp. 435–450. DOI:10.1080/00221686.2007.9521778. eprint: https://doi.org/10.1080/00221686.2007.9521778.

Baptist, M. J., A. V. de Groot, and W. E. van Duin (2016). Contrasting biogeomorphic processes affecting salt-marsh development of the Mokbaai, Texel, The Netherlands. *Earth Surface Processes and Landforms* 41.9, pp. 1241–1249. DOI:HTTPS://DOI.ORG/10.1002/ESP.3949. eprint: https://onlinelibrary.wiley.com/doi/pdf/10.1002/esp.3949.

Barbier, E. B., S. D. Hacker, C. Kennedy, E. W. Koch, A. C. Stier, and B. R. Silliman (2011). The value of estuarine and coastal ecosystem services. *Ecological Monographs* 81.2, pp. 169–193. DOI:10.1890/10-1510.1. eprint: https://esajournals.onlinelibrary.wiley.com/doi/pdf/10.1890/10-1510.1.

Beets, D. J. and A. J. F. van der Spek (2000). The Holocene evolution of the barrier and the back-barrier basins of Belgium and the Netherlands as a function of late Weichselian morphology, relative sea-level rise and sediment supply. *Netherlands Journal of Geosciences - Geologie en Mijnbouw* 79.1, pp. 3–16. DOI:10.1017/S0016774600021533.

Belliard, J.-P., N. Di Marco, L. Carniello, and M. Toffolon (2016). Sediment and vegetation spatial dynamics facing sea-level rise in microtidal salt marshes: Insights from an ecogeomorphic model. *Advances in water resources* 93, pp. 249–264.

Benedet, L., J. Dobrochinski, D. Walstra, A. Klein, and R. Ranasinghe (2016). A morphological modeling study to compare different methods of wave climate schematization and evaluate strategies to reduce erosion losses from a beach nourishment project. *Coastal Engineering* 112, pp. 69–86. DOI:HTTPS://DOI.ORG/10.1016/J.COASTALENG.2016.02.005.

Berendsen, H. J. and E. Stouthamer (2000). Late Weichselian and Holocene palaeogeography of the Rhine–Meuse delta, The Netherlands. *Palaeogeography, Palaeoclimatology, Palaeoecology* 161.3, pp. 311–335. DOI:HTTPS://DOI.ORG/10.1016/S0031-0182(00)00073-0.

Bertalanffy, L. V. (1950). The Theory of Open Systems in Physics and Biology. *Science* 111.2872, pp. 23–29.

Bertin, X., A. Oliveira, and A. B. Fortunato (2009). Simulating morphodynamics with unstructured grids: Description and validation of a modeling system for coastal applications. *Ocean Modelling* 28.1. The Sixth International Workshop on Unstructured Mesh Numerical Modelling of Coastal, Shelf and Ocean Flows, pp. 75–87. DOI:HTTPS://DOI.ORG/10.1016/J.OCEMOD.2008.11.001.

Best, J. (2019). Anthropogenic stresses on the world's big rivers. *Nature Geoscience* 12.1, pp. 7–21.

Bij de Vaate, I., M. Z. M. Brückner, M. G. Kleinhans, and C. Schwarz (2020). On the Impact of Salt Marsh Pioneer Species-Assemblages on the Emergence of Intertidal Channel Networks. *Water Resources Research* 56.3. e2019WR025942 2019WR025942, e2019WR025942. DOI:HTTPS://DOI.ORG/10.1029/2019WR025942. eprint: https://agupubs.onlinelibrary.wiley.com/doi/pdf/10.1029/2019WR025942.

Blum, M., A. Sivers, T. Zayac, and R. Goble (2003). Middle Holocene sea-level and evolution of the Gulf of Mexico coast. *Transaction Gulf Coast Association of Geological Societies* 53, pp. 64–77.

Boechat Albernaz, M. (2022). *Yoda Repository, Utrecht University, DOI: 10.24416/UU01-LWNX9B*. https://public.yoda.uu.nl/geo/UU01/LWNX9B.html. Software.

Boechat Albernaz, M. (2019). *SVN Repository*. https://svn.oss.deltares.nl/repos/delft3d/branches.

Boechat Albernaz, M., L. Roelofs, H. J. Pierik, and M. G. Kleinhans (2020). Natural levee evolution in vegetated fluvial-tidal environments. *Earth Surface Processes and Landforms* 45.15, pp. 3824–3841. DOI:HTTPS://DOI.ORG/10.1002/ESP.5003. eprint: https://onlinelibrary.wiley.com/doi/pdf/10.1002/esp.5003.

Boechat Albernaz, M., G. Ruessink, H. Jagers, and M. G. Kleinhans (2019). Effects of wave orbital velocity parameterization on nearshore sediment transport and decadal morphodynamics. *Journal of Marine Science and Engineering* 7.6, p. 188. DOI:DOI.ORG/10.3390/JMSE7060188.

Bolla Pittaluga, M., R. Repetto, and M. Tubino (2003). Correction to "Channel bifurcation in braided rivers: Equilibrium configurations and stability". *Water Resources Research* 39.3, pp. 1–13. DOI:10.1029/2003WR002754.

Bolla Pittaluga, M., G. Coco, and M. G. Kleinhans (2015). A unified framework for stability of channel bifurcations in gravel and sand fluvial systems. *Geophysical Research Letters* 42.18, pp. 7521–7536. DOI:10.1002/2015GL065175.

Booij, N., R. C. Ris, and L. H. Holthuijsen (1999). A third-generation wave model for coastal regions: 1. Model description and validation. *Journal of Geophysical Research: Oceans* 104.C4, pp. 7649–7666. DOI:10.1029/98JC02622. eprint: https://agupubs.onlinelibrary.wiley.com/doi/pdf/10.1029/98JC02622.

Bouma, T. et al. (2013). Organism traits determine the strength of scale-dependent bio-geomorphic feedbacks: A flume study on three intertidal plant species. *Geomorphology* 180-181, pp. 57–65. DOI:HTTPS://DOI.ORG/10.1016/J.GEOMORPH.2012.09.005.

Boyd, R., R. Dalrymple, and B. Zaitlin (1992). Classification of clastic coastal depositional environments. *Sedimentary Geology* 80.3. Research Conference on Quaternary Coastal Evolution, pp. 139–150. DOI:HTTPS://DOI.ORG/10.1016/0037-0738(92)90037-R.

Braat, L., T. van Kessel, J. R. F. W. Leuven, and M. G. Kleinhans (2017). Effects of mud supply on large-scale estuary morphology and development over centuries to millennia. *Earth Surface Dynamics* 5.4, pp. 617–652. DOI:10.5194/ESURF-5-617-2017.

Braat, L., J. R. F. W. Leuven, I. R. Lokhorst, and M. G. Kleinhans (2019). Effects of estuarine mudflat formation on tidal prism and large-scale morphology in experiments. *Earth Surface Processes and Landforms* 44.2, pp. 417–432. DOI:10.1002/ESP.4504. eprint: https://onlinelibrary.wiley.com/doi/pdf/10.1002/esp.4504.

Briere, C., A. Giardino, and J. van der Werf (2011). Morphological modeling of bar dynamics with DELFT3D: the quest for optimal free parameter settings using an automatic calibration technique. *Coastal Engineering Proceedings* 1.32, p. 60. DOI:10.9753/ICCE.V32.SEDIMENT.60.

Brierley, G. J., R. J. Ferguson, and K. J. Woolfe (1997). What is a fluvial levee?. *Sedimentary Geology* 114.1, pp. 1–9. DOI:HTTPS://DOI.ORG/10.1016/S0037-0738(97)00114-0.

Brinkkemper, J. (Mar. 2018). Short-wave sand transport in the surf zone. PhD thesis.

Brown, S. et al. (2014). Shifting perspectives on coastal impacts and adaptation. *Nature Climate Change* 4.9. cited By 58, pp. 752–755. DOI:10.1038/NCLIMATE2344.

Brückner, M. (2020). *SVN Repository*. https://github.com/Mbruckner42.

Brückner, M., L. Braat, C. Schwarz, and M. Kleinhans (2020). What came first, mud or biostabilizers? Elucidating interacting effects in a coupled model of mud, saltmarsh, microphytobenthos and estuarine morphology. *Water Resources Research*. DOI:10.1029/2019WR026945.

Brückner, M. Z. M., C. Schwarz, W. M. van Dijk, M. van Oorschot, H. Douma, and M. G. Kleinhans (2019). Salt Marsh Establishment and Eco-Engineering Effects in Dynamic Estuaries Determined by Species Growth and Mortality. *Journal of Geophysical Research: Earth Surface*. DOI:10.1029/2019JF005092. eprint: https://agupubs.onlinelibrary.wiley.com/doi/pdf/10.1029/2019JF005092.

Brückner, M. Z., C. Schwarz, G. Coco, A. Baar, M. Boechat Albernaz, and M. G. Kleinhans (2021). Benthic species as mud patrol - modelled effects of bioturbators and biofilms on large-scale estuarine mud and morphology. *Earth Surface Processes and Landforms* n/a.n/a. DOI:HTTPS://DOI.ORG/10.1002/ESP.5080. eprint: https://onlinelibrary.wiley.com/doi/pdf/10.1002/esp.5080.

Bruun, P. (1954). *Coast erosion and the development of beach profiles*. Vol. 44. US Beach Erosion Board.

Bruun, P. (1962). Sea-level rise as a cause of shore erosion. *Journal of the Waterways and Harbors division* 88.1, pp. 117–132.

Bruun, P. and F. Gerritsen (1959). Natural by-passing of sand at coastal inlets. *Journal of the Waterways and Harbors Division* 85.4, pp. 75–108.

Burns, C., N. Mountney, D. Hodgson, and L. Colombera (2017). Anatomy and dimensions of fluvial crevasse-splay deposits: Examples from the Cretaceous Castlegate Sandstone and Neslen Formation, Utah, U.S.A.. *Sedimentary Geology* 351, pp. 21–35. DOI:HTTPS://DOI.ORG/10.1016/J.SEDGEO.2017.02.003.

Burns, C., N. Mountney, D. Hodgson, and L. Colombera (2019). Stratigraphic architecture and hierarchy of fluvial overbank splay deposits. *Journal of the Geological Society* 176.4, pp. 629–649.

Caldwell, R. L. and D. A. Edmonds (2014). Journal of Geophysical Research : Earth Surface. *Journal of Geophysical Research: Earth Surface* 119, pp. 961–982. DOI:10.1002/2013JF002965.RECEIVED.

Canestrelli, A., W. Nardin, D. Edmonds, S. Fagherazzi, and R. Slingerland (2014). Importance of frictional effects and jet instability on the morphodynamics of river mouth bars and levees. *Journal of Geophysical Research: Oceans* 119.1, pp. 509–522.

Carniello, L., A. Defina, and L. D'Alpaos (2009). Morphological evolution of the Venice lagoon: Evidence from the past and trend for the future. *Journal of Geophysical Research: Earth Surface* 114.F4. DOI:HTTPS://DOI.ORG/10.1029/2008JF001157. eprint: https://agupubs.onlinelibrary.wiley.com/doi/pdf/10.1029/2008JF001157.

Carrasco, A. R., T. Plomaritis, J. Reyns, Ó. Ferreira, and D. Roelvink (2018). Tide circulation patterns in a coastal lagoon under sea-level rise. *Ocean Dynamics* 68.9, pp. 1121–1139. DOI:10.1007/s10236-018-1178-0.

Cayocca, F. (2001). Long-term morphological modeling of a tidal inlet: the Arcachon Basin, France. *Coastal Engineering* 42.2, pp. 115–142. DOI:HTTPS://DOI.ORG/10.1016/S0378-3839(00)00053-3.

Cazanacli, D. and N. D. Smith (1998). A study of morphology and texture of natural levees—Cumberland Marshes, Saskatchewan, Canada. *Geomorphology* 25.1, pp. 43–55. DOI:HTTPS://DOI.ORG/10.1016/S0169-555X(98)00032-4.

Cohen, K., E. Stouthamer, H. Pierik, and A. Geurts (2012). Digitaal Basisbestand Paleogeografie van de Rijn-Maas Delta. DANS. DOI:HTTPS://DOI.ORG/10.17026/DANS-X7G-SJTW.

Contti Neto, N., A. Pomeroy, R. Lowe, and M. Ghisalberti (2022). Seagrass Meadows Reduce Wind-Wave Driven Sediment Resuspension in a Sheltered Environment. *Frontiers in Marine Science* 8. DOI:10.3389/FMARS.2021.733542.

Cooper, J. A. G. et al. (2020). Sandy beaches can survive sea-level rise. *Nature Climate Change* 10.11, pp. 993–995.

Cooper, J. A. G. and O. H. Pilkey (2004). Sea-level rise and shoreline retreat: time to abandon the Bruun Rule. *Global and Planetary Change* 43.3, pp. 157–171. DOI:HTTPS://DOI.ORG/10.1016/J.GLOPLACHA.2004.07.001.

Corenblit, D. et al. (2011). Feedbacks between geomorphology and biota controlling Earth surface processes and landforms: A review of foundation concepts and current understandings. *Earth-Science Reviews* 106.3, pp. 307–331. DOI:HTTPS://DOI.ORG/10.1016/J.EARSCIREV.2011.03.002.

Cox, J. R., Y. Huismans, S. M. Knaake, J. R. F. W. Leuven, N. E. Vellinga, M. van der Vegt, A. J. F. Hoitink, and M. G. Kleinhans (2021). Anthropogenic Effects on the Contemporary Sediment Budget of the Lower Rhine-Meuse Delta Channel Network. *Earth's Future* 9.7. e2020EF001869 2020EF001869, e2020EF001869. DOI:HTTPS : / / DOI . ORG / 10 . 1029 / 2020EF001869. eprint: https : / / agupubs . onlinelibrary.wiley.com/doi/pdf/10.1029/2020EF001869.

Crosato, A. and E. Mosselman (2009). Simple physics-based predictor for the number of river bars and the transition between meandering and braiding. *Water Resources Research* 45.3, pp. 1–14. DOI:10.1029/2008WR007242.

D'Alpaos, A. (2011). The mutual influence of biotic and abiotic components on the long-term ecomorphodynamic evolution of salt-marsh ecosystems. *Geomorphology* 126.3. Geomorphology on Multiscale Feedbacks in Ecogeomorphology, pp. 269–278. DOI:HTTPS : / / DOI . ORG / 10 . 1016 / J . GEOMORPH.2010.04.027.

D'Alpaos, A., S. Lanzoni, M. Marani, and A. Rinaldo (2007). Landscape evolution in tidal embayments: Modeling the interplay of erosion, sedimentation, and vegetation dynamics. *Journal of Geophysical Research: Earth Surface* 112.F1. DOI:10.1029/2006JF000537. eprint: https://agupubs.onlinelibrary.wiley.com/doi/pdf/10.1029/2006JF000537.

D'Alpaos, A., S. Lanzoni, M. Marani, and A. Rinaldo (2010). On the tidal prism–channel area relations. *Journal of Geophysical Research: Earth Surface* 115.F1. DOI:HTTPS : / / DOI . ORG / 10 . 1029 / 2008JF001243. eprint: https://agupubs.onlinelibrary.wiley.com/doi/pdf/10.1029/2008JF001243.

D'Alpaos, A. and M. Marani (2016). Reading the signatures of biologic–geomorphic feedbacks in salt-marsh landscapes. *Advances in Water Resources* 93. Ecogeomorphological feedbacks of water fluxes, sediment transport and vegetation dynamics in rivers and estuaries, pp. 265–275. DOI:HTTPS://DOI.ORG/10.1016/J.ADVWATRES.2015.09.004.

Dam, G., M. Van der Wegen, R. Labeur, and D. Roelvink (2016). Modeling centuries of estuarine morphodynamics in the Western Scheldt estuary. *Geophysical Research Letters* 43.8, pp. 3839–3847.

Dam, G. and A. J. Bliek (2013). Using a sand–mud model to hindcast the morphology near Waarde, the Netherlands. In: *Proceedings of the Institution of Civil Engineers-Maritime Engineering*. Vol. 166. Thomas Telford Ltd, pp. 63–75.

Dastgheib, A. and J. Roelvink (2010). Effect of different sediment mixtures on the long-term morphological simulation of tidal basins. *River, Coastal and Estuarine Morphodynamics: RCEM 2009*, pp. 913–918.

Davies, A. and P. Robins (2017). Residual flow, bedforms and sediment transport in a tidal channel modelled with variable bed roughness. *Geomorphology* 295, pp. 855–872.

Davies, N. S. and M. R. Gibling (2011). Evolution of fixed-channel alluvial plains in response to Carboniferous vegetation. *Nature Geoscience* 4 (9), pp. 629–633. DOI:10.1038/NGEO1237.

Davis, R. A. and M. O. Hayes (1984). What is a Wave-Dominated Coast?. In: *Hydrodynamics and Sedimentation in Wave-Dominated Coastal Environments*. Ed. by B. Greenwood and R. Davis. Vol. 39. Developments in Sedimentology. Elsevier, pp. 313–329. DOI:HTTPS://DOI.ORG/10.1016/S0070-4571(08)70152-3.

De Swart, H. and J. Zimmerman (2009). Morphodynamics of tidal inlet systems. *Annual review of fluid mechanics* 41, pp. 203–229.

De Vriend, H. (1991a). Mathematical modelling and large-scale coast al behaviour. *Journal of Hydraulic Research* 39.6.

De Vriend, H. J. (1991b). Mathematical modelling and large-scale coastal behaviour: Part 2: Predictive models. *Journal of hydraulic research* 29.6, pp. 741–753.

Dean, R. (1977). Equilibrium beach profiles: US Atlantic coast and Gulf coasts. *Ocean Eng.Tech.Rep. 12 Univ. of Delaware, Newark* 12, p. 45.

Dean, R. and M. Perlin (1986). Intercomparison of near-bottom kinematics by several wave theories and field and laboratory data. *Coastal Engineering* 9.5, pp. 399–437. DOI:HTTPS://DOI.ORG/10.1016/0378-3839(86)90006-2.

Dean, R. G. (1991). Equilibrium Beach Profiles: Characteristics and Applications. *Journal of Coastal Research* 7.1, pp. 53–84.

De Haas, T., H. Pierik, A. van der Spek, K. Cohen, B. van Maanen, and M. Kleinhans (2018). Holocene evolution of tidal systems in The Netherlands: Effects of rivers, coastal boundary conditions, eco-engineering species, inherited relief and human interference. *Earth-Science Reviews* 177, pp. 139–163. DOI:HTTPS://DOI.ORG/10.1016/J.EARSCIREV.2017.10.006.

De Haas, T., L. van der Valk, K. M. Cohen, H. J. Pierik, S. A. H. Weisscher, M. P. Hijma, A. J. F. van der Spek, and M. G. Kleinhans (2019). Long-term evolution of the Old Rhine estuary: Unravelling effects of changing boundary conditions and inherited landscape. *The Depositional Record* 5.1, pp. 84–108. DOI:10.1002/DEP2.56. eprint: https://onlinelibrary.wiley.com/doi/pdf/10.1002/dep2.56.

Deltares (2017). Delft3D-FLOW: Simulation of multi-dimensional hydrodynamic flows and transport phenomena, including sediments. *User Manual*.

Deltares (2020). *SVN Repository*. https://svn.oss.deltares.nl/repos/delft3d/tags/delft3d4/7545.

Deng, J., B. G. Jones, K. Rogers, and C. D. Woodroffe (2018). Wind influence on the orientation of estuarine landforms: An example from Lake Illawarra in southeastern Australia. *Earth Surface Processes and Landforms* 43.14, pp. 2915–2925. DOI:10.1002/ESP.4459.

Den Heijer, K. C., F. Baart, and M. van Koningsveld (2012). Assessment of dune failure along the Dutch coast using a fully probabilistic approach. *Geomorphology* 143-144. Thresholds for storm impacts along European coastlines, pp. 95–103. DOI:HTTPS://DOI.ORG/10.1016/J.GEOMORPH.2011.09.010.

De Smit, J. C., M. Z. M. Bruckner, K. I. Mesdag, M. G. Kleinhans, and T. J. Bouma (2021). Key Bioturbator Species Within Benthic Communities Determine Sediment Resuspension Thresholds. *Frontiers in Marine Science* 8, p. 1344. DOI:10.3389/FMARS.2021.726238.

DGT (2011). *Modelo Digital do Terreno (Resolução 2 m) - Zonas Costeiras de Portugal Continental - 2011*. https://www.dgterritorio.gov.pt/dados-abertos.

Dissanayake, D., J. Roelvink, and M. Van der Wegen (2009). Modelled channel patterns in a schematized tidal inlet. *Coastal Engineering* 56.11-12, pp. 1069–1083.

Donatelli, C., N. K. Ganju, T. S. Kalra, S. Fagherazzi, and N. Leonardi (2019). Changes in hydrodynamics and wave energy as a result of seagrass decline along the shoreline of a microtidal back-barrier estuary. *Adv. Water Resour*.

Donatelli, C., X. Zhang, N. K. Ganju, A. L. Aretxabaleta, S. Fagherazzi, and N. Leonardi (June 2020). A nonlinear relationship between marsh size and sediment trapping capacity compromises salt marshes' stability. *Geology* 48.10, pp. 966–970. DOI:10.1130/G47131.1. eprint: https://pubs.geoscienceworld.org/geology/article-pdf/48/10/966/5146642/966.pdf.

Dronkers, J. (1986). Tidal asymmetry and estuarine morphology. *Netherlands Journal of Sea Research* 20.2-3, pp. 117–131.

Dronkers, J. (1998). Morphodynamics of the Dutch delta. *Physics of Estuaries and Coastal Seas*, pp. 297–304.

Dubarbier, B., B. Castelle, V. Marieu, and G. Ruessink (2015). Process-based modeling of cross-shore sandbar behavior. *Coastal Engineering* 95, pp. 35–50. DOI:HTTPS://DOI.ORG/10.1016/J.COASTALENG.2014.09.004.

Dubarbier, B., B. Castelle, G. Ruessink, and V. Marieu (2017). Mechanisms controlling the complete accretionary beach state sequence. *Geophysical Research Letters* 44.11, pp. 5645–5654. DOI:10.1002/2017GL073094. eprint: https://agupubs.onlinelibrary.wiley.com/doi/pdf/10.1002/2017GL073094.

Dunn, F. E., S. E. Darby, R. J. Nicholls, S. Cohen, C. Zarfl, and B. M. Fekete (2019). Projections of declining fluvial sediment delivery to major deltas worldwide in response to climate change and

anthropogenic stress. *Environmental Research Letters* 14.8, p. 084034. DOI:10.1088/1748-9326/ab304e.

Edmonds, D. and R. Slingerland (2007). Mechanics of river mouth bar formation: Implications for the morphodynamics of delta distributary networks. *Journal of Geophysical Research: Earth Surface* 112.F2.

Edmonds, D. A., R. L. Caldwell, E. S. Brondizio, and S. M. O. Siani (2020). Coastal flooding will disproportionately impact people on river deltas. *Nature Communications* 11.1, p. 4741.

Edmonds, D. A. and R. L. Slingerland (2010). Significant effect of sediment cohesion on delta morphology. *Nature Geoscience* 3.2, pp. 105–109.

Elgar, S. and R. T. Guza (1986). Nonlinear model predictions of bispectra of shoaling surface gravity waves. *Journal of Fluid Mechanics* 167, pp. 1–18. DOI:10.1017/S0022112086002690.

Elias, E. P., A. J. Van der Spek, S. G. Pearson, and J. Cleveringa (2019). Understanding sediment bypassing processes through analysis of high-frequency observations of Ameland Inlet, the Netherlands. *Marine Geology* 415, p. 105956. DOI:HTTPS://DOI.ORG/10.1016/J.MARGEO.2019.06.001.

Engelund, F. (1974). Flow and bed topography in channel bends. *Jounal of the Hydraulics Division* 100.11, pp. 1631–1647.

Engelund, F. and E. Hansen (1967). A monograph on sediment transport in alluvial streams. *Technical University of Denmark 0stervoldgade 10, Copenhagen K*.

Escoffier, F. F. (1940). *The stability of tidal inlets*. Tech. rep. United States Engineer Office Mobile United States.

Escoffier, F. F. (1977). *Hydraulics and Stability of Tidal Inlets*. Tech. rep. ESCOFFIER (FRANCIS F) FORT BELVOIR VA.

Eslami, S., P. Hoekstra, N. Nguyen Trung, S. Ahmed Kantoush, D. Van Binh, D. Duc Dung, T. Tran Quang, and M. van der Vegt (2019). Tidal amplification and salt intrusion in the Mekong Delta driven by anthropogenic sediment starvation. *Scientific Reports* (1). DOI:10.1038/s41598-019-55018-9.

Eslami, S. et al. (2021). Projections of salt intrusion in a mega-delta under climatic and anthropogenic stressors. *Communications Earth & Environment* 2.1, p. 142. DOI:10.1038/s43247-021-00208-5.

Esposito, C. R., Z. Shen, T. E. Törnqvist, J. Marshak, and C. White (2017). Efficient retention of mud drives land building on the Mississippi Delta plain.. *Earth Surface Dynamics* 5.3.

Fagherazzi, S. et al. (2012). Numerical models of salt marsh evolution: Ecological, geomorphic, and climatic factors. *Reviews of Geophysics* 50.1.

Filgueira--Rivera, M., N. D. Smith, and R. L. Slingerland (2007). Controls on natural levee development in the Columbia River, British Columbia, Canada. *Sedimentology* 54.4, pp. 905–919. DOI:10.1111/j.1365-3091.2007.00865.x.

FitzGerald, D. M. and I. V. Buynevich (2003). Encyclopedia of sediments and sedimentary rocks. In: ed. by G. V. Middleton. Chap. Barrier Islands.

FitzGerald, D. M., N. C. Kraus, and E. B. Hands (2000). *Natural mechanisms of sediment bypassing at tidal inlets*. Tech. rep. ENGINEER RESEARCH, DEVELOPMENT CENTER VICKSBURG MS COASTAL, and HYDRAULICS LAB.

Fitzgerald, D. M., S. Penland, and D. Nummedal (1984). Control of barrier island shape by inlet sediment bypassing: East Frisian Islands, West Germany. *Marine Geology* 60.1. Hydrodynamics and Sedimentation in Wave-Dominated Coastal Environments, pp. 355–376. DOI:HTTPS://DOI.ORG/10.1016/0025-3227(84)90157-9.

FitzGerald, D. M. (1996). Geomorphic Variability and Morphologic and Sedimentologic Controls on Tidal Inlets. *Journal of Coastal Research*, pp. 47–71.

FitzGerald, D. M., C. J. Hein, J. E. Connell, Z. J. Hughes, I. Y. Georgiou, and A. B. Novak (2021). Largest marsh in New England near a precipice. *Geomorphology* 379, p. 107625. DOI:HTTPS://DOI.ORG/10.1016/J.GEOMORPH.2021.107625.

FitzGerald, D. M., C. J. Hein, Z. Hughes, M. Kulp, I. Georgiou, and M. Miner (2018). Runaway Barrier Island Transgression Concept: Global Case Studies. In: *Barrier Dynamics and Response to Changing*

Climate. Ed. by L. J. Moore and A. B. Murray. Cham: Springer International Publishing, pp. 3–56. DOI:10.1007/978-3-319-68086-6_1.

Fokker, P., F. van Leijen, B. Orlic, H. van der Marel, and R. Hanssen (2018). Subsidence in the Dutch Wadden Sea. *Netherlands Journal of Geosciences* 97.3, pp. 129–181. DOI:10.1017/NJG.2018.9.

Friedrichs, C. T. and D. G. Aubrey (1988). Non-linear tidal distortion in shallow well-mixed estuaries: a synthesis. *Estuarine, Coastal and Shelf Science* 27.5, pp. 521–545. DOI:HTTPS://DOI.ORG/10.1016/0272-7714(88)90082-0.

Funabiki, A., Y. Saito, V. V. Phai, H. Nguyen, and S. Haruyama (2012). Natural levees and human settlement in the Song Hong (Red River) delta, northern Vietnam. *The Holocene* 22.6, pp. 637–648.

Gallagher, E. L., S. Elgar, and R. T. Guza (Feb. 1998). Observations of sand bar evolution on a natural beach. *Journal of Geophysical Research: Oceans* 103.C2, pp. 3203–3215. DOI:10.1029/97JC02765.

Ganju, N., D. Schoellhamer, and B. Jaffe (2009). Hindcasting of decadal-timescale estuarine bathymetric change with a tidal-timescale model. *Journal of Geophysical Research: Earth Surface* 114.4. DOI:10.1029/2008JF001191.

Geleynse, N., J. E. Storms, D.-J. R. Walstra, H. A. Jagers, Z. B. Wang, and M. J. Stive (2011). Controls on river delta formation; insights from numerical modelling. *Earth and Planetary Science Letters* 302.1, pp. 217–226. DOI:HTTPS://DOI.ORG/10.1016/J.EPSL.2010.12.013.

Gibling, M. R. (2006). Width and Thickness of Fluvial Channel Bodies and Valley Fills in the Geological Record: A Literature Compilation and Classification. *Journal of Sedimentary Research* 76.5, pp. 731–770. DOI:10 . 2110 / JSR . 2006 . 060. eprint: https : / / pubs . geoscienceworld . org / jsedres / article - pdf/76/5/731/2821853/731.pdf.

Giosan, L., J. Syvitski, S. Constantinescu, and J. Day (2014). Climate change: protect the world's deltas. *Nature News* 516.7529, p. 31.

Gleason, C. J. (2015). Hydraulic geometry of natural rivers: A review and future directions. *Progress in Physical Geography: Earth and Environment* 39.3, pp. 337–360. DOI:10.1177/0309133314567584. eprint: https://doi.org/10.1177/0309133314567584.

González, M. and R. Medina (2001). On the application of static equilibrium bay formulations to natural and man-made beaches. *Coastal Engineering* 43.3, pp. 209–225. DOI:HTTPS://DOI.ORG/10.1016/S0378-3839(01)00014-X.

Grasmeijer, B., G. Dam, and M. Taal (2013). *Actualisatierapport Delft3D Schelde-estuarium (in Dutch)*. Tech. rep. International Marine & Dredging Consultants.

Grasmeijer, B. (Jan. 2002). Process-Based Cross-Shore Modeling of Barred Beaches.

Gruijters, S. H. L. L., J. Schokker, and J. G. Veldkamp (2004). *Kartering moeilijk erodeerbare lagen in het Schelde estuarium (in Dutch)*. rapport NITG 03213B1208. TNO.

Grunnet, N. M., D.-J. R. Walstra, and B. Ruessink (2004). Process-based modelling of a shoreface nourishment. *Coastal Engineering* 51.7, pp. 581–607. DOI:HTTPS://DOI.ORG/10.1016/J.COASTALENG.2004.07.016.

Guo, L., M. van der Wegen, J. A. Roelvink, and Q. He (2014). The role of river flow and tidal asymmetry on 1-D estuarine morphodynamics. *Journal of Geophysical Research: Earth Surface* 119.11, pp. 2315–2334. DOI:HTTPS://DOI.ORG/10.1002/2014JF003110. eprint: https://agupubs.onlinelibrary.wiley.com/doi/pdf/10.1002/2014JF003110.

Guo, L., M. van der Wegen, D. (Roelvink, Z. B. Wang, and Q. He (2015). Long-term, process-based morphodynamic modeling of a fluvio-deltaic system, part I: The role of river discharge. *Continental Shelf Research* 109, pp. 95–111. DOI:HTTPS://DOI.ORG/10.1016/J.CSR.2015.09.002.

Hein, C. J., D. M. FitzGerald, L. H. de Souza, I. Y. Georgiou, I. V. Buynevich, A. H. d. F. Klein, J. T. de Menezes, W. J. Cleary, and T. L. Scolaro (2016). Complex coastal change in response to autogenic basin infilling: An example from a sub-tropical Holocene strandplain. *Sedimentology* 63.6, pp. 1362–1395.

Hein, C. J., D. M. FitzGerald, E. A. Carruthers, B. D. Stone, W. A. Barnhardt, and A. M. Gontz (2012). Refining the model of barrier island formation along a paraglacial coast in the Gulf of Maine. *Marine Geology* 307-310, pp. 40–57. DOI:HTTPS://DOI.ORG/10.1016/J.MARGEO.2012.03.001.

Hiatt, M. and P. Passalacqua (2015). Hydrological connectivity in river deltas: The first-order importance of channel-island exchange. *Water Resources Research* 51.4, pp. 2264–2282. DOI:10.1002/2014WR016149. eprint: https://agupubs.onlinelibrary.wiley.com/doi/pdf/10.1002/2014WR016149.

Hijma, M. P. and K. M. Cohen (2019). Holocene sea-level database for the Rhine-Meuse Delta, The Netherlands: Implications for the pre-8.2 ka sea-level jump. *Quaternary Science Reviews* 214, pp. 68–86. DOI:HTTPS://DOI.ORG/10.1016/J.QUASCIREV.2019.05.001.

Hsu, J. R. C. and C. Evans (1989). Parabolic bay shapes and applications. *Proceedings of the Institution of Civil Engineers* 87.4, pp. 557–570. DOI:10.1680/IICEP.1989.3778.

Huismans, Y., A. van der Spek, Q. Lodder, R. Zijlstra, E. Elias, and Z. B. Wang (2022). Development of intertidal flats in the Dutch Wadden Sea in response to a rising sea level: Spatial differentiation and sensitivity to the rate of sea level rise. *Ocean & Coastal Management* 216, p. 105969. DOI:HTTPS://DOI.ORG/10.1016/J.OCECOAMAN.2021.105969.

Ikeda, S. (1982). Lateral Bed Load Transport on Side Slopes. *Journal of the Hydraulics Division, ASCE* 108.11, pp. 1369–1373.

Ikeda, S. (1984). Lateral bed-load transport on side slopes - closure. *Journal of Hydraulic Engineering* 110.2, pp. 200–203.

Ikeda, S. and T. Nishimura (1986). Flow and Bed Profile in Meandering Sand Silt Rivers. *Journal of Hydraulic Engineering* 112.7, pp. 562–579. DOI:10.1061/(ASCE)0733-9429(1986)112:7(562).

Ishii, Y., K. Hori, A. Momohara, T. Nakanishi, and W. Hong (2016). Middle to late-Holocene decreased fluvial aggradation and widespread peat initiation in the Ishikari lowland (northern Japan). *The Holocene* 26.12, pp. 1924–1938. DOI:10.1177/0959683616646189. eprint: https://doi.org/10.1177/0959683616646189.

Isobe, M. and K. Horikawa (1982). Study on Water Particle Velocities of Shoaling and Breaking Waves. *Coastal Engineering in Japan* 25.1, pp. 109–123. DOI:10.1080/05785634.1982.11924340. eprint: https://doi.org/10.1080/05785634.1982.11924340.

Johnston, G. H., S. R. David, and D. A. Edmonds (2019). Connecting Fluvial Levee Deposition to Flood-Basin Hydrology. *Journal of Geophysical Research: Earth Surface* 124.7, pp. 1996–2012. DOI:10.1029/2019JF005014. eprint: https://agupubs.onlinelibrary.wiley.com/doi/pdf/10.1029/2019JF005014.

Jones, C. G., J. H. Lawton, and M. Shachak (1994). Organisms as Ecosystem Engineers. *Oikos* 69.3, pp. 373–386.

Kirwan, M. L., G. R. Guntenspergen, A. D'Alpaos, J. T. Morris, S. M. Mudd, and S. Temmerman (2010). Limits on the adaptability of coastal marshes to rising sea level. *Geophysical Research Letters* 37.23. DOI:HTTPS://DOI.ORG/10.1029/2010GL045489. eprint: https://agupubs.onlinelibrary.wiley.com/doi/pdf/10.1029/2010GL045489.

Kirwan, M. L. and J. P. Megonigal (2013). Tidal wetland stability in the face of human impacts and sea-level rise. *Nature* 504.7478, pp. 53–60. DOI:10.1038/NATURE12856.

Kirwan, M. L. and A. B. Murray (2007). A coupled geomorphic and ecological model of tidal marsh evolution. *Proceedings of the National Academy of Sciences* 104.15, pp. 6118–6122. DOI:10.1073/PNAS.0700958104. eprint: https://www.pnas.org/content/104/15/6118.full.pdf.

Kirwan, M. L., A. B. Murray, and W. S. Boyd (2008). Temporary vegetation disturbance as an explanation for permanent loss of tidal wetlands. *Geophysical Research Letters* 35.5. DOI:10.1029/2007GL032681. eprint: https://agupubs.onlinelibrary.wiley.com/doi/pdf/10.1029/2007GL032681.

Kirwan, M. L., S. Temmerman, E. E. Skeehan, G. R. Guntenspergen, and S. Fagherazzi (2016). Overestimation of marsh vulnerability to sea level rise. *Nature Climate Change* 6.3, pp. 253–260.

Kiss, T., M. Balogh, K. Fiala, and G. Sipos (2018). Morphology of fluvial levee series along a river under human influence, Maros River, Hungary. *Geomorphology* 303, pp. 309–321.

Klasz, G., W. Reckendorfer, H. Gabriel, C. Baumgartner, R. Schmalfuss, and D. Gutknecht (2014). Natural levee formation along a large and regulated river: The Danube in the National Park Donau-Auen, Austria. *Geomorphology* 215, pp. 20–33.

Kleinhans, M. G., T. de Haas, E. Lavooi, and B. Makaske (2012). Evaluating competing hypotheses for the origin and dynamics of river anastomosis. *Earth Surface Processes and Landforms* 37.12,

pp. 1337–1351. DOI:10.1002/ESP.3282. eprint: https://onlinelibrary.wiley.com/doi/pdf/10.1002/esp.3282.

Kleinhans, M. G., H. R. A. Jagers, E. Mosselman, and C. J. Sloff (2008). Bifurcation dynamics and avulsion duration in meandering rivers by one-dimensional and three-dimensional models. *Water Resources Research* 44.8, pp. 1–31. DOI:10.1029/2007WR005912.

Kleinhans, M. G., C. J. Buskes, and H. W. de Regt (2010a). Philosophy of earth science. *Philosophies of the Sciences*, pp. 213–236.

Kleinhans, M. G., H. J. Weerts, and K. M. Cohen (2010b). Avulsion in action: reconstruction and modelling sedimentation pace and upstream flood water levels following a Medieval tidal-river diversion catastrophe (Biesbosch, The Netherlands, 1421–1750 AD). *Geomorphology* 118.1-2, pp. 65–79.

Kleinhans, M. G., B. de Vries, L. Braat, and M. van Oorschot (2018). Living landscapes: Muddy and vegetated floodplain effects on fluvial pattern in an incised river. *Earth Surface Processes and Landforms* 43.14, pp. 2948–2963. DOI:10.1002/ESP.4437. eprint: https://onlinelibrary.wiley.com/doi/pdf/10.1002/esp.4437.

Kleinhans, M. G., R. I. Ferguson, S. N. Lane, and R. J. Hardy (2013). Splitting rivers at their seams: bifurcations and avulsion. *Earth Surface Processes and Landforms* 38.1, pp. 47–61. DOI:10.1002/ESP.3268. eprint: https://onlinelibrary.wiley.com/doi/pdf/10.1002/esp.3268.

Kleinhans, M. G. and J. H. van den Berg (2011). River channel and bar patterns explained and predicted by an empirical and a physics-based method. *Earth Surface Processes and Landforms* 36.6, pp. 721–738. DOI:10.1002/ESP.2090.

Kleinhans, M., O. Montfort, P. Dankers, L. Van Rijn, and W. Bonne (2005). Mud dynamics on the shoreface and upper shelf, Noordwijk, The Netherlands.

Koch, F. and C. Flokstra (1981). Bed level computations for curved alluvial channels. In: *19th International association for hydraulic research congress*.

Lanzoni, S. and A. D'Alpaos (2015). On funneling of tidal channels. *Journal of Geophysical Research: Earth Surface* 120.3, pp. 433–452. DOI:10.1002/2014JF003203. eprint: https://agupubs.onlinelibrary.wiley.com/doi/pdf/10.1002/2014JF003203.

Latrubesse, E. M. and E. Franzinelli (2002). The Holocene alluvial plain of the middle Amazon River, Brazil. *Geomorphology* 44.3-4, pp. 241–257.

Latteux, B. (1995). Techniques for long-term morphological simulation under tidal action. *Marine Geology* 126.1, pp. 129–141. DOI:HTTPS://DOI.ORG/10.1016/0025-3227(95)00069-B.

Lenstra, K. J. H., W. Ridderinkhof, and M. van der Vegt (2019). Unraveling the Mechanisms That Cause Cyclic Channel-Shoal Dynamics of Ebb-Tidal Deltas: A Numerical Modeling Study. *Journal of Geophysical Research: Earth Surface* 124.12, pp. 2778–2797. DOI:10.1029/2019JF005090. eprint: https://agupubs.onlinelibrary.wiley.com/doi/pdf/10.1029/2019JF005090.

Leonard, L. A. and M. E. Luther (1995). Flow hydrodynamics in tidal marsh canopies. *Limnology and Oceanography* 40.8, pp. 1474–1484. DOI:10.4319/LO.1995.40.8.1474. eprint: https://aslopubs.onlinelibrary.wiley.com/doi/pdf/10.4319/lo.1995.40.8.1474.

Leonard, L. A., P. A. Wren, and R. L. Beavers (2002). Flow dynamics and sedimentation in Spartina alterniflora and Phragmites australis marshes of the Chesapeake Bay. *Wetlands* 22.2, pp. 415–424. DOI:10.1672/0277-5212(2002)022[0415:FDASIS]2.0.CO;2.

Leonardi, N., A. Canestrelli, T. Sun, and S. Fagherazzi (2013). Effect of tides on mouth bar morphology and hydrodynamics. *Journal of Geophysical Research: Oceans* 118.9, pp. 4169–4183.

Lesser, G. (2009). An approach to medium-term coastal morphological modelling. PhD thesis. TU Delft.

Lesser, G., J. Roelvink, J. van Kester, and G. Stelling (2004). Development and validation of a three-dimensional morphological model. *Coastal Engineering* 51.8. Coastal Morphodynamic Modeling, pp. 883–915. DOI:HTTPS://DOI.ORG/10.1016/J.COASTALENG.2004.07.014.

Leuven, J. R. F. W., L. Braat, W. M. van Dijk, T. de Haas, E. P. van Onselen, B. G. Ruessink, and M. G. Kleinhans (2018a). Growing Forced Bars Determine Nonideal Estuary Planform. *Journal*

of Geophysical Research: Earth Surface 123.11, pp. 2971–2992. DOI:HTTPS://DOI.ORG/10.1029/2018JF004718. eprint: https://agupubs.onlinelibrary.wiley.com/doi/pdf/10.1029/2018JF004718.

Leuven, J. R. F. W., T. de Haas, L. Braat, and M. G. Kleinhans (2018b). Topographic forcing of tidal sandbar patterns for irregular estuary planforms. *Earth Surface Processes and Landforms* 43.1, pp. 172–186. DOI:HTTPS://DOI.ORG/10.1002/ESP.4166. eprint: https://onlinelibrary.wiley.com/doi/pdf/10.1002/esp.4166.

Leuven, J. R. F. W., H. J. Pierik, M. v. d. Vegt, T. J. Bouma, and M. G. Kleinhans (2019). Sea-level-rise-induced threats depend on the size of tide-influenced estuaries worldwide. *Nature Climate Change* 9.12, pp. 986–992.

Lokhorst, I. R., L. Braat, J. R. F. W. Leuven, A. W. Baar, M. van Oorschot, S. Selaković, and M. G. Kleinhans (2018). Morphological effects of vegetation on the tidal–fluvial transition in Holocene estuaries. *Earth Surface Dynamics* 6.4, pp. 883–901. DOI:10.5194/ESURF-6-883-2018.

Lorenzo-Trueba, J., V. R. Voller, C. Paola, R. R. Twilley, and A. E. Bevington (2012). Exploring the role of organic matter accumulation on delta evolution. *Journal of Geophysical Research: Earth Surface* 117.F4. DOI:HTTPS://DOI.ORG/10.1029/2012JF002339. eprint: https://agupubs.onlinelibrary.wiley.com/doi/pdf/10.1029/2012JF002339.

Louisiana, C. and R. Authority (2012). Louisiana's Comprehensive Master Plan for a Sustainable Coast. *Coastal Protection and Restoration Authority of Louisiana, Baton Rouge*.

Luijendijk, A. P., R. Ranasinghe, M. A. de Schipper, B. A. Huisman, C. M. Swinkels, D. J. Walstra, and M. J. Stive (2017). The initial morphological response of the Sand Engine: A process-based modelling study. *Coastal Engineering* 119, pp. 1–14. DOI:HTTPS://DOI.ORG/10.1016/J.COASTALENG.2016.09.005.

Makaske, B., H. J. Berendsen, and M. H. Van Ree (2007). Middle Holocene avulsion-belt deposits in the central Rhine–Meuse delta, The Netherlands. *Journal of Sedimentary Research* 77.2, pp. 110–123.

Makaske, B., D. G. Smith, and H. J. A. Berendsen (2002). Avulsions, channel evolution and floodplain sedimentation rates of the anastomosing upper Columbia River, British Columbia, Canada. *Sedimentology* 49.5, pp. 1049–1071. DOI:10.1046/J.1365-3091.2002.00489.X. eprint: https://onlinelibrary.wiley.com/doi/pdf/10.1046/j.1365-3091.2002.00489.x.

Malej, M., J. M. mith, and G. Salgado-Dominguez (2015). Introduction to phase-resolving wave modeling with FUNWAVE. *ERDC/CHL CHETNERDC/CHL CHET* I87.

Marani, M., A. D'Alpaos, S. Lanzoni, and M. Santalucia (2011). Understanding and predicting wave erosion of marsh edges. *Geophysical Research Letters* 38.21. DOI:10.1029/2011GL048995. eprint: https://agupubs.onlinelibrary.wiley.com/doi/pdf/10.1029/2011GL048995.

Marani, M., A. D'Alpaos, S. Lanzoni, L. Carniello, and A. Rinaldo (2007). Biologically-controlled multiple equilibria of tidal landforms and the fate of the Venice lagoon. *Geophysical Research Letters* 34.11. DOI:10.1029/2007GL030178. eprint: https://agupubs.onlinelibrary.wiley.com/doi/pdf/10.1029/2007GL030178.

Marani, M., C. Da Lio, and A. D'Alpaos (2013). Vegetation engineers marsh morphology through multiple competing stable states. *Proceedings of the National Academy of Sciences* 110.9, pp. 3259–3263. DOI:10.1073/PNAS.1218327110. eprint: https://www.pnas.org/content/110/9/3259.full.pdf.

Marciano, R., Z. B. Wang, A. Hibma, H. J. D. Vriend, and A. Defina (2005). Modeling of channel patterns in short tidal basins. *Journal of Geophysical Research* 110, pp. 1–13. DOI:10.1029/2003JF000092.

Mariotti, G. and A. Canestrelli (2017a). Long-term morphodynamics of muddy backbarrier basins: Fill in or empty out?. *Water Resources Research* 53.8, pp. 7029–7054.

Mariotti, G., F. Falcini, N. Geleynse, M. Guala, T. Sun, and S. Fagherazzi (2013). Sediment eddy diffusivity in meandering turbulent jets: Implications for levee formation at river mouths. *Journal of Geophysical Research: Earth Surface* 118.3, pp. 1908–1920.

Mariotti, G. (2020). Beyond marsh drowning: The many faces of marsh loss (and gain). *Advances in Water Resources* 144, p. 103710. DOI:HTTPS://DOI.ORG/10.1016/J.ADVWATRES.2020.103710.

Mariotti, G. and A. Canestrelli (2017b). Long-term morphodynamics of muddy backbarrier basins: Fill in or empty out?. *Water Resources Research* 53.8. cited By 3, pp. 7029–7054. DOI:10.1002/2017WR020461.

Mariotti, G. and S. Fagherazzi (2010). A numerical model for the coupled long-term evolution of salt marshes and tidal flats. *Journal of Geophysical Research: Earth Surface* 115.F1. DOI:10.1029/2009JF001326. eprint: https://agupubs.onlinelibrary.wiley.com/doi/pdf/10.1029/2009JF001326.

Maximova, T., S. Ides, T. De Mulder, and F. Mostaert (2009a). *LTV O & M thema Veiligheid - Deelproject 1: Verbetering hydrodynamisch NeVla model ten behoeve van scenario-analyse (in Dutch)*. WL rapporten 756_05. Antwerp, Belgium: Flanders Hydraulics Research & Deltares.

Maximova, T., S. Ides, T. De Mulder, and F. Mostaert (2009b). *Verbetering randvoorwaardenmodel. Deelrapport 4: Extra aanpassingen Zeeschelde (in Dutch)*. WL rapporten 753_09. Antwerp, Belgium: Flanders Hydraulics Research.

Maximova, T., S. Ides, J. Vanlede, T. De Mulder, and F. Mostaert (2009c). *Verbetering 2D randvoorwaardenmodel. Deelrapport 3: kalibratie bovenlopen (in Dutch)*. WL rapporten 753_09. Antwerp, Belgium: Flanders Hydraulics Research.

McMahon, W. J. and N. S. Davies (2018). The shortage of geological evidence for pre-vegetation meandering rivers. *Fluvial Meanders and Their Sedimentary Products in the Rock Record*, pp. 119–148.

Meijles, E. W., P. Kiden, H.-J. Streurman, J. van der Plicht, P. C. Vos, W. R. Gehrels, and R. E. Kopp (2018). Holocene relative mean sea-level changes in the Wadden Sea area, northern Netherlands. *Journal of Quaternary Science* 33.8, pp. 905–923. DOI:HTTPS://DOI.ORG/10.1002/JQS.3068. eprint: https://onlinelibrary.wiley.com/doi/pdf/10.1002/jqs.3068.

Meyer-Peter, E. and R. Müller (1948). Formulas for bed-load transport. In: *IAHSR 2nd meeting, Stockholm, appendix 2*. IAHR.

Minderhoud, P. S. J., H. Middelkoop, G. Erkens, and E. Stouthamer (Jan. 2020). Groundwater extraction may drown mega-delta: projections of extraction-induced subsidence and elevation of the Mekong delta for the 21st century. *Environmental Research Communications* 2.1, p. 011005. DOI:10.1088/2515-7620/AB5E21.

Mohrig, D., P. L. Heller, C. Paola, and W. J. Lyons (Dec. 2000). Interpreting avulsion process from ancient alluvial sequences: Guadalope-Matarranya system (northern Spain) and Wasatch Formation (western Colorado). *GSA Bulletin* 112.12, pp. 1787–1803. DOI:10.1130/0016-7606(2000)112<1787:IAPFAA>2.0.CO;2. eprint: https://pubs.geoscienceworld.org/gsabulletin/article-pdf/112/12/1787/3383751/i0016-7606-112-12-1787.pdf.

Moore, L. J., E. B. Goldstein, O. D. Vinent, D. Walters, M. Kirwan, R. Lauzon, A. B. Murray, and P. Ruggiero (2018). The role of ecomorphodynamic feedbacks and landscape couplings in influencing the response of barriers to changing climate. In: *Barrier Dynamics and Response to Changing Climate*. Springer, pp. 305–336.

Murray, A. B. and C. Paola (2003). Modelling the effect of vegetation on channel pattern in bedload rivers. *Earth Surface Processes and Landforms* 28.2, pp. 131–143. DOI:10.1002/ESP.428. eprint: https://onlinelibrary.wiley.com/doi/pdf/10.1002/esp.428.

Nahon, A., X. Bertin, A. B. Fortunato, and A. Oliveira (2012). Process-based 2DH morphodynamic modeling of tidal inlets: A comparison with empirical classifications and theories. *Marine Geology* 291-294, pp. 1–11. DOI:HTTPS://DOI.ORG/10.1016/J.MARGEO.2011.10.001.

Nardin, W. and S. Fagherazzi (2012). The effect of wind waves on the development of river mouth bars. *Geophysical Research Letters* 39.12. DOI:10.1029/2012GL051788. eprint: https://agupubs.onlinelibrary.wiley.com/doi/pdf/10.1029/2012GL051788.

Nardin, W. and S. Fagherazzi (2018). The Role of Waves, Shelf Slope, and Sediment Characteristics on the Development of Erosional Chenier Plains. *Geophysical Research Letters* 45.16, pp. 8435–8444. DOI:10.1029/2018GL078694. eprint: https://agupubs.onlinelibrary.wiley.com/doi/pdf/10.1029/2018GL078694.

Nardin, W., L. Larsen, S. Fagherazzi, and P. Wiberg (2018). Tradeoffs among hydrodynamics, sediment fluxes and vegetation community in the Virginia Coast Reserve, USA. *Estuarine, Coastal and Shelf Science* 210, pp. 98–108. DOI:HTTPS://DOI.ORG/10.1016/J.ECSS.2018.06.009.

Nardin, W., S. Lera, and J. Nienhuis (2020). Effect of offshore waves and vegetation on the sediment budget in the Virginia Coast Reserve (VA). *Earth Surface Processes and Landforms* 45.12, pp. 3055–3068. DOI:HTTPS://DOI.ORG/10.1002/ESP.4951. eprint: https://onlinelibrary.wiley.com/doi/pdf/10.1002/esp.4951.

Nicholas, A. P. (2013). Modelling the continuum of river channel patterns. *Earth Surface Processes and Landforms* 1196.June, pp. 1187–1196. DOI:10.1002/ESP.3431.

Nienhuis, J. H., A. D. Ashton, D. A. Edmonds, A. J. F. Hoitink, A. J. Kettner, J. C. Rowland, and T. E. Törnqvist (2020). Global-scale human impact on delta morphology has led to net land area gain. *Nature* (7791). DOI:10.1038/s41586-019-1905-9.

Nienhuis, J. H. and A. D. Ashton (2016). Mechanics and rates of tidal inlet migration: Modeling and application to natural examples. *Journal of Geophysical Research: Earth Surface* 121.11, pp. 2118–2139. DOI:10.1002/2016JF004035. eprint: https://agupubs.onlinelibrary.wiley.com/doi/pdf/10.1002/2016JF004035.

Nienhuis, J. H., A. D. Ashton, W. Nardin, S. Fagherazzi, and L. Giosan (2016). Alongshore sediment bypassing as a control on river mouth morphodynamics. *Journal of Geophysical Research: Earth Surface* 121.4, pp. 664–683. DOI:10.1002/2015JF003780. eprint: https://agupubs.onlinelibrary.wiley.com/doi/pdf/10.1002/2015JF003780.

Nienhuis, J. H., T. E. Törnqvist, and C. R. Esposito (2018). Crevasse Splays Versus Avulsions: A Recipe for Land Building With Levee Breaches. *Geophysical Research Letters* 45.9, pp. 4058–4067. DOI:10.1029/2018GL077933. eprint: https://agupubs.onlinelibrary.wiley.com/doi/pdf/10.1029/2018GL077933.

Nnafie, A., T. Van Oyen, B. De Maerschalck, M. van der Vegt, and M. v. d. Wegen (2018). Estuarine channel evolution in response to closure of secondary basins: An observational and morphodynamic modeling study of the Western Scheldt Estuary. *Journal of Geophysical Research: Earth Surface* 123.1, pp. 167–186.

O'Brien, M. P. (1967). Equilibrium flow areas of tidal inlets on sandy coasts. In: *Coastal Engineering 1966*, pp. 676–686.

Olabarrieta, M., W. R. Geyer, G. Coco, C. T. Friedrichs, and Z. Cao (2018). Effects of Density-Driven Flows on the Long-Term Morphodynamic Evolution of Funnel-Shaped Estuaries. *Journal of Geophysical Research: Earth Surface* 123.11, pp. 2901–2924. DOI:10.1029/2017JF004527. eprint: https://agupubs.onlinelibrary.wiley.com/doi/pdf/10.1029/2017JF004527.

Olabarrieta, M., W. R. Geyer, and N. Kumar (2014). The role of morphology and wave-current interaction at tidal inlets: An idealized modeling analysis. *Journal of Geophysical Research: Oceans* 119.12, pp. 8818–8837. DOI:10.1002/2014JC010191. eprint: https://agupubs.onlinelibrary.wiley.com/doi/pdf/10.1002/2014JC010191.

Oorschot, M. v., M. Kleinhans, G. Geerling, and H. Middelkoop (2016). Distinct patterns of interaction between vegetation and morphodynamics. *Earth Surface Processes and Landforms* 41.6, pp. 791–808.

Oppenheimer, M. et al. (2019). Sea Level Rise and Implications for Low-Lying Islands, Coasts and Communities. In: *In: IPCC Special Report on the Ocean and Cryosphere in a Changing Climate*. Ed. by H. Portner et al.

Paola, C. and V. R. Voller (2005). A generalized Exner equation for sediment mass balance. *Journal of Geophysical Research: Earth Surface* 110.F4. DOI:10.1029/2004JF000274. eprint: https://agupubs.onlinelibrary.wiley.com/doi/pdf/10.1029/2004JF000274.

Paola, C., V. Ganti, D. Mohrig, A. C. Runkel, and K. M. Straub (2018). Time Not Our Time: Physical Controls on the Preservation and Measurement of Geologic Time. *Annual Review of Earth and Planetary Sciences* 46.1, pp. 409–438. DOI:10.1146/ANNUREV-EARTH-082517-010129. eprint: https://doi.org/10.1146/annurev-earth-082517-010129.

Paola, C. et al. (2001). Experimental stratigraphy. *GSA TODAY* 11.7, pp. 4–9.
Parker, G. (1979). Hydraulic geometry of active gravel rivers. *Journal of the Hydraulic Division, American Society of Civil Engineers* 105.9, pp. 1185–1201.
Parker, G. (1978). Self-formed straight rivers with equilibrium banks and mobile bed. Part 1. The sand-silt river. *Journal of Fluid Mechanics* 89.1, pp. 109–125. DOI:10.1017/s0022112078002499.
Partheniades, E. (1965). Erosion and Deposition of Cohesive Soils. *Journal of the Hydraulics Division* 91 (1), pp. 105–139.
Pearson, S. G., B. C. van Prooijen, E. P. L. Elias, S. Vitousek, and Z. B. Wang (2020). Sediment Connectivity: A Framework for Analyzing Coastal Sediment Transport Pathways. *Journal of Geophysical Research: Earth Surface* 125.10. e2020JF005595 10.1029/2020JF005595, e2020JF005595. DOI:HTTPS://DOI.ORG/10.1029/2020JF005595. eprint: https://agupubs.onlinelibrary.wiley.com/doi/pdf/10.1029/2020JF005595.
Perez-Arlucea, M. and N. D. Smith (Jan. 1999). Depositional patterns following the 1870s avulsion of the Saskatchewan River (Cumberland Marshes, Saskatchewan, Canada). *Journal of Sedimentary Research* 69.1, pp. 62–73. DOI:10.2110/JSR.69.62. eprint: https://pubs.geoscienceworld.org/jsedres/article-pdf/69/1/62/2812573/62.pdf.
Pierik, H., K. Cohen, P. Vos, A. van der Spek, and E. Stouthamer (2017a). Late Holocene coastal-plain evolution of the Netherlands: the role of natural preconditions in human-induced sea ingressions. *Proceedings of the Geologists' Association* 128.2, pp. 180–197. DOI:HTTPS://DOI.ORG/10.1016/J.PGEOLA.2016.12.002.
Pierik, H., E. Stouthamer, and K. Cohen (2017b). Natural levee evolution in the Rhine-Meuse delta, the Netherlands, during the first millennium CE. *Geomorphology* 295, pp. 215–234. DOI:HTTPS://DOI.ORG/10.1016/J.GEOMORPH.2017.07.003.
Pierik, H. J., E. Stouthamer, T. Schuring, and K. M. Cohen (2018). Human-caused avulsion in the Rhine-Meuse delta before historic embankment (The Netherlands). *Geology* 46.11, pp. 935–938.
Pierik, H. J. et al. (2023). Vegetation and peat accumulation steer Holocene tidal–fluvial basin filling and overbank sedimentation along the Old Rhine River, The Netherlands. *Sedimentology* 70.1, pp. 179–213. DOI:HTTPS://DOI.ORG/10.1111/SED.13038. eprint: https://onlinelibrary.wiley.com/doi/pdf/10.1111/sed.13038.
Powell, M. A., R. J. Thieke, and A. J. Mehta (2006). Morphodynamic relationships for ebb and flood delta volumes at Florida's tidal entrances. *Ocean Dynamics* 56.3, pp. 295–307.
Raabe, A. L., A. H. da F. Klein, M. González, and R. Medina (2010). MEPBAY and SMC: Software tools to support different operational levels of headland-bay beach in coastal engineering projects. *Coastal Engineering* 57.2. Hydrodynamics and Applications of Headland-Bay Beaches, pp. 213–226. DOI:HTTPS://DOI.ORG/10.1016/J.COASTALENG.2009.10.008.
Ranasinghe, R. (2020). On the need for a new generation of coastal change models for the 21st century. *Scientific Reports* 10.1, p. 2010. DOI:10.1038/s41598-020-58376-x.
Ranasinghe, R., C. Swinkels, A. Luijendijk, D. Roelvink, J. Bosboom, M. Stive, and D. Walstra (2011). Morphodynamic upscaling with the MORFAC approach: Dependencies and sensitivities. *Coastal Engineering* 58.8, pp. 806–811. DOI:HTTPS://DOI.ORG/10.1016/J.COASTALENG.2011.03.010.
Richardson, D., G. O. J. Porter, R. Zimmerman, C. Carlson, K. Overman, and C. Carlson (2018). *Integrated Topography and Bathymetry for the Eastern Shore of Virginia ver 10. Environmental Data Initiative*. https://doi.org/10.6073/pasta/63a22558d6650fae8232b6a8814a90d5.
Rienecker, M. M. and J. D. Fenton (1981). A Fourier approximation method for steady water waves. *Journal of Fluid Mechanics* 104, pp. 119–137.
Rijkswaterstaat (2017). *The yearly coastal measurements (in Dutch: De JAarlijkse KUStmetingen or JARKUS)*. https://opendap.deltares.nl/thredds/catalog/opendap/rijkswaterstaat/jarkus/caralog.html.
Ris, R. C., L. H. Holthuijsen, and N. Booij (1999). A third-generation wave model for coastal regions: 2. Verification. *Journal of Geophysical Research: Oceans* 104.C4, pp. 7667–7681. DOI:10.1029/1998JC900123. eprint: https://agupubs.onlinelibrary.wiley.com/doi/pdf/10.1029/1998JC900123.

Robbins, M. G., J. L. Shawler, and C. J. Hein (2022). Contribution of longshore sand exchanges to mesoscale barrier-island behavior: Insights from the Virginia Barrier Islands, U.S. East Coast. *Geomorphology* 403, p. 108163. DOI:HTTPS://DOI.ORG/10.1016/J.GEOMORPH.2022.108163.

Roelvink, J. (2006). Coastal morphodynamic evolution techniques. *Coastal Engineering* 53.2. Coastal Hydrodynamics and Morphodynamics, pp. 277–287. DOI:HTTPS://DOI.ORG/10.1016/J.COASTALENG.2005.10.015.

Roelvink, J. and I. Brøker (1993). Cross-shore profile models. *Coastal Engineering* 21.1. Special Issue Coastal Morphodynamics: Processes and Modelling, pp. 163–191. DOI:HTTPS://DOI.ORG/10.1016/0378-3839(93)90049-E.

Roelvink, J. and M. Stive (1989). Bar-generating cross-shore flow mechnisms on a beach. *Journal of Geophysical Research: Oceans* 94, pp. 4785–4800.

Rowland, J. C., W. E. Dietrich, and M. T. Stacey (2010). Morphodynamics of subaqueous levee formation: Insights into river mouth morphologies arising from experiments. *Journal of Geophysical Research: Earth Surface* 115.F4.

Ruessink, B. G., Y. Kuriyama, A. J. H. M. Reniers, J. A. Roelvink, and D. J. R. Walstra (2007). Modeling cross-shore sandbar behavior on the timescale of weeks. *Journal of Geophysical Research: Earth Surface* 112.3, pp. 1–15. DOI:10.1029/2006JF000730.

Ruessink, B., G. Ramaekers, and L. van Rijn (2012). On the parameterization of the free-stream nonlinear wave orbital motion in nearshore morphodynamic models. *Coastal Engineering* 65, pp. 56–63. DOI:HTTPS://DOI.ORG/10.1016/J.COASTALENG.2012.03.006.

Savenije, H. H. G. (2015). Prediction in ungauged estuaries: An integrated theory. *Water Resources Research* 51.4, pp. 2464–2476. DOI:HTTPS://DOI.ORG/10.1002/2015WR016936. eprint: https://agupubs.onlinelibrary.wiley.com/doi/pdf/10.1002/2015WR016936.

Schrijvershof, R. and J. Vroom (2016). *Effecten van realistische (extreme) stortstrategieën in de Westerschelde (in Dutch)*. Tech. rep. Deltares.

Schuerch, M. et al. (2018). Future response of global coastal wetlands to sea-level rise. *Nature* 561.7722, pp. 231–234. DOI:10.1038/s41586-018-0476-5.

Schuttelaars, H. and H. De Swart (1999). Initial formation of channels and shoals in a short tidal embayment. *Journal of fluid mechanics* 386, pp. 15–42.

Schuurman, F., W. a. Marra, and M. G. Kleinhans (2013). Physics-based modeling of large braided sand-bed rivers: Bar pattern formation, dynamics, and sensitivity. *Journal of Geophysical Research: Earth Surface* 118.4, pp. 2509–2527. DOI:10.1002/2013JF002896.

Schuurman, F., W. Ta, S. Post, M. Sokolewicz, M. Busnelli, and M. Kleinhans (2018). Response of braiding channel morphodynamics to peak discharge changes in the Upper Yellow River. *Earth Surface Processes and Landforms*.

Schwarz, C., T. Bouma, L. Zhang, S. Temmerman, T. Ysebaert, and P. Herman (2015). Interactions between plant traits and sediment characteristics influencing species establishment and scale-dependent feedbacks in salt marsh ecosystems. *Geomorphology* 250, pp. 298–307. DOI:HTTPS://DOI.ORG/10.1016/J.GEOMORPH.2015.09.013.

Schwarz, C., O. Gourgue, J. van Belzen, Z. Zhu, T. J. Bouma, J. van de Koppel, G. Ruessink, N. Claude, and S. Temmerman (2018). Self-organization of a biogeomorphic landscape controlled by plant life-history traits. *Nature Geoscience* 11.9, pp. 672–677. DOI:10.1038/s41561-018-0180-Y.

Schwarz, C., F. van Rees, D. Xie, M. G. Kleinhans, and B. van Maanen (2022). Salt marshes create more extensive channel networks than mangroves. *Nature Communications* 13.1, p. 2017. DOI:10.1038/s41467-022-29654-1.

Sekine, M. and G. Parker (1992). Bed-load transport on transverse slope. *Journal of Hydraulic Engineering* 118.4, pp. 513–535.

Seminara, G. and M. Turbino (2001). Sand bars in tidal channels. Part 1. Free bars. *Journal of fluid mechanincs* 440.2001, pp. 49–74.

Shen, Z., T. E. Törnqvist, B. Mauz, E. L. Chamberlain, A. G. Nijhuis, and L. Sandoval (Oct. 2015). Episodic overbank deposition as a dominant mechanism of floodplain and delta-plain aggrada-

tion. *Geology* 43.10, pp. 875–878. DOI:10.1130/G36847.1. eprint: https://pubs.geoscienceworld.org/geology/article-pdf/43/10/875/3547509/875.pdf.

Shiers, M., N. Mountney, D. Hodgson, and S. Cobain (2014). Depositional controls on tidally influenced fluvial successions, Neslen Formation, Utah, USA. *Sedimentary Geology* 311, pp. 1–16. DOI:HTTPS://DOI.ORG/10.1016/J.SEDGEO.2014.06.005.

Short, A. D. (1992). Beach systems of the central Netherlands coast: Processes, morphology and structural impacts in a storm driven multi-bar system. *Marine Geology* 107.1, pp. 103–137. DOI:HTTPS://DOI.ORG/10.1016/0025-3227(92)90071-O.

Siders, A., M. Hino, and K. J. Mach (2019). The case for strategic and managed climate retreat. *Science* 365.6455, pp. 761–763. DOI:10.1126/SCIENCE.AAX8346. eprint: https://science.sciencemag.org/content/365/6455/761.full.pdf.

Sievers, J., M. Rubel, and P. Milbradt (2020). *EasyGSH-DB: Bathymetrie (1996-2016). Bundesanstalt für Wasserbau*. https://doi.org/10.48437/02.2020.K2.7000.0002.

Silvestri, S., A. Defina, and M. Marani (2005). Tidal regime, salinity and salt marsh plant zonation. *Estuarine, Coastal and Shelf Science* 62.1, pp. 119–130. DOI:HTTPS://DOI.ORG/10.1016/J.ECSS.2004.08.010.

Slingerland, R. and N. D. Smith (1998). Necessary conditions for a meandering-river avulsion. *Geology* 26.5, pp. 435–438. DOI:10.1130/0091-7613(1998)026<0435.

Sloff, K. and E. Mosselman (2012). Bifurcation modelling in a meandering gravel-sand bed river. *Earth Surface Processes and Landforms* 37.14, pp. 1556–1566. DOI:10.1002/ESP.3305.

Smajgl, A., T. Toan, D. Nhan, J. Ward, N. Trung, L. Tri, V. Tri, and P. Vu (2015). Responding to rising sea levels in the Mekong Delta. *Nature Climate Change* 5.2, p. 167.

Smith, N. D. and M. Pérez-Arlucea (2004). Effects of peat on the shapes of alluvial channels: examples from the Cumberland Marshes, Saskatchewan, Canada. *Geomorphology* 61.3, pp. 323–335. DOI:HTTPS://DOI.ORG/10.1016/J.GEOMORPH.2004.01.006.

Smith, N. D. and M. Pérez-Arlucea (2008). Natural levee deposition during the 2005 flood of the Saskatchewan River. *Geomorphology* 101.4, pp. 583–594. DOI:HTTPS://DOI.ORG/10.1016/J.GEOMORPH.2008.02.009.

Soulsby, R., L. Hamm, G. Klopman, D. Myrhaug, R. Simons, and G. Thomas (1993). Wave-current interaction within and outside the bottom boundary layer. *Coastal Engineering* 21.1. Special Issue Coastal Morphodynamics: Processes and Modelling, pp. 41–69. DOI:HTTPS://DOI.ORG/10.1016/0378-3839(93)90045-A.

Stark, J., P. Meire, and S. Temmerman (2017). Changing tidal hydrodynamics during different stages of eco-geomorphological development of a tidal marsh: A numerical modeling study. *Estuarine, Coastal and Shelf Science* 188, pp. 56–68. DOI:HTTPS://DOI.ORG/10.1016/J.ECSS.2017.02.014.

Stauble, D. K. and M. A. Cialone (1996). Sediment dynamics and profile interactions: DUCK94. *Proceedings of the 25th International Conference on Coastal Engineering* 25, pp. 3921–3934.

Stive, M. (1986). A model for cross-shore sediment transport. *20th International Conference on Coastal Engineering*, pp. 1550–1564.

Storms, J. E. A., M. J. F. Stive, D. (A. Roelvink, and D. J. Walstra (n.d.). Initial Morphologic and Stratigraphic Delta Evolution Related to Buoyant River Plumes. (). DOI:10.1061/40926(239)56.

Storms, J. E., R. M. Hoogendoorn, R. A. Dam, A. Hoitink, and S. Kroonenberg (2005). Late-holocene evolution of the Mahakam delta, East Kalimantan, Indonesia. *Sedimentary Geology* 180.3-4, pp. 149–166.

Stouthamer, E. (2001). Sedimentary products of avulsions in the Holocene Rhine–Meuse Delta, The Netherlands. *Sedimentary Geology* 145.1, pp. 73–92. DOI:HTTPS://DOI.ORG/10.1016/S0037-0738(01)00117-8.

Stouthamer, E. (2005). Reoccupation of channel belts and its influence on alluvial architecture in the Holocene Rhine–Meuse delta, The Netherlands. *SEPM Special Publications* 83, pp. 319–339.

Stouthamer, E. and H. J. Berendsen (2007). Avulsion: The relative roles of autogenic and allogenic processes. *Sedimentary Geology* 198.3, pp. 309–325. DOI:HTTPS://DOI.ORG/10.1016/J.SEDGEO.2007.01.017.

Struiksma, N., K. W. Olesen, C. Flokstra, and H. J. De Vriend (1985). Bed deformation in curved alluvial channels. *Journal of Hydraulic Research* 23.1, pp. 57–79. DOI:10.1080/00221688509499377.

Syvitski, J. P. M., C. J. Vörösmarty, A. J. Kettner, and P. Green (2005). Impact of Humans on the Flux of Terrestrial Sediment to the Global Coastal Ocean. *Science* 308.5720, pp. 376–380. DOI:10.1126/SCIENCE.1109454. eprint: https://science.sciencemag.org/content/308/5720/376.full.pdf.

Tal, M. and C. Paola (2007). Dynamic single-thread channels maintained by the interaction of flow and vegetation. *Geology* 35.4, pp. 347–350.

Talmon, A., N. Struiksma, and M. Van Mierlo (1995). Laboratory measurements of the direction of sediment transport on transverse alluvial-bed slopes. *Journal of Hydraulic Research* 33.4, pp. 495–517. DOI:10.1080/00221689509498657.

Temmerman, S., T. Bouma, J. V. de Koppel, D. V. der Wal, M. D. Vries, and P. Herman (2007). Vegetation causes channel erosion in a tidal landscape. *Geology* 35.7, pp. 631–634. DOI:10.1130/G23502A.1.

Temmerman, S., P. Meire, T. J. Bouma, P. M. Herman, T. Ysebaert, and H. J. De Vriend (2013). Ecosystem-based coastal defence in the face of global change. *Nature* 504.7478, pp. 79–83.

Thorn, C. E. and M. R. Welford (1994). The Equilibrium Concept in Geomorphology. *Annals of the Association of American Geographers* 84.4, pp. 666–696. DOI:10.1111/J.1467-8306.1994.TB01882.X. eprint: https://onlinelibrary.wiley.com/doi/pdf/10.1111/j.1467-8306.1994.tb01882.x.

Tonnon, P., B. Huisman, G. Stam, and L. van Rijn (2018). Numerical modelling of erosion rates, life span and maintenance volumes of mega nourishments. *Coastal Engineering* 131, pp. 51–69. DOI:HTTPS://DOI.ORG/10.1016/J.COASTALENG.2017.10.001.

Törnqvist, T. E. and J. S. Bridge (2002). Spatial variation of overbank aggradation rate and its influence on avulsion frequency. *Sedimentology* 49.5, pp. 891–905. DOI:10.1046/J.1365-3091.2002.00478.X. eprint: https://onlinelibrary.wiley.com/doi/pdf/10.1046/j.1365-3091.2002.00478.x.

Törnqvist, T. E., J. L. González, L. A. Newsom, K. van der Borg, A. F. de Jong, and C. W. Kurnik (July 2004). Deciphering Holocene sea-level history on the U.S. Gulf Coast: A high-resolution record from the Mississippi Delta. *GSA Bulletin* 116.7-8, pp. 1026–1039. DOI:10.1130/B2525478.1. eprint: https://pubs.geoscienceworld.org/gsabulletin/article-pdf/116/7-8/1026/3390591/i0016-7606-116-7-1026.pdf.

Townend, I., Z. B. Wang, M. Stive, and Z. Zhou (2016). Development and extension of an aggregated scale model: Part 1 - Background to ASMITA. *China Ocean Engineering* 30.4, pp. 483–504.

Trowbridge, J. and D. Young (Aug. 1989). Sand transport by unbroken water waves under sheet flow conditions. *Journal of Geophysical Research: Oceans* 94.C8, pp. 10971–10991. DOI:10.1029/JC094IC08P10971.

Umitsu, M. (1985). Natural Levees and Landform Evolutions in the Bengal Lowland. *Geographical review of Japan, Series B.* 58.2, pp. 149–164. DOI:10.4157/GRJ1984B.58.149.

van der Molen, J. and H. de Swart (2001). Holocene wave conditions and wave-induced sand transport in the southern North Sea. *Continental Shelf Research* 21.16, pp. 1723–1749. DOI:HTTPS://DOI.ORG/10.1016/S0278-4343(01)00018-8.

Van der Vegt, H., J. E. A. Storms, D. J. R. Walstra, and N. C. Howes (2016). Can bed load transport drive varying depositional behaviour in river delta environments ?. *Sedimentary Geology* 345, pp. 19–32. DOI:10.1016/J.SEDGEO.2016.08.009.

Van der Wegen, M. and B. Jaffe (2014). Processes governing decadal-scale depositional narrowing of the major tidal channel in San Pablo Bay, California, USA. *Journal of Geophysical Research: Earth Surface* 119.5. cited By 8, pp. 1136–1154. DOI:10.1002/2013JF002824.

Van der Spek, A. J. (2018). The development of the tidal basins in the Dutch Wadden Sea until 2100: the impact of accelerated sea-level rise and subsidence on their sediment budget – a synthesis. *Netherlands Journal of Geosciences* 97.3, pp. 71–78. DOI:10.1017/NJG.2018.10.

Van der Spek, A. J. and D. J. Beets (1992). Mid-Holocene evolution of a tidal basin in the western Netherlands: a model for future changes in the northern Netherlands under conditions of acceler-

ated sea-level rise?. *Sedimentary Geology* 80.3. Research Conference on Quaternary Coastal Evolution, pp. 185–197. DOI:HTTPS://DOI.ORG/10.1016/0037-0738(92)90040-X.

Van der Vegt, H., J. Storms, D. Walstra, and N. Howes (2016). Can bed load transport drive varying depositional behaviour in river delta environments?. *Sedimentary Geology* 345, pp. 19–32. DOI:HTTPS://DOI.ORG/10.1016/J.SEDGEO.2016.08.009.

Van der Wegen, M. and J. A. Roelvink (2008). Long-term morphodynamic evolution of a tidal embayment using a two-dimensional, process-based model. *Journal of Geophysical Research: Oceans* 113.C3. DOI:HTTPS://DOI.ORG/10.1029/2006JC003983. eprint: https://agupubs.onlinelibrary.wiley.com/doi/pdf/10.1029/2006JC003983.

Van der Wegen, M. and J. A. Roelvink (2012). Reproduction of estuarine bathymetry by means of a process-based model: Western Scheldt case study, the Netherlands. *Geomorphology* 179, pp. 152–167. DOI:10.1016/J.GEOMORPH.2012.08.007.

Van Dijk, W. M., F. Schuurman, W. I. Van de Lageweg, and M. G. Kleinhans (2014). Bifurcation instability and chute cutoff development in meandering gravel-bed rivers. *Geomorphology* 213, pp. 277–291.

Van Kessel, T., A. Spruyt-de Boer, J. Van der Werf, L. Sittoni, B. Van Pooijen, and H. Winterwerp (2012). *Bed module for sand-mud mixtures*. Tech. rep. Delft, The Netherlands: Deltares.

van Kessel, T., J. Vanlede, and J. de Kok (2011). Development of a mud transport model for the Scheldt estuary. *Continental Shelf Research* 31.10, Supplement. Proceedings of the 9th International Conference on Nearshore and Estuarine Cohesive Sediment Transport Processes, S165–S181. DOI:HTTPS://DOI.ORG/10.1016/J.CSR.2010.12.006.

van Maren, D. (2007). Grain size and sediment concentration effects on channel patterns of silt-laden rivers. *Sedimentary Geology* 202.1, pp. 297–316. DOI:HTTPS://DOI.ORG/10.1016/J.SEDGEO.2007.04.001.

Van Rijn, L., D. Walstra, and M. v. Ormondt (2004). Description of TRANSPOR2004 and Implementation in Delft3D-ONLINE. *Z3748*.

van Rijn, L. C. (1997). Sediment transport and budget of the central coastal zone of Holland. *Coastal Engineering* 32.1, pp. 61–90. DOI:HTTPS://DOI.ORG/10.1016/S0378-3839(97)00021-5.

Van Belzen, J. et al. (2017). Vegetation recovery in tidal marshes reveals critical slowing down under increased inundation. *Nature Communications* 8.1, p. 15811. DOI:10.1038/NCOMMS15811.

Van Bendegom, L. (1947). Enige beschouwingen over riviermofologie en rivierverbetering. *De Ingenieur* 59.4, pp. 1–11.

Van Dijk, W., M. Hiatt, J. van der Werf, and M. G. Kleinhans (2018). Effect of perturbations by shoal margin collapses on the morphodynamics of a sandy estuary. *Earth Surface Processes and Landforms*.

Van Dinter, M. (2013). The Roman Limes in the Netherlands: how a delta landscape determined the location of the military structures. *Netherlands Journal of Geosciences - Geologie en Mijnbouw* 92.1, pp. 11–32. DOI:10.1017/S0016774600000251.

Van Dobben, H. F., A. V. de Groot, and J. P. Bakker (2022). Salt Marsh Accretion With and Without Deep Soil Subsidence as a Proxy for Sea-Level Rise. *Estuaries and Coasts*. DOI:10.1007/S12237-021-01034-W.

Van Maanen, B., G. Coco, and K. R. Bryan (2015). On the ecogeomorphological feedbacks that control tidal channel network evolution in a sandy mangrove setting. *Proceedings of the Royal Society A: Mathematical, Physical and Engineering Sciences* 471.2180, p. 20150115. DOI:10.1098/RSPA.2015.0115. eprint: https://royalsocietypublishing.org/doi/pdf/10.1098/rspa.2015.0115.

Van Maanen, B., G. Coco, K. R. Bryan, and C. T. Friedrichs (2013). Modeling the morphodynamic response of tidal embayments to sea-level rise. *Ocean Dynamics* 63.11, pp. 1249–1262. DOI:10.1007/s10236-013-0649-6.

Van Oorschot, M., M. G. Kleinhans, G. W. Geerling, G. Egger, R. S. E. W. Leuven, and H. Middelkoop (2017). Modeling invasive alien plant species in river systems: Interaction with native ecosystem engineers and effects on hydro-morphodynamic processes. *Water Resources Research* 53.8, pp. 6945–

6969. DOI:10.1002/2017WR020854. eprint: https://agupubs.onlinelibrary.wiley.com/doi/pdf/10.1002/2017WR020854.
Van Rijn, L. C., D. J. R. Walstra, and M. van Ormondt (2004). Description of TRANSPOR2004 and implementation in Delft3D-ONLINE. *WL | Hydraulics - Final report*.
Van Rijn, L. (1995). Sand budget and coastline changes of the central coast of Holland between Den Helder and Hoek van Holland, period 1964-2040.
Van Rijn, L., D. Walstra, B. Grasmeijer, J. Sutherland, S. Pan, and J. Sierra (2003). The predictability of cross-shore bed evolution of sandy beaches at the time scale of storms and seasons using process-based Profile models. *Coastal Engineering* 47.3, pp. 295–327. DOI:HTTPS://DOI.ORG/10.1016/S0378-3839(02)00120-5.
Van Rijn, L. C. (2007a). Unified View of Sediment Transport by Currents and Waves. I: Initiation of Motion, Bed Roughness, and Bed-Load Transport. *Journal of Hydraulic Engineering* 133.6, pp. 649–667. DOI:10.1061/(ASCE)0733-9429(2007)133:6(649).
Van Rijn, L. C. (2007b). Unified View of Sediment Transport by Currents and Waves. II: Suspended Transport. *Journal of Hydraulic Engineering* 133.6, pp. 668–689. DOI:10.1061/(ASCE)0733-9429(2007)133:6(668).
Van Rijn, L. C. (2011). *Principles of fluid flow and surface waves in rivers, estuaries, seas, and oceans*. 2011th ed. Acqua. DOI:978.90.79955.02.8.
Van Rijn, L. C., D.-J. R. Walstra, and M. van Ormondt (2007). Unified View of Sediment Transport by Currents and Waves. IV: Application of Morphodynamic Model. *Journal of Hydraulic Engineering* 133.7, pp. 776–793. DOI:10.1061/(ASCE)0733-9429(2007)133:7(776).
Van Thiel de Vries, J. (2009). Dune erosion during storm surges. PhD thesis. Delft, The Netherlands: Delft University of Technology.
Van Veen, J., A. J. F. van der Spek, M. J. F. Stive, and T. Zitman (Nov. 2005). Ebb and Flood Channel Systems in the Netherlands Tidal Waters1. *Journal of Coastal Research* 21.6 (216), pp. 1107–1120. DOI:10.2112/04-0394.1. eprint: https://meridian.allenpress.com/jcr/article-pdf/21/6(216)/1107/1293932/04-0394_1.pdf.
Van Wesenbeeck, B. K., G. Wolters, J. A. A. Antolínez, S. A. Kalloe, B. Hofland, W. P. de Boer, C. Çete, and T. J. Bouma (2022). Wave attenuation through forests under extreme conditions. *Scientific Reports* 12.1, p. 1884. DOI:10.1038/s41598-022-05753-3.
Vellinga, P. (1982). Beach and dune erosion during storm surges. *Coastal Engineering* 6.4, pp. 361–387. DOI:HTTPS://DOI.ORG/10.1016/0378-3839(82)90007-2.
Vermeersen, B. L. et al. (2018). Sea-level change in the Dutch Wadden Sea. *Netherlands Journal of Geosciences* 97.3, pp. 79–127. DOI:10.1017/NJG.2018.7.
Villaret, C., J.-M. Hervouet, R. Kopmann, U. Merkel, and A. G. Davies (2013). Morphodynamic modeling using the Telemac finite-element system. *Computers & Geosciences* 53. Modeling for Environmental Change, pp. 105–113. DOI:HTTPS://DOI.ORG/10.1016/J.CAGEO.2011.10.004.
Vos, P. (2015). Origin of the Dutch Coastal Landscape. PhD thesis. Utrecht University.
Vousdoukas, M. I., R. Ranasinghe, L. Mentaschi, T. A. Plomaritis, P. Athanasiou, A. Luijendijk, and L. Feyen (2020). Sandy coastlines under threat of erosion. *Nature Climate Change* 10.3, pp. 260–263.
Vroom, J., P. L. M. De Vet, and J. J. Van der Werf (2015). *Validatie waterbeweging Delft3D NeVla model Westerscheldemonding (in Dutch)*. Tech. rep. Deltares.
Walstra, D. J. R., L. C. van Rijn, M. van Ormondt, C. Briere, and A. M. Talmon (2007a). The Effects of Bed Slope and Wave Skewness on Sediment Transport and Morphology. In: *Coastal Sediments '07*. DOI:10.1061/40926(239)11. eprint: https://ascelibrary.org/doi/pdf/10.1061/40926.28239.2911.
Walstra, D. J. R., L. C. van Rijn, M. van Ormondt, C. Briere, and A. M. Talmon (2007b). The effects of bed slope and wave skewness on sediment transport and morphology. *6th International Symposium on Coastal Engineering and Science of Coastal Sediment Processes*, pp. ---. DOI:10.1061/40926(239)11.
Walstra, D., R. Hoekstra, P. Tonnon, and B. Ruessink (2013). Input reduction for long-term morphodynamic simulations in wave-dominated coastal settings. *Coastal Engineering* 77, pp. 57–70. DOI:HTTPS://DOI.ORG/10.1016/J.COASTALENG.2013.02.001.

Walstra, D., A. Reniers, R. Ranasinghe, J. Roelvink, and B. Ruessink (2012). On bar growth and decay during interannual net offshore migration. *Coastal Engineering* 60, pp. 190–200. DOI:HTTPS://DOI.ORG/10.1016/J.COASTALENG.2011.10.002.

Walton, T. L. and W. D. Adams (1976). Capacity of Inlet Outer Bars to Store Sand. In: *Coastal Engineering 1976*, pp. 1919–1937. DOI:10.1061/9780872620834.112. eprint: https://ascelibrary.org/doi/pdf/10.1061/9780872620834.112.

Wang, Z., P. Hoekstra, H. Burchard, H. Ridderinkhof, H. de Swart, and M. Stive (2012). Morphodynamics of the Wadden Sea and its barrier island system. *Ocean & Coastal Management* 68. Special Issue on the Wadden Sea Region, pp. 39–57. DOI:HTTPS://DOI.ORG/10.1016/J.OCECOAMAN.2011.12.022.

Wang, Z., J. De Ronde, A. Van der Spek, and E. Elias (2009). Responses of the Dutch coastal system to the (semi-) closures of tidal basins. In: *ICEC 2009, Sendai, Japan*. Tohoku University, pp. 203–210.

Wang, Z. B., E. P. Elias, A. J. van der Spek, and Q. J. Lodder (2018). Sediment budget and morphological development of the Dutch Wadden Sea: impact of accelerated sea-level rise and subsidence until 2100. *Netherlands Journal of Geosciences* 97.3, pp. 183–214. DOI:10.1017/NJG.2018.8.

Warner, J. C., C. R. Sherwood, R. P. Signell, C. K. Harris, and H. G. Arango (2008). Development of a three-dimensional, regional, coupled wave, current, and sediment-transport model. *Computers & Geosciences* 34.10. Predictive Modeling in Sediment Transport and Stratigraphy, pp. 1284–1306. DOI:HTTPS://DOI.ORG/10.1016/J.CAGEO.2008.02.012.

Wijnberg, K. M. and J. H. Terwindt (1995). Extracting decadal morphological behaviour from high-resolution, long-term bathymetric surveys along the Holland coast using eigenfunction analysis. *Marine Geology* 126.1, pp. 301–330. DOI:HTTPS://DOI.ORG/10.1016/0025-3227(95)00084-C.

Winterwerp, J. C., Z. Zhou, G. Battista, T. V. Kessel, H. R. A. Jagers, D. S. V. Maren, and M. V. D. Wegen (2018). Efficient Consolidation Model for Morphodynamic Simulations in Low-SPM Environments. *Journal of Hydraulic Engineering* 144.8, p. 04018055. DOI:10.1061/(ASCE)HY.1943-7900.0001477.

Wright, L. and B. Thom (1977). Coastal depositional landforms: a morphodynamic approach. *Progress in Physical Geography: Earth and Environment* 1.3, pp. 412–459. DOI:10.1177/030913337700100302. eprint: https://doi.org/10.1177/030913337700100302.

Xie, D., C. Schwarz, M. Z. M. Brückner, M. G. Kleinhans, D. H. Urrego, Z. Zhou, and B. van Maanen (2020). Mangrove diversity loss under sea-level rise triggered by bio-morphodynamic feedbacks and anthropogenic pressures. *Environmental Research Letters* 15.11, p. 114033. DOI:10.1088/1748-9326/ABC122.

Xu, F., G. Coco, J. Tao, Z. Zhou, C. Zhang, S. Lanzoni, and A. D'Alpaos (2019). On the Morphodynamic Equilibrium of a Short Tidal Channel. *Journal of Geophysical Research: Earth Surface* 124.2, pp. 639–665. DOI:10.1029/2018JF004952. eprint: https://agupubs.onlinelibrary.wiley.com/doi/pdf/10.1029/2018JF004952.

Yamasaki, S. and I. Tange (1981). Growth responses of Zizania latifolia, Phragmites australis and Miscanthus sacchariflorus to varying inundation. *Aquatic Botany* 10, pp. 229–239.

Zhou, Z., M. Olabarrieta, L. Stefanon, A. D'Alpaos, L. Carniello, and G. Coco (2014). A comparative study of physical and numerical modeling of tidal network ontogeny. *Journal of Geophysical Research: Earth Surface* 119.4, pp. 892–912.

Zhou, Z. et al. (2017). Is "Morphodynamic Equilibrium" an oxymoron?. *Earth-Science Reviews* 165, pp. 257–267. DOI:HTTPS://DOI.ORG/10.1016/J.EARSCIREV.2016.12.002.

Zhu, Z., V. Vuik, P. J. Visser, T. Soens, B. van Wesenbeeck, J. van de Koppel, S. N. Jonkman, S. Temmerman, and T. J. Bouma (2020). Historic storms and the hidden value of coastal wetlands for nature-based flood defence. *Nature Sustainability*.

Zijlema, M., G. Stelling, and P. Smit (2011). SWASH: An operational public domain code for simulating wave fields and rapidly varied flows in coastal waters. *Coastal Engineering* 58.10, pp. 992–1012. DOI:HTTPS://DOI.ORG/10.1016/J.COASTALENG.2011.05.015.

Acknowledgements

This thesis marks the end of an important chapter in my life that I am beyond glad to conclude. In average, I had a really nice experience. I truly appreciated the freedom to explore and dive deep into the (bio)morphodynamics. However, the standard deviation was rather large, especially outside the professional life, and that made this journey a bumpy roller coast. But one thing was never an option: quitting. And here I am! Therefore, I acknowledge everything and everyone that paved this road and helped me to become a Dr.

First, my parents, family and close (but mostly far!) friends. Even though most of them had no idea about my research, they were always there to support and create nice moments and good memories. Here, fortunately, I have too many people to mention, so just a sample of the physically nearby friends: Kaji and Amaury (no hard feelings that you abandoned me here!); Daniel, Gi, Rafa and Pitu for the fun weekends; the Piccolinsky family for the good times, technical discussions and adventures; and the late-comers Scherr and Marleen for the quality food experiences and the fun times together. To Ana Paula who encouraged me to get into the PhD adventure and to Mel who helped me to get out of it. My time in Werkhoven at the Molenzolder was special among the Porte family. Hartlijk bedankt Leny and Marius for everything. A very special thanks to my mom. She managed to keep 3 naughty boys in the good path all by herself as a primary school teacher. I am as proud of her as she is (probably) proud of me now. Obrigado, Mãe!

A kid from Tremembé-SP, fio, does not easily end up in a PhD track at Utrecht University. I own this to some special people that helped me to come this far. To my ant and portuguese teacher, Tia Gildete, and to my Godparents Inês and Alfredo that always encouraged and supported me to go beyond the ordinary. To my professors João Thadeu de Menezes and Antonio Klein that opened up my ways in Oceanography and research (after I paid the sieving entry-fee of the Geo-lab!). The final but decisive push towards my international carrier was made by Duncan FitzGerald and Christopher Hein that brought me to the USA for an internship in their research group at Boston University. After that I was never the same and the entire world up end in front of me. I can't say enough thanks to these people, especially to Chris. Thanks, folks!

Then, finally on the PhD track itself, thanks to Maarten Kleinhans and for his ERC Consolidator grant that financially supported my PhD. Above all, thanks Maarten for hiring this (by the time) rather unknown person from a far land, and for your unconditional support. We had our agreements and disagreements, but I hope that I managed to fulfill the expectations for you project.

My sincere acknowledgements to Gerben Ruessink who gave me the key insight to improve my long-term morphological simulations with waves. Here, I further extend my acknowledgments to Deltares, to Dirk Jan Walstra, Bert Jagers, Bart Grasmeijer and Pieter Koen Tonnon for the assistance and discussions while working on the source code of Delft3D. The new version of Delft3D was the turning point of my PhD and I can't say enough thanks here.

This work was also possible due to my geological legs. So thanks to Tjalling who unfortunately (for me!) changed path within the department, but was always around, and to Harm Jan who brilliantly took it over. Thanks to Ad van der Spek and Sitze for the fruitful discussions and your efforts to help me with the geological data and insights. By the end I could not incorporate everything in this thesis - the Oude Rijn case is still open! And also to my amazing (prize winner) MSc student and now PhD candidate (and paranymph!) Lonneke. You folks were amazing!

Another key point for this thesis was the possibility to work on the powerful (and amazing) SURFSara and Eejit clusters. A HUGE thanks to Edwin who helped me until the models were compiled and running. Also thanks to Maxime (SURFSara) and to the Physical Geography department for making it possible. I hope more people from the department will benefit from it in the near future. Speaking of the department, thanks to the Physical Geography department for their support, especially during the pandemic.

It was a pleasure to be among the bike-lovers. Thanks Tjalling for showing me some nice bikes routes around de Utrechtse Heuvelrug and in Limburg when I didn't know the area - they are still among my favorites. Thanks to Anne and Marjolein for all the chocolates and ice creams from the cycling rides and bets! And Op de Stad Fiets (also know as Klaas) for the bike and wave-related discussions.

Thanks to my friends and colleagues from the department. Specially to Sepehr for the quality coffee breaks and for the friendship beyond the work environment. To my project and Son's of Maarten band: Anne, Lisanne, Jasper, Wout, Matt, Sanja, Steven, Jana, Muriel, Will and to the PhD crowd: Sepehr, Tim, Joeri, Jannis, Daan, Joost, Daniel, for the friday drinks and polemic coffee break discussions. And the potluck crowd for the fun times, specially to Jana for all her energy to organize everything!

Finally, thanks to WaterProof for reconnecting me to the world outside and for the chance to play with water, sand and mud in the lab. And thanks to the nice colleagues that made this rough time of consultancy and thesis a little easier!

Once again, thanks to my family and friends that helped me to go through it.

About the author

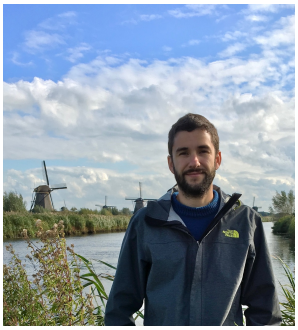

Olá, it's me, Márcio!

Márcio has a complementary expertise in oceanography and coastal engineering earned through international experience in academia and consultancy. Since 2008, his work focuses on the morphodynamics of coastal, estuarine and fluvial environments in different temporal-spatial scales. His skills in morphodynamics seamlessly combine knowledge, analytical tools, numerical models, field data and laboratory experiments.

Formal Education

PhD Candidate in Physical Geography
Utrecht University – Faculty of Geosciences, Utrecht, The Netherlands
Period: October 2016 to January 2021

MSc in Civil Engineering (Hydraulics)
Coastal and Marine Engineering and Management (CoMEM)
Graduated at TU Delft, the Netherlands
Joint program of TU Delft, the Netherlands & UPC, Spain & NTNU, Norway
Period: August 2011 to June 2013

BSc in Oceanography
Universidade do Vale do Itajaí (UNIVALI) – Itajaí/SC, Brazil
Period: August 2005 to August 2010

List of Publications and Academic Activities

Published Journal articles

Boechat Albernaz, M., Brückner, M., van Maanen, B., van der Spek, A. J. F., Maarten G. Kleinhans (2023) Vegetation reconfigures barrier coasts and affects tidal basin infilling under sea level rise *Journal of Geophysical Research: Earth Surface* 128

Boechat Albernaz, M., Roelofs, L; Pierik, H.J., Kleinhans, M.G. (2020) Natural levee evolution in vegetated fluvial-tidal environments. *Earth Surface Processes and Landforms* 45: 3824–3841

Boechat Albernaz, M.; Ruessink, G.; Jagers, H.R.A.B.; Kleinhans, M.G. (2019) Effects of Wave Orbital Velocity Parameterization on Nearshore Sediment Transport and Decadal Morphodynamics. *Journal of Marine Science and Engineering* 7(6), 188.

Co-Authoring articles

Harm Jan Pierik, Jelle I.M. Moree, Karianne M. van der Werf, Lonneke Roelofs, **Marcio Boechat Albernaz**, Antoine Wilbers, Bert van der Valc, Marieke van Dinter, Wim Hoek, Tjalling de Haas, Maarten G. Kleinhans (2023) Vegetation and peat accumulation steer Holocene tidal–fluvial basin filling and overbank sedimentation along the Old Rhine River, The Netherlands. *Sedimentology* 70: 179-213.

Brückner, M.; Schwarz, C.; Coco, G.; Baar, A.; **Boechat Albernaz, M.**, Kleinhans, M.G. (2021) Benthic species as mud patrol-modelled effects of bioturbators and biofilms on large-scale estuarine mud and morphology. *Earth Surface Processes and Landforms* 46:1128-1144

Weisscher, S.A.H., **Boechat Albernaz, M.**, Leuven, J.R.F.W., Van Dijk, W.M., Shimizu, Y., Kleinhans. M.G. (2020) Implementing a hydrodynamic model to complement water depth and flow velocity data for physical scale experiments of rivers and estuaries. *Earth Surface Dynamics* 8(4), 955-972

Baar, A.W., **Boechat Albernaz, M**, Van Dijk, W.M., and Kleinhans, M.G. (2019) Critical dependence of morphodynamic models of fluvial and tidal systems on empirical downslope sediment transport. *Nature Communications* 10, 4903

Hein, C.J., Fitzgerald, D.M., Klein, A.H.D.F., **Albernaz, M.B.**, de Menezes, J.T. and Cleary, W.J., (2014). Reply to the Discussion by Dillenburg et al. on "Evidence for a transgressive barrier within a regressive strandplain system: implications for complex response to environmental change" by Hein et al.(2013), Sedimentology 60, 469–502: A transgressive barrier at Pinheira, Southern Brazil around 3 ka?. *Sedimentology*, 61(7), pp.2213-2217.

Hein, C.J., FitzGerald, D.M., Clearly, W., Menezes, J.T., and Klein, A.H.F., **Albernaz, M.B.** (2014) "Coastal response to late-stage transgression and sea-level highstand" *Geological Society of America Bulletin* (GSAB)

Hein, C.J., FitzGerald, D.M., Clearly, W., **Albernaz, M.B.**, Menezes, J.T., and Klein, A.H.F. (2013) "Evidence for a transgressive barrier within a regressive strandplain system: Implications for complex coastal response to environmental change" *Sedimentology* (60) 2, p. 469-502

Other Publications

Albernaz, M.B., Ansanelli, L., de Luca, C., Fiedler, M.F.M., Giovannini, S.G.T., Siqueira, B., Yassuda, E.A. (2016) Effects of TEBAR Pier at São Sebastião Channel Hydrodynamics and Shoreline Evolution at Ilha Bela, *Conf. Proceedings at IX PIANC COPEDEC*, Rio de Janeiro – Brazil.

Albernaz, M.B. (2013) Sustainable long term coastal protection and development based on sand nourishments. *MSC thesis*. Delft University of Technology. June 2013. Supervisor: Prof. Dr. Eng. Marcel Stive

Design of sand bypass system in Zeebrugge, Belgium. *Multidisciplinary Project*. TU Delft. June 2012.Supervisor: Dr. Eng. Jan van Overeem

Albernaz, M.B. (2010) Long term analysis of morphodynamic processes at Balneário Camboriú beach applying multivariate analysis. *BSc thesis*, Universidade do Vale do Itajaí. Supervisor: Dr. João Thadeu de Menezes in: Portuguese

Albernaz, M.B.; Menezes, J.T. (2010) Mapping, Identification and description of morphological and sedimentological characteristics as well as present infrastructure at Bombinhas/SC beaches *Congresso Brasileiro de Oceanografia* (CBO). in: Portuguese

Selected Conferences and Events

EGU 2020 – Share EGU, online
Display: "Biogeomorphodynamic of fluvial-tidal levees and accommodation space infilling"

AGU Fall Meeting 2019 - San Francisco, USA
Oral presentation: "Raising the land: fluvial-tidal levees and accommodation space infilling"

ICEC 2018 - Caen, France
Oral presentation: "Cross-shore effect of orbital motion parameterization on wave-related sediment transport in the nearshore"

SIESD 2018 summer school – St. Anthony Falls Laboratory – Minneapolis, USA

Delft Software Days 2018 – Deltares – Delft, NL
Oral presentation: "From milliseconds to centuries: long-term coastal morphology modelled with a new wave orbital motion parameterization"

RCEM 2017 - Padova, Italy
Poster session: "Morphological evolution of estuary mouths with wave-current interactions modelled over centuries"